Adaptive Output Feedback Control of Flexible Systems

A Thesis
Presented to
The Academic Faculty

by

Bong-Jun Yang

In Partial Fulfillment
of the Requirements for the Degree
Doctor of Philosophy

School of Aerospace Engineering
Georgia Institute of Technology
April 2004

Adaptive Output Feedback Control of Flexible Systems

Approved by:

Anthony J. Calise, Committee Chair

Wassim M. Haddad

James I. Craig

Naira Hovakimyan
(AOE, Virginia Tech.)

Wayne J. Book
(ME)

Date Approved: 8 April 2004

DEDICATION

To my parents

ACKNOWLEDGEMENTS

I would like to thank my committee members for suggestions and corrections that greatly improved this dissertation. First I would like to thank my advisors, Dr. Anthony J. Calise and James I. Craig for their support, advice, and guidance over the years that I have been working with them. While I was doubtful and my idea was superficial, they could concretely envision what would be achieved, and, without them, I could have never come to this stage. Their passion for research has had a great influence on me and I have learned from them how to view things from different aspects. I would also like to thank Dr. Wassim M. Haddad to whom I always feel indebted for his excellent teaching and great books. I thank Dr. Wayne J. Book for providing opportunity to work with Lyannae George and Ryan Krauss on the project in the intelligent machine dynamics lab, without which Chapter 8 would have been missing in my thesis. Finally, I must say that I miss many discussions that I had with Dr. Naira Hovakimyan. She has been a tremendous help to my study at Georgia Tech.

I thank now-gone Dr.s, Hungu Lee, Seungjae ("Franz") Lee, Manu Sharma, Flavio Nardi, Haijun Shen, Tomohisa Hayakawa and still-present Dr.s, Professor Eric Johnson and Nakwan Kim, for their assistance and help. I am grateful for my former and current lab mates, Hesham El-Shirbiny, Ali Kutay, Suresh Kannan, Matt Johnson, Yoonghyun ("John") Shin, Ramachandra Sattigeri, Suraj Unnikrishnan, Venkatesh Madyastha, Choong-Yil Kim, Dr. Hyuk Ryu for many hours of discussions, advice and assistance. In particular, my special gratitude goes to Matt Johnson, whom I first resort to about very many things around me, for managing our lab to be well equipped and comfortable.

I am greatly indebted to my family for their long-time, patient support and encouragement, especially to my parents. From birth to now, they have shaped what I was born as into who I am. Finally, my special thanks go to my significant other, Jiyoon, who has become a joyful company along this journey.

TABLE OF CONTENTS

LIST OF FIGURES

SUMMARY

Neural network-based adaptive output feedback approaches that augment a linear control design are described in this thesis, and emphasis is placed on their real-time implementation with flexible structural systems. Two different control architectures that are robust to parametric uncertainties and unmodelled dynamics are presented. A key feature of these approaches is that the order of the system need not be known. The unmodelled effects can consist of minimum phase internal dynamics of the system together with external disturbance process acting on the system. Within this context, adaptive compensation for external disturbances is addressed.

In the first approach, internal model-following control, augmenting elements are designed using feedback inversion. The effect of an actuator limit is treated using control hedging, and the effect of other actuation nonlinearities, such as dead zone and backlash, is mitigated by a disturbance observer-based control design. The effectiveness of the approach is illustrated through simulation and experimental testing with a three-disk torsional system, which is subjected to control voltage limit and stiction.

While the internal model-following control is limited to minimum phase systems, due to the inversion-based augmenting control design, the second approach, external model-following control, does not involve feedback linearization and can be applied to non-minimum phase systems. The unstable zero dynamics are assumed to have been modelled in the design of the existing linear controller. The laboratory tests for this method include a three-disk torsional pendulum, an inverted pendulum, and a flexible-base robot manipulator.

The external model-following control architecture is further extended in three ways. The first extension is an approach for control of multivariable nonlinear systems. The second extension is a decentralized adaptive control approach for large-scale interconnected systems. The third extension is to make use of an adaptive observer to augment a linear observer-based controller. In this extension, augmenting terms for the adaptive observer

can be used to achieve adaptation in both the observer and the controller simultaneously. Simulations to illustrate these approaches include an inverted pendulum with its cart serially attached to two carts (one unmodelled), three spring-coupled inverted pendulums, and an inverted pendulum with its initial condition in a range in which a linear model is not valid.

CHAPTER 1

INTRODUCTION

1.1 Motivation

A major limitation on the operational performance of air, land, and space systems is the mechanical flexibility in their structural and mechanical elements. Systems made of light materials exhibit a high degree of flexibility and encounter unavoidable deflection and vibration problems. As a result, an active control system that compensates for flexibility and that suppresses vibration is an essential part of the development of high-performance, lightweight systems. Designing an effective controller for flexible systems, however, is an challenging task. The difficulties associated with control design in flexible systems include structural parameter uncertainties and their variations over time, low damping over wide range of modal frequencies, unmodelled closely spaced modes, structural nonlinearities, and operation under a wide range of loadings and disturbances. In most instances there is a large degree of uncertainty associated with flexible structures. In addition, flexible systems containing a mechanical structure with distributed parameters are typically represented by partial differential equations while most present control algorithms have been developed for lumped parameter systems. Therefore, approximation of distributed parameter systems by finite order models for control design purposes introduced a further degree of uncertainty. The presence of a high degree of uncertainty combined with the desire for high performance provides sufficient motivation for developing approaches to adaptive control of flexible systems.

Adaptive control is a natural strategy to enhance performance of uncertain systems with minimal sacrifice in performance. Early state feedback approaches in adaptive control were developed for linear systems [1–4], and for nonlinear systems with linearly parameterized uncertainty [2, 5]. Recent progress in state feedback adaptive control include approaches that do not require any parameterization of state-dependent uncertainties [6, 7]. Design

approaches for adaptive output feedback control are more limited in their applicability due to the fact that a state observer must be employed in the feedback architecture. In this respect, a high-gain observer introduced in [8] has had a great influence on the literature that followed [9–15]. Ref. [8] highlighted a destabilizing effect of the high-gain observer, a so-called peaking phenomenon [16, 17], and suggested the employment of saturation in control input to prevent it. The peaking phenomenon has proven to be a fundamental obstacle in extending global results in linear systems to nonlinear systems [17]. In the case of uncertain nonlinear systems, results on adaptive output feedback control have been restricted to the class of nonlinear systems either affine in uncertain parameters [14, 18] or with uncertainties dependent only upon available measurements [19, 20].

The use of a neural network (NN) in adaptive control greatly broadened the class of systems that can be treated by adaptive control. Whereas in most classical adaptive control approaches [2–4, 19, 21] uncertainties are restricted to linearly parameterized uncertainties, NN-based adaptive control allows for *functional uncertainty* as well. It is well established that a NN can approximate any continuous function to any desired accuracy on a compact set [22, 23]. This universal approximator property of NNs has lead to their evolution as a powerful tool for designing adaptive controllers for uncertain nonlinear systems [24]. In the early to mid 1990's, the feasibility of using NNs in identification and control for uncertain nonlinear systems was illustrated through various simulation studies [25–28]. The potential of employing NNs to compensate for flexibility in the uncertain systems was demonstrated in [29–33]. These approaches were essentially experimental evaluation of the simulation studies in [25, 27] and lacked a stability proof. Since the mid 1990's, several researchers have proposed control methods that employ NNs together with stability proofs based on Lyapunov's direct method in a state feedback setting [34–37]. In [38], the NN control method in [36] was tested in a single-link flexible beam and shown to outperform conventional PD and PID controllers. Extensions to NN-based adaptive output feedback have been developed either by employing a high-gain observer [39–41], or by incorporating a second NN in the estimation process [42, 43].

Applying an adaptive technique for control of uncertain systems, in most cases, implies

replacement of an existing control system. Because of the high cost in this process, it is highly desirable to consider an adaptive approach that can be implemented in a form that augments an existing controller. In particular, within various fields of applications, there exists a legacy of experience with an existing control system architecture, and control designers would prefer to augment their controllers with an adaptive process rather than replace them with a totally new control system. This rationale has been a main driving force for applying adaptive control to augment existing control systems in space robotics [44], power systems [45, 46], temperature regulation [47], and flight control systems [48, 49], to name a few. Incorporating a NN as a tool for augmenting adaptive control was also tried in [50, 51] in a state feedback setting.

Since the late 1990's, NN-based adaptive control in conjunction with a baseline *inverting* controller has been applied to flight control systems and led to successful implementation results [52–57]. This success initiated an attempt to employ NN-based adaptive methods for augmenting a baseline linear controller in [58–61]. These methods were, however, based on state feedback, and assumed that the dimension of the system is known. This prevented these approaches from being applied to control of flexible systems in which only a set of measurements are available, and for which unmodelled dynamics are the rule rather than the exception.

In inversion–based NN adaptive control, major progress towards the output feedback problem was made in [62, 63] by employing the approximation scheme in [64]. Whereas the approaches in [39–41] employ a high-gain observer to generate the NN inputs needed to approximate the uncertainty, the approach in [64] made use of time delayed values of input/output data, and greatly simplified the approximation process. This approximation scheme was further proved in [65], and an upper bound for the NN approximation error was established. The approaches in [62, 63] can be applied to a broad class of minimum phase nonlinear systems in which regulated outputs have a known vector relative degree. The approaches are robust to parametric uncertainties and unmodelled dynamics. Laboratory experiments have illustrated their effectiveness in a real-time environment [66, 67].

The objective of this thesis is to provide a output feedback methodology that employs

NN-based adaptive control to augment a fixed-gain linear controller. The problem formulation involves how the adaptive designs in [62,63] can be used to augment a fixed-gain linear controller. The resulting approaches are robust to parametric uncertainties and unmodelled dynamics, and can be applied to control of flexible systems. The thesis also includes experimental results to show the effectiveness of the control designs in a real-time, complex environment.

1.2 Contributions of Thesis

This thesis extends the previous augmenting approaches in [58–61] from state feedback to output feedback, with emphasis on real-time implementation to flexible systems. The problem formulation involves extending the approaches in [62,63] from augmenting an *inverting* baseline controller to augmenting a *linear* controller, so that the approaches can be used for adaptive control of flexible systems. An important assumption in the development of an augmenting approach is that the relative degree of the system is known. This assumption is a fundamental requirement for robust control system design.

A key feature of the method is that the order of the system dynamics need not be known. The unmodelled effects can consist of minimum phase internal dynamics of the system together with external disturbance processes acting on the system. Within this context, we present a new approach to adaptive compensation for external disturbances. Unlike the output regulator [68] and disturbance accommodating control [69], we do not need to know the frequencies of external sinusoidal disturbances.

Figure 1.1 organizes the results presented in this thesis. The approaches fall into two classes depending on control architectures: internal model-following control and external model-following control. Their distinction lies between emphasizing closed-loop behavior versus plant behavior. In internal model-following control the true plant is modified by the adaptive element so that its behavior is close to that of the plant model. In external model-following control, the adaptive element is used to modify the closed-loop behavior so that it is close to that of the reference model. In both architectures, the disturbance only affect the plant dynamics, and not the model dynamics, therefore both architectures are

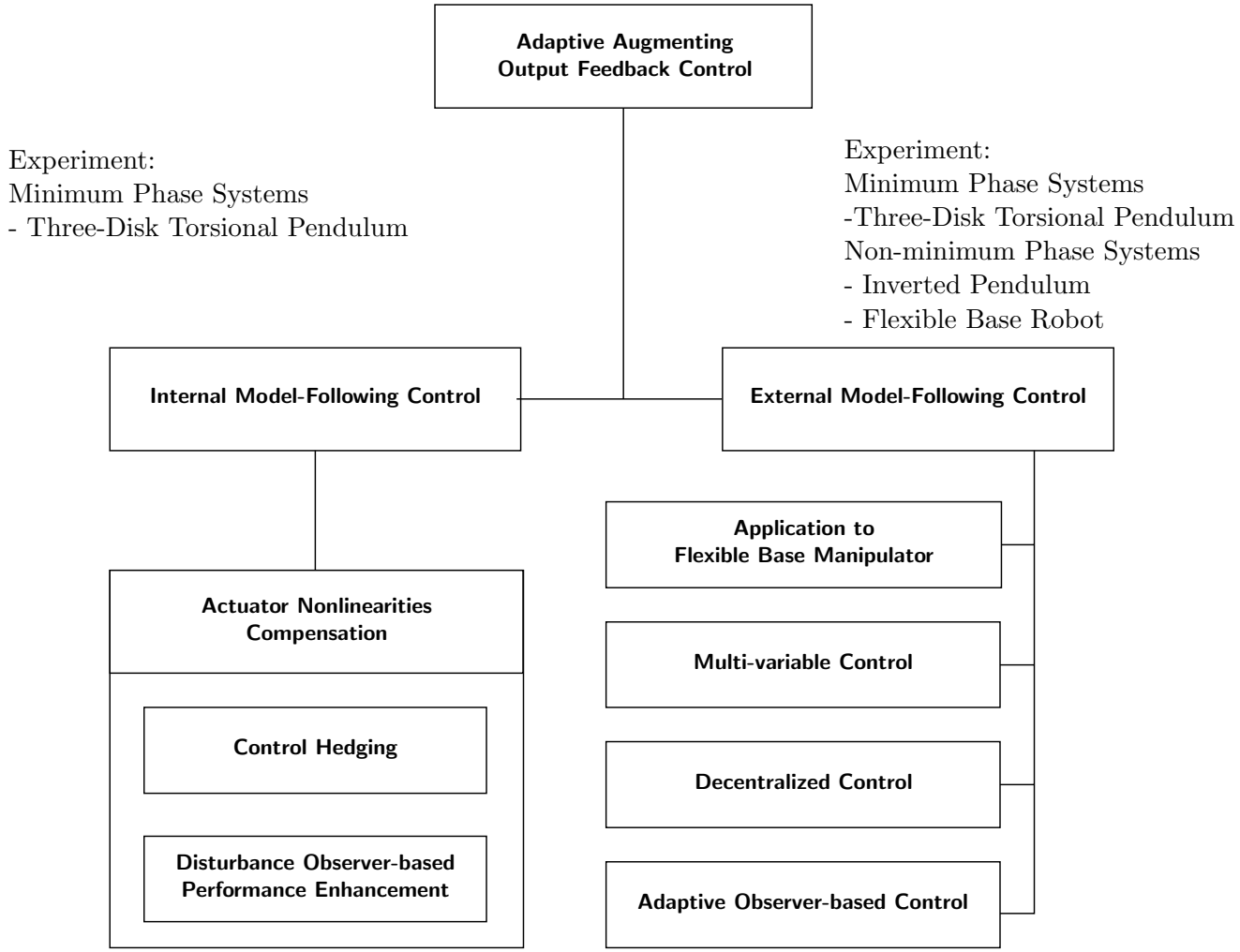

Fig. 1.1: Organization Diagram for Adaptive Augmenting Output Feedback Control

well suited for disturbance rejection.

Within the internal model-following control architecture, we describe how we can compensate for actuator nonlinearities. From the perspective of adaptive control, common actuator nonlinearities can be grouped into two classes: dead zone, backlash, and hysteresis generally limit the control system performance when the control demand is low, and amplitude/rate saturation degrades performance when the control demand is high. Inspired by pseudo-control hedging (PCH) [57, 70] developed in the architecture of inverting controller, we develop a method, called control hedging (CH), to protect the adaptive process in the case of input saturation. While the problem of input saturation has been well recognized in the literature [57, 70–75], the treatment of other class of nonlinearities is relatively new,

and adaptive methods to compensate for them have appeared only recently in the literature [76–80]. For this class of nonlinearities, we pay attention to the results in [81, 82] that establish structural equivalences among model based disturbance compensating controllers. We note that the internal model-following control architecture is equivalent to a robust internal-loop compensator (RIC) architecture in [82], which has been shown equivalent to a disturbance observer. Subsequently, we realize the disturbance observer in the internal model-following architecture to achieve the result in [77], i.e., performance enhancement by compensating for actuator nonlinearities. When this scheme is combined with CH, we obtain a method highly effective for a great variety of actuator nonlinearities (dead zone, backlash, and saturation). Internal model-following control and CH are tested in a laboratory experiment consisting of a three-disk torsional pendulum system subject to control voltage saturation. Disturbance observer-based performance enhancement is illustrated through simulations in which the actuator is subject to dead zone and saturation.

External model-following control is an extension of the method in [61] from state feedback to output feedback. In this architecture, as in [61], the external model, the so-called "reference model", is utilized in the design of adaptive elements. The reference model is the closed-loop system consisting of the plant model regulated by the existing controller, and is assumed to meet the performance specifications. NN-based adaptive elements based on the design method in [63] are added to force the output of the system to track that of the reference model. Whereas the internal model-following architecture employs *feedback inversion* in the adaptive control design, the adaptive design in the external model-following architecture does not depend on inversion. Hence, the method can be applied to non-minimum phase systems. Laboratory tests for this architecture include the three-disk torsional pendulum noted earlier, an inverted pendulum, and vibration control for a large flexible-base manipulator.

As a final step in this thesis, we extend external model-following control in three ways. First, the framework of external model-following control is extended to a multi-input multi-output (MIMO) setting following the design in [83]. Another extension is a *decentralized* scheme for large-scale interconnected systems. Decentralized control problems often arise

from either the physical inability to share subsystem information or the lack of computing capabilities for a single central controller in large-scale interconnected systems. By employing the external model-following control method, we develop a decentralized scheme for interconnected systems with unknown interconnections. That is, each subsystem is regulated by a NN-based adaptive control to compensate for interconnected effects to achieve *implicit cooperation* [84, 85] for the whole composite system. Finally, we show how the adaptive observer in [86] can be employed to adaptively tackle the unmatched uncertainty. The observer in [86] augments an existing linear observer by injecting uncertainty estimates generated by a NN. In this extension, we show how the adaptive observer in [86] can be used to achieve adaptation in both the observer and a controller simultaneously. This is in contrast to the control architectures in [42, 43] where two NNs are used for observer and controller design.

1.3 Thesis Outline

The thesis is organized following the diagram in Figure 1.1. In Chapter 2, the internal model-following control architecture is described. The adaptive NN-based elements are added to compensate for modelling uncertainties between the system and the plant model. The main assumptions are known relative degree and the minimum phase property of the regulated output. Experimental results with a three-disk torsional pendulum system illustrate the validity of the method in Section 2.7.

In Chapter 3, we address the problem of actuator nonlinearities in the framework of Chapter 2. The CH technique is described in Section 3.2. Experiments are carried out by limiting control voltage with the three-disk torsional pendulum. The results show its effectiveness in handling input saturation. In Section 3.3, the control design to deal with actuator nonlinearities such as dead zone and backlash is described. The problem is formulated assuming that the plant model is fully linearizable. The simulation results show that the method, combined with CH, is effective with dead zone and saturation nonlinearities as well as when the system is subject to dynamic friction.

In Chapter 4, external model-following control is developed. In this architecture, the

adaptive control design does not involve feedback linearization, so the method can be applied to non-minimum phase systems. Main assumptions are that the system has known relative degree and that the non-minimum phase zeros are accounted for to a sufficient degree of accuracy in the nominal design. Experimental results in Section 4.4 with the three-disk torsional pendulum show the same level of performance as that in Section 2.7. In Section 4.5, the method is also tested with an inverted pendulum to prove its validity in control of a non-minimum phase system.

In Chapter 5, we extend the augmenting method developed in Chapter 4 to a MIMO setting. The basic assumption is that the vector relative degree of the nonlinear system is known and that the non-minimum phase zeros are accounted for to a sufficient degree of accuracy in the nominal design. Simulation results with an inverted pendulum that is connected to an additional cart illustrate the approach.

In Chapter 6, we develop a decentralized control method for large-scale interconnected systems, in which each subsystem is regulated by the centralized control method in Chapter 4. It is assumed that all the controllers share information about the system reference models. Based on this information, a linearly parameterized NN for each subsystem is introduced to partially cancel the effect of the interconnections on local tracking performance. Simulations are performed with a system consisting of three inverted pendulums connected by springs and dampers.

In Chapter 7, we show how an adaptive observer can be used to enhance the performance of the observer and controller simultaneously when the existing system employs a linear observer. This problem also falls under the architecture of Chapter 4. In this process, we show how an unmatched uncertainty is treated by an adaptive signal. The approach is illustrated with an inverted pendulum with initial conditions in which a controller based a linear model is destabilizing.

In Chapter 8, the control methodology in Chapter 4 is applied to control of a large, flexible-base manipulator. The testbed consists of a micromanipulator serially attached to the tip of a flexible cantilevered beam. Section 8.4 describes how the method is modified so as to augment a two-time scale controller. Experimental results in Section 8.5 show that

the adaptive control achieves vibration suppression for the base in the transient period and high-accuracy positioning for the micromanipulator in steady state.

Finally, we conclude the thesis and recommend some future research direction in Chapter 9. Throughout the manuscript, $\|\cdot\|$ denotes Euclidean norm, and $\|\cdot\|_F$ denotes Frobenius norm unless otherwise mentioned. That is, $\|A\|_F = \sqrt{\mathrm{tr}(AA^T)}$.

CHAPTER 2

OUTPUT FEEDBACK AUGMENTATION IN INTERNAL MODEL-FOLLOWING CONTROL

This chapter describes the internal model-following control implemented with a NN-based adaptive element. The control framework involves a mechanism which forces the system to follow the plant model, the model used in the design of an existing control system. Performance of the controlled system is guaranteed by the existing controller when the system behaves like the plant model. The basic approach involves formulating an architecture for which the associated error equations have a form suitable for applying existing results for adaptive output feedback control. The approach is applicable to non-affine, nonlinear systems with both parametric uncertainties and unmodelled dynamics. The approach is particularly well suited for control of flexible structural systems. Its effectiveness is illustrated through simulation results with a mass-spring-damper system, and it is further tested on a laboratory experiment consisting of a three disk torsional pendulum system.

2.1 Introduction

This chapter describes the internal model-following control implemented with a NN-based adaptive element. Previous adaptive output feedback control approaches have been applied within a control architecture that uses an inverting type of controller for the non-adaptive portion of the control system [62, 63]. Considering that the vast majority of controllers are locally linear controllers, it would be highly desirable to retrofit such systems with an adaptive element, rather than to replace them with an inverting controller. This is particularly so in applications calling for control of flexible systems.

Several attempts to develop a method for adding an adaptive element to an existing controller architecture have recently appeared in the literature [49, 51, 58–61, 87]. Some of the methods [58–61] are restricted to state feedback, and impose restrictive conditions with

respect to properties of the regulated variable, and the manner in which the uncertainty affects the plant. For example, they might require that the regulated output has full relative degree (meaning that the number of times the regulated variable must be differentiated before the control appears equals the number of state variables needed to describe the plant dynamics), or that the plant uncertainty is matched (meaning that the uncertainty enters the plant dynamics in the same manner as the control). Since the methods [51, 58–61] are based on matching the state response of an idealized model with that of the true plant, they cannot be applied to a system of higher order than the model used in the design process. Consequently, they are not robust to the unmodelled dynamics. The methods in [49, 87] use an adaptive technique called *input error method* [2, p.102] for reconfigurable flight control. It requires, however, that the open loop system is stable. State feedback is also very restrictive, and flexible systems with large degrees of freedom provide a good example in which a state feedback approach is not practical.

The controller architecture in this chapter relies on recent developments in the area of nonlinear adaptive output feedback control [62, 63]. It can be applied to a linear controller architecture without any of the restrictions mentioned above. The main restrictions are that the system to be controlled is minimum phase, and that the relative degree of the regulated output variable is known at least over the band of frequencies that the plant is regulated. Knowledge of relative degree is a fundamental requirement for any robust control system design. In a linear setting, this assumption amounts to saying that the roll-off at the crossover frequency is known. If applied absolutely, then it means that the high frequency roll-off is known.

The approach can also be applied to control of distributed parameter systems, provided that their dynamics can be approximated to sufficient accuracy by a finite dimensional model. In this setting, the order of the model need not be known. It is assumed that a known lower order approximate model, having the same relative degree as that of the accurate model, is employed in the design of the linear controller [88].

This chapter is organized as follows: First we describe the control system architecture in Section 2.2. Section 2.3 develops the error equation needed to apply an existing approach to

adaptive output feedback augmentation. Section 2.4 summarizes the approach used for the adaptive portion of the design and presents a new result concerning adaptive disturbance cancellation. Section 2.5 presents results related to observability of the system subject to the external disturbance that is required for adaptive disturbance cancellation. Section 2.6 illustrates the approach using a multiple spring-mass model for a flexible system. Section 2.7 considers a three-disk torsional pendulum laboratory experiment and describes the controller design and the experimental results. Conclusions are given in Section 2.8. For simplicity we have limited the development to single-input single-output(SISO) systems, but extensions to multi-input multi-output (MIMO) systems can be carried out following the steps in [83, 89].

2.2 Control Architecture

Figure 2.1 depicts the conceptual layout for augmenting a linear controller. The nominal feedback control system consists of the true plant under regulation of a linear controller. It is assumed that the linear controller is designed based on a linear plant model, so that $y_m(t)$ tracks $y_c(t)$. The linear controller produces the output $u_{lc}(t)$ that is normally used to regulate the plant. The shaded portion of the diagram highlights the elements to be added to the nominal system. The adaptive process augments the linear controller by adding a signal $u_{ad}(t)$ to the linear controller output to form the new plant input $u(t)$. The adaptive controller shown is essentially the method of adaptive control design described in [62]. It could just as well be replaced by the method of adaptive control design described in [63], or any other method of adaptive control design that requires only the output variables to be available for feedback. It is assumed that the plant model is the model used to design the existing controller and that the relative degree of the plant model matches that of the true plant over the bandwidth of interest. Normally, this model is not used to actually control the plant. Here it is used to generate the error signal, $e_1 = y_m - y$, which is needed by the adaptive controller. What is important is the form of the equations that describe the dynamics of this error signal, e_1, and that it has the correct form for which the theory of adaptive control design is applicable. This will be shown in the next section.

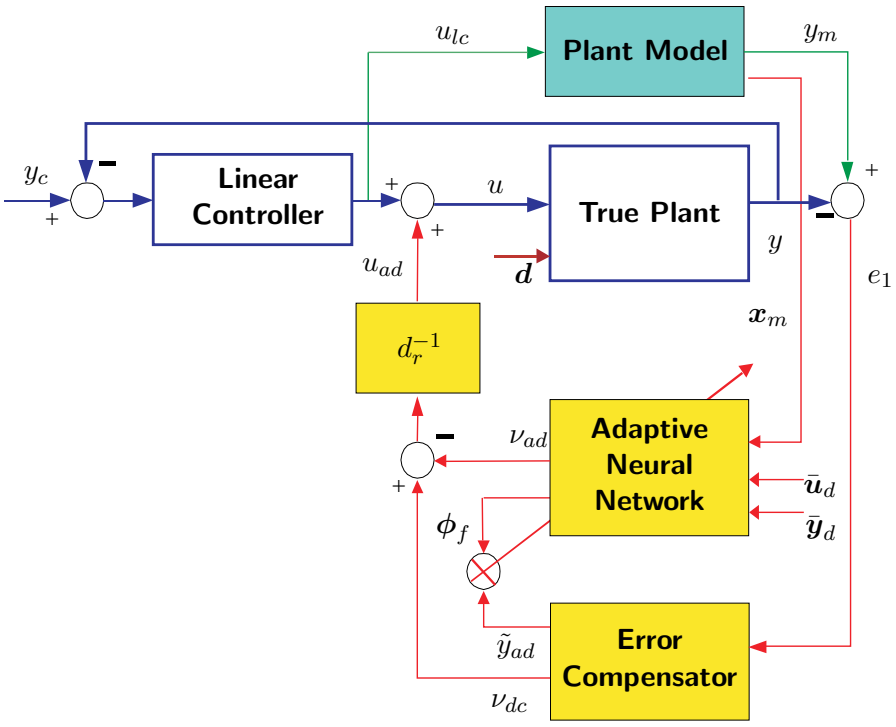

Fig. 2.1: Adaptive Control Augmentation Diagram in the Internal Model-Following Architecture.

2.3 Output Tracking Error Equation

Let the true plant dynamics Σ_p over the bandwidth of interest be described by

$$\dot{\boldsymbol{x}}_p = \boldsymbol{f}_p(\boldsymbol{x}_p, u, \boldsymbol{d}), \quad y = h_p(\boldsymbol{x}_p, \boldsymbol{d}), \tag{2.1}$$

where $\boldsymbol{x}_p \in \mathcal{D}_p \subset \mathbb{R}^{n_p}$ is the state of the system, $u(t) \in \mathcal{D}_u \subset \mathbb{R}$ is the control variable, $y(t) \in \mathbb{R}$ is the regulated output and $\boldsymbol{d}(t) \in \mathbb{R}^{n_s}$ is the external disturbance. There may be additional outputs that are not regulated but that are available for feedback. These may be included with a slight modification of the overall design approach, so for simplicity in presentation they are not explicitly treated in the development. We regard the functions $\boldsymbol{f}_p : \mathcal{D}_p \times \mathbb{R} \times \mathbb{R}^{n_s} \to \mathbb{R}^{n_p}$ and $h_p : \mathcal{D}_p \times \mathbb{R}^{n_s} \to \mathbb{R}$ as uncertain but sufficiently smooth. That is, all needed derivatives exist and are continuous. We assume that $\boldsymbol{f}_p(0,0,0) = 0$, and $h_p(0,0) = 0$. If there are unmodelled dynamics, the system dimension n_p is unknown.

Assumption 2.1. *The system (2.1) has known relative degree [90] equal to r on the domain*

$\mathcal{D}_p$.

The *bounded* disturbance vector $\boldsymbol{d}(t)$ evolves according to its own dynamics defined by

$$\dot{\boldsymbol{x}}_d = \boldsymbol{f}_d(\boldsymbol{x}_d), \quad \boldsymbol{d} = \boldsymbol{h}_d(\boldsymbol{x}_d), \tag{2.2}$$

where $\boldsymbol{x}_d(t) \in \mathcal{D}_d \subseteq \mathbb{R}^{n_d}$, and n_d is the unknown dimension of exogenous disturbance dynamics. The functions $\boldsymbol{f}_d : \mathcal{D}_d \to \mathbb{R}^{n_d}$ and $\boldsymbol{h}_d : \mathcal{D}_d \to \mathbb{R}^{n_s}$ are sufficiently smooth, but also uncertain, due to the fact that even though disturbances have finite bandwidth, they are usually unknown functions of time. The augmented system consisting of the plant and disturbance dynamics can now be expressed as

$$\begin{aligned} \dot{\boldsymbol{x}} &= \begin{bmatrix} \dot{\boldsymbol{x}}_p \\ \dot{\boldsymbol{x}}_d \end{bmatrix} = \begin{bmatrix} \boldsymbol{f}_p(\boldsymbol{x}_p, u, \boldsymbol{h}_d(\boldsymbol{x}_d)) \\ \boldsymbol{f}_d(\boldsymbol{x}_d) \end{bmatrix} = \boldsymbol{f}(\boldsymbol{x}, u), \\ y &= h_p(\boldsymbol{x}_p, \boldsymbol{h}_d(\boldsymbol{x}_d)) = h(\boldsymbol{x}). \end{aligned} \tag{2.3}$$

Assumption 2.1 implies

$$\begin{aligned} y^{(i)} =& h_i(\boldsymbol{x}), \ 0 \le i \le r-1 \\ y^{(r)} =& h_r(\boldsymbol{x}, u) \ i.e., \frac{\partial h_i}{\partial u} = 0, \quad \forall i \quad 0 \le i \le r-1 \\ & \text{and} \quad \frac{\partial h_r}{\partial u} \neq 0, \quad \forall (\boldsymbol{x}, u) \in \mathcal{D}_x (\triangleq \mathcal{D}_p \times \mathcal{D}_d) \times \mathcal{D}_u. \end{aligned} \tag{2.4}$$

That is, the system in (2.3) can, by a diffeomorphism on $\mathcal{D}_x \times \mathcal{D}_u$, be transformed into the following normal form [90]:

$$\begin{aligned} \dot{\boldsymbol{\xi}} =& A_\xi \boldsymbol{\xi} + \boldsymbol{b}_\xi h_r(\boldsymbol{z}_o, \boldsymbol{\xi}, \boldsymbol{x}_d, u) \\ \dot{\boldsymbol{z}}_o =& \boldsymbol{f}_o(\boldsymbol{z}_o, \boldsymbol{\xi}, \boldsymbol{x}_d) \\ \dot{\boldsymbol{x}}_d =& \boldsymbol{f}_d(\boldsymbol{x}_d), \\ y =& \xi_1 = \boldsymbol{c}_\xi^T \boldsymbol{\xi}, \end{aligned} \tag{2.5}$$

where $\boldsymbol{\xi}^T \triangleq \begin{bmatrix} y, & \cdots, & y^{(r-1)} \end{bmatrix}$ so that $\boldsymbol{\xi} \in \mathcal{D}_\xi \subseteq \mathbb{R}^r$, and $\boldsymbol{z}_o \in \mathcal{D}_{z_o} \in \mathbb{R}^{n-r}$. The set

$\mathcal{D}_\xi \times \mathcal{D}_{z_o}$ is diffeomorphic to $\mathcal{D}_p$. The system matrices are given by

$$A_\xi = \begin{bmatrix} 0 & 1 & 0 & \cdots & 0 \\ 0 & 0 & 1 & \cdots & 0 \\ \vdots & & \ddots & & \vdots \\ \vdots & & & 0 & 1 \\ 0 & \cdots & \cdots & 0 & 0 \end{bmatrix}_{r\times r}, \; \boldsymbol{b}_\xi = \begin{bmatrix} 0 \\ 0 \\ \vdots \\ 0 \\ 1 \end{bmatrix}_r, \; \boldsymbol{c}_\xi = \begin{bmatrix} 1 \\ 0 \\ \vdots \\ 0 \\ 0 \end{bmatrix} \tag{2.6}$$

Assumption 2.2. *The system $\dot{\boldsymbol{z}}_o = \boldsymbol{f}_o(\boldsymbol{z}_o, \boldsymbol{\xi}, \boldsymbol{x}_d)$ is input-to-state stable [91, p.217], with $\boldsymbol{\xi}$ and $\boldsymbol{x}_d$ viewed as its input.*

Assumption 2.3. *The system (2.3) is locally observable for all $\boldsymbol{x} \in \mathcal{D}_x$.*

Let the plant model $P_n(s)$ be described by

$$\begin{aligned} \dot{\boldsymbol{x}}_m &= A_m \boldsymbol{x}_m + \boldsymbol{b}_m u_{lc} \\ y_m &= \boldsymbol{c}_m^T \boldsymbol{x}_m \\ y_m^{(r)} &\triangleq \hat{h}_r(\boldsymbol{x}_m, u_{lc}) = \boldsymbol{c}_r^T \boldsymbol{x}_m + d_r u_{lc}, \end{aligned} \tag{2.7}$$

where $\boldsymbol{x}_m \in \mathcal{D}_m \subseteq \mathbb{R}^m$ $(m \leq n_p)$ and

$$\boldsymbol{c}_r^T = \boldsymbol{c}_m^T A_m^r, \; d_r = \boldsymbol{c}_m^T A_m^{r-1} \boldsymbol{b}_m. \tag{2.8}$$

The linear control signal u_{lc} is the output of the following compensator $C(s)$

$$\begin{aligned} \dot{\boldsymbol{x}}_c &= A_c \boldsymbol{x}_c + \boldsymbol{b}_c (y_c - y) \\ u_{lc} &= \boldsymbol{c}_c^T \boldsymbol{x}_c + d_c (y_c - y), \end{aligned} \tag{2.9}$$

where $\boldsymbol{x}_c \in \mathcal{D}_c \subset \mathbb{R}^{n_c}$. The plant model in (2.7) regulated by the linear controller in (2.9), with the replacement of y by y_m, results in the following nominal closed loop system

$$\begin{aligned} \dot{\bar{\boldsymbol{x}}}_{\text{nom}} &= \bar{A} \bar{\boldsymbol{x}}_{\text{nom}} + \bar{\boldsymbol{b}}_c y_c(t) \\ y_{\text{nom}} &= \bar{\boldsymbol{c}}^T \bar{\boldsymbol{x}}_{\text{nom}}, \end{aligned} \tag{2.10}$$

where $\boldsymbol{x}_{\text{nom}} \in \mathcal{D}_{\text{nom}} \subset \mathbb{R}^{m+n_c}$ and,

$$\bar{A} = \begin{bmatrix} A_m - \boldsymbol{b}_m d_c \boldsymbol{c}_m^T & \boldsymbol{b}_m \boldsymbol{c}_c^T \\ -\boldsymbol{b}_c \boldsymbol{c}_m^T & A_c \end{bmatrix}, \; \bar{\boldsymbol{b}}_c = \begin{bmatrix} \boldsymbol{b}_m d_c \\ \boldsymbol{b}_c \end{bmatrix}, \; \bar{\boldsymbol{c}} = \begin{bmatrix} \boldsymbol{c}_m \\ 0 \end{bmatrix}, \tag{2.11}$$

where $y_c(t)$ is a bounded reference command. It is reasonable to assume that the controller in (2.9) is designed so that performance specifications are satisfied by the nominal system in (2.10). Therefore, $\bar{A}$ in (2.11) is Hurwitz. This, in turn, guarantees that the trajectories given by (2.10) are bounded and restricted to $\mathcal{D}_{\text{nom}}$ for all $t \geq 0$ for bounded $y_c(t)$.

Using Eqs.(2.4)-(2.8), the following error dynamics can be derived

$$\begin{aligned} e_1^{(r)} &= -d_r(u - u_{lc}) - \Delta(\boldsymbol{x}, \boldsymbol{x}_m, u) \\ &= -d_r u_{ad} - \Delta(\boldsymbol{x}, \boldsymbol{x}_m, u), \end{aligned} \tag{2.12}$$

where $e_1 = y_m - y$, and

$$\Delta(\boldsymbol{x}, \boldsymbol{x}_m, u) = h_r(\boldsymbol{x}, u) - \boldsymbol{c}_r^T \boldsymbol{x}_m - d_r u. \tag{2.13}$$

It can be seen from Eq.(2.12) that the goal of u_{ad} is to stabilize the error dynamics and cancel $\Delta(\boldsymbol{x}, \boldsymbol{x}_m, u)$. Thus, u_{ad} in Eq.(2.12) is expressed as

$$u_{ad} = d_r^{-1}(\nu_{dc} - \nu_{ad}), \tag{2.14}$$

where ν_{dc} is the output of a linear controller, with e_1 as its input, that is designed to stabilize the error dynamics in Eq.(2.12) when $\Delta(\boldsymbol{x}, \boldsymbol{x}_m, u) = 0$, and ν_{ad} is the output of a NN, whose weights are adapted in a way to guarantee a bounded error response. Substituting Eq.(2.14) into Eq.(2.12) results in the final form of the error equation

$$e_1^{(r)} = -\nu_{dc} + \nu_{ad} - \Delta. \tag{2.15}$$

Remark 2.1. In a linear system, Assumption 2.2 implies that the zeros of the system in (2.1) lie in the left half complex plane. With the regulated output as e_1, in a completely linear setting, it can be shown that the closed loop eigenvalues of the plant model when regulated by the linear controller, together with zeros for the system in (2.3) constitute the eigenvalues of the zero dynamics for the closed loop system depicted in Figure 2.1.

From Eqs.(2.12) and (2.13), it follows that Δ depends on ν_{ad} through u, whereas ν_{ad} is designed to cancel Δ.

Assumption 2.4. *There exists a fixed point to the equation* $\nu_{ad} = \Delta(\boldsymbol{x}, \boldsymbol{x}_m, \nu_{ad})$ *uniformly in* $\boldsymbol{x} \in \mathcal{D}_x, \boldsymbol{x}_m \in \mathcal{D}_m$ *on* $\mathcal{D}_u$.

According to the Brouwer fixed point theorem, any continuous mapping with its range contained in the bounded domain must have at least one fixed point [92, p. 163]. A typical assumption when a control signal is involved in an uncertainty, for example, sliding mode control [91, p. 603], is

$$|\Delta(\boldsymbol{x}, \boldsymbol{x}_m, u)| \leq \rho(\boldsymbol{x}, \boldsymbol{x}_m) + k_u|u|, \tag{2.16}$$

where a continuous function $\rho(\boldsymbol{x}, \boldsymbol{x}_m) \geq 0$ and $k_u \in [0,\ 1)$ are assumed to be known. Whenever (2.16) is satisfied, Assumption 2.4 holds. Furthermore, we do not assume that the bounds in (2.16) are known. Existence and uniqueness of a fixed point is guaranteed when the mapping $\nu_{ad} \rightarrow \Delta$ is a contraction. It can be shown that the map $\nu_{ad} \rightarrow \Delta$ is a contraction if and only if the following two conditions are satisfied [62]

$$\begin{aligned} &\text{sign}(d_r) = \text{sign}(\frac{\partial h_r}{\partial u}) \\ &\left|\frac{\partial h_r}{\partial u}\right| /2 < |d_r| < \infty. \end{aligned} \tag{2.17}$$

These conditions mean that control reversal is not permitted and there is a lower bound on the estimate of the control effectiveness d_r of the plant model. A different development that uses the mean value theorem to eliminate the fixed point assumption can be found in [40, 89].

2.4 Adaptive Output Feedback Augmentation

The approach in [62] allows for designing the signals ν_{dc} and ν_{ad} in Eq.(2.15) using only available measurements. The error compensator has two outputs

$$\begin{bmatrix} \nu_{dc}(s) \\ \tilde{y}_{ad}(s) \end{bmatrix} = \frac{1}{D_{dc}(s)} \begin{bmatrix} N_{dc}(s) \\ N_{ad}(s) \end{bmatrix} e_1(s), \tag{2.18}$$

where the first output ν_{dc} is designed to stabilize the error dynamics in Eq.(2.15) and the second output $\tilde{y}_{ad}$ is a training signal for a NN which is a linear combination of the error compensator states and its input, the tracking error e_1. With the error compensator in Eq.(2.18), the error equation given in Eq.(2.15) results in the following transfer function

from $\nu_{ad} - \Delta$ to $\tilde{y}_{ad}$:

$$\begin{aligned}\tilde{y}_{ad}(s) =& \frac{N_{ad}(s)}{s^r D_{dc}(s) + N_{dc}(s)}(\nu_{ad} - \Delta) \\ \equiv& G(s)(\nu_{ad} - \Delta).\end{aligned} \tag{2.19}$$

A linearly parameterized NN is used to approximate Δ in Eq.(2.13). It is a *universal approximator* if a set of basis functions can be selected over a compact domain of approximation. For example, it has been shown that an arbitrary continuous function can be approximated to any desired accuracy on a compact domain using radial basis functions [93]. The result has been extended to map the uncertainty of an *observable* plant, generally a function of states and control, from available input/output history [64, 65]. That is, given $\epsilon > 0$, there exist a $n_0 \in \mathbb{N}$ and a $d^* > 0$ such that for every $n_h \geq n_0$ and $0 < d \leq d^*$, Δ can be approximated by a linearly parameterized NN over a compact domain with bounded weights $\boldsymbol{W}$ and a suitable set of basis functions $\boldsymbol{\phi}(\cdot)$ that provide a universal approximation. Thus,

$$\Delta = \boldsymbol{W}^T \boldsymbol{\phi}(\boldsymbol{\eta}) + \varepsilon(\boldsymbol{\eta}), \;\; \|\varepsilon(\boldsymbol{\eta}, d)\| < \epsilon, \quad (\boldsymbol{x}, \boldsymbol{x}_m, u) \in \mathcal{D}_x \times \mathcal{D}_m \times \mathcal{D}_u, \tag{2.20}$$

where $\varepsilon(\boldsymbol{\eta})$ is the NN reconstruction error, n_h is the number of neurons, and $\boldsymbol{\eta}$ is the network input vector

$$\begin{aligned}\boldsymbol{\eta}(t) &= \begin{bmatrix} 1 & \boldsymbol{x}_m(t)^T & \bar{u}_d^T(t) & \bar{y}_d^T(t) \end{bmatrix}^T, \quad \|\boldsymbol{\eta}\| \leq \eta^* \\ \bar{u}_d^T(t) &= [u(t) \quad u(t-d) \quad \cdots u(t-(n_1-r-1)d)]^T, \\ \bar{y}_d^T(t) &= [y(t) \quad y(t-d) \cdots y(t-(n_1-1)d)]^T,\end{aligned} \tag{2.21}$$

where $n_1 \geq n$ is the length of a sliding window of measurements, r is the relative degree, and $d > 0$ is a time delay. The output of the adaptive element in Figure 2.1 is designed as

$$\nu_{ad} = \widehat{\boldsymbol{W}}^T \boldsymbol{\phi}(\boldsymbol{\eta}), \tag{2.22}$$

where $\widehat{\boldsymbol{W}}$ are estimates of the weights $\boldsymbol{W}$ in Eq.(2.20) that are adjustable on-line.

In order to obtain an adaptation rule dependent only upon available signals, $G(s)$ is required to be strictly positive real (SPR) [62]. $G(s)$ can be made SPR by properly choosing

$N_{ad}(s)$ in case $r = 1$. If $r > 1$, a stable low pass filter $T^{-1}(s)$ is introduced so that $G(s)T(s)$ is SPR

$$\tilde{y}_{ad}(s) = G(s)T(s)[T^{-1}(s)(\nu_{ad} - \Delta)], \tag{2.23}$$

where the polynomial $T(s)$ is Hurwitz but can otherwise be freely chosen along with $N_{ad}(s)$ of the error compensator in Eq.(2.18).

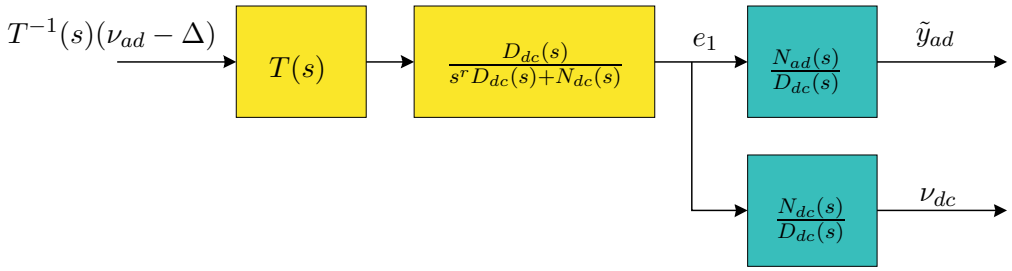

Fig. 2.2: Block Diagram for the Error Compensator and the SPR Filter.

The filtered NN reconstruction error, $\psi \triangleq T^{-1}(s)(\nu_{ad} - \Delta)$, can be written as follows [62]:

$$\psi = \widetilde{\boldsymbol{W}}^T \boldsymbol{\phi}_f + \theta - \varepsilon_f, \tag{2.24}$$

where $\boldsymbol{\phi}_f$ and ε_f are the signals $\boldsymbol{\phi}$ and ε, respectively, after being filtered through $T^{-1}(s)$, and θ is the mismatch term given by

$$\theta(s) = T^{-1}(s)(\widetilde{\boldsymbol{W}}^T \boldsymbol{\phi}) - \widetilde{\boldsymbol{W}}^T \boldsymbol{\phi}_f, \tag{2.25}$$

that can be bounded as

$$|\theta| \leq \alpha \left\| \widetilde{\boldsymbol{W}} \right\|_F, \ \alpha > 0, \tag{2.26}$$

where $\widetilde{\boldsymbol{W}} = \widehat{\boldsymbol{W}} - \boldsymbol{W}$ represents weight deviations from the optimal weights $\boldsymbol{W}$. The transfer function from ψ to e_1 is realized as follows (see Figure 2.2):

$$\begin{aligned} \dot{\boldsymbol{z}}_e &= A_e \boldsymbol{z}_e + \boldsymbol{b}_e \psi \\ e_1 &= \boldsymbol{c}_1^T \boldsymbol{z}_e. \end{aligned} \tag{2.27}$$

The transfer functions from e_1 to $\tilde{y}_{ad}$ and ν_{dc} are realized as follows:

$$\begin{aligned} \dot{\boldsymbol{z}}_{dc} &= A_{dc} \boldsymbol{z}_{dc} + \boldsymbol{b}_{dc} e_1 \\ \tilde{y}_{ad} &= \boldsymbol{c}_{ad}^T \boldsymbol{z}_{dc} + d_{ad} e_1 \\ \nu_{dc} &= \boldsymbol{c}_{dc}^T \boldsymbol{z}_{dc} + d_{dc} e_1, \end{aligned} \tag{2.28}$$

where A_{dc} is assumed Hurwitz. Combining Eq.s (2.27) and (2.28) leads to the following *non-minimal* realization for the tracking error dynamics in Figure 2.2.

$$\begin{aligned} \dot{\boldsymbol{z}} &= A_{cl}\boldsymbol{z} + \boldsymbol{b}_{cl}\psi, \quad \boldsymbol{z} \in \mathbb{R}^{n_z} \\ \tilde{y}_{ad} &= \boldsymbol{c}_{cl}^T\boldsymbol{z},\ \nu_{dc} = \boldsymbol{c}_{\nu}^T\boldsymbol{z},\ e_1 = \boldsymbol{c}_{e_1}^T\boldsymbol{z}, \end{aligned} \tag{2.29}$$

where

$$\begin{aligned} A_{cl} &= \begin{bmatrix} A_e & \mathbf{0} \\ \boldsymbol{b}_{dc}\boldsymbol{c}_1^T & A_{dc} \end{bmatrix},\ \boldsymbol{b}_{cl} = \begin{bmatrix} \boldsymbol{b}_e \\ 0 \end{bmatrix},\ \boldsymbol{c}_{cl}^T = \begin{bmatrix} d_{ad}\boldsymbol{c}_1^T & \boldsymbol{c}_{ad}^T \end{bmatrix} \\ \boldsymbol{c}_{\nu}^T &= \begin{bmatrix} d_{dc}\boldsymbol{c}_1^T & \boldsymbol{c}_{dc}^T \end{bmatrix},\ \boldsymbol{c}_{e_1}^T = \begin{bmatrix} \boldsymbol{c}_1^T & \mathbf{0} \end{bmatrix}. \end{aligned} \tag{2.30}$$

Since the transfer function from ψ to $\tilde{y}_{ad}$ is SPR, by the Meyer-Kalman-Yakubovitz Lemma [4, p.129], there exist $Q > 0$ and $P > 0$ such that

$$\begin{aligned} A_{cl}^T P + P A_{cl} + Q &= 0 \\ P\boldsymbol{b}_{cl} &= \boldsymbol{c}_{cl}. \end{aligned} \tag{2.31}$$

The SPR filter $T^{-1}(s)$ is realized by

$$\begin{aligned} \dot{\boldsymbol{z}}_f &= A_f\boldsymbol{z}_f + \boldsymbol{b}_f\boldsymbol{\phi}, \quad \boldsymbol{z}_f \in \mathbb{R}^{n_f} \\ \boldsymbol{\phi}_f &= \boldsymbol{c}_f^T\boldsymbol{z}_f. \end{aligned} \tag{2.32}$$

The SPR filter is designed to be stable, so for any $Q_f > 0$ there exist $P_f > 0$ such that

$$A_f^T P_f + P_f A_f + Q_f = 0. \tag{2.33}$$

The signals $\boldsymbol{\phi}_f$ are used in the following NN adaptation rule

$$\dot{\widehat{\boldsymbol{W}}} = -\Gamma_W[\tilde{y}_{ad}\boldsymbol{\phi}_f + \sigma\widehat{\boldsymbol{W}}], \tag{2.34}$$

where $\Gamma_W > 0$ is the adaptation gain, defining the "learning rate" and $\sigma\hat{W}$ is the $\sigma-$modification term [1, pp.85-88]. The procedure for designing the error compensator, the SPR filter $T(s)$, and the stability proof for the NN adaptation law is given in [62].

Theorem 2.1. *With assumptions 2.1-2.4, the error signals of the system comprised of the dynamics in Eq.(2.15), together with the feedback control law $u = u_{lc} + d_r^{-1}(\nu_{dc} - \nu_{ad})$ and the NN adaptation rule in Eq.(2.34), are uniformly ultimately bounded.*

Proof. The result follows from the theorems given in [62] and the fact that (2.3) is locally observable.

Theorem 2.1 guarantees boundedness of the output tracking error e_1 and NN weights $\widehat{\boldsymbol{W}}$. Since the linear controller is designed to stabilize the plant model, it immediately follows that if $y_c(t)$ and $e_1(t)$ are bounded, then $e(t) = y_c - y$ is bounded. It is also apparent that when $e_1 = 0$ we recover the tracking performance associated with the existing controller design, with the plant model substituted for the true plant. In particular, for this idealized setting, the disturbances $\boldsymbol{d}(t)$ will be cancelled.

2.5 Observability of the Augmented System

Theorem 2.2. *If the linear system*

$$\dot{\boldsymbol{x}} = A\boldsymbol{x},\ y = C\boldsymbol{x}$$

is observable, where $A = \frac{\partial \boldsymbol{f}}{\partial \boldsymbol{x}}\,|_{\boldsymbol{x}=\boldsymbol{x}_0}$ *and* $C = \frac{\partial h}{\partial \boldsymbol{x}}\,|_{\boldsymbol{x}=\boldsymbol{x}_o}$*, then the nonlinear system in (2.3) is locally observable at the point* $\boldsymbol{x}_0$*.*

Proof. See [94, pp.272-280,Theorem 2.6].

Define

$$\begin{aligned} A &= \left[\begin{array}{cc} \frac{\partial \boldsymbol{f}_p}{\partial \boldsymbol{x}_p} & \frac{\partial \boldsymbol{f}_p}{\partial \boldsymbol{d}}\frac{\partial \boldsymbol{h}_d}{\boldsymbol{x}_d} \\ 0 & \frac{\partial \boldsymbol{f}_d}{\partial \boldsymbol{x}_d} \end{array}\right]_{\boldsymbol{x}=\boldsymbol{x}_0} = \left[\begin{array}{cc} A_p & B_pC_d \\ 0 & A_d \end{array}\right] \\ C &= \left[\frac{\partial h_p}{\partial \boldsymbol{x}_p} \quad \frac{\partial h_p}{\partial \boldsymbol{d}}\frac{\partial \boldsymbol{h}_d}{\partial \boldsymbol{x}_d}\right]_{\boldsymbol{x}=\boldsymbol{x}_0} = \left[\begin{array}{cc} C_p & D_pC_d \end{array}\right]. \end{aligned} \tag{2.35}$$

The following theorem establishes a sufficient condition for the local observability of the augmented nonlinear system in (2.3).

Theorem 2.3. *Consider the system of matrices defined in (2.35) together with the following assumptions:*

1. (A_p, C_p) *observable.*

2. (A_d, C_d) *observable.*

3. $\begin{bmatrix} B_p \\ D_p \end{bmatrix}$ *has full column rank .*

Then the augmented nonlinear system in (2.3) is locally observable at $\boldsymbol{x} = \boldsymbol{x}_0$ *if* A_p *and* A_d *have no common eigenvalues.*

Proof. See Appendix A.

Condition 2 means that the realization of the disturbance model is locally minimal, and condition 3 means that the realization of the influence that the disturbance has on the plant is locally minimal. Therefore these two conditions are not restrictive. The following corollary shows that, subject to the assumptions in Theorem 2.3, nonlinear systems are almost always observable.

Corollary 2.1. *Under the assumptions stated in Theorem 2.3, the augmented system in (2.35) is not observable if and only if* A_p *and* A_d *share a common eigenvalue* $\lambda \in C$*, and* $\bar{\boldsymbol{C}}\boldsymbol{q}_2$ *lies in the column space of* $\begin{bmatrix} C_p^T & \lambda I_{n_p} - A_p^T \end{bmatrix}^T$*, where* $\bar{C} = \begin{bmatrix} D_p \\ -B_p \end{bmatrix} C_d$ *and* $\boldsymbol{q}_2$ *is the eigenvector of* A_d *associated with* λ*.*

Proof. See Appendix A.

Theorem 2.3 taken together with Corollary 2.1 suggests that the adaptive element should be able to cancel the effect of $\boldsymbol{d}(t)$ on $y(t)$, modulo the effect due to a component of $\boldsymbol{d}(t)$ satisfying a very narrow set of conditions. The *generic* property of observability further justifies that the observability assumption is not restrictive [94, pp.272-280].

2.6 Simulation Results with a Mass Spring Damper System

A simple two degree of freedom spring-mass-damper system shown in Figure 2.3 is used to illustrate the approach. The plant model used to design the existing controller is shown on the left, and the true plant appears on the right. There is both unmatched parametric error and unmatched unmodeled dynamics associated with the design of the existing controller. A comparison of the Bode plots associated these models is given in Figure 2.4. Note that the unmodeled modes of the true plant are quite close to the modelled modes. This represents a

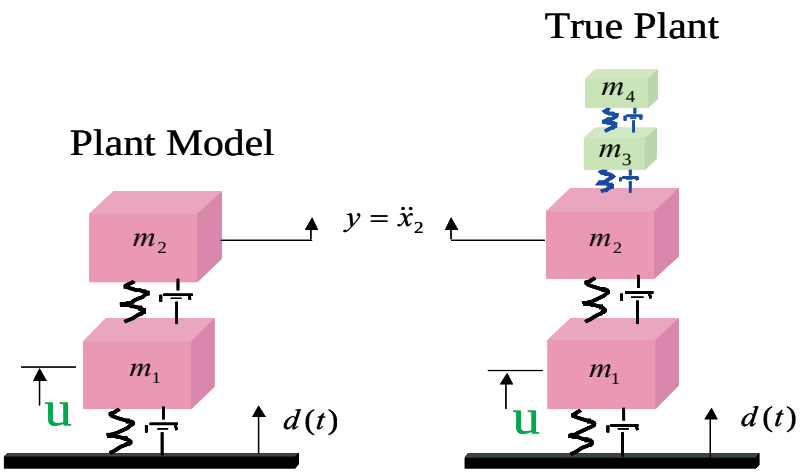

Fig. 2.3: Mass Spring Damper System:Plant Model and True Plant Dynamics

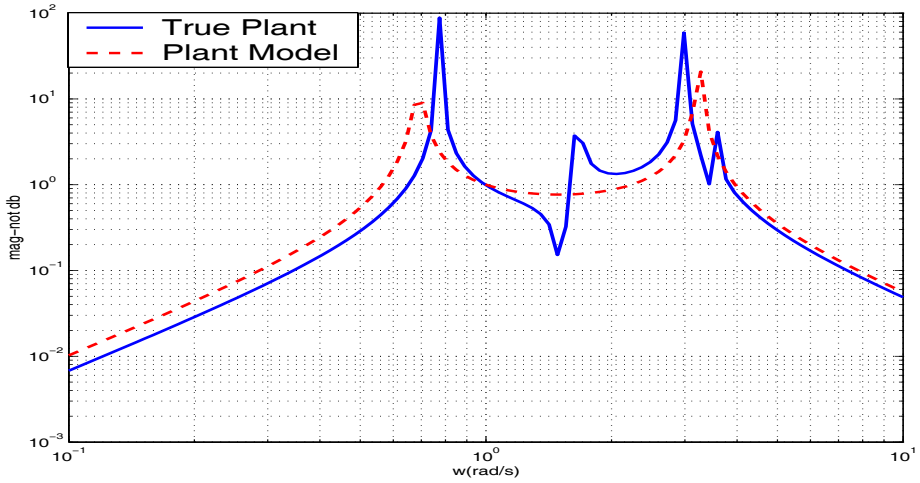

Fig. 2.4: Mass Spring Damper System:Bode Plots for the Plant Model and True Plant

difficult design challenge because all of the modes are closely spaced. The disturbance $d(t)$ is a base displacement, consisting of a sum of sinusoids with frequencies close to the natural modes of the true plant. The output to be regulated is the acceleration of the second mass. The existing controller is an LQG design that minimizes

$$J = E\{y^2\} + kE\{u_{lc}^2\}$$

with $d(t)$ modelled as a white noise process and $k = 0.01$. The parameter values are: $\hat{m}_1 = \hat{m}_2 = 1, \hat{k}_1 = 1, \hat{k}_2 = 5, \hat{c}_1 = 0.05, \hat{c}_2 = 0.01$ for the plant model, and $m_1 = 1, m_2 = 0.8, k_1 = 1.5, k_2 = 3.5, c_1 = 0.005, c_2 = 0.01, m_3 = 0.2, m_4 = 0.1, k_3 = 0.8, k_4 = 0.7, c_3 = 1 \times 10^{-9}$ and $c_4 = 1 \times 10^{-10}$ for the true plant.

The relative degree of the regulated output equals 1 for both the plant model and the true plant dynamics when regarded over an infinite frequency band. However, for frequencies within the design bandwidth, it is better approximated as equal to 2. That is, the transfer functions contain a zero that is far beyond the loop crossover frequency. This can also be seen by noting that $\boldsymbol{c}_p^T A_p \boldsymbol{b}_p = c_2/m_1 m_2 = 0.0125$ for the true plant and $\boldsymbol{c}_m^T A_m \boldsymbol{b}_m = 0.01$ for the plant model. Physically this means that the acceleration of the second mass is influenced primarily by the force exerted through the spring that couples it to the first mass (rather than through the damper). Consequently the adaptive portion of the design was performed using $r = 2$.

The output responses of the open loop plant, the plant controlled by the existing controller, and the plant controlled using the architecture in Figure 2.1 are compared in Figure 2.5. Note that the existing controller does provide a level of response reduction in com-

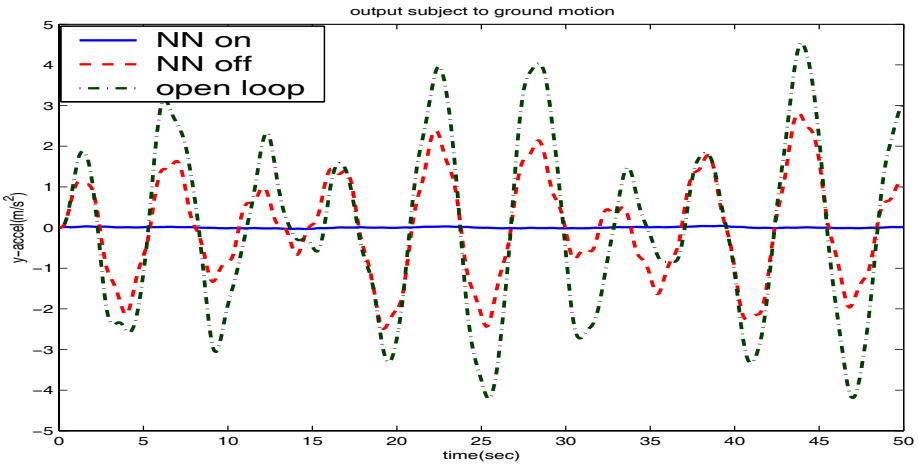

Fig. 2.5: Mass Spring Damper System:Output Comparison Plot.

parison to the open loop response. However, this response, if allowed to continue, becomes unstable. That is, the existing controller, when applied to the plant model, provides a stable response by design, but when applied to the true plant it is destabilizing due to the presence of parametric uncertainty and unmodelled dynamics in the plant model. When the adaptive element is added to the existing controller, the response is not only stabilized, it is nearly reduced to zero. That is, the disturbance is not only attenuated, it is nearly cancelled by the adaptive element, due to the fact that adaptive element is able to control not only the

unmodelled dynamics of the true plant, but also the dynamics of the disturbance. Similar results were obtained when unmatched force disturbances were applied to the other masses. Figure 2.6 shows that the adaptive signal comes very close to perfectly cancelling Δ when a force disturbance is applied to the third mass. Although not shown, the same result was

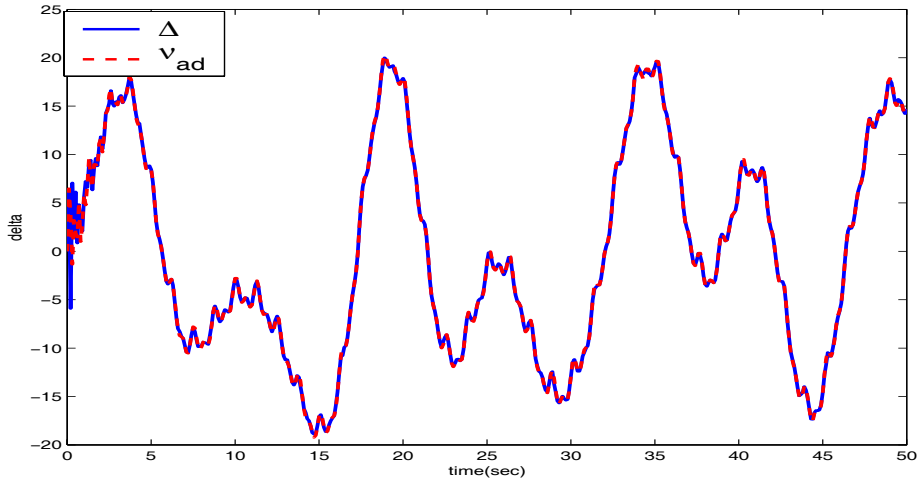

Fig. 2.6: Mass Spring Damper System:Uncertainty Δ and ν_{ad}

obtained regardless of where the disturbance was introduced into the system dynamics.

2.7 Experimental Results with a Three-Disk Torsional System

Figure 2.7 depicts a torsional pendulum system which is made up of three disks connected by a vertical flexible shaft [95]. The actuation device, a brushless DC servo motor, applies torque to the bottom disk. A disturbance can also be applied to the top disk. The equations of motion for the system are as follows:

$$\begin{aligned} J_1\ddot{\theta}_1 + B\dot{\theta}_1 + K(\theta_1 - \theta_2) + f_{c_1}(\dot{\theta}_1, \theta_1, \theta_2) &= K_d V_d, \\ J_2\ddot{\theta}_2 + B\dot{\theta}_2 - K\theta_1 + 2K\theta_2 - K\theta_3 + f_{c_2}(\dot{\theta}_2, \theta_1, \theta_2, \theta_3) &= 0, \\ J_3\ddot{\theta}_3 + B\dot{\theta}_3 - K(\theta_2 - \theta_3) + f_{c_3}(\dot{\theta}_3, \theta_2, \theta_3) &= K_{vt} u, \end{aligned} \tag{2.36}$$

where $J_i = 0.103\text{kg}\cdot\text{m}^2$ $(i = 1, 2, 3)$ are the moments of inertia, $B = 0.0018\text{kg}\cdot\text{m/s}$ is the viscous damping coefficient, $K = 2.2625\text{kg}\cdot\text{m}^2/\text{s}^2$ is the spring constant, $K_d = 0.05\frac{\text{N}\cdot\text{m}}{\text{V}}$ is the gain from disturbance voltage to torque, $K_{vt} = 0.42\frac{\text{N}\cdot\text{m}}{\text{V}}$ is the gain from control voltage to torque, and f_{c_i} represents nonlinearities, such as coulomb friction. The control input

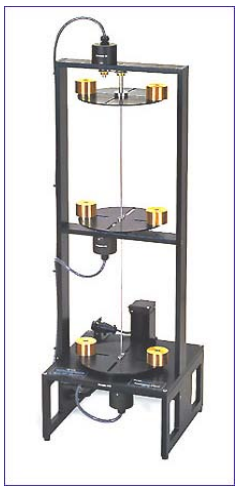

Fig. 2.7: The Three-disk Torsional Pendulum System (shown without the disturbance drive on the top disk).

u is the voltage applied to the control motor, and the disturbance input V_d is the voltage applied to the disturbance drive attached to the rim of the top disk.

2.7.1 Bottom Disk Control-a Collocated Control Problem

When the regulated output variable is the angular displacement of the bottom disk θ_3, the output is *collocated* with the control u. The output has relative degree 2 if the dynamics of the DC motor are treated as lying outside the bandwidth of the design. With $f_{c_i} = 0$, the transfer function from applied voltage to the regulated output is given by the 6th order model

$$\frac{y}{u} = \frac{K_a(s^2 + 2\zeta_{z_1}\omega_{z_1}s + \omega_{z_1}^2)(s^2 + 2\zeta_{z_2}\omega_{z_2}s + \omega_{z_2}^2)}{s(s+c)(s^2 + 2\zeta_{p_1}\omega_{p_1}s + \omega_{p_1}^2)(s^2 + 2\zeta_{p_2}\omega_{p_2}s + \omega_{p_2}^2)}. \tag{2.37}$$

The parameters were determined experimentally to be: $K_a = 40.46$, $\zeta_{z_1} = 0.009$, $\omega_{z_1} = 9.87$, $\zeta_{z_2} = 0.0035$, $\omega_{z_2} = 25.8$, $c = 0.1786$, $\zeta_{p_1} = 0.00559$, $\omega_{p_1} = 16$(rad/sec) and $\zeta_{p_2} = 0.00323$, $\omega_{p_2} = 27.7$(rad/sec). The zero dynamics for the system in (2.36), with $f_{c_i} = 0$, are given by:

$$\begin{aligned} J_1\ddot{\theta}_1 + B\dot{\theta}_1 + K(\theta_1 - \theta_2) &= K_d V_d \\ J_2\ddot{\theta}_2 + B\dot{\theta}_2 - K\theta_1 + 2K\theta_2 &= 0 \\ \dot{\boldsymbol{x}}_d = f_d(\boldsymbol{x}_d),\ V_d &= h_d(\boldsymbol{x}_d) \end{aligned} \tag{2.38}$$

where $\boldsymbol{x}_d$ represents the states of the *bounded* disturbance dynamics. The eigenvalues associated with the zero dynamics are $-0.089 \pm 15.97i$ and $-0.893 \pm 27.66i$. Therefore the system is globally exponentially minimum phase. Thus Assumptions 2.1-2.2 are easily verified.

To simulate the presence of unmodelled dynamics, the following low frequency model for the plant dynamics that does not include the flexible modes is assumed

$$\frac{y_m}{u} = \frac{K_n}{s(s+c)}, \tag{2.39}$$

where $K_n = 13.49$ is determined so that low frequency gain of the plant model matches that of the 6th order plant. Figure 2.8 compares the frequency response of the assumed plant model with that of the higher fidelity model. The agreement is quite good at low

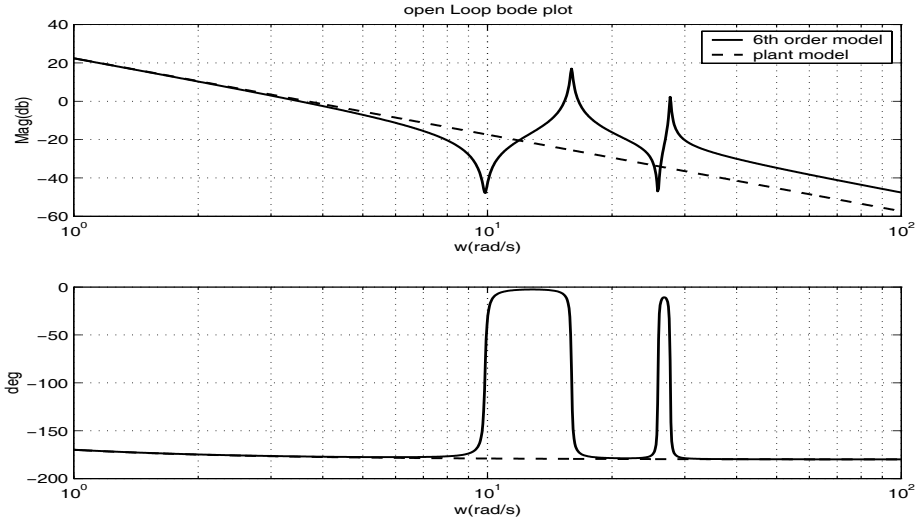

Fig. 2.8: Frequency Responses for the 6th Order Model and the Plant Model for the Torsional Pendulum with the Bottom Disk Regulated

frequencies but differs significantly at high frequencies due to the unmodelled flexible modes. Comparison of Eq.(2.36) with Eq.(2.39) leads to the following modelling error:

$$\Delta = -\frac{B}{J_3}\dot{\theta}_3 + \frac{K}{J_3}(\theta_2 - \theta_3) - \frac{1}{J_3} f_{c_3}(\dot{\theta}_3, \theta_2, \theta_3) + \frac{K_{vt}}{J_3} u + c\dot{y}_m - K_n u. \tag{2.40}$$

By simple manipulation, we can assure that Assumption 2.4 is satisfied if $K_n - K_{vt}/J_3 \neq D_r$.

The linear controller is designed as a lead compensator that results in a dominant mode at $\omega_n = 3$ rad/sec and $\zeta = 0.8$ for the nominal system design. This results in

$$u_{lc} = K_1 \frac{s + b_1}{s + a_1}(y_c - y), \tag{2.41}$$

where $K_1 = 0.67, a_1 = 4.8, b_1 = 0.1786$. The error compensator and the SPR filter are designed as

$$\begin{bmatrix} \nu_{dc}(s) \\ \tilde{y}_{ad}(s) \end{bmatrix} = \frac{1}{s+42.6} \begin{bmatrix} 427(s+3.44) \\ 40(s+5) \end{bmatrix} e_1, \quad T^{-1}(s) = \frac{1}{s+1}. \tag{2.42}$$

A radial basis function NN with 78 neurons is used to approximate the system uncertainty.

$$\phi_k(\boldsymbol{\eta}) = e^{-\|\boldsymbol{\eta}-\boldsymbol{\eta}_{c_k}\|^2/2\sigma_k}, \sigma_k = \sqrt{5}, k = 1, \ldots, 78. \tag{2.43}$$

The centers $\boldsymbol{\eta}_{c_k}$ are randomly selected over a grid of possible values for the vector $\boldsymbol{\eta}$. All of the NN inputs are normalized using an estimate for their maximum values. The NN input is constructed as in (2.21) using 2 delayed values of control signal u and 5 delayed values of output y with a delay $d = 0.1$sec. That is, $\bar{u}_d^T(t) = [u(t) \quad u(t-d) \quad u(t-2d)]^T$, $\bar{y}_d^T(t) = [y(t) \quad y(t-d) \cdots y(t-5d)]^T$. To circumvent a fixed point iteration in the real-time environment, the control signal is further delayed before it is used as the network input. In simulation, this was compared to obtaining a fixed point solution, and the results were indistinguishable. Adaptation gains are chosen as $\Gamma_W = 100, \sigma = 0.5$.

Figures 2.9 compares the response of the regulated output with and without the adaptive element for a square wave command of 20°. The response with the controller in (2.41) but without the adaptive element is shown dashed. The reference command and the response with the adaptive element are shown solid. The absence of the flexible modes in the response with the adaptive element shows that the augmented controller provides adaptation to the unmodelled flexible modes. Furthermore, the output response without the adaptive element exhibits a large steady state error. This is caused by stiction which is also unmodelled in the nominal controller design. The output response with the adaptive element removes the steady state error, showing that the effect of stiction on the output response is removed.

An alternative approach to removing steady state error is to add integral action in the linear controller. A lead/lag controller was designed with integral action (low frequency pole of the compensator at zero) to provide approximately the same transient response when applied to the linear model in (2.39). This design increased the loop crossover frequency from

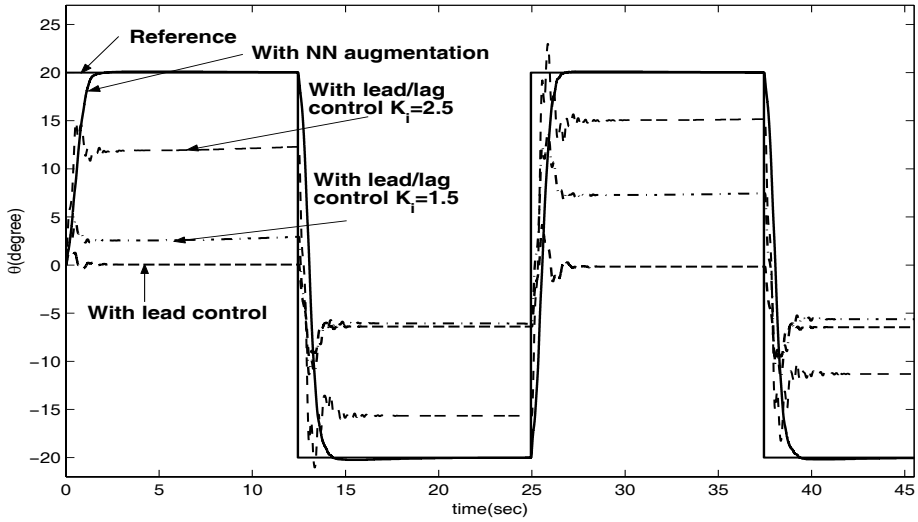

Fig. 2.9: Comparison of Output Responses with/without the Adaptive Element and Integral Control.

1.8 rad/sec to 2.5 rad/sec and reduced the phase margin from 70° to 55.6°. However, due to the nonlinear stiction characteristic of the actuator, this resulted in a nonlinear response to a step command that ultimately staircases to a near zero steady state error. In essence, the integrator repeatedly winds up until it overcomes the stiction. The experimental results for a response to a square wave command is depicted in Figure 2.9 for the design value of the integral gain (K_i=1.5), and a higher value of integral gain (K_i=2.5). The staircase behavior is not seen in this response due to the fact that the command is not held constant for a sufficient duration. The increased destabilizing effect that this controller has on the flexible modes can also be seen. In contrast, the response with the adaptive element (and without integral control) is nearly identical to the ideal model response (the response of the plant model regulated by the lead controller), does not exhibit a nonlinear characteristic, and completely eliminates the effect of the unmodelled modes.

To demonstrate both good tracking and attenuation of disturbances by the augmented controller, a set of reference commands and disturbances are combined in an experiment with the results shown in Figure 2.10. For this case, the bandwidth of the linear controller is increased to $\omega_n = 5$ rad/sec. A disturbance is applied as an external torque to the system using a friction drive motor which is attached to the rim of the top disk. This introduces unmodelled dynamics associated with the disturbance process. Hence, the disturbance is

not matched since it is non-collocated with the control. The voltage applied to the rim drive motor is

$$V_d(t) = \begin{cases} 0.7 \sin 15.7t & (0 \leq t \leq 22) \\ 0.4(\sin t + \sin 3t + \sin 15.7t + \sin 27.7t) & (22 \leq t \leq 45) \end{cases} \tag{2.44}$$

where $V_d(t)$ is the voltage applied to the disturbance drive motor. With the disturbance in (2.44), it is straightforward to check that the disturbance dynamics have eigenvalues that are distinct from those of the plant dynamics in (2.37). The augmented dynamics consisting of plant dynamics and disturbance dynamics are observable by Theorem 3. Thus Assumption 2.3 is satisfied.

In Figure 2.10 the upper traces show the output response (angular position of the lower disk) while the lower trace shows the control voltage. The reference command is zero for the first 22 seconds and is a 0.2 Hz square wave of magnitude 20° for the remaining 23 seconds. The results during the first 7 seconds show the open loop response. The linear controller is activated at t=7 sec. and is able to noticeably reduce the output response to the disturbance. At t=14 sec., the adaptive element is turned on and is able to essentially cancel the effect of the disturbance in the output response. At t=22 sec. the adaptive element is turned off and the square wave is applied as the command to test tracking performance. At the same time, the disturbance signal, $V_d(t)$, is modified as defined in (2.44). Under these conditions, the linear controller is clearly not able to track the reference command, and the response deviates wildly. At t=29 sec., the adaptive element is turned on again and is quickly able to begin tracking the command with increasing fidelity as the NN adapts.

2.7.2 Middle Disk Control-a Non-collocated Control Problem

When the regulated output variable is the angular displacement of the middle disk θ_2, the output variable is *non-collocated* with the control u. The output has relative degree 4. To ensure observability of the system, two more masses are added on the bottom disk increase the moment of inertia, and this results in moments of inertia for the system in (2.36) as

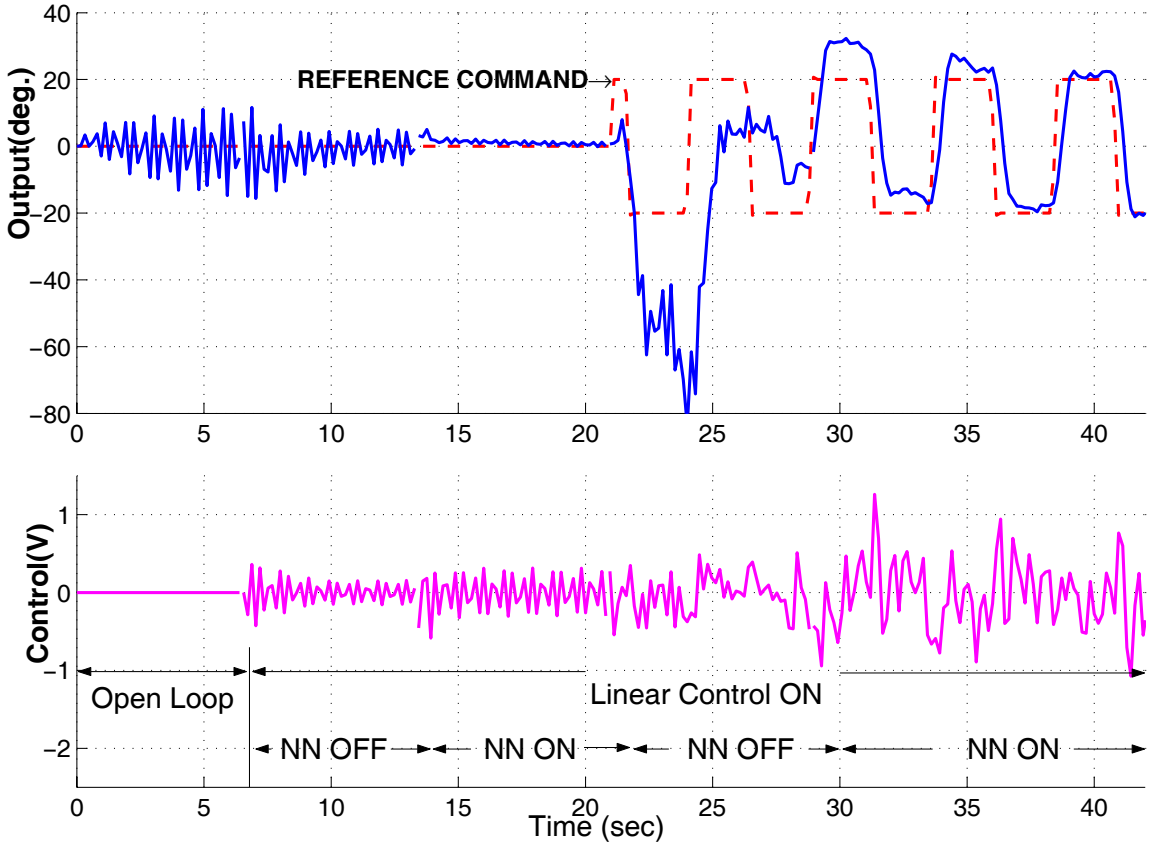

Fig. 2.10: Experimental Results with/without the Adaptive Element with the Bottom Disk Regulated

$J_1 = J_2 = 0.0078, J_3 = 0.0138$. The transfer function from u to θ_2 is as follows:

$$\frac{\theta_2}{u} = \frac{K_a(s^2 + 2\zeta_{z_1}\omega_{z_1}s + \omega_{z_1}^2)}{s(s+c)(s^2 + 2\zeta_{p_1}\omega_{p_1}s + \omega_{p_1}^2)(s^2 + 2\zeta_{p_2}\omega_{p_2}s + \omega_{p_2}^2)} \tag{2.45}$$

The parameters are : $K_a = 10170$, $\zeta_{z_1} = 0.0064$, $\omega_{z_1} = 18.4$, $c = 0.1877$, $\zeta_{p_1} = 0.0059$, $\omega_{p_1} = 16(rad/sec)$ and $\zeta_{p_2} = 0.0037$, $\omega_{p_2} = 30.7(rad/sec)$. The zero dynamics , similar to that shown in (2.38), are given by:

$$\begin{aligned} J_1\ddot{\theta}_1 + B\dot{\theta}_1 + K(\theta_1 - \theta_2) &= K_d V_d \\ \dot{\boldsymbol{x}}_d &= f_d(\boldsymbol{x}_d) \\ V_d &= h_d(\boldsymbol{x}_d) \end{aligned} \tag{2.46}$$

The associated eigenvalues are $-0.089 \pm 15.97i$. Therefore, the system is globally exponentially minimum phase.

In the plant model, the shaft which connects the top and middle disk is assumed rigid. Furthermore, it is assumed that the moments of inertia in (2.36) are of the same value, i.e.,$J_i = 0.103$ $(i = 1, 2, 3)$, which results in the following transfer function:

$$\frac{\theta_2}{u} = \frac{K}{s(s+c)(s^2 + 2\zeta_n\omega_n s + \omega_n^2)} \tag{2.47}$$

where $K = 5159,\ c = 0.18,\ \zeta_n = 0.0046,\ \omega_n = 19.6$. The system matrices for the plant model in (2.47) are as follows:

$$A_m = \begin{bmatrix} 0 & 1 & 0 & 0 \\ -127.5 & -0.1786 & 127.5 & 0 \\ 0 & 0 & 0 & 1 \\ 255 & 0 & -255 & -0.1786 \end{bmatrix}, \boldsymbol{b}_m = \begin{bmatrix} 0 \\ 0 \\ 0 \\ 40.47 \end{bmatrix}, \quad \boldsymbol{c}_m = \begin{bmatrix} 1 \\ 0 \\ 0 \\ 0 \end{bmatrix} \tag{2.48}$$

Figure 2.11 compares the frequency response of the assumed plant model with that of the 6th order model in (2.45).

The linear controller in (2.9) is designed as a LQG controller:

$$A_c = \begin{bmatrix} -1.5 & 1 & 0 & 0 \\ -128.7 & -0.2 & 128.7 & 0 \\ -1.5 & 0 & 0 & 1 \\ 992.6 & -22.8 & -1016.9 & -133.8 \end{bmatrix}, \boldsymbol{b}_c = \begin{bmatrix} -1.55 \\ -1.20 \\ -1.54 \\ -1.19 \end{bmatrix}, \quad \boldsymbol{c}_c = \begin{bmatrix} -18.26 \\ 0.56 \\ 18.83 \\ 3.30 \end{bmatrix}, \ d_c = 0 \tag{2.49}$$

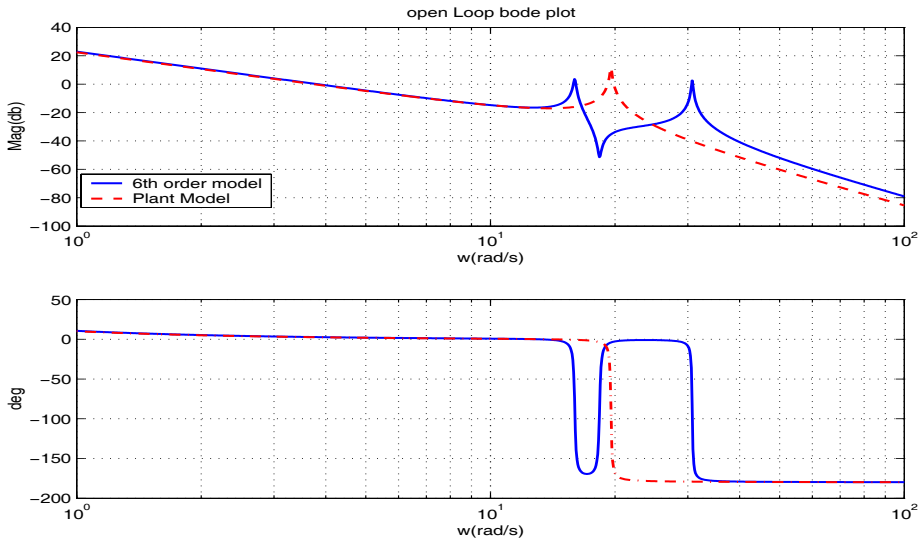

Fig. 2.11: Frequency Responses for the 6th Order Model and the Plant Model with the Middle Disk Regulated.

The experiment is carried out in the same manner as was done for the case of collocated control, and representative output responses are shown in Figure 2.12. It shows that the LQG controller performs very poorly due to the modelling error, even though it showed good tracking and reasonable disturbance attenuation in simulation with the plant model. With the augmented controller, the responses are similar to those in Figure 2.10, however, NN adaptation is slower compared to that observed in the collocated control case.

2.8 Conclusions

This chapter describes an approach for augmenting an existing linear controller design with a neural network based adaptive element. The adaptive control forces the system output to track the plant model output. The main assumptions are that the relative degree of the plant is known within the bandwidth of the control design, and that the augmented system describing the plant and disturbance dynamics is observable. An analysis of the augmented nonlinear system shows that the observability condition is almost always satisfied so long as the plant is observable. Numerical examples with a mass-spring-damper system show that the overall system is highly effective from the perspective of adaptation to both unmatched unmodeled dynamics and disturbances. This is further illustrated by the experimental

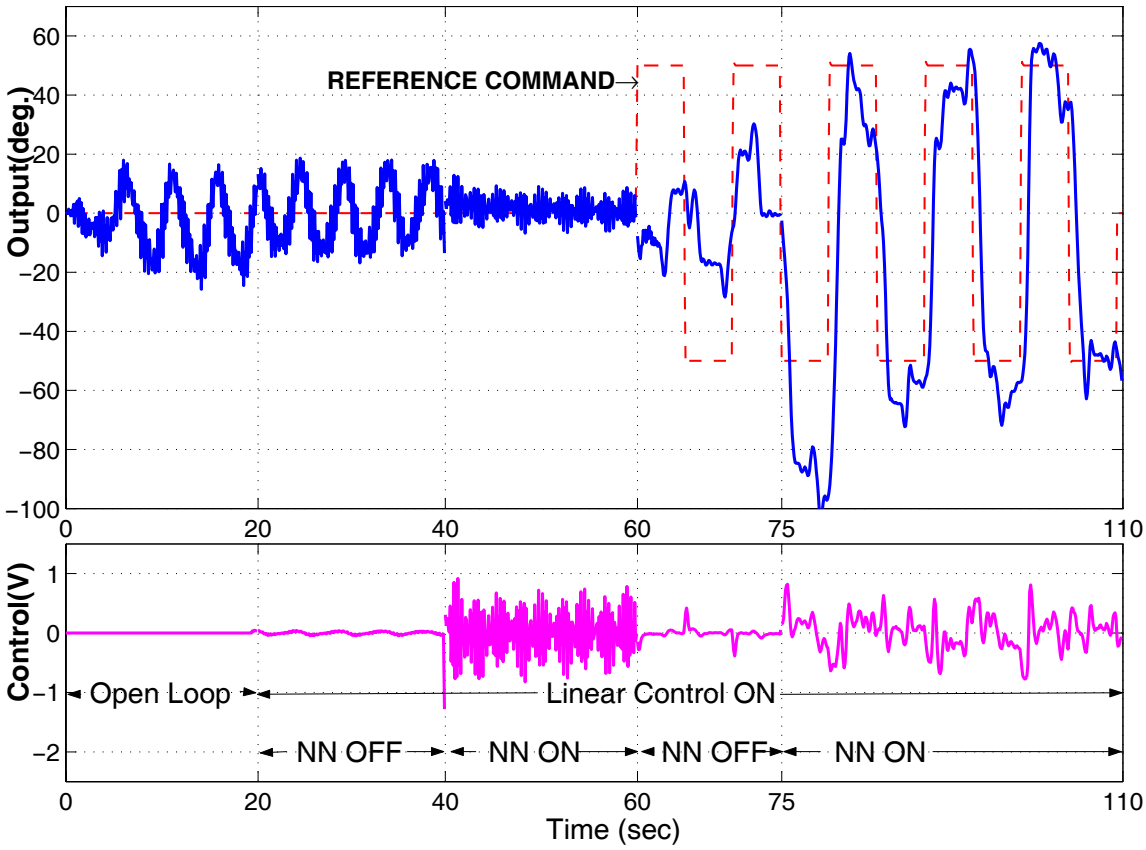

Fig. 2.12: Experimental Results on the Middle Disk Control

results with the three-disk torsional pendulum.

CHAPTER 3

ADDRESSING ACTUATOR NONLINEARITIES IN INTERNAL MODEL-FOLLOWING CONTROL

In this chapter, we describe a control design to deal with actuator nonlinearities to guarantee stability and enhance the performance of an adaptive control system described in Chapter 2. The effect of an actuator limit is treated using control hedging. The other class of actuator nonlinearities, such as dead zone and backlash are addressed by a disturbance observer design. In this case, the basic approach involves showing that the augmenting adaptive output feedback architecture is structurally equivalent to a robust internal-loop compensator (RIC), which has been shown equivalent to a disturbance observer. It is shown that this combination is highly effective for a variety of actuator nonlinearities (dead zone, backlash, and saturation). Control hedging is tested on a three-disk torsional pendulum. The overall approach is illustrated using the three-disk torsional system with dynamic friction, when the actuator is subject to dead zone and saturation.

3.1 Introduction

Actuator nonlinearities have been a major obstacle in guaranteeing stability and performance of adaptive control systems. From the perspective of control design, common actuator nonlinearities can be grouped into two classes. Whereas dead zone, backlash, and hysteresis limit the control system performance when the control demand is low, amplitude and rate saturations degrade the performance, and raises a question of stability when the control demand is high.

While actuator nonlinearity is often present, most control design methods either ignore them, or treat a single type of nonlinearity. In the first class of actuation characteristics, such as amplitude and rate saturation, many approaches have accounted for the capacity of the actuation device in relation to the control system performance in both adaptive

and non-adaptive control designs [57, 71–75, 96]. In particular, Ref. [57, 97] developed an approach called "pseudo-control hedging" (PCH) that is applicable when augmenting a nonlinear, state feedback inverting controller with an adaptive element in the presence of control saturation, and other nonlinear effects. The role of PCH is to protect the adaptive process from attempting to adapt to the effects of actuator nonlinearities. Its validity in a real-time setting has also been shown through various flight tests and simulations [98, 99]. We show how to incorporate the PCH method in a NN-based output feedback setting which augments a linear controller, and refer to it as "control hedging" (CH). The method was introduced in [100], and its stability has been proved in [101] in case of input saturation. In the first part of this chapter, we formulate the problem in a more general setting than that in [101] and provide a stability anaylsis. A class of *static* actuator characteristics can be extended to those which can be approximated by a Lipschitz function in the range of control signal. This class includes amplitude saturation as a special case, for it is globally Lipschitz [91, pp.70-71].

While the first class of actuator nonlinearities are problematic in relation to stability of adaptive control system, the other class of nonlinearities, such as dead zone and backlash are more problematic in relation to its effect on performance since nonlinearities in this class manifest their presence at low command levels. This class of nonlinearities renders the system response sluggish and may result in a limit cycle in its steady-state. Thus, these nonlinearities have been tackled by seeking an inverse of a selected characteristic [76, 78, 80]. In [76, 80], parametric uncertainties are addressed by adaptive inverse compensation. In [78], an inverse for dead zone is sought by employing a NN which includes neurons whose activation functions provide *a jump function basis set* to approximate a *discontinuous* dead zone inverse. In a non-adaptive control setting, Ref. [77] provides an interesting use of a disturbance observer to compensate for actuator nonlinearities. A disturbance observer has typically been used in high-precision robotic motion control systems [77, 82, 102–106] to compensate for external disturbances. This method estimates the effects of external disturbances and modelling errors to cancel them and subsequently to make the system behave like the plant model. The results in [77] indicate that the disturbance

observer can greatly mitigate the effect of actuator nonlinearities of the second class. In [82], a method called robust internal-loop compensation (RIC) was proposed and shown structurally equivalent to the disturbance observer. In the second part of this chapter, we show that the control architecture in Chapter 2 is equivalent to that of RIC. Using this structural equivalence, we apply the results in [77] to the adaptive control architecture in Chapter 2, and incorporate CH to protect the adaptive process. It is shown that this combination is highly effective for multiple types of actuator nonlinearities (dead zone, backlash, and saturation).

This chapter is organized as follows. CH is described in Section 3.2. Its formulation and a stability analysis are presented in the sections 3.2.1 and 3.2.2. The experimental results with the three-disk torsional system with control voltage limit is provided in Section 3.2.3. Section 3.3 describes the disturbance observer design. In Section 3.3.1, a structural equivalence between a disturbance observer and the internal model-following control architecture is established using the RIC framework. In Section 3.3.2 we describe the method of augmenting adaptive control based on [63]. The design involves deriving error dynamics and constructing a reduced error observer to generate a teaching signal for an adaptation law. Simulation results are presented in Section 3.3.4. Conclusions are given in Section 3.4.

3.2 Control Hedging

3.2.1 Control Hedging Architecture

PCH is introduced to protect an adaptive process, by preventing it from attempting to adapt to selected input nonlinearities (such as those due to amplitude and rate saturation) [70]. This is accomplished by modelling and removing the effect of these characteristics in the error dynamics. For example, this permits the adaptive process to continue to estimate the modelling error, so that when the process comes out of saturation, the correct adaptive control is immediately available. The approach was originally developed for use when augmenting an inverting controller. The implementation of PCH consists of calculating the difference between a commanded pseudo-control signal, and an estimate of the achievable pseudo-control. This difference is referred to as the hedge signal because it is subtracted

from the dynamics of a command filter. Its implementation in the context of augmenting a linear controller is illustrated in Figure 3.1. In this setting the difference is formed at the level of the control signal, rather than the pseudo-control signal, so we refer to it as control hedging (CH), rather than PCH.

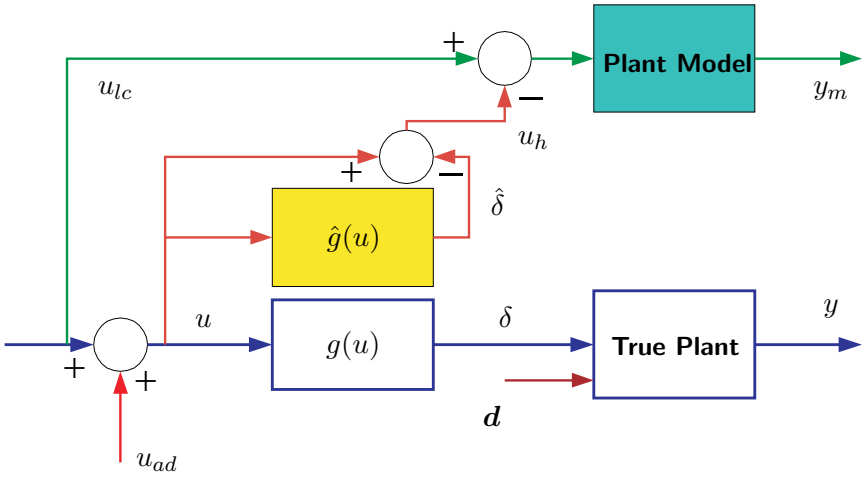

Fig. 3.1: Implementation of Control Hedging.

The nonlinear input characteristic is defined as

$$\delta \triangleq g(u),\ |\delta| \leq \delta_0, \tag{3.1}$$

where u is the commanded control input and δ_0 is the control limit. With the input nonlinearity, the dynamics in (2.3) are written as

$$\begin{aligned} \dot{\boldsymbol{x}} &= \boldsymbol{f}(\boldsymbol{x}, g(u)),\ y = h(\boldsymbol{x}) \\ y^{(r)} &= h_r(\boldsymbol{x}, g(u)). \end{aligned} \tag{3.2}$$

If δ is available for feedback, then $\hat{\delta} = \delta$. Otherwise, we assume it is estimated using

$$\hat{\delta} = \hat{g}(u),\ |\hat{\delta}| \leq \hat{\delta}_0, \tag{3.3}$$

where $\hat{\delta}_0$ is an estimate for δ_0. Further we assume that the estimate for the input satisfies a Lipschitz condition. This assumption is required for stability analysis.

Assumption 3.1. *There exists $L > 0$ such that $\|\hat{g}(u_1) - \hat{g}(u_2)\| \leq L\,|u_1 - u_2|$ for $\forall\ u_1, u_2 \in \mathcal{U}$.*

Note that input saturation globally satisfies the assumption 3.1 with $L = 1$.

With CH, the plant model dynamics in (2.7) are modified as follows:

$$\begin{aligned} \dot{\boldsymbol{x}}_m &= A_m \boldsymbol{x}_m + \boldsymbol{b}_m (u_{lc} - u_h), \;\; u_h = u - \hat{\delta} \\ y_m &= \boldsymbol{c}_m^T \boldsymbol{x}_m \\ y_m^{(r)} &= \boldsymbol{c}_r^T \boldsymbol{x}_m + d_r (u_{lc} - u_h), \end{aligned} \tag{3.4}$$

where

$$u_h = u_{lc} + d_r^{-1}(\nu_{dc} - \nu_{ad}) - \hat{g}(u_{lc} + d_r^{-1}(\nu_{dc} - \nu_{ad})). \tag{3.5}$$

The control hedging signal u_h represents an estimate for the deficient part of commanded control signal due to the nonlinearity of the actuator. For example, with amplitude saturation, u_h is shown dashed in Figure 3.2.

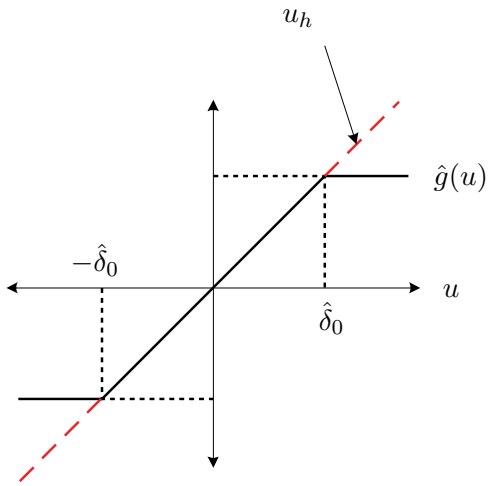

Fig. 3.2: Control Hedging Signal u_h with Input Saturation

The plant model dynamics in (3.4) regulated by the linear controller in (2.9) can be described by

$$\dot{\bar{\boldsymbol{x}}} = \bar{A}\bar{\boldsymbol{x}} + \bar{\boldsymbol{b}}_c y_c + \bar{\boldsymbol{b}}_c e_1 - \bar{\boldsymbol{b}} u_h, \tag{3.6}$$

where $\bar{\boldsymbol{x}}^T = [\boldsymbol{x}_m^T, \; \boldsymbol{x}_c^T]$, $\bar{\boldsymbol{b}}^T = [\boldsymbol{b}_m^T, \; 0^T]$. Define the plant model error vector $\boldsymbol{e}_m \triangleq \bar{\boldsymbol{x}}_{\text{nom}} - \bar{\boldsymbol{x}}$, then comparing (3.6) to (2.10) leads to the following *plant model error dynamics*:

$$\dot{\boldsymbol{e}}_m = \bar{A}\boldsymbol{e}_m - \bar{\boldsymbol{b}}_c e_1 + \bar{\boldsymbol{b}} u_h, \quad \boldsymbol{e}_m \in \Omega_{\boldsymbol{e}_m} \subseteq \mathbb{R}^{m+n_c}, \tag{3.7}$$

where the domain $\Omega_{\boldsymbol{e}_m} \triangleq \{\boldsymbol{e}_m \in \mathbb{R}^{m+n_c} \ : \ \bar{\boldsymbol{x}}_{\text{nom}} \in \mathcal{D}_m, \ \bar{\boldsymbol{x}} \in \mathcal{D}_m \times \mathcal{D}_c\}$. The sets $\mathcal{D}_{\text{nom}}$, $\mathcal{D}_m$, and $\mathcal{D}_c$ are defined in the following lines after (2.10), (2.7), and (2.9), respectively. Since $\bar{A}$ is Hurwitz by design, for any $Q_n > 0$, there exists $P_n > 0$ such that

$$\bar{A}^T P_n + P_n \bar{A} + Q_n = 0. \tag{3.8}$$

With the form of $\hat{h}_r$ in (2.7) and $\hat{\delta}$ in (3.3), $y^{(r)}$ in (3.2) can be written as

$$\begin{aligned} y^{(r)} =& \hat{h}_r(\boldsymbol{x}_m, \hat{g}(u)) + \Delta(x, \boldsymbol{x}_m, u) \\ =& \boldsymbol{c}_r^T \boldsymbol{x}_m + d_r \hat{\delta} + \Delta(\boldsymbol{x}, \boldsymbol{x}_m, u), \end{aligned} \tag{3.9}$$

where

$$\Delta(\boldsymbol{x}, \boldsymbol{x}_m, u) = h_r(\boldsymbol{x}, g(u)) - \boldsymbol{c}_r^T \boldsymbol{x}_m - d_r \hat{\delta}. \tag{3.10}$$

Comparing Eq.(3.4) and Eq.(3.9) leads to the following *output tracking error dynamics*:

$$e_1^{(r)} = -d_r u_{ad} - \Delta(\boldsymbol{x}, \boldsymbol{x}_m, u). \tag{3.11}$$

Using Eq.(2.14), the output tracking error dynamics in (2.12) is finally written as

$$e_1^{(r)} = -\nu_{dc} + \nu_{ad} - \Delta. \tag{3.12}$$

Note that the error dynamics maintain the same form as in Eq.(2.15), while the definition of the modelling error Δ has changed from that in Eq.(2.13) to that in Eq.(3.10). This implies that Theorem 2.1 remains valid so long as Assumptions 2.2 and 2.4 are not violated with Δ being defined as in (3.10). it is also notable that without CH, Assumption 2.4 is violated in case of input saturation [101].

3.2.2 Stability Analysis with CH

For stability analysis, we introduce the following definition:

$$u_h^* = u_{lc} + d_r^{-1}(\nu_{dc} - \nu_{ad}^*) - \hat{g}(u_{lc} + d_r^{-1}(\nu_{dc} - \nu_{ad}^*)). \tag{3.13}$$

The term u_h^* represents u_h in (3.5) when NN adaptation is exact. That is, $\nu_{ad} = \nu_{ad}^* = \boldsymbol{W}\boldsymbol{\phi}(\boldsymbol{\eta})$. With Eq.s (2.9) and (2.28), u_h^* can be explicitly written as

$$u_h^* = d_c y_c + J_1 \bar{\boldsymbol{x}}_{\text{nom}} - J_1 \boldsymbol{e}_m + J_2 \boldsymbol{z} - d_r^{-1} \boldsymbol{W}\boldsymbol{\phi} - \hat{g}(d_c y_c + J_1 \bar{\boldsymbol{x}}_{\text{nom}} - J_1 \boldsymbol{e}_m + J_2 \boldsymbol{z} - d_r^{-1} \boldsymbol{W}\boldsymbol{\phi}), \tag{3.14}$$

where $J_1 = \left[-d_c \boldsymbol{c}_m^T,\ \boldsymbol{c}_c^T\right]$, and $J_2 = \left[(d_c + d_r^{-1} d_{dc})\boldsymbol{c}_1^T,\ d_r^{-1}\boldsymbol{c}_{dc}^T\right]$. Note that u_h^* depends on the nominal closed loop performance(through $\bar{\boldsymbol{x}}_{\text{nom}},\ y_c$), the modelling error (through $\boldsymbol{W}^T\boldsymbol{\phi}(\boldsymbol{\eta})$), and the degree of NN adaptation to the modelling error (through $\boldsymbol{e}_m,\ \boldsymbol{z}$). The following technical assumption requires that u_h^* satisfies a linear growth condition on $\Omega_{\boldsymbol{e}_m}$. In case of input saturation, the assumption implies that the deficient control depicted in Figure 3.2 satisfies the linear growth condition when NN adaptation is exact.

Assumption 3.2. *The signal u_h^* is bounded as follows:*

$$|u_h^*| \leq \mu_1 \|\boldsymbol{e}_m\| + \mu_2 \|\boldsymbol{z}\| + \mu_4,\ \text{for } \boldsymbol{e}_m \in \Omega_{\boldsymbol{e}_m}, \tag{3.15}$$

where $\mu_1, \mu_2, \mu_4 \geq 0$.

Compared to u_h^* in (3.13), u_h in (3.5) can be expressed as

$$u_h = u_h^* + d_r^{-1}[\nu_{ad}^* - \nu_{ad}] + [\hat{g}(u_{lc} + d_r^{-1}(\nu_{dc} - \nu_{ad}^*)) - \hat{g}(u_{lc} + d_r^{-1}(\nu_{dc} - \nu_{ad}))] \tag{3.16}$$

Using Eq.(3.15), with Assumption 3.1, u_h is bounded by

$$|u_h| \leq \mu_1 \|\boldsymbol{e}_m\| + \mu_2 \|\boldsymbol{z}\| + \mu_3 \left\|\widetilde{\boldsymbol{W}}\right\| + \mu_4,\ \text{for } \boldsymbol{e}_m \in \Omega_{\boldsymbol{e}_m}, \tag{3.17}$$

where $\mu_3 = (1 + L)\|\boldsymbol{\phi}\|$.

We will show via Lyapunov's direct method that the signals $\boldsymbol{e}_m$ in (3.7), $\boldsymbol{z}$ in (2.29), $\boldsymbol{z}_f$ in (2.32), and NN weight errors $\widetilde{\boldsymbol{W}}$ are bounded. With that objective in mind, we define the error vector $\zeta^T \triangleq [\ \boldsymbol{e}_m^T\ \boldsymbol{z}^T\ \boldsymbol{z}_f^T\ \widetilde{\boldsymbol{W}}^T\ ]$ and its domain

$$\Omega_o \triangleq \left\{\zeta \in \Omega_{\boldsymbol{e}_m} \times \mathbb{R}^{n_z + n_f + n_h}\ :\ \bar{\boldsymbol{x}}_{\text{nom}} \in \mathcal{D}_{\text{nom}},\ \bar{\boldsymbol{x}} \in \mathcal{D}_m \times \mathcal{D}_c\right\}, \tag{3.18}$$

which includes the origin. Let us consider a convex compact set $\mathcal{B}_R \triangleq \{\zeta \in \Omega_o\ :\ \|\zeta\| \leq R,\ R > 0\}$ so that for every $\zeta \in \mathcal{B}_R$, the NN approximation implied in (2.20), with Δ defined in (3.10), is valid. Consider the following Lyapunov function candidate

$$V(\zeta) = \zeta^T T \zeta = \frac{1}{2}\boldsymbol{e}_m^T P_n \boldsymbol{e}_m + \frac{1}{2}\boldsymbol{z}^T P \boldsymbol{z} + \frac{1}{2}\boldsymbol{z}_f P_f \boldsymbol{z}_f + \frac{1}{2}\text{tr}\{\widetilde{\boldsymbol{W}}^T \Gamma_W^{-1} \widetilde{\boldsymbol{W}}\}, \tag{3.19}$$

where $P_n, P, P_f > 0$ are solutions of (3.8), (2.31), (2.33) respectively and T is defined to be:

$$T = \frac{1}{2}\begin{bmatrix} P_n & 0 & 0 & 0 \\ 0 & P & 0 & 0 \\ 0 & 0 & P_f & 0 \\ 0 & 0 & 0 & \Gamma_W^{-1} \end{bmatrix}. \tag{3.20}$$

Introduce T_m, T_M which are minimal and maximal eigenvalues of T respectively. Then $T_m \|\zeta\|^2 \leq V(\zeta) \leq T_M \|\zeta\|^2$. Let $\alpha = \sqrt{\frac{T_m}{T_M}} R, \mathcal{B}_\alpha = \{\zeta \in \mathcal{B}_R \ : \ \|\zeta\| \leq \alpha\}$.

Theorem 3.1. *Suppose $\zeta(0) \in \mathcal{B}_\alpha$ and,*

$$R > \sqrt{\frac{T_M}{T_m}} C \geq C, \tag{3.21}$$

where C is defined later in (B.8). Subject to assumptions 2.1-3.2, the control law $u = u_{lc} + d_r^{-1}(\nu_{dc} - \nu_{ad})$ with plant model dynamics in (3.4) guarantees that the signal ζ is uniformly ultimately bounded with the bound $\sqrt{\frac{T_M}{T_m}} C$, provided the following conditions hold

$$\begin{aligned} \gamma_1 &> \gamma_4 \\ \lambda_{\min}(Q) &> 2\epsilon \|P\boldsymbol{b}_{cl}\| + \frac{4\gamma_2^2}{\gamma_1} \\ \lambda_{\min}(Q_f) &> \|P_f \boldsymbol{b}_f\| \|\boldsymbol{\phi}\| \\ \sigma &> 1 + \frac{\gamma_3^2}{\gamma_1} + \frac{\alpha^2 \|P\boldsymbol{b}_{cl}\|^2}{\lambda_{\min}(Q)}, \end{aligned}$$

where $\gamma_1 = \frac{1}{2}\lambda_{\min}(Q_n) - \mu_1 \left\|P_n \bar{\boldsymbol{b}}\right\|, \gamma_2 = \left\|P_n \bar{\boldsymbol{b}}_c \boldsymbol{c}_{e_1}^T\right\| + \mu_2 \left\|P_n \bar{\boldsymbol{b}}\right\|, \ \gamma_3 = \mu_3 \left\|P_n \bar{\boldsymbol{b}}\right\|, \ \gamma_4 = \mu_4 \left\|P_n \bar{\boldsymbol{b}}\right\|$.

Proof. see Appendix B.

The uniform ultimate boundedness of $\boldsymbol{e}_m$ and $\boldsymbol{z}$ guarantees, using (2.10) and (2.29), that the tracking error is bounded; $|y_c - y| \leq |y_c - y_{\text{nom}}| + |y_{\text{nom}} - y_m| + |e_1| \leq |y_c - y_{\text{nom}}| + \left\|\boldsymbol{c}_m^T\right\| \|\boldsymbol{e}_m\| + \left\|\boldsymbol{c}_1^T\right\| \|\boldsymbol{z}_e\|$, where $|y_c - y_{\text{nom}}|$ represents the nominal tracking error bound for the system in (2.10).

Remark 3.1. The assumption that $\zeta(0) \in \mathcal{B}_\alpha$ implies that the control system initially belongs to the domain where stabilization is possible, for whenever $\zeta \in \mathcal{B}_\alpha$ and $\|\zeta\| > C$, $\dot{L} < 0$.

If the system initially belongs to the region in which it cannot be stabilized, the control hedging signal u_h goes unbounded and results in $\boldsymbol{e}_m \notin \Omega_{\boldsymbol{e}_m}$ after some time.

Remark 3.2. The assumption that $R > \sqrt{\frac{T_M}{T_m}} C \geq C$ implies both an upper and a lower bound for the adaptation gain. Define $\bar{\gamma} \triangleq \max \Gamma_W$, $\underline{\gamma} \triangleq \min \Gamma_W$, $\bar{\lambda} = \max\left(\lambda_{\max} P_n,\ \lambda_{\max} P,\ \lambda_{\max} P_f\right)$, $\underline{\lambda} = \min\left(\lambda_{\min} P_n,\ \lambda_{\min} P,\ \lambda_{\min} P_f\right)$, where $\lambda(\cdot)$ denotes a eigenvalue. If the adaptation gain is large such that $\underline{\gamma} > \frac{1}{\underline{\lambda}}$, Eq.(3.21) implies an upper bound $\overline{\gamma} < \frac{R^2}{C^2 \underline{\lambda}}$ for the adaptation gain. Likewise, for $\bar{\gamma} < \frac{1}{\bar{\lambda}}$, Eq.(3.21) leads to an lower bound $\underline{\gamma} > \frac{C^2}{R^2 \underline{\lambda}}$ for the adaptation gain.

Remark 3.3. The closed loop system when the NN adaptation is exact, i.e., $\nu_{ad} = \nu_{ad}^*$ ($\hat{\boldsymbol{W}} = \boldsymbol{W}$) $\Rightarrow u_h = u_h^*$, is defined as a *non-adaptive subsystem* in [70]. The performance of this system represents the best performance that can be achieved with CH together with the NN based adaptive element. The uniform ultimate bounded region, in this case, further shrinks, because all the constants related to $\widetilde{\boldsymbol{W}}$ vanishes from C in (B.8).

3.2.3 Experimental Results with the Three-disk Torsional System

The CH technique is tested in the three-disk torsional pendulum system with the bottom disk regulated as in Section 2.7.1. In practice the applied control voltage must be limited because excessive angular displacement between two disks can damage the flexible shaft connecting them. This amounts to introducing a form of control saturation, but the CH method can be employed to allow the adaptive process to continue during saturation.

In the first experiment, the control voltage is limited to 0.18 V. Fig. 3.3 compares the output tracking performances when the square wave is the reference command. The response without CH shows similar phenomenon as integrator wind-up, i.e. big overshoot. With CH, the control system moves out of initial phase saturation and gradually tracks the reference command without input saturation.

In the next experiment, a control limit of 0.3 volts is introduced. Since it is implemented in software, δ in (3.1) equals $\hat{\delta}$ in (3.3). The reference command is set to zero, and the disturbance is constructed as $V_d(t) = 0.5(\sin t + \sin 3t + \sin 12t + \sin 15.7t + \sin 27.7t)$. Since the control voltage limit is set to a value which does not permit cancellation of the

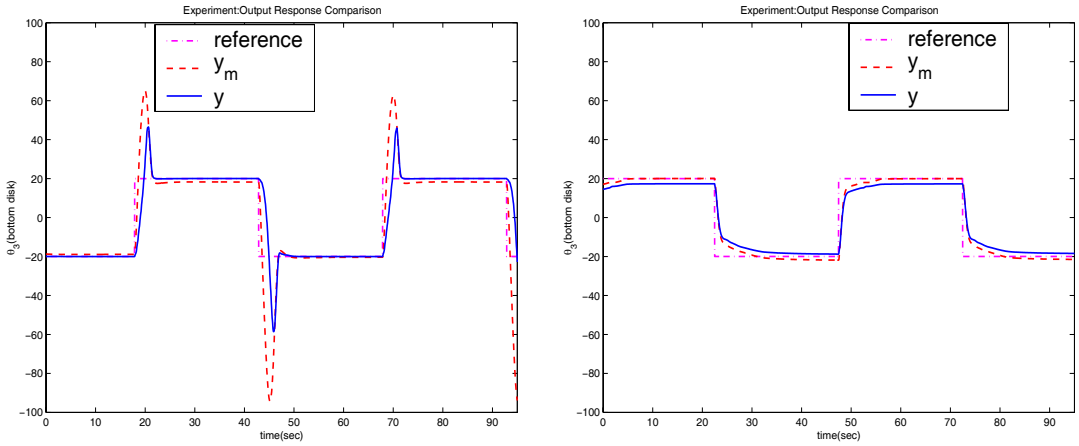

(a) without CH (b) with CH

Fig. 3.3: Responses of Plant Model y_m and the Output y without External Disturbance

disturbance, the disturbance is expected to be only partially attenuated. The main focus in this experiment is to show that the CH technique insures correct adaptation while the actuator is in saturation. The results are presented in Figure 3.4. Figure 4(a) shows the response when the adaptive element is active, but without CH. Incorrect adaptation is evidenced by a growing response and the difference between the actual plant(y) and the plant model(y_m) under the continual input saturation as shown in Figure 4(c). The NN weights also diverge due to control saturation. Figure 4(b) shows the response for the same controller, but with CH active. Note that although the disturbance is not completely cancelled, the output tracks the plant model response reasonably well. This illustrates that correct adaptation is achieved with CH, even when there is a significant amount of control saturation. The NN weight histories (not shown) were also bounded.

3.3 Disturbance Observer-based Performance Enhancement

In this section, we address the second class of actuator nonlinearities, such as dead zone and backlash. We consider the nonlinear system Σ_p in (3.2) expressed in its normal form

$$\begin{aligned} \dot{\boldsymbol{\xi}} &= A_\xi \boldsymbol{\xi} + \boldsymbol{b}_\xi h_r(\boldsymbol{z}_o, \boldsymbol{\xi}, g(u)) \\ \dot{\boldsymbol{z}}_o &= \boldsymbol{f}_o(\boldsymbol{z}_o, \boldsymbol{\xi}) \\ y &= \boldsymbol{c}_\xi^T \boldsymbol{\xi}, \end{aligned} \tag{3.22}$$

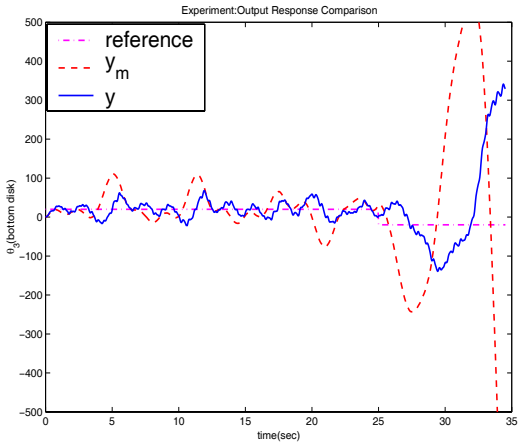

(a) Responses of Plant Model, y_m, and the output, y without CH

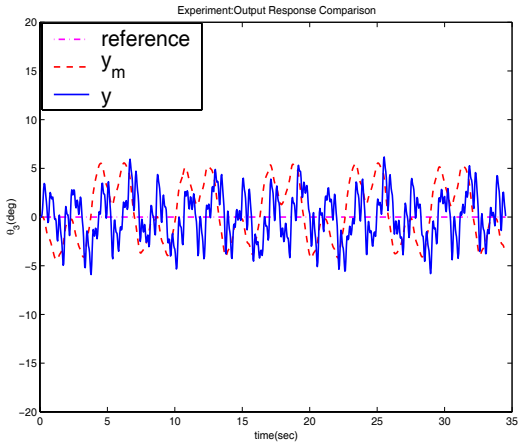

(b) Responses of Plant Model, y_m, and the output, y with CH

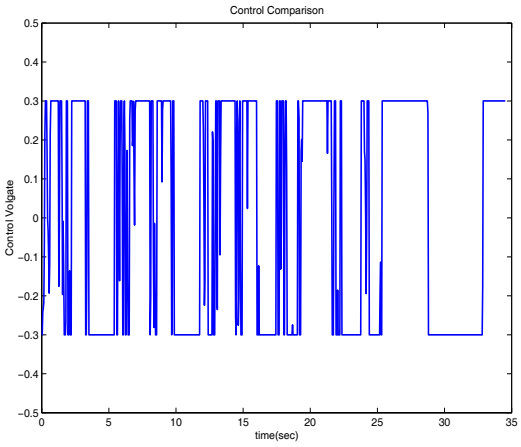

(c) Control Signal without CH

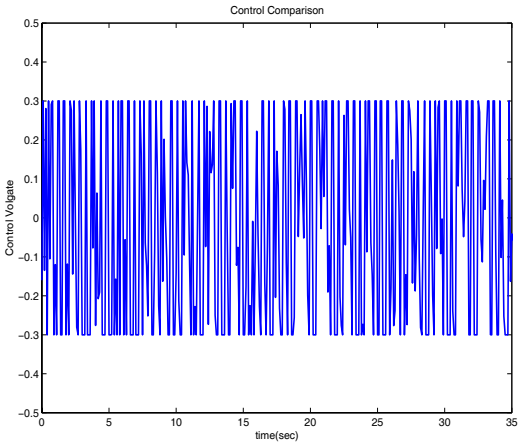

(d) Control Signal with CH

Fig. 3.4: Comparison of Output Responses with/without CH when subjected to External Disturbances

where explicit dependence on the external disturbance $\boldsymbol{d}$ is removed for simplicity of presentation.

In addition to a known relative degree, the linear plant model $P_n(s)$ in (2.7) is further assumed to have no zeros. In other words,

Assumption 3.3. *The linear plant model $P_n(s)$ is fully linearizable.*

Thus, the linear plant model is described by

$$\begin{aligned}\dot{\boldsymbol{\xi}}_m =& A_m\boldsymbol{\xi}_m + \boldsymbol{b}_m u \\ y_m =& \boldsymbol{c}_m^T\boldsymbol{\xi}_m, \quad y_m^{(r)} = \hat{h}_r(\boldsymbol{\xi}_m, u) = \boldsymbol{c}_r^T\boldsymbol{\xi}_m + d_r u\end{aligned} \tag{3.23}$$

where $\boldsymbol{\xi}_m \in \mathbb{R}^r$, $\boldsymbol{c}_m = \boldsymbol{c}_\xi$, and

$$\begin{aligned}A_m =& \begin{bmatrix} 0 & 1 & 0 & \cdots & 0 \\ 0 & 0 & 1 & \cdots & 0 \\ \vdots & & \vdots & \ddots & \vdots \\ 0 & & \cdots & & 1 \\ a_1 & a_2 & \cdots & a_{r-1} & a_r \end{bmatrix}_{r\times r}, \ \boldsymbol{b}_m = \begin{bmatrix} 0 \\ 0 \\ \vdots \\ 0 \\ d_r \end{bmatrix}_r, \\ \boldsymbol{c}_r^T =& \boldsymbol{c}_m^T A_m^r = \begin{bmatrix} a_1 & \dots & a_r \end{bmatrix}, \ d_r = \boldsymbol{c}_m^T A_m^{r-1}\boldsymbol{b}_m.\end{aligned} \tag{3.24}$$

Our objective in this section is to show how we can systematically design the augmenting signal u_{ad} in (2.14) when actuator nonlinearities are present in the adaptive control framework in Chapter 2.

3.3.1 Structural Equivalence between Disturbance Observer and Internal Model Following Architecture

Figure 3.5 represents a typical closed loop system. This is the same as the system depicted in Figure 2.1 with augmenting elements removed. If $\Sigma_p = P_n(s)$, all performance specifications are satisfied, and the closed loop system becomes identical with the nominal closed-loop system in (2.10). Figure 3.6 illustrates how an inner-loop disturbance observer is used to augment the outer-loop controller of Figure 3.5. Its goal is to force the system Σ_p to behave like the plant model $P_n(s)$ by rejecting external disturbances and modelling errors satisfying a *matching condition*. Its architecture is depicted in Figure 3.6 for the case in

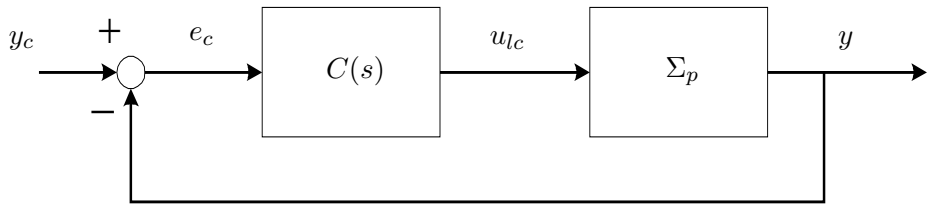

Fig. 3.5: Typical Feedback Control System

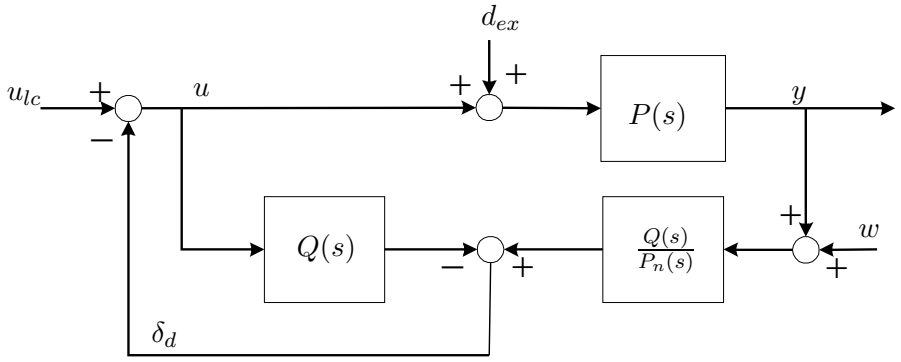

Fig. 3.6: Disturbance Observer Architecture

which the system is linear, $\Sigma_p = P(s)$. The terms d_{ex}, w represent external disturbance and sensor noise, respectively. The Q-filter is designed to reject disturbances below a cut-off frequency [82]. From Figure 3.6, the output y is expressed as

$$y = [P_n(s)u_{lc} + P_n(s)\{1 - Q(s)\}d_{ex} - Q(s)w]\,\frac{P(s)}{X(s)}, \tag{3.25}$$

where $X(s) = P_n(s) + [P(s) - P_n(s)]Q(s)$. From (3.25), we can see that it is desirable that $|1 - Q(j\omega)| \simeq 0$ to reject external disturbances, while $|Q(j\omega)|$ should be small in order to reduce the effect of sensor noise w. Thus, the design of $Q(s)$ is s compromise between these conflicting objectives, which can be formulated as a mixed sensitivity optimization problem [106, 107].

A common form for the Q-filter, proposed in [107], is

$$Q(s) = \frac{1 + \sum_{k=1}^{N_q - r} a_k(\tau s)^k}{1 + \sum_{k=1}^{N_q} a_k(\tau s)^k}, \tag{3.26}$$

in which a_k, τ are design parameters. A structural equivalence between the disturbance

observer and RIC is established when the Q-filter is selected as

$$Q(s) = \frac{P_n(s)K(s)}{1 + P_n(s)K(s)}, \tag{3.27}$$

in which $K(s)$ is the compensator designed for the unity feedback system in Figure 3.5, with $C(s)$ and Σ_p replaced by $K(s)$ and $P_n(s)$, respectively. The relation in (3.27) implies that if a compensator $K(s)$ is designed for $P_n(s)$ in order to satisfy a given robustness criterion, such as gain/phase margin, the Q-filter is automatically designed.

The feedback control system with RIC as an internal-loop compensator is depicted in Figure 3.7. The analysis in [82] reveals that with $u^* = 0$, the estimated disturbance δ_d in

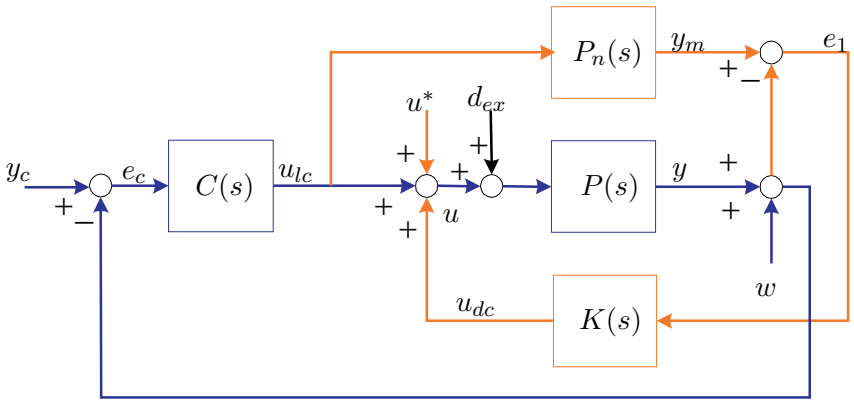

Fig. 3.7: The Robust Internal-loop Compensator (RIC) Architecture

Figure 3.6 is reformulated as

$$\delta_d = -u_{dc} = -K(s)e_1, \tag{3.28}$$

in which e_1 is defined by $e_1 = y_m - y$. The control signal u^* is an additional control input used to compensate for plant uncertainty. It can be designed using either a fixed gain method or an adaptive method. From Figure 3.7 it follows that

$$y = \left[\frac{\{1 + L_n(s)\}P(s)C(s)}{X_c(s)}\right] y_d + \left[\frac{P(s)}{X_c(s)}\right] d_{ex} - \left[\frac{L(s) + \{1 + L_n(s)\}P(s)C(s)}{X_c(s)}\right] w, \tag{3.29}$$

where $L(s) = P(s)K(s)$, $L_n(s) = P_n(s)K(s)$, $X_c(s) = 1 + L(s) + \{1 + L_n(s)\}P(s)C(s)$. With the following definition for d_{eq}

$$d_{eq} \triangleq \left[\frac{P(s)}{P_n(s)} - 1\right] u + \left[\frac{P(s)}{P_n(s)}\right] d_{ex}, \tag{3.30}$$

which is depicted in Figure 3.8, we have the transfer function from d_{eq} to y

$$\frac{y(s)}{d_{eq}(s)} = \frac{P_n(s)}{[1 + P_n(s)C(s)][1 + L_n(s)]}. \tag{3.31}$$

Then, with $w = 0$, the relationship among e_c, y_c and d_{eq} can be expressed as

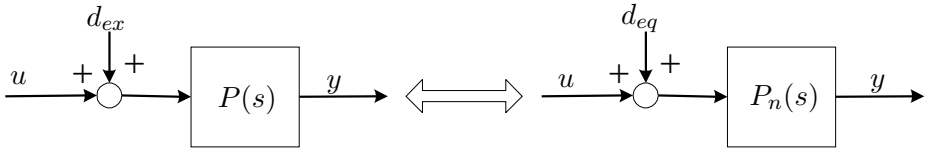

Fig. 3.8: Reconstruction of the System using Equivalent Disturbance

$$e_c(s) = \frac{1}{1 + P_n(s)C(s)} \left[y_c - \frac{P_n(s)}{1 + L_n(s)} d_{eq} \right]. \tag{3.32}$$

The effect of d_{eq} on e_c decreases by a factor of $1 + L_n(s)$ compared to the control loop in Figure 3.5. A stability analysis based on small-gain theorem can be found in [82] for the case of multiplicative model uncertainty, $P(s) = P_n(s)[1 + \Delta(s)]$.

Figure 3.9 depicts the architecture in Chapter 2 in which the adaptive controller is designed using the approach in [63]. The adaptive controller can also be replaced by that in [62], which is utilized in Chapter 2. It is apparent that the architecture in Figure 3.9 is equivalent to the RIC framework in Figure 3.7 . With $u^* = -u_{nn}$, the architectures are identical if $\Sigma_p = P(s)$. Thus, we can design a linear controller $K(s)$ in Figure 3.9, using RIC, to achieve performance enhancement when actuator nonlinearities (dead zone and backlash) belong to the class defined in [77]. In addition, when a class of nonlinearities described in Section 3.2 are present, the CH technique can be introduced. In this case, the architecture in the dotted box in Figure 3.9 is modified as that in Figure 3.1. The rationale of CH combined with the RIC design is as follows. When actuation is nonlinear at low control command levels, the RIC controller boosts the control command. When actuation is nonlinear at high control command levels, CH modifies the control command to $P_n(s)$ to protect the adaptive process.

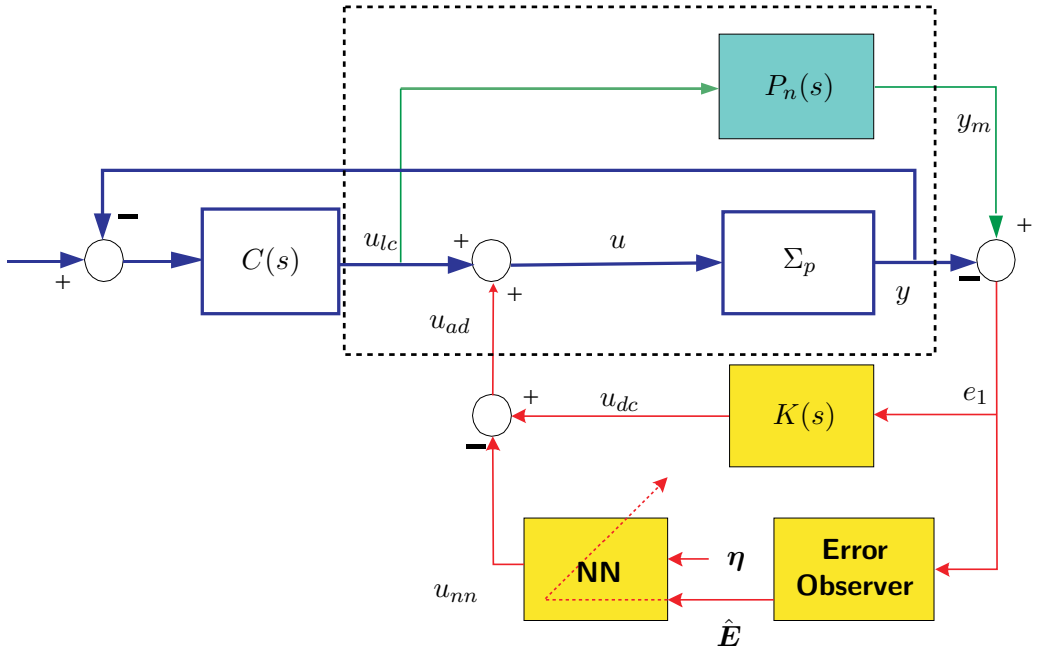

Fig. 3.9: Internal Model Following Architecture with Adaptive Elements

3.3.2 Augmenting Control Design

With CH introduced, the plant model dynamics in (3.23) are modified as:

$$y_m(s) = P_n(s)(u_{lc} - u_h), \tag{3.33}$$

which is realized as in (3.4) with system matrices given in (3.24). Define the tracking error vector

$$\boldsymbol{e} = \boldsymbol{\xi}_m - \boldsymbol{\xi}. \tag{3.34}$$

With the following control signal augmentation:

$$u = u_{lc} + u_{ad} = u_{lc} + u_{dc} - u_{nn}, \tag{3.35}$$

comparing (3.22) to (3.4) leads to the following tracking error dynamics:

$$\begin{aligned} \dot{\boldsymbol{e}} =& A_m \boldsymbol{e} + \boldsymbol{b}_m(-u_{dc} + u_{nn} - \Phi(\boldsymbol{z}_o, \boldsymbol{\xi}, u)) \\ \dot{\boldsymbol{z}}_o =& \boldsymbol{f}(\boldsymbol{z}_o, \boldsymbol{\xi}) \\ e_1 =& \boldsymbol{c}_m^T \boldsymbol{e}, \end{aligned} \tag{3.36}$$

where u_{dc} is the control signal designed by RIC, and u_{nn} is an adaptive signal to approximately cancel the uncertainty $\Phi(\boldsymbol{z}_o, \boldsymbol{\xi}, u)$, which is defined by

$$\Phi(\boldsymbol{z}_o, \boldsymbol{\xi}, \boldsymbol{\xi}_m, u) = \frac{1}{d_r}[h_r(\boldsymbol{z}_o, \boldsymbol{\xi}, g(u)) - \hat{h}_r(\boldsymbol{\xi}, \hat{g}(u))] = \frac{1}{d_r}[h_r(\boldsymbol{z}_o, \boldsymbol{\xi}, g(u)) - \boldsymbol{c}_r^T \boldsymbol{\xi} - d_r \hat{g}(u)]. \tag{3.37}$$

Remark 3.4. Note that the control u_{ad} in (3.35) is equivalent to that in (2.14). However, unlike Δ in (3.10), the uncertainty $\Phi(\boldsymbol{z}_o, \boldsymbol{\xi}, u)$ in (3.37) is defined without $\boldsymbol{x}_m$. The uncertainty also implies that the effect of actuator nonlinearities is adaptively compensated by the employed NN. Therefore, the role of u_{dc} is to further reject the NN reconstruction error by incorporating disturbance observer design.

A single hidden layer NN (SHLNN) is used to approximate Φ in (3.37). Since the uncertainty Φ is a function of states and control, we recall the main result from [65] that enables approximation of unknown bounded processes using finite input/output history.

Theorem 3.2. *For arbitrary $\epsilon > 0$, there exist a $n_0 \in \mathbb{N}$, a $d^* > 0$, and bounded constant weights M, N such that for every $n_h \geq n_0$ and $0 < d \leq d^*$,*

$$\Phi(\boldsymbol{z}_o, \boldsymbol{\xi}, u) = M^T \boldsymbol{\sigma}(N^T \boldsymbol{\eta}) + \varepsilon(\boldsymbol{\eta}, d), \;\; \|\varepsilon(\boldsymbol{\eta}, d)\| \leq \epsilon, \tag{3.38}$$

where $\varepsilon(\boldsymbol{\eta})$ is the NN reconstruction error, n_h is the number of neurons in the hidden layer, and $\boldsymbol{\eta}$ is the network input vector defined in (2.21), with $\boldsymbol{x}_m$ removed, $\boldsymbol{\sigma}$ being a vector of squashing functions $\sigma(\cdot)$, its i^{th} element being defined as $\left[\boldsymbol{\sigma}(N^T\boldsymbol{\eta})\right]_i = \sigma\left[(N^T\boldsymbol{\eta})_i\right]$.

The adaptive signal u_{nn} is designed as

$$u_{nn} = \widehat{M}^T \boldsymbol{\sigma}(\widehat{N}^T \boldsymbol{\eta}) \tag{3.39}$$

where $\widehat{M}$ and $\widehat{N}$ are estimates of M and N to be adapted on-line.

To design $K(s)$ using RIC, a critical step involves defining an equivalent disturbance d_{eq} as in (3.30). We define it as the approximation error between u_{nn} and Φ in (3.37)

$$d_{eq} \triangleq -u_{nn} + \Phi(\boldsymbol{z}_o, \xi, u). \tag{3.40}$$

This implies that the NN approximation error is further attenuated by u_{dc}. The linear controller $K(s)$ is described by

$$\begin{aligned} \dot{\boldsymbol{x}}_{dc} &= A_{dc}\boldsymbol{x}_{dc} + b_{dc}e_1 \\ u_{dc} &= \boldsymbol{c}_{dc}^T\boldsymbol{x}_{dc} + \boldsymbol{d}_{dc}e_1\,. \end{aligned} \tag{3.41}$$

Applying u_{dc} in (3.41) to (3.36) leads to the following error dynamics

$$\begin{aligned} \dot{\boldsymbol{E}} &= F\boldsymbol{E} - \boldsymbol{g}_E d_{eq} \\ \boldsymbol{Z} &= \boldsymbol{c}_E^T\boldsymbol{E}, \end{aligned} \tag{3.42}$$

where $\boldsymbol{E}^T = [\ \boldsymbol{e}^T \quad \boldsymbol{x}_{dc}^T\ ]$, and

$$F = \begin{bmatrix} A_m - \boldsymbol{b}_m d_{dc}\boldsymbol{c}_m^T & -\boldsymbol{b}_m\boldsymbol{c}_{dc}^T \\ \boldsymbol{b}_{dc}\boldsymbol{c}_m^T & A_{dc} \end{bmatrix},\ \boldsymbol{g}_E = \begin{bmatrix} \boldsymbol{b}_m \\ 0 \end{bmatrix},\ \boldsymbol{c}_E^T = \begin{bmatrix} \boldsymbol{c}_m^T \\ I \end{bmatrix}. \tag{3.43}$$

Since F is Hurwitz, for any $Q_E > 0$, there exists a $P_E > 0$ such that

$$F^T P_E + P_E F + Q_E = 0. \tag{3.44}$$

Note that the error dynamics in (3.42) have the same form as in [63], thus the NN weights update law can be derived in the same manner as in [63]. The NN weights update law requires teaching signals which are generated by the estimator for the error dynamics in (3.42).

3.3.3 Reduced Error Observer and Adaptation Law

With the definition of d_{eq} in (3.40), the error dynamics in (3.36) can be equivalently described by

$$e_1(s) = P_n(s)[-u_{dc} - d_{eq}]. \tag{3.45}$$

According to (3.28), u_{dc} is an estimate for the equivalent disturbance as shown in Figure 3.6. Therefore, by the relation between $Q(s)$ and $K(s)$ in (3.27), Eq.(3.45) can be rearranged as follows

$$e_1(s) = -P_n(s)(1 - Q(s))d_{eq}. \tag{3.46}$$

Since the Q-filter is designed so that $(1 - Q(s))d_{eq} \approx 0$ below a cut-off frequency, we construct an error observer assuming $(1 - Q(s))d_{eq} \approx 0$ for the dynamics in (3.46)

$$\begin{aligned} \dot{\hat{\boldsymbol{e}}} &= A_m \hat{\boldsymbol{e}} + L(e_1 - \hat{e}_1) \\ \hat{e}_1 &= \boldsymbol{c}_m^T \hat{\boldsymbol{e}}, \end{aligned} \tag{3.47}$$

The observer gain L is designed so that $A_m - L\boldsymbol{c}_m^T$ is Hurwitz.

Using the estimate in (3.47), the teaching signal for the NN is constructed as

$$\widehat{\boldsymbol{E}} = \begin{bmatrix} \hat{\boldsymbol{e}}^T & \boldsymbol{x}_{dc}^T \end{bmatrix}^T. \tag{3.48}$$

The NN weights $\widehat{M},\ \widehat{N}$ are updated according to the following adaptation laws [63]

$$\begin{aligned} \dot{\widehat{M}} &= -\Gamma_M[(\hat{\boldsymbol{\sigma}} - \hat{\sigma}'\widehat{N}^T\boldsymbol{\eta})\widehat{\boldsymbol{E}}^T P_E \bar{\boldsymbol{b}} + k\widehat{M}], \\ \dot{\widehat{N}} &= -\Gamma_N[\boldsymbol{\eta}\widehat{\boldsymbol{E}} P_E \bar{\boldsymbol{b}} \widehat{M}^T \hat{\sigma}' + k\widehat{N}] \end{aligned} \tag{3.49}$$

in which $\Gamma_M,\ \Gamma_N > 0$ are positive definite adaptation gain matrices, $k > 0$ is a $\sigma-$modification constant, $\hat{\boldsymbol{\sigma}} \triangleq \boldsymbol{\sigma}(\widehat{N}\boldsymbol{\eta})$, $\hat{\sigma}'$ is the Jacobian computed at the estimates: $\hat{\sigma}' = \sigma'(\widehat{N}\boldsymbol{\eta})$.

Theorem 3.3. *Consider the system in (3.22) that satisfies Assumptions 2.1–3.3. Together with the NN adaptation rule in (3.49), the control law in (3.35) guarantees that the signal e_c is ultimately bounded.*

Proof. Ultimate boundedness with CH has been addressed in Theorem 3.1. Following the lines in [63], it can be shown that the tracking error, e_1, is bounded. Then, Assumption 2.2 ensures that $\boldsymbol{z}_o$ is bounded. Since the linear controller $C(s)$ is designed to stabilize the plant model $P_n(s)$, it immediately follows that if y_c and e_1 are bounded, then e_c is bounded.

3.3.4 Illustrative Design Example

We illustrate the proposed approach using the three-disk torsional pendulum in Figure 2.7. In this simulation, the equations of motion for the system are as follows:

$$\begin{aligned} J_1\ddot{\theta}_1 + K(\theta_1 - \theta_2) + f_{c_1}(\dot{\theta}_1) &= 0, \\ J_2\ddot{\theta}_2 - K\theta_1 + 2K\theta_2 - K\theta_3 + f_{c_2}(\dot{\theta}_2) &= 0, \\ J_3\ddot{\theta}_3 - K(\theta_2 - \theta_3) + f_{c_3}(\dot{\theta}_3) &= K_{vt}g(u), \end{aligned} \tag{3.50}$$

where $f_{c_i},\ i = 1, 2, 3$ represents dynamic friction torque as in [108].

$$\dot{z}_i = \dot{\theta}_i - \frac{\sigma_f |\dot{\theta}_i|}{G(\dot{\theta}_i)} z_i,\ G(\dot{\theta}_i) = T_c + (T_s - T_c)\exp\left(-(\frac{\dot{\theta}_i}{\dot{\theta}_s})^2\right)$$
$$f_{c_i} = \sigma_0 z_i + \sigma_1 \dot{z}_i + \sigma_2 \dot{\theta}_i,\ i = 1, 2, 3, \tag{3.51}$$

where $T_c = 0.075$ N $\cdot$ m is the Coulomb friction level, $T_s = 0.083$ N $\cdot$ m is the stiction torque, and $\dot{\theta}_s = 0.0001$ rad/s is the Stribeck velocity. The constants $\sigma_f = 4$ N $\cdot$ m, $\sigma_0 = 2$ N $\cdot$ m, $\sigma_1 = 0.1$ N $\cdot$ m $\cdot$ s are friction parameters, and $\sigma_2 = 0.0018$ kg $\cdot$ m/s represents a viscous damping coefficient. This model of dynamic friction is generally adopted in adaptive dynamic compensation approaches [109, 110]. The control input u is the voltage applied to the control motor, and the stiction value T_c corresponds to the control voltage $0.2V$ with the given gain K_{vt}. The actuator nonlinearity $g(u)$ consists of dead zone and saturation with $u_d = \pm 0.1V$ and $u_{lim} = 1.2V$ as depicted in Figure 3.10. However, the estimate for the actuator $\hat{g}(u)$ only considers the saturation characteristic.

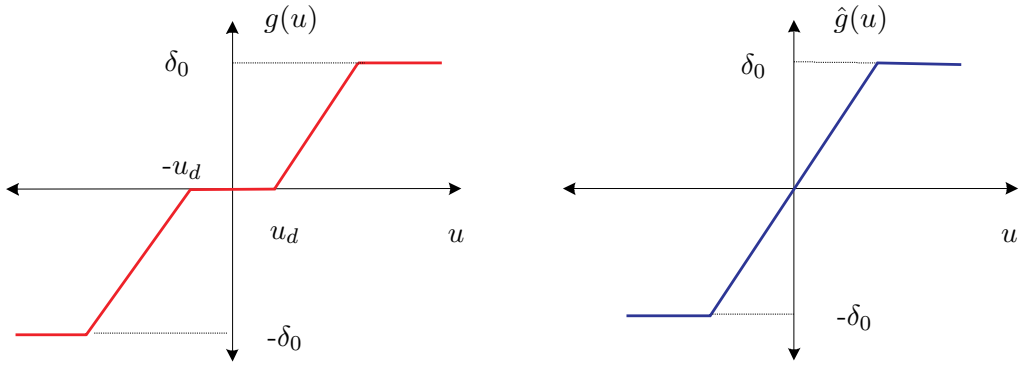

Fig. 3.10: Actuator Characteristic $g(u)$ and its Estimate $\hat{g}(u)$ in CH.

The bottom disk angle θ_3 is selected as the regulated variable. That is, all the parameters related to the existing control system are the same as in Section 2.7.1. Since CH is employed to address actuator saturation, the modelling error in (2.40) is modified as in (3.37)

$$\Phi = \frac{1}{K_n}[\frac{K}{J_3}(\theta_2 - \theta_3) - \frac{1}{J_3} f_{c_3}(\dot{\theta}_3) + \frac{K_{vt}}{J_3} g(u) + c\dot{\theta}_3 - K_n \hat{g}(u)]. \tag{3.52}$$

The RIC controller $K(s)$ is designed in the same manner as $C(s)$, which puts the dominant mode at $\omega_{=}20rad/s$ and $\zeta = 0.8$. This results in

$$u_{dc} = 29.65\frac{s + 0.18}{s + 32} e_1. \tag{3.53}$$

Using the relation in (3.27), the frequency response of $Q(s)$ and $1 - Q(s)$ are shown in Figure 3.11. Figure 3.11 shows that additional controller $K(s)$ is designed so that 20db

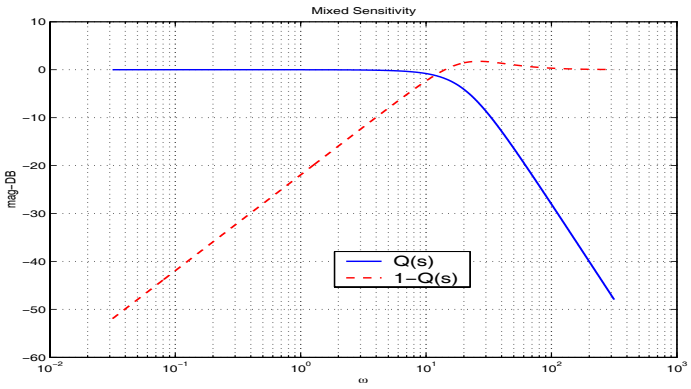

Fig. 3.11: Frequency Response of $Q(s)$ and $1 - Q(s)$.

gain decrease is achieved around $\omega = 1$rad/s with respect to the external disturbance.

The reduced error observer is designed so that the eigenvalues of $A_m - L\boldsymbol{c}_m^T$ are located at $-82.12 \pm 82.12i$. The SHLNN is introduced to approximate the uncertainty Φ. It has 20 hidden layers, with 6 delayed values of y for $\bar{\boldsymbol{y}}_d$ combined with 4 delayed values of u for $\bar{\boldsymbol{u}}_d$ as its input vector, and has the following learning rates and $\sigma-$modification factor:

$$\Gamma_M = 0.5I,\ \Gamma_N = 0.5I,\ k = 1.3.$$

Figure 3.12(a) compares output responses of the system in (3.50) regulated only by the controller $C(s)$ in (2.41) to that of the plant model in (2.39) regulated by the same controller. The reference command is made up of a square wave of 1 rad. at 0.2 Hz. The response is oscillatory and exhibits a large steady state error. When $C(s)$ is augmented by the controller architecture in Figure 3.9, the steady-state error and oscillations are drastically decreased as shown in Figure 3.12(b). The commanded control signal u and the achieved control signal $g(u)$ are compared in Figure 3.13(a). The modelling error Φ and the adaptive signal u_{nn} are compared in Figure 3.13(b) to illustrate NN adaptation. The overall compensation scheme is further justified by the results in Figure 3.14. Without the adaptive signal u_{nn}, as shown in Figure 3.14(a), the plant model output y_m and the system output y do not converge to each other. Without u_{dc}, Figure 3.14(b) shows that bounded tracking is achieved, but is much more oscillatory than that in Figure 3.12(b).

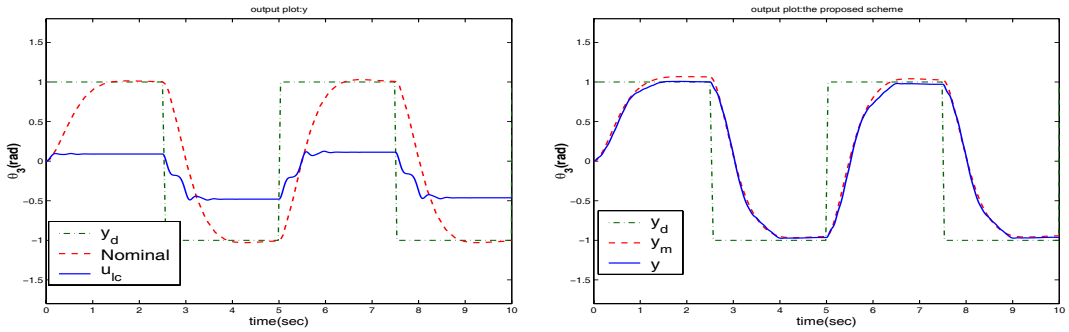

(a) Comparison of the Nominal Loop Response and the Output Regulated only by u_{lc}.

(b) Output Response with $u = u_{lc} + u_{dc} - u_{nn}$

Fig. 3.12: Comparison of Output Responses when the System is Regulated Only by u_{lc} and the Proposed Scheme

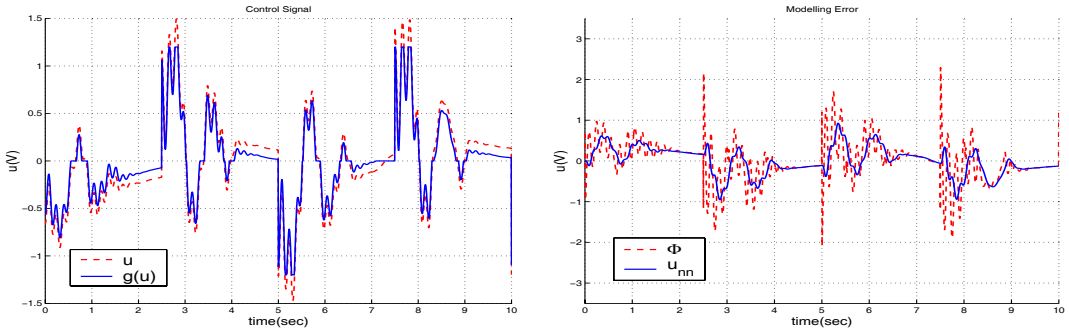

(a) Comparison of u and $g(u)$

(b) Comparison of Φ and u_{nn}

Fig. 3.13: Control Signals and Actuator Outputs with the Proposed Scheme

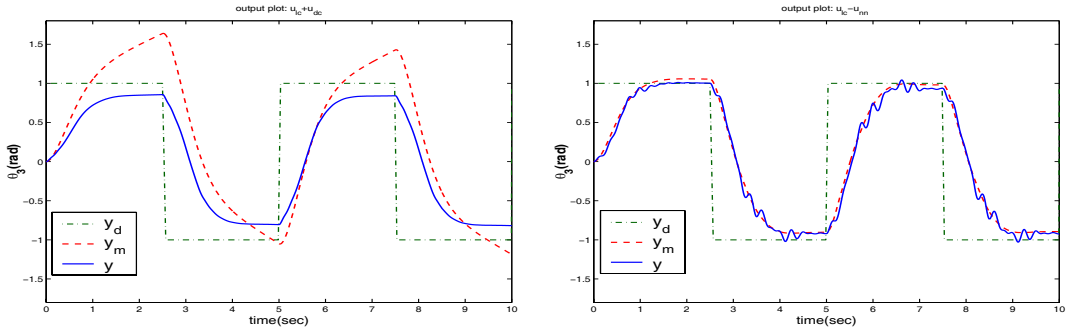

(a) Output Responses when $u = u_{lc} + u_{dc}$

(b) Output Responses when $u = u_{lc} - u_{nn}$

Fig. 3.14: Output Responses without u_{dc} or u_{nn}.

The role of CH can be illustrated when the magnitude of the reference command increases to 3 rad. The responses with and without CH are compared in Figure 3.15. Without CH, the plant model output y_m and the system output y significantly deviate from each other as shown in Figure 3.15(a). Whenever the actuator is in saturation, without CH, the adaptive signal u_{nn} loses track of the uncertainty Φ as shown in Figures 3.15(c) and 3.15(e). With CH, almost perfect tracking is maintained with correct NN adaptation as shown in Figures 3.15(b), 3.15(d) and 3.15(f).

3.4 Conclusions

This chapter describes a control design that addresses actuator nonlinearities in the internal model-following control architecture. A key ingredient of control design is control hedging and the structural equivalence between the architecture of the internal model-following control and that of a disturbance observer using the framework of robust internal-loop compensation. Multiple types of actuator nonlinearities can be effectively compensated when the disturbance observer is combined with control hedging. Experimental results with the three-disk torsional pendulum illustrate the effectiveness of control hedging with control voltage saturation. Simulation results further demonstrate the validity of the approach when the actuator nonlinearities consist of dead zone and saturation.

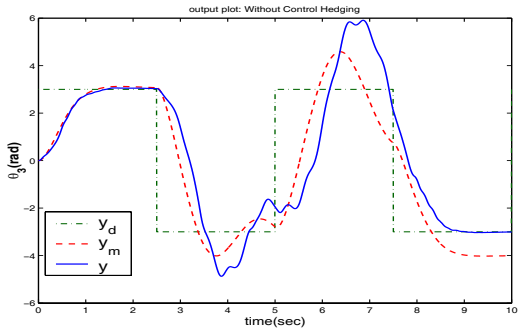

(a) Output Responses Without CH

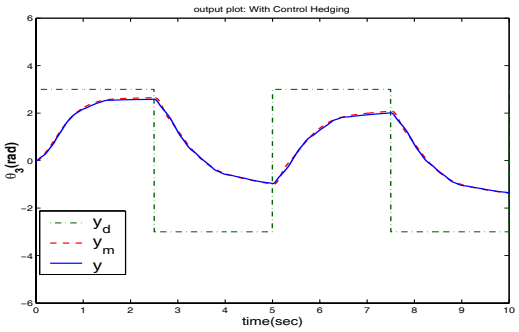

(b) Output Responses with CH

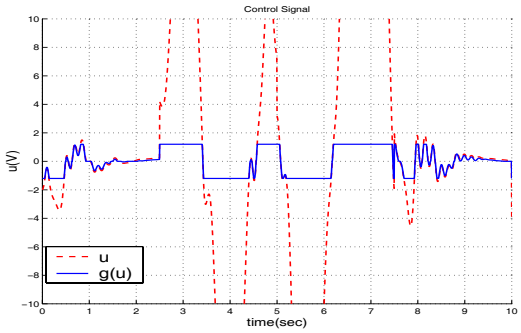

(c) u and $g(u)$ Without CH

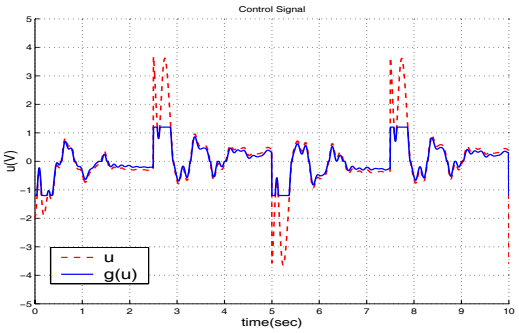

(d) u and $g(u)$ With CH

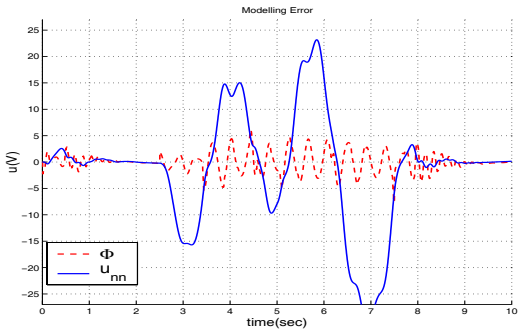

(e) Φ and u_{nn} Without CH

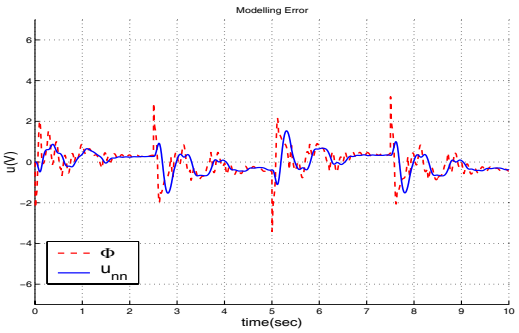

(f) Φ and u_{nn} With CH

Fig. 3.15: Comparison of Responses with/without CH

CHAPTER 4

OUTPUT FEEDBACK AUGMENTATION IN EXTERNAL MODEL-FOLLOWING CONTROL

In this chapter, we address augmenting a fixed gain linear controller with an output feedback adaptive element in the framework of external model-following control. In this architecture, adaptive control does not rely on feedback linearization, thus it can be applied to non-minimum phase systems. We assume a linear model for the plant dynamics that has the same relative degree as the true plant dynamics. We further assume that this linear model represents the non-minimum phase zeros of the true plant to a sufficient degree of accuracy, and that the linear controller takes into account the presence of these zeros. By this, we mean that a conic sector bound holds on the modelling error of the non-minimum phase internal dynamics. Any unmodelled dynamics, present within the bandwidth of the control design, is assumed to be globally exponentially stable and globally Lipschitz. The approach is experimentally validated using the three-disk torsional pendulum and an inverted pendulum.

4.1 Introduction

While stabilization and tracking problems in minimum phase systems are well understood in state and output feedback settings [5, 19, 20, 68], feedback control system design for *non-minimum* phase systems remains a challenging problem in nonlinear control theory. Early state feedback results in control of non-minimum phase systems include the nonlinear regulator equation [111] and non-causal inversion [112, 113]. In an output feedback setting, most approaches [9, 12] employ a high-gain observer [13] to realize a feedback controller based on partial states (time derivatives of the output up to the relative degree of the system). In [14], a stabilization problem for a non-minimum phase system with parametric uncertainty has been solved by employing a high gain observer.

In this chapter we revisit the problem formulation in Chapter 2 and develop a methodology that does not rely on feedback inversion, so it can be applied to non-minimum phase systems. From the perspective of augmenting adaptive control, the method extends the state feedback method in [61] to an output feedback method. As in [61], we make use of a reference model, the linear design model regulated by a linear controller. Main assumptions are that the relative degree of the regulated output variable is the same as that of the linear model used in the design of the linear controller, and that the zero dynamics of the linear model represent the internal dynamics of the non-minimum phase system to sufficient accuracy. By this, we mean that the unstable zero dynamics are recognized and addressed in the design of the linear controller. In linear systems, unstable zero dynamics are not as problematic as nonlinear systems, regardless of limitations on achievable performance [114]. To compensate for the modelling errors that arise from linear approximation of the nonlinear system, a NN-based adaptive element is introduced to augment the linear controller. This rationale is in line with that in [14] in the sense that we make use of unstable zero dynamics for feedback purposes, in contrast to feedback inversion which renders the zero dynamics unobservable in the output.

This chapter is organized as follows: After we present the control problem in Section 4.2, the approach for augmenting a linear controller with an adaptive element is described in Section 4.3. Experimental results with the torsional pendulum follow to demonstrate the validity of the approach for flexible systems in Section 4.4. Section 4.5 presents experimental results for an inverted pendulum to show its applicability to non-minimum phase systems. Conclusions are given in Section 4.6.

4.2 Control Architecture

The conceptual layout for augmenting a linear controller in the external model-following control architecture is depicted in Figure 4.1. The shaded portion of the diagram highlights the elements to be added. In the typical closed-loop system, the true plant is regulated by a linear controller that is designed using a linear model so that y_m tracks the reference command y_c. We assume that the linear controller meets all the design specifications in

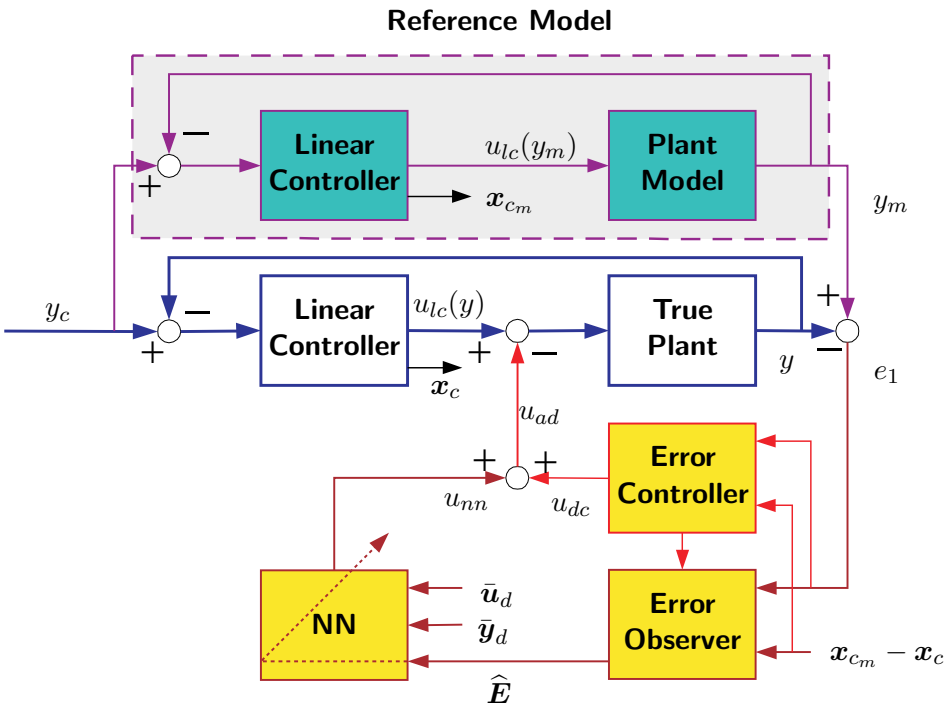

Fig. 4.1: Output Feedback Augmentation in the External Model Following Architecture

the absence of modelling errors. This closed-loop system constitutes the reference model, which specifies the best performance that can be achieved by the adaptive control design. The adaptive process augments the linear controller by adding u_{ad} to the linear controller output $u_{lc}(y)$ to render the tracking error $e_1 = y_m - y$ ultimately bounded. This is achieved by employing the adaptive control method in [63]. The error observer is employed to estimate the states of the error dynamics $\widehat{\boldsymbol{E}}$ to construct a teaching signal for a NN. The NN reconstructs the system uncertainty from a finite history of available input/output $\bar{\boldsymbol{u}}_d, \bar{\boldsymbol{y}}_d$ to form the adaptive signal u_{nn}. The architecture provides an additional control degree of freedom u_{dc}. To accelerate NN adaptation and reduce the ultimate bound on the tracking error, a linear controller can be employed depending on specific applications.

4.3 Error Dynamics and Adaptive Output Feedback Augmentation

Consider the system presented in normal form in (2.5). Without loss of generality, explicit dependence on external disturbances is removed for simplicity of presentation. After a

suitable change of coordinates in the state space, the linear plant model in (2.7) can also be put in the normal form

$$\begin{aligned}
\dot{\xi}_{m_1} =& \xi_{m_2} \\
& \vdots \\
\dot{\xi}_{m_r} =& \boldsymbol{h}_0^T \boldsymbol{z}_m + a_1 \xi_{m_1} + \cdots + a_r \xi_{m_r} + d_r u \\
\dot{\boldsymbol{z}}_m =& F_0 \boldsymbol{z}_m + \boldsymbol{g}_0 \xi_{m_1} \\
y_l =& \xi_{m_1}
\end{aligned} \tag{4.1}$$

where $\boldsymbol{z}_m \in \mathbb{R}^{m-r}$ are the states of the internal dynamics. Compared to the plant model in (4.1), the system in (2.5) can be written as:

$$\begin{aligned}
\dot{\xi}_1 =& \xi_2 \\
& \vdots \\
\dot{\xi}_r =& \boldsymbol{h}_0^T \boldsymbol{z}_1 + a_1 \xi_1 + \cdots + a_r \xi_r + d_r [u + \Delta_1(\boldsymbol{z}_1, \boldsymbol{z}_2, \boldsymbol{\xi}, u)] \\
\dot{\boldsymbol{z}}_1 =& F_0 \boldsymbol{z}_1 + \boldsymbol{g}_0 \xi_1 + \boldsymbol{\Delta}_2(\boldsymbol{z}_1, \boldsymbol{z}_2, \boldsymbol{\xi}) \\
\dot{\boldsymbol{z}}_2 =& \boldsymbol{f}_2(\boldsymbol{z}_1, \boldsymbol{z}_2, \boldsymbol{\xi}) \\
y =& \xi_1
\end{aligned} \tag{4.2}$$

where $\boldsymbol{z}_o^T = [\boldsymbol{z}_1^T \ \boldsymbol{z}_2^T]$ and $\boldsymbol{z}_1 \in R^{m-r}$ represents the part of the states of the internal dynamics that are modelled through $\boldsymbol{z}_m$ in (4.1), and $\boldsymbol{z}_2 \in R^{n-m}$ are introduced to represent any unmodelled dynamics if $m < n$. The terms Δ_1 and $\boldsymbol{\Delta}_2$ represent the matched and unmatched uncertainties respectively, defined as

$$\begin{aligned}
\Delta_1(\boldsymbol{z}_1, \boldsymbol{z}_2, \boldsymbol{\xi}, u) &= \frac{1}{d_r}[h(\boldsymbol{z}_1, \boldsymbol{z}_2, \boldsymbol{\xi}, u) - \boldsymbol{h}_0^T \boldsymbol{z}_1 - a_1 \xi_1 \cdots - a_r \xi_r - d_r u] \\
\boldsymbol{\Delta}_2(\boldsymbol{z}_1, \boldsymbol{z}_2, \boldsymbol{\xi}) &= \boldsymbol{f}_1(\boldsymbol{z}_1, \boldsymbol{z}_2, \boldsymbol{\xi}) - F_0 \boldsymbol{z}_1 - \boldsymbol{g}_0 \xi_1
\end{aligned} \tag{4.3}$$

Assumption 4.1. *The zero solution of $\dot{\boldsymbol{z}}_2 = \boldsymbol{f}_2(0, \boldsymbol{z}_2, 0)$ is globally exponentially stable, and the function $\boldsymbol{f}_2(\boldsymbol{z}_1, \boldsymbol{z}_2, \boldsymbol{\xi})$ is globally Lipschitz in its arguments.*

The plant model in (4.1), when regulated by (2.9), constitutes a "reference model". Defining $\boldsymbol{\xi}_m^T \triangleq [\ \xi_{m_1} \ \cdots \ \xi_{m_r}\ ]$ and denoting $\boldsymbol{x}_{c_m}$ the states of the controller in (2.9)

when applied to (4.1), i.e. when y is replaced by y_m in (2.9), the "reference model" can be written as:

$$\begin{aligned} \dot{\bar{\boldsymbol{x}}}_l &= \bar{A}\bar{\boldsymbol{x}}_l + \bar{\boldsymbol{b}}_c y_c, \quad \bar{\boldsymbol{x}}_l \in \mathbb{R}^{m+n_c} \\ y_m &= \bar{\boldsymbol{c}}^T \bar{\boldsymbol{x}}_l \end{aligned} \tag{4.4}$$

where $\bar{\boldsymbol{x}}_l^T = \begin{bmatrix} \boldsymbol{\xi}_l^T & \boldsymbol{z}_m^T & \boldsymbol{x}_{c_m}^T \end{bmatrix}$,

$$\bar{A} = \begin{bmatrix} F_\xi - \boldsymbol{g}_\xi d_c \boldsymbol{c}_\xi^T & B_z & \boldsymbol{g}_\xi \boldsymbol{c}_c^T \\ \boldsymbol{g}_0 \boldsymbol{c}_\xi^T & F_0 & 0 \\ -\boldsymbol{b}_c \boldsymbol{c}_\xi^T & 0 & A_c \end{bmatrix}, \ \bar{\boldsymbol{b}}_c = \begin{bmatrix} \boldsymbol{g}_\xi d_c \\ 0 \\ \boldsymbol{b}_c \end{bmatrix}, \ \bar{\boldsymbol{c}} = \begin{bmatrix} \boldsymbol{c}_\xi \\ 0 \\ 0 \end{bmatrix}, \tag{4.5}$$

and

$$F_\xi = \begin{bmatrix} 0 & 1 & 0 & \cdots \\ 0 & 0 & 1 & \cdots \\ \vdots & \vdots & \vdots & \vdots \\ a_1 & a_2 & \cdots & a_r \end{bmatrix}_{r\times r}, \ B_z = \begin{bmatrix} 0 \\ 0 \\ \vdots \\ \boldsymbol{h}_0^T \end{bmatrix}_{r\times(m-r)}, \ \boldsymbol{g}_\xi = \begin{bmatrix} 0 \\ 0 \\ \vdots \\ d_r \end{bmatrix}_r, \ \boldsymbol{c}_\xi = \begin{bmatrix} 1 \\ 0 \\ \vdots \\ 0 \end{bmatrix}_r. \tag{4.6}$$

Note that the reference model in (4.4) is equivalent to the nominal closed loop system in (2.10). Thus, $\bar{A}, \bar{\boldsymbol{b}}_c, \bar{\boldsymbol{c}}$ in (4.5) are matrices obtained by a coordinate transformation from (2.10).

Let

$$u = u_{lc} - u_{ad} \tag{4.7}$$

When the control signal u, with u_{lc} defined in (2.9), is applied to the system in (4.2), it results in the following closed loop system:

$$\begin{aligned} \dot{\bar{\boldsymbol{x}}} &= \bar{A}\bar{\boldsymbol{x}} + \bar{\boldsymbol{b}}_c y_c - \bar{\boldsymbol{b}} u_{ad} + \boldsymbol{\Delta} \\ \dot{\boldsymbol{z}}_2 &= \boldsymbol{f}_2(\boldsymbol{z}_2, \boldsymbol{z}_1, \boldsymbol{\xi}) \\ y &= \bar{\boldsymbol{c}}^T \bar{\boldsymbol{x}}\,, \end{aligned} \tag{4.8}$$

in which $\bar{\boldsymbol{x}}^T = \begin{bmatrix} \boldsymbol{\xi}^T & \boldsymbol{z}_1^T & \boldsymbol{x}_c^T \end{bmatrix}$, $\bar{\boldsymbol{b}}^T = \begin{bmatrix} \boldsymbol{g}_\xi^T & 0 & 0 \end{bmatrix}$, $\boldsymbol{\Delta}^T = \begin{bmatrix} \boldsymbol{\Delta}_1^T & \boldsymbol{\Delta}_2^T & 0 \end{bmatrix}$ $\boldsymbol{\Delta}_1^T = \begin{bmatrix} 0 & \cdots & d_r \Delta_1 \end{bmatrix}$.

With the following definition of the error vector

$$\boldsymbol{E} \triangleq \bar{\boldsymbol{x}}_l - \bar{\boldsymbol{x}} \tag{4.9}$$

comparing (4.4) and (4.8), the error dynamics can be written as:

$$\begin{aligned} \dot{\boldsymbol{E}} =& \bar{A}\boldsymbol{E} + \bar{\boldsymbol{b}}(u_{ad} - \Delta_1) - B\boldsymbol{\Delta}_2 \\ \boldsymbol{z}_2 =& \boldsymbol{f}_2(\boldsymbol{z}_2, \boldsymbol{z}_1, \boldsymbol{\xi}) \\ \boldsymbol{Z} =& \bar{C}\boldsymbol{E}\,, \end{aligned} \tag{4.10}$$

where $\boldsymbol{Z}$ represents the signals available for feedback:

$$\boldsymbol{Z} = \begin{bmatrix} y_l - y \\ \boldsymbol{x}_{cl} - \boldsymbol{x}_c \end{bmatrix} = \underbrace{\begin{bmatrix} \boldsymbol{c}_m & 0 \\ 0 & I \end{bmatrix}}_{\bar{C}} \boldsymbol{E}\,, \tag{4.11}$$

and $B^T = \begin{bmatrix} 0 & I & 0 \end{bmatrix}$, $I \in R^{(m-r)\times(m-r)}$. Since $\bar{A}$ is Hurwitz by design, there exist a $P_n = P_n^T > 0$ such that for an arbitrary $Q_n > 0$,

$$\bar{A}^T P_n + P_n \bar{A} + Q_n = 0 \tag{4.12}$$

Note that this is the equivalent equation in (3.8), for $\bar{A}$ is the transformed matrix from that in (3.8).

The control signal u_{ad} is designed to approximately cancel Δ_1. Notice from (4.7) and (4.3) that Δ_1 depends on u_{ad} through u, and that the role of u_{ad} is to cancel Δ_1.

Assumption 4.2. *There exists a fixed point to the equation $u_{ad} = \Delta(\boldsymbol{z}_0, \boldsymbol{\xi}, u)$ uniformly in $(\boldsymbol{z}_o, \boldsymbol{\xi}) \in \mathcal{D}_{z_o} \times \mathcal{D}_\xi$ on $\mathcal{D}_u$.*

The set $\mathcal{D}_{z_o} \times \mathcal{D}_\xi$ is defined in the lines after (2.5). This assumption is exactly the same as Assumption 2.4 except the definition of uncertainty. Thus, the same analysis after the assumption 2.4 remains valid.

The unmatched uncertainty $\boldsymbol{\Delta}_2$ is assumed to satisfy a *linear* bound in the error norm as in [115].

Assumption 4.3. $\|\boldsymbol{\Delta}_2(\boldsymbol{z}_1, \boldsymbol{z}_2, \boldsymbol{\xi})\| \le \pi_1 \left\| \begin{bmatrix} \boldsymbol{\xi} \\ \boldsymbol{z}_1 \end{bmatrix} \right\| + \pi_2 \|\boldsymbol{z}_2\| + \pi_3\,, \quad (\boldsymbol{z}_1, \boldsymbol{z}_2, \boldsymbol{\xi}) \in \mathcal{D}_{z_o} \times \mathcal{D}_\xi$

with some $\pi_1, \pi_2, \pi_3 > 0$.

A SHLNN is used to approximate $\Delta_1(\boldsymbol{z}_o, \boldsymbol{\xi}, u)$ in (4.3), which can be approximated using input/output delayed values, $\boldsymbol{\eta}$ in (2.21) with $\boldsymbol{x}_m$ removed, as in Theorem 3.2. That is, the NN input is as follows

$$\boldsymbol{\eta}(t) = \begin{bmatrix} 1 & \bar{u}_d^T(t) & \bar{y}_d^T(t) \end{bmatrix}^T, \quad \|\boldsymbol{\eta}\| \leq \eta^*, \tag{4.13}$$

where $\bar{u}_d t)$, $\bar{y}_d(t)$ are defined in the following lines after (2.21). The adaptive signal u_{ad} is designed as in (3.39)

$$u_{ad} = u_{nn} = \hat{M}^T \boldsymbol{\sigma}(\hat{N}^T \boldsymbol{\eta}). \tag{4.14}$$

The weight adaptation laws are similar to the ones in [63]. To this end, we introduce the following linear error observer for the dynamics in (4.10):

$$\begin{aligned} \dot{\widehat{\boldsymbol{E}}} &= \bar{A}\widehat{\boldsymbol{E}} + K(\boldsymbol{z} - \widehat{\boldsymbol{z}}) \\ \widehat{\boldsymbol{Z}} &= \bar{C}\widehat{\boldsymbol{E}}, \end{aligned} \tag{4.15}$$

where K is chosen to make $\bar{A} - K\bar{C}$ stable. Then, the NN weights update laws are the same as (3.49) except that P_n is a solution to the equation in (4.12)

$$\begin{aligned} \dot{\widehat{M}} &= -\Gamma_M[(\hat{\boldsymbol{\sigma}} - \hat{\sigma}'\widehat{N}^T\boldsymbol{\eta})\widehat{\boldsymbol{E}}^T P_n \bar{\boldsymbol{b}} + k\widehat{M}], \\ \dot{\widehat{N}} &= -\Gamma_N[\boldsymbol{\eta}\widehat{\boldsymbol{E}} P_n \bar{\boldsymbol{b}} \widehat{M}^T \hat{\sigma}' + k\widehat{N}] \end{aligned} \tag{4.16}$$

Theorem 4.1. *Consider the system in (4.2) regulated by the control law in (4.7). Subject to Assumptions 2.1, 2.3, 4.1–4.3, together with the NN adaptation rule in (4.16), the signals $\boldsymbol{E}$ in (4.9) and the NN weights $\widehat{M}, \widehat{N}$ are uniformly ultimately bounded.*

Proof. The theorem is a special case of the MIMO theorem 5.2 in Chapter 5.

In many realistic applications, it is of great interest to achieve tracking performance with the smallest possible bound. Towards this end, the control law in (4.7) can be augmented by an additional controller which accelerates the adaptation process and corrects NN adaptation while NN learning is at its initial phase. Consider the following modification of the adaptive control signal u_{ad}

$$u_{ad} = u_{nn} + u_{dc} \tag{4.17}$$

where u_{nn} represents the adaptive signal defined in (4.14), and u_{dc} is a linear control signal, designed to robustify the error dynamics in (4.10), and designed as

$$\begin{aligned} \dot{\boldsymbol{x}}_{dc} &= A_{dc}\boldsymbol{x}_{dc} + B_{dc}\boldsymbol{Z} \\ u_{dc} &= \boldsymbol{c}_{dc}^{T}\boldsymbol{x}_{dc} + \boldsymbol{d}_{dc}\boldsymbol{Z}. \end{aligned} \tag{4.18}$$

Applying the controller in (4.18) to the dynamics in (4.10) leads to the following redefined error dynamics:

$$\dot{\boldsymbol{E}}_a = L_a\boldsymbol{E}_a + \begin{bmatrix} \bar{\boldsymbol{b}} \\ 0 \end{bmatrix}(u_{nn} - \Delta_1) - \begin{bmatrix} B \\ 0 \end{bmatrix}\boldsymbol{\Delta}_2\,. \tag{4.19}$$

where

$$\boldsymbol{E}_a = \begin{bmatrix} \boldsymbol{E} \\ \boldsymbol{x}_{dc} \end{bmatrix},\ L_a = \begin{bmatrix} \bar{A} + \bar{\boldsymbol{b}}\boldsymbol{d}_{dc}\bar{C} & \bar{\boldsymbol{b}}\boldsymbol{c}_{dc} \\ B_{dc}\bar{C} & A_{dc} \end{bmatrix}. \tag{4.20}$$

Notice that with the choice of design gains in (4.18), the eigenvalues of L_a can always be placed in the open left-half plane. The dynamics in (4.19) are similar to that in (4.10), except for the dimension of the error vector. Thus its stability analysis is similar to that used for (4.10).

Remark 4.1. Introducing the additional control signal u_{dc} leads to the similar control signal as in Chapter 2 and Section 3.3. Whereas these control designs involve either stabilizing a r chain of integrators in Chapter 2 or estimating external disturbances as shown in Figure 3.6 in Section 3.3, in this chapter, it is designed so as to further robustify the error dynamics in (4.10) influenced by the NN reconstruction error $u_{ad} - \Delta_1$ and the unmatched uncertainty $\boldsymbol{\Delta}_2$.

4.4 Experimental Results with the Three-disk Torsional System

The approach is tested in the same laboratory setting as in Section 2.7. That is, the same existing control system as that in Section 2.7 is augmented by the adaptive elements in this chapter. In case of a collocated control problem, the bottom disk control, the plant model

in (2.39) is realized in its normal form with the following system matrices

$$F_\xi = \begin{bmatrix} 0 & 1 \\ 0 & -0.18 \end{bmatrix},\ \boldsymbol{g}_\xi = \begin{bmatrix} 0 \\ 13.49 \end{bmatrix},\ \boldsymbol{c}_\xi = \begin{bmatrix} 1 \\ 0 \end{bmatrix} \tag{4.21}$$

In design of augmenting elements, we employ a reduced observer rather than the full order observer in (4.15), for the states of the controller are available. That is, with the definition $\boldsymbol{e}^T = [y_m - y,\ \dot{y}_m - \dot{y}]$, we design a reduced order observer to obtain an estimate for $\boldsymbol{e}$

$$\dot{\hat{\boldsymbol{e}}} = F_\xi \hat{\boldsymbol{e}} + \boldsymbol{g}_\xi [u_{lc}(y_m) - u_{lc}(y)] + \boldsymbol{g}_\xi u_{dc} + K(e_1 - \hat{e}_1) \tag{4.22}$$

where $u_{lc}(y_m)$ is the linear control signal in the reference model and $u_{lc}(y)$ is the linear control signal in the system, as they are depicted in Figure 4.1. The observer gain K is decided so that the eigenvalues of $A_m - K\boldsymbol{c}_m^T$ are $-46.2 \pm 46.2i$. Then the error vector in (4.15) needed for training of the NN is constructed as

$$\widehat{\boldsymbol{E}} = \begin{bmatrix} \hat{\boldsymbol{e}} \\ x_{cl} - x_c \end{bmatrix} \tag{4.23}$$

A SHLNN is introduced to approximate the uncertainty Δ_1 that is defined by

$$\Delta_1 = \frac{1}{K_n}[-\frac{B}{J_3}\dot{\theta}_3 + \frac{K}{J_3}(\theta_2 - \theta_3) - \frac{1}{J_3} f_{c_3}(\dot{\theta}_3, \theta_2, \theta_3) + \frac{K_{vt}}{J_3} u + c\dot{\theta}_3 - K_n u]. \tag{4.24}$$

Note that $\dot{y}_m$ in (2.40) is replaced by $\dot{\theta}_3$. The NN has 5 hidden layer neurons, with 5 delayed values of y for $\bar{\boldsymbol{y}}_d$ combined with 3 delayed values of u for $\bar{\boldsymbol{u}}_d$ as its input vector, and has the following learning rates and $\sigma-$modification gain

$$\Gamma_M = 0.5I,\ \Gamma_N = 0.5I,\ k = 1.3.$$

The additional control u_{dc} is added to accelerate NN adaptation. It is designed as a linear quadratic Gaussian(LQG) controller so as to attenuate effects of the disturbance, and of the NN reconstruction error $u_{nn} - \Delta_1$ in (4.10).

In the first experiment, the performance of output tracking with and without the proposed adaptive element is compared when a square wave command of 20° at 20 Hz is applied. Figure 4.2 compares the response of the regulated output. The response without

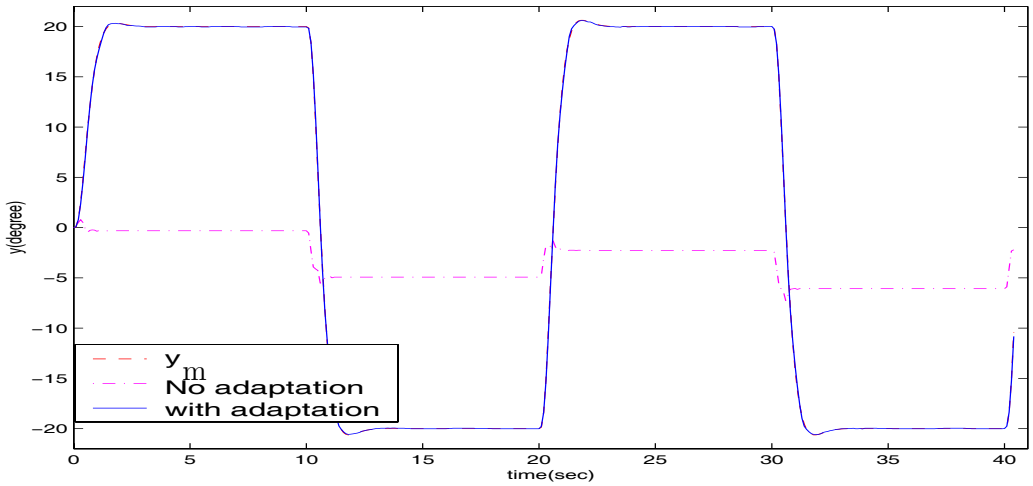

Fig. 4.2: Comparison of the Output Response of the Bottom Disk with/without the Adaptive Element in the External Model Following Architecture

the adaptive element is shown dash-dotted and the output of the reference model is dashed. The absence of the flexible modes in the response with the adaptive element shows that the augmented controller provides adaptation to the unmodelled flexible modes. In addition, the adaptive elements remove the steady state error caused by stiction and result in almost perfect tracking for y_m.

In another set of experiments, disturbance attenuation is evaluated with $y_c = 0$. A disturbance was introduced using a friction drive motor attached to the rim of the top disk as in Section 2.7. The disturbance is made up of sinusoids:

$$V_d(t) = 0.5 \sin t + 0.3 \sin 2t + 0.2 \sin 10t + 0.2 \sin 15.7t + 0.2 \sin 27.7t \tag{4.25}$$

The output responses of the open loop plant, the plant controlled without the adaptive element, and the plant controlled with the adaptive element are compared in Figure 4.3. The response of the open loop system is shown dotted, the output of the system regulated only by the linear controller is dash-dotted, and the output of the system with the adaptive element is solid. Note that the linear controller provides a level of response reduction in comparison to the open loop response. When the adaptive element is added to the linear controller, the response is nearly reduced to zero. This result is analogous to the experimental results in Section 2.7.1.

The other case, the middle disk control problem, is evaluated in a similar manner.

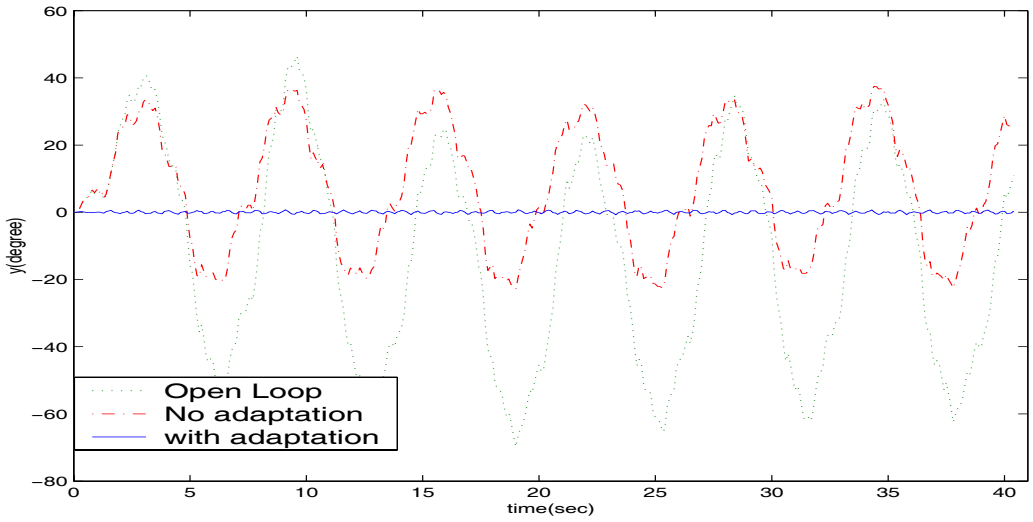

Fig. 4.3: Comparison of Output Responses of the Bottom Disk under Sinusoidal Disturbances in the External Model Following Architecture

After the system in (2.48) is transformed to its normal form, the reduced error observer is designed similarly as in (4.22) with the following definition for $\boldsymbol{e}^T = [y_m - y, \dot{y}_m - \dot{y}, \ldots, y_m^{(3)} - y^{(3)}]$. The observer gain K is decided so that the eigenvalues of $F_\xi - K\boldsymbol{c}_\xi^T$ are $-182.3 \pm 440.5i, -440.1 \pm 182.5i$. The SHLNN and the additional control signal u_{dc} are designed in the similar manner as in the bottom disk control problem.

Figure 4.4 compares output responses with and without the adaptive element when the same square wave as in the bottom disk control is applied. It is notable that the linear controller without the adaptive element almost completely fails to overcome the stiction due to increased inertia which is not captured in the plant model. Compared to perfect tracking shown in Figure 4.2, the response with the adaptive element is more oscillatory. The steady state error is, however, effectively eliminated. Figure 4.5 compares the output responses, when the same disturbance as in (4.25) is applied. The control law with adaptation shows significant disturbance rejection compared to that of the linear control law without the adaptive element. However, the disturbance attenuation is not as drastic as Figure 4.3.

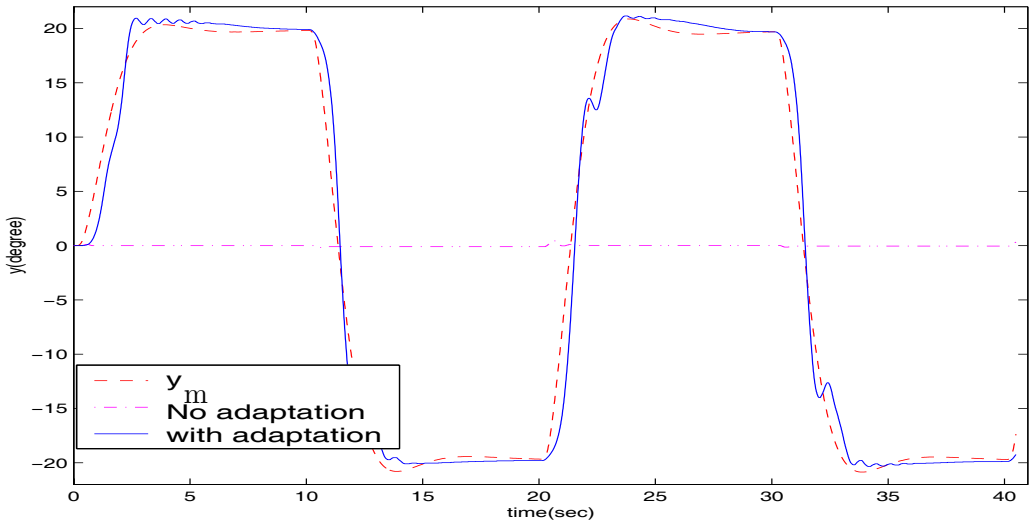

Fig. 4.4: Comparison of the Output Response of the Middle Disk with and without the Adaptive Element in the External Model Following Architecture

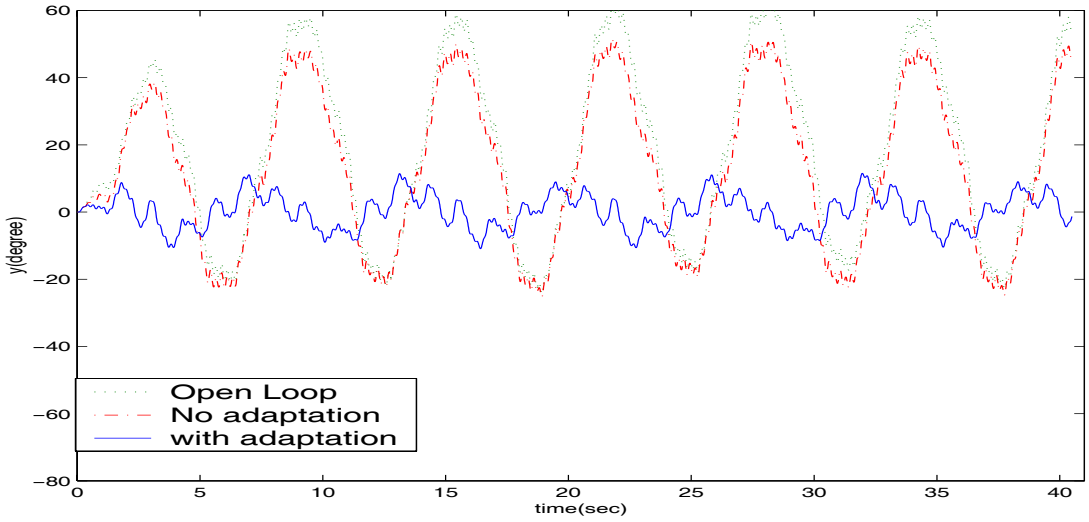

Fig. 4.5: Output Response of the Middle Disk under Sinusoidal Disturbances

4.5 Experimental Results with an Inverted Pendulum

An inverted pendulum regulation is a typical example of a non-minimum phase control problem [12,14,116]. In this section, we apply the method for control of an inverted pendulum in a real-time setting. Figure 4.6 depicts an inverted pendulum mechanism, Quanser Inc. [117]. It consists of a motor driven cart, which is equipped with two quadrature encoders. One encoder (0.05mm resolution) measures the position of the cart via a pinion (x), which meshes with the track. The other encoder(0.09° resolution) measures the angle of

the pendulum (θ), which is free to swing at the side of the cart. The equations of motion

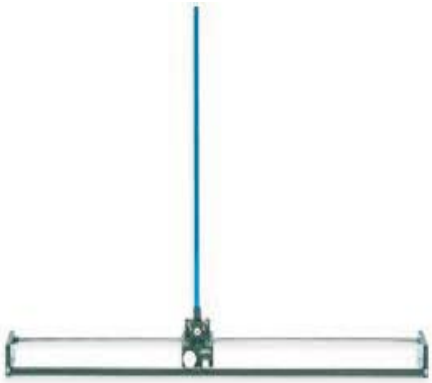

Fig. 4.6: Inverted Pendulum Apparatus from Quanser Inc.

for the system are as follows:

$$\begin{aligned}(M+m)\ddot{x} + c_M\dot{x} + ml_p\ddot{\theta}\cos\theta - ml_p\dot{\theta}^2\sin\theta + \Psi(\dot{x},x) &= F \\ ml_p\cos\theta\ddot{x} + (J_p + ml_p^2)\ddot{\theta} + c_m\dot{\theta} - mgl_p\sin\theta &= 0\end{aligned} \tag{4.26}$$

where x is the displacement of the cart along the track (m), F is the force applied to the cart (N), M is the mass of the cart (kg), m is the mass of the rod (kg), l_p is the position of the center of gravity of the rod (half of full length)(m), $J_p = \frac{1}{3}ml_p^2$ is a moment of inertia of the rod with respect to its center of gravity ($kg \cdot m^2$), g is the gravitational acceleration ($kg \cdot m/sec^2$), c_M, c_m are the viscous damping coefficients, and $\Psi(\dot{x},x)$ is an uncertain nonlinearity which is caused by the cart moving mechanism, i.e., combined effects of stiction, coulomb friction, and backlash. There are also unmodelled dynamics due to flexibility in the direction perpendicular to the track. The force, F, is a consequence of an input voltage u applied to a DC motor and the cart velocity, according to the following equations:

$$F = \frac{K_m K_g}{R_m r}u - \frac{K_m^2 K_g^2}{R_m r^2}\dot{x} = a_1 u - a_2\dot{x} \tag{4.27}$$

where K_m is a back EMF constant(Volts/(rad/sec)), K_g is a gear ratio in motor gearbox, R_m is a motor armature resistance (Ohms), and r is the radius of motor pinion that meshes with

the track (m). The system parameters are $M = .815,\ m = 0.21,\ l_p = 0.305,\ g = 9.8,\ a_1 = 2.33,\ a_2 = 10.42$. The control objective is to regulate x so that it tracks the reference command y_c, using measured outputs $x,\ \theta$, while balancing the inverted pendulum.

With the definition, $\xi_1 = x, \xi_2 = \dot{x}, z_1 = \theta, z_2 = \frac{\dot{x}}{l_p}\cos\theta + \frac{4}{3}\dot{\theta}$, the system in (4.26) is put into a normal form:

$$\begin{aligned}
\dot{\xi}_1 &= \xi_2 \\
\dot{\xi}_2 &= \frac{1}{M + m(1 - 3/4\cos\theta^2)}\big[\ a_1 u - a_2\xi_2 \\
&\quad - c_M\xi_2 - \Psi(\xi_1, \xi_2) + ml_p\dot{\theta}^2\sin\theta \\
&\quad + \frac{3}{4}c_m\dot{\theta}\cos\theta - \frac{3}{4}mg\sin\theta\cos\theta\ \big] \\
\dot{z}_1 &= \frac{3}{4}z_2 - \frac{3\cos\theta}{4l_p}\xi_2 \\
\dot{z}_2 &= \frac{g}{l_p}\sin\theta - \frac{c_m}{ml_p}\dot{\theta} - \frac{1}{l_p}\xi_2\dot{\theta}\sin\theta
\end{aligned} \tag{4.28}$$

Its zero dynamics are given by:

$$\begin{aligned}
\dot{z}_1 &= \frac{3}{4}z_2 \\
\dot{z}_2 &= \frac{g}{l_p}\sin z_1 - \frac{3c_m}{4ml_p}z_2.
\end{aligned} \tag{4.29}$$

Linearization of z_1, z_2 dynamics in (4.29) about the desired equilibrium point $(z_1, z_2) = (0, 0)$, reveals an eigenvalue at $\frac{c_m}{ml_p}\left[-\frac{3}{8} + \frac{1}{2}\sqrt{1 + \frac{3m^2gl_p}{c_m^2}}\right] > 0$. Therefore the system is non-minimum phase.

The plant model is constructed linearizing Eq.(4.26) with $J_p = 0$. Furthermore, the uncertain nonlinearity $\Psi(\dot{x}, x)$ and viscous damping terms (c_M, c_m) are not accounted in the linear model. With $\xi_{m_1} = x,\ \xi_{m_2} = \dot{x},\ z_{m_1} = \theta,\ z_{m_2} = \frac{\dot{x}}{l_p} + \dot{\theta}$, it is put into the following normal form:

$$\begin{aligned}
\dot{\xi}_{m_1} &= \xi_{m_2} \\
\dot{\xi}_{m_2} &= \frac{1}{M}[a_1 u - a_2\xi_{m_2} - mg\theta] \\
\dot{z}_{m_1} &= z_{m_2} - \frac{1}{l_p}\xi_{m_2} \\
\dot{z}_{m_2} &= \frac{g}{l_p}\theta
\end{aligned} \tag{4.30}$$

Comparing (4.30) with (4.28) leads to the following matched and unmatched uncertainties.

$$\Delta_1 = \frac{1}{a_1}\Big[\frac{M}{M+m(1-3/4\cos\theta^2)}\big[a_1u - a_2\xi_2 - c_M\xi_2 - \Psi(\xi_1,\xi_2) + ml_p\dot{\theta}^2\sin\theta + \frac{3}{4}c_m\dot{\theta}\cos\theta$$
$$- \frac{3}{4}mg\sin\theta\cos\theta\big] + mg\theta - a_1u + a_2\xi_2\Big]$$
$$\boldsymbol{\Delta}_2 = \begin{bmatrix} -\frac{1}{4}z_2 + \frac{1}{l_p}\xi_2(1-\frac{3}{4}\cos\theta) \\ \frac{g}{l_p}(\sin\theta-\theta) - \frac{c_m}{ml_p}\dot{\theta} - \frac{1}{l_p}\xi_2\dot{\theta}\sin\theta \end{bmatrix} \tag{4.31}$$

The linear controller is designed as a LQG controller based on the plant model in (4.30), in which two measured outputs $\xi_1,\ z_1(=\theta)$ are available. In the experimental tests, it was observed that a high bandwidth design is stabilizing, while a low bandwidth design results in an unstable system. To address the effectiveness of the approach, we augment the low bandwidth design. The LQG controller places the eigenvalues of $\bar{A}$ at -0.3, $-4.9 \pm 1.3i$, $-8.2 \pm 5.9i$, $-10.3 \pm 2.4i$, -31.6.

The reduced order error observer as in (4.22) is designed so that its poles are located at -1.0, -99.9, $-26.5 \pm 24.0i$. The additional controller is not necessary, so $u_{dc} = 0$. Since two outputs are available, network inputs are constructed as follows

$$\boldsymbol{\eta}^T = [\xi_1,\ \xi_1(t-d),\ z_1,\ z_1(t-d), u],\ d = 0.01sec.$$

The NN consists of 6 neurons in the hidden layer and its parameters are

$$\Gamma_M = 150I,\ \Gamma_N = 150I,\ k = 1.2.$$

Figures 4.7 and 4.8 show the experimental results with $y_c = 0$. The pendulum is swung up to the vertical position by hand before the the proposed controller starts at t=7.8 sec. While the linear controller is augmented by the adaptive NN, the cart position and the angle of the pendulum are regulated within $\pm 0.05(m)$ and $\pm 1^\circ$. When the NN is turned off at t=44.6 sec., the control system immediately goes unstable.

Figures 4.9 and 4.10 show the output responses when a square wave command of 0.15 m at 0.01 Hz is applied. The result shows that y_m is tracked with a bounded error, while the inverted pendulum is rapidly stabilized after a short transient.

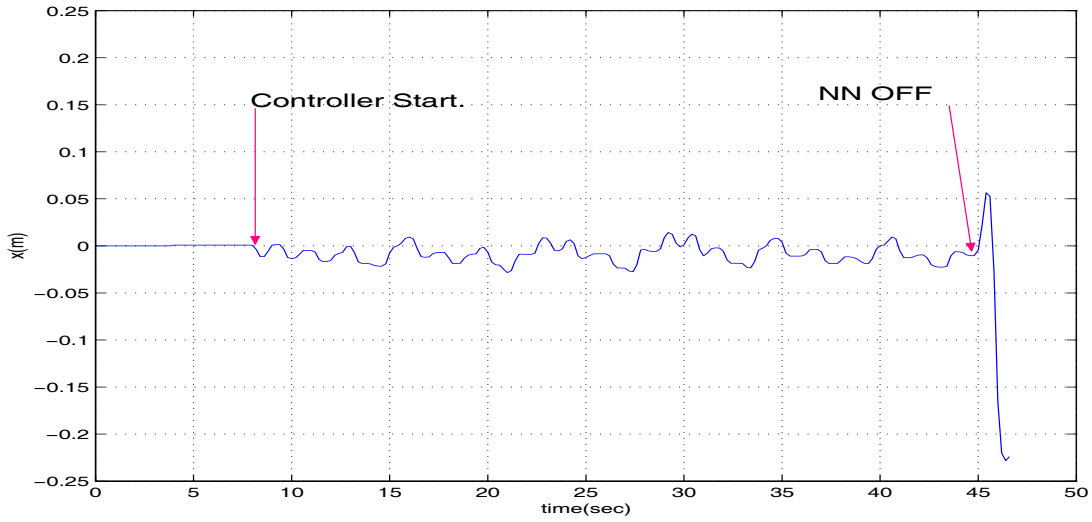

Fig. 4.7: Cart Position with $y_c = 0$.

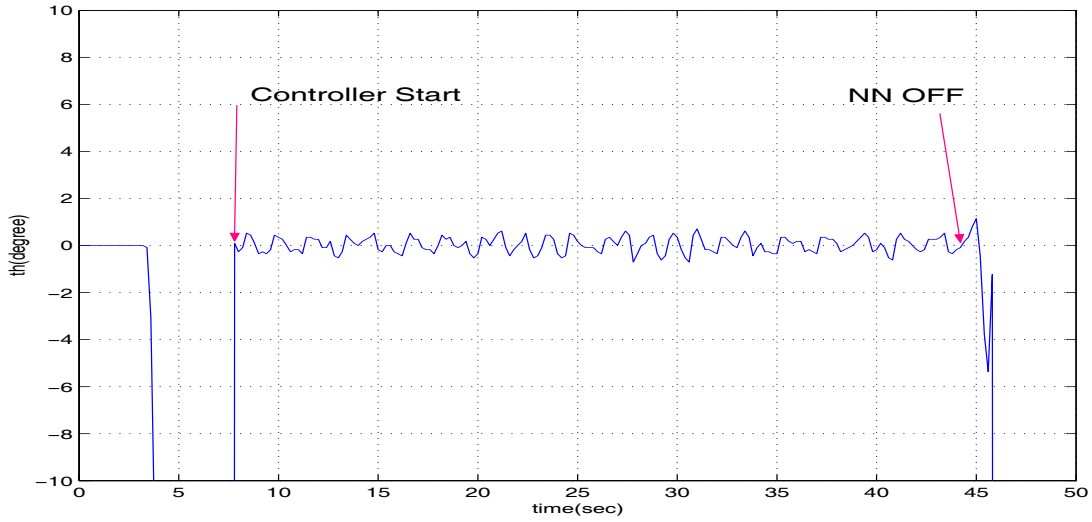

Fig. 4.8: Angle of the Pendulum with $y_c = 0$.

4.6 Conclusions

This chapter describes an approach for augmenting a linear controller with an adaptive element that can be applied to both minimum phase and non-minimum phase uncertain nonlinear systems. The framework involves an external model-following architecture. The key properties of the design are that only output variables are used, and it is adaptive to both parametric errors and unmodelled/unmatched dynamics and disturbances. The main assumptions are that the relative degree of the regulated output is known, and that the unmatched uncertainty in the error dynamics satisfies a conic sector bound. In the case of

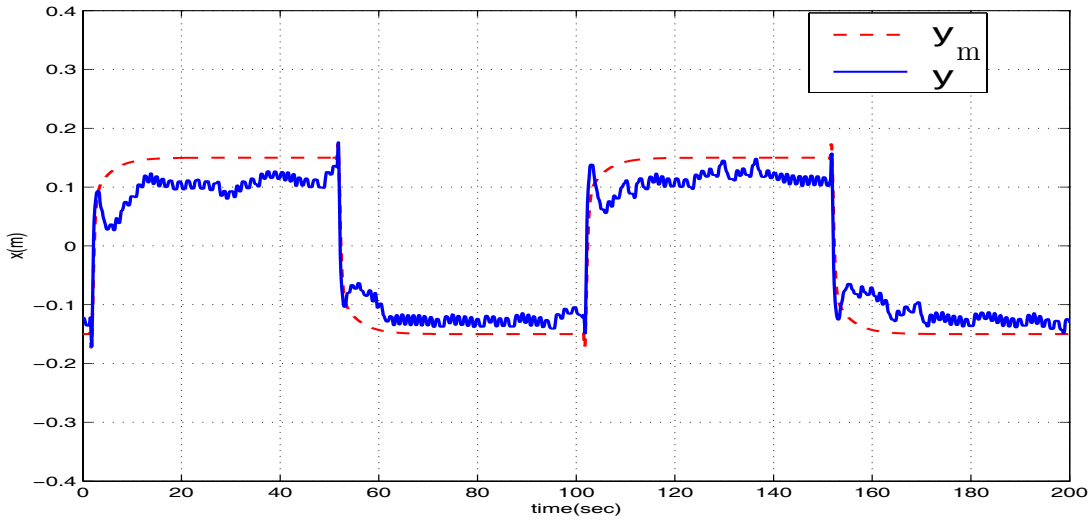

Fig. 4.9: Cart Position with a Square Wave Command y_c.

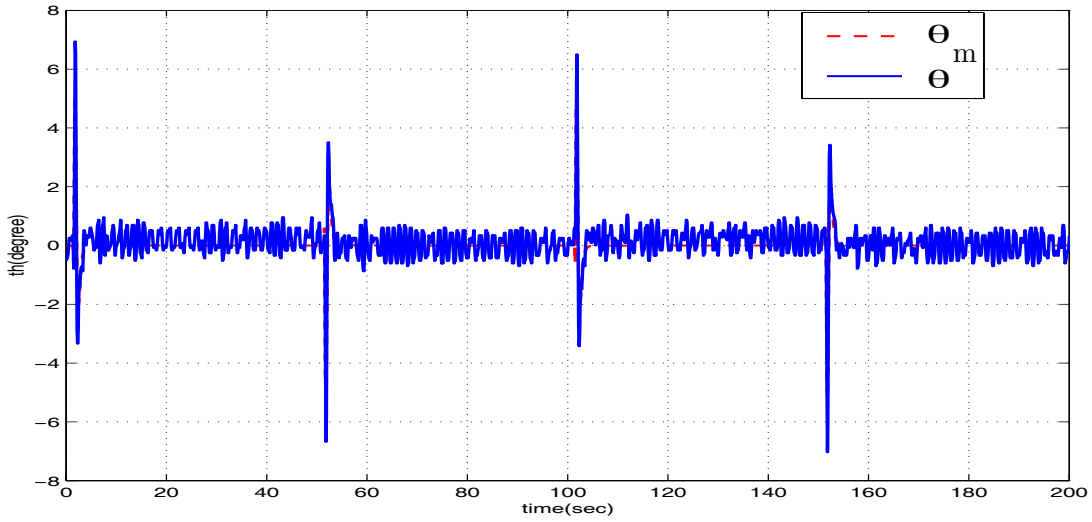

Fig. 4.10: Angle of the Pendulum with a Square Wave Command y_c.

unstable zero dynamics, the unstable zeros must be accounted for in the design of the linear controller.

Experimental results obtained using a three-disk torsional pendulum laboratory model, which is minimum phase, shows that the proposed control law achieves significant improvement in tracking and disturbance attenuation. Experimental results with an inverted pendulum further illustrate the effectiveness of the approach for control of a non-minimum phase nonlinear system.

CHAPTER 5

ADAPTIVE CONTROL AUGMENTATION FOR MULTI-INPUT MULTI-OUTPUT SYSTEMS

This chapter extends the approach in Chapter 4 to mutlivariable nonlinear systems. The basic assumptions are that the vector relative degree of the nonlinear system is known and that the non-minimum phase zeros of the nonlinear systems are modelled to a sufficient accuracy. Ultimate boundedness of error signals is shown using Lyapunov's direct method.

5.1 Introduction

A fundamental goal for many research efforts in control theory is the development of systematic design methods for controlling system outputs in the presence of structured uncertainties, such as parameter variations, and unstructured uncertainties, such as unmodelled dynamics and disturbances. While for linear systems stabilization and tracking can be achieved by output feedback via standard methods [118, 119], for nonlinear systems this is not an obvious task. Most of the nonlinear control methodologies, robust or adaptive, impose the assumption that the zero dynamics are asymptotically stable [18–20], and thus are limited to minimum phase systems. Output feedback control of *non-minimum* phase nonlinear systems remains as one of the challenging problems in control theory. In [9] output feedback stabilization of a class of nonlinear non-minimum phase systems is considered, and a useful solution is obtained for systems linearizable by state feedback. Ref. [14] also addresses this problem and proposes an elegant solution for robust semiglobal practical stabilization based on auxiliary constructions.

In this chapter we address the problem of adaptive output feedback control of observable and stabilizable multivariable non-minimum phase systems with well-defined vector relative degree. This is done from the perspective of augmenting a fixed gain linear design that is assumed to satisfy performance requirements in the absence of modelling errors. We assume

that the linear model of the system dynamics has the same vector relative degree and represents the non-minimum phase zero dynamics of the nonlinear system up to a *tolerable* accuracy. By this, we mean that the modelling error associated with the non-minimum phase zero dynamics satisfies a sector bound. This assumption permits these dynamics to be managed by a robust control component. Any unmodelled dynamics, present within the bandwidth of the control design, is assumed to be globally exponentially stable and globally Lipschitz.

From the perspective of classical adaptive control, we relax the assumptions on affinity in the control and/or the unknown parameters by invoking a NN for modelling the uncertainties in the control range [36, 39, 42]. Similar to the approaches in [62, 63], the NN reconstructs the unknown dynamics from a finite history of available measurements [65]. This property allows us to formulate and address the synthesis problem for systems with *unknown* dimension, as long as the vector relative degree is known. The adaptive laws are written in terms of the output of a linear observer for the nominal system's error dynamics as in [63]. Ultimate boundedness of error signals is shown through Lyapunov's direct method. The benefits of the approach are that it is robust to both parametric uncertainties and unmodelled dynamics, and that it is applicable to non-minimum phase systems.

This chapter is organized as follows. In Section 5.2 we define the system dynamics, the linear model used for the design of the linear controller, the linear control law and state the problem formulation. In Section 5.3 we state assumptions on the relationship between the linear model and the nonlinear system and formulate the approach. Section 5.4 addresses the design of the adaptive element and derivation of the error dynamics. In Section 5.5 we present the proof on ultimate boundedness of error signals. An illustrative example is given in Section 5.6. Conclusions are in Section 5.7.

5.2 Problem Formulation

Let the dynamics of an *observable* and *stabilizable* nonlinear multi-input-multi-output (MIMO) system be given by the following equations:

$$\begin{aligned} \dot{\boldsymbol{x}} &= \boldsymbol{f}_0(\boldsymbol{x},\boldsymbol{u}) \\ \boldsymbol{y} &= \boldsymbol{g}(\boldsymbol{x})\,, \end{aligned} \tag{5.1}$$

where $\boldsymbol{x} \in \mathcal{D}_x \subset \mathbb{R}^n$ is the state of the system, $\boldsymbol{u} \in \mathcal{D}_u \subset \mathbb{R}^m$, $\boldsymbol{y} \in \mathbb{R}^m$ are the system input (control) and output (measurement) signals, respectively, and $\boldsymbol{f}_0(\boldsymbol{x},\boldsymbol{u}) : \mathbb{R}^n \times \mathbb{R}^m \to \mathbb{R}^n$, $\boldsymbol{g}(\boldsymbol{x}) : \mathbb{R}^n \to \mathbb{R}^m$ are sufficiently smooth partially known functions, n need not be known. Extensions to situations in which there are m regulated outputs and other outputs that are not regulated are straightforward, and consequently are not explicitly treated here.

Assumption 5.1. *The dynamical system in (5.1) has the vector relative degree* $\boldsymbol{r} \triangleq \begin{bmatrix} r_1 & r_2 & \cdots & r_m \end{bmatrix}^T$, *such that* $r \triangleq r_1 + r_2 + \cdots + r_m \leq n$.

Following [68], there exists a mapping $\boldsymbol{\xi} = \Phi(\boldsymbol{x})$

$$\Phi(\boldsymbol{x}) = \begin{bmatrix} \boldsymbol{\phi}_1 \\ \boldsymbol{\phi}_2 \\ \vdots \\ \boldsymbol{\phi}_m \end{bmatrix}, \quad \boldsymbol{\phi}_i \triangleq \begin{bmatrix} L^0_{\boldsymbol{f}_0} g_i \\ L^1_{\boldsymbol{f}_0} g_i \\ \vdots \\ L^{(r_i-1)}_{\boldsymbol{f}_0} g_i \end{bmatrix}, \tag{5.2}$$

with $L^{(i)}_{\boldsymbol{f}_0} g_j$ being the Lie derivatives, g_i's the elements of $\boldsymbol{g}$ in (5.1), that transforms the system (5.1) into the so called normal form [90]

$$\begin{aligned} \dot{\boldsymbol{z}} &= \boldsymbol{f}(\boldsymbol{\xi},\boldsymbol{z}) \\ \dot{\xi}_i^1 &= \xi_i^2, \\ &\vdots \\ \xi_i^{(r_i)} &= h_i(\boldsymbol{\xi},\boldsymbol{z},\boldsymbol{u}) \\ y_i &= \xi_i^1, \quad i = 1,\cdots,m\,, \end{aligned} \tag{5.3}$$

where $h_i(\boldsymbol{\xi},\boldsymbol{z},\boldsymbol{u}) = h_i(\boldsymbol{x},\boldsymbol{u}) = L^{(r_i)}_{\boldsymbol{f}_0} g_i$, $\boldsymbol{\xi} \triangleq \begin{bmatrix} \boldsymbol{\xi}_1^T & \cdots & \boldsymbol{\xi}_m^T \end{bmatrix}^T$, $\boldsymbol{\xi}_i \triangleq \begin{bmatrix} \xi_i^1 & \cdots & \xi_i^{(r_i)} \end{bmatrix}^T$, and $\boldsymbol{z}$ are the states associated with the internal dynamics. Comparing with (5.1), notice

that

$$\boldsymbol{y} = C\boldsymbol{\xi}, \tag{5.4}$$

where

$$C = \begin{bmatrix} \boldsymbol{c}_1^T & 0 & \cdots & 0 \\ 0 & \boldsymbol{c}_2^T & \cdots & 0 \\ \vdots & \vdots & \ddots & \\ 0 & 0 & \cdots & \boldsymbol{c}_m^T \end{bmatrix}_{m \times r}, \quad \boldsymbol{c}_i^T = \begin{bmatrix} 1 & 0 & \cdots & 0 \end{bmatrix}_{1 \times r_i}. \tag{5.5}$$

Assume there exists a linear design model of the system dynamics in (5.3) that has the same vector relative degree and is transformable to normal form

$$\begin{aligned} \dot{\boldsymbol{z}}_l &= F_0 \boldsymbol{z}_l + G_0 \boldsymbol{\xi}_l \\ \dot{\xi}_{l_i}^1 &= \xi_{l_i}^2, \\ &\vdots \\ \xi_{l_i}^{(r_i)} &= \boldsymbol{h}_i^T \boldsymbol{z}_l + \boldsymbol{a}_i^T \boldsymbol{\xi}_l + \boldsymbol{b}_i^T \boldsymbol{u} \\ y_{l_i} &= \xi_{l_i}^1, \quad , \quad i = 1, \cdots, m \end{aligned} \tag{5.6}$$

where $\boldsymbol{\xi}_l = \begin{bmatrix} \boldsymbol{\xi}_{l_1}^T & \dots & \boldsymbol{\xi}_{l_m}^T \end{bmatrix}^T$, $\boldsymbol{\xi}_{l_i} = \begin{bmatrix} \xi_{l_i}^1 & \dots & \xi_{l_i}^{(r_i)} \end{bmatrix}^T$, $\boldsymbol{z}_l \in \mathbb{R}^{n_m - r}$ are the states of the zero dynamics, $\boldsymbol{a}_i = \begin{bmatrix} \boldsymbol{a}_{i1}^T & \dots & \boldsymbol{a}_{im}^T \end{bmatrix}^T$, $\boldsymbol{a}_{ij} = \begin{bmatrix} a_{ij}^1 & \dots & a_{ij}^{(r_j)} \end{bmatrix}^T$, $\boldsymbol{b}_i = \begin{bmatrix} b_i^1 & \dots & b_i^m \end{bmatrix}^T$ and $n_m \leq n$ is the dimension of the linear system. Consider the following stabilizing linear controller for the dynamics in (5.6):

$$\begin{aligned} \dot{\boldsymbol{x}}_c &= A_c \boldsymbol{x}_c + B_c(\boldsymbol{y}_c - \boldsymbol{y}) \\ \boldsymbol{u}_{lc} &= C_c \boldsymbol{x}_c + D_c(\boldsymbol{y}_c - \boldsymbol{y}), \end{aligned} \tag{5.7}$$

where $\boldsymbol{x}_c \in \mathbb{R}^{n_c}$ are the states of the controller, $\boldsymbol{y}_c \in \mathbb{R}^m$ is a bounded reference input of interest to track, and A_c, B_c, C_c, D_c are matrices of appropriate dimensions. Let

$$\|\boldsymbol{y}_c\| \leq \beta_c. \tag{5.8}$$

The linear design model in (5.6), when regulated by (5.7), define a "closed-loop reference model". Denoting $\boldsymbol{x}_{cl}$ the states of the controller in (5.7) when applied to (5.6), i.e. when

$\boldsymbol{y}$ is replaced by $\boldsymbol{y}_l$ in (5.7), the closed-loop reference model can be written as:

$$\underbrace{\begin{bmatrix} \dot{\boldsymbol{\xi}}_l \\ \dot{\boldsymbol{z}}_l \\ \dot{\boldsymbol{x}}_{cl} \end{bmatrix}}_{\dot{\boldsymbol{x}}_l} = \underbrace{\begin{bmatrix} A - BD_cC & B_z & BC_c \\ G_0 & F_0 & 0 \\ -B_cC & 0 & A_c \end{bmatrix}}_{\bar{A}} \underbrace{\begin{bmatrix} \boldsymbol{\xi}_l \\ \boldsymbol{z}_l \\ \boldsymbol{x}_{cl} \end{bmatrix}}_{\boldsymbol{x}_l} + \underbrace{\begin{bmatrix} BD_c \\ 0 \\ B_c \end{bmatrix}}_{\bar{B}} \boldsymbol{y}_c$$

$$\boldsymbol{y}_l = \underbrace{\left[\begin{array}{c|c|c} \mathrm{C} & 0 & 0 \\ \hline 0 & 0 & 0 \\ \hline 0 & 0 & \mathrm{I} \end{array}\right]}_{\bar{C}} \begin{bmatrix} \boldsymbol{\xi}_l \\ \boldsymbol{z}_l \\ \boldsymbol{x}_{cl} \end{bmatrix}, \tag{5.9}$$

where

$$A = \begin{bmatrix} A_{11} & A_{12} & \cdots & A_{1m} \\ A_{21} & A_{22} & \cdots & A_{2m} \\ \vdots & \vdots & \ddots & \vdots \\ A_{m1} & A_{m2} & \cdots & A_{mm} \end{bmatrix}, \quad A_{ii} = \begin{bmatrix} 0 & 1 & 0 & \cdots & 0 \\ 0 & 0 & 1 & & 0 \\ \vdots & \vdots & & \ddots & \\ 0 & 0 & & & 1 \\ a_{ii}^1 & a_{ii}^2 & a_{ii}^3 & \cdots & a_{ii}^{(r_i)} \end{bmatrix}_{r_i \times r_i},$$

$$A_{ij}\Big|_{i \neq j} = \begin{bmatrix} 0 & 0 & 0 & \cdots & 0 \\ 0 & 0 & 0 & & 0 \\ \vdots & \vdots & & \ddots & \\ 0 & 0 & & & 0 \\ a_{ij}^1 & a_{ij}^2 & a_{ij}^3 & \cdots & a_{ij}^{(r_j)} \end{bmatrix}_{r_i \times r_j}, \quad B_z = \begin{bmatrix} B_z^1 \\ B_z^2 \\ \vdots \\ B_z^m \end{bmatrix}_{r \times (n_m - r)},$$

$$B_z^i = \begin{bmatrix} 0 \\ 0 \\ \vdots \\ \boldsymbol{h}_i^T \end{bmatrix}_{r_i \times (n_m - r)}, \quad B = \begin{bmatrix} B_1 \\ B_2 \\ \vdots \\ B_m \end{bmatrix}_{r \times m}, B_1 = \begin{bmatrix} 0 & \cdots & 0 \\ \vdots & & \\ b_1 & \cdots & 0 \end{bmatrix}_{r_1 \times m},$$

$$B_i = \begin{bmatrix} 0 & 0 & \cdots & 0 & 0 \\ \vdots & & & & \\ 0 & \cdots & b_i & \cdots & 0 \end{bmatrix}_{r_i \times m}, \quad B_m = \begin{bmatrix} 0 & \cdots & 0 \\ \vdots & & \\ 0 & \cdots & b_m \end{bmatrix}_{r_m \times m}.$$

The dynamics in (5.9) can be written in the following compact form

$$\begin{aligned} \dot{\boldsymbol{x}}_l =& \bar{A}\boldsymbol{x}_l + \bar{B}\boldsymbol{y}_c \\ \boldsymbol{y}_m =& \bar{C}\boldsymbol{x}_l \,, \end{aligned} \tag{5.10}$$

where $\boldsymbol{x}_l \in \mathbb{R}^{n_m+n_c}$, and $\bar{A}$ is Hurwitz. Note that Eq.(5.10) is a MIMO version of the reference model in (4.4.) We immediately note that given Hurwitz $\bar{A}$, there exists a positive definite matrix $P = P^T$ solving the Lyapunov equation

$$\bar{A}^T P_n + P_n \bar{A} = -Q_n \tag{5.11}$$

for arbitrary $Q_n > 0$.

The objective is to augment the linear control law $\boldsymbol{u}_{lc}$ in (5.7) with an adaptive element so that when applied to the system (5.3) the output $\boldsymbol{y}$ tracks $\boldsymbol{y}_c$. In what follows, we will derive error dynamics for the signal $\boldsymbol{y}_l - \boldsymbol{y}$ and prove through Lyapunov's direct method that it is ultimately bounded. This in turn ensures that $\boldsymbol{y}$ tracks $\boldsymbol{y}_c$ with bounded errors.

5.3 The Approach

To derive the error dynamics we need the following assumption, establishing the relationship between the system in (5.3) and the linear model in (5.6).

Assumption 5.2. *The $\boldsymbol{z}$ dynamics in (5.3) can be decomposed as:*

$$\dot{\boldsymbol{z}}_1 = \boldsymbol{f}_1(\boldsymbol{\xi}, \boldsymbol{z}_1, \boldsymbol{z}_2) = F_0\boldsymbol{z}_1 + G_0\boldsymbol{\xi} + \boldsymbol{\Delta}_2(\boldsymbol{\xi}, \boldsymbol{z}_1, \boldsymbol{z}_2),\ \boldsymbol{z}_1 \in \mathbb{R}^{n_m-r} \tag{5.12}$$

$$\dot{\boldsymbol{z}}_2 = \boldsymbol{f}_2(\boldsymbol{\xi}, \boldsymbol{z}_1, \boldsymbol{z}_2),\ \boldsymbol{z}_2 \in \mathbb{R}^{n-n_m} \,, \tag{5.13}$$

where the equilibrium $\boldsymbol{z}_2 = 0$ of $\dot{\boldsymbol{z}}_2 = \boldsymbol{f}_2(0, 0, \boldsymbol{z}_2)$ is globally exponentially stable, the function $\boldsymbol{f}_2(\boldsymbol{\xi}, \boldsymbol{z}_1, \boldsymbol{z}_2) : \mathbb{R}^n \to \mathbb{R}^{n-n_m}$ is globally Lipschitz in its arguments, and $\boldsymbol{\Delta}_2 = \boldsymbol{f}_1(\boldsymbol{\xi}, \boldsymbol{z}_1, \boldsymbol{z}_2) - F_0\boldsymbol{z}_1 - G_0\boldsymbol{\xi}$ can be viewed as modeling error in the dynamics of $\boldsymbol{z}_1$, satisfying the following upper bound with known constants [115]:

$$\|\boldsymbol{\Delta}_2\| \leq \beta_0 \|\boldsymbol{\xi}\| + \beta_1 \|\boldsymbol{z}_1\| + \beta_2 \|\boldsymbol{z}_2\| + \beta_3 \,, \quad \beta_0, \beta_1, \beta_2, \beta_3 > 0. \tag{5.14}$$

Remark 5.1. From a converse Lyapunov theorem one can deduce that there exists a Lyapunov function $V_{\boldsymbol{z}_2}(\boldsymbol{z}_2)$ satisfying the following conditions [91]

$$\begin{aligned} c_1\|\boldsymbol{z}_2\|^2 &\leq V_{\boldsymbol{z}_2}(\boldsymbol{z}_2) \leq c_2\|\boldsymbol{z}_2\|^2 \\ \frac{\partial V_{\boldsymbol{z}_2}}{\partial \boldsymbol{z}_2}\boldsymbol{f}_2(0,0,\boldsymbol{z}_2) &\leq -c_3\|\boldsymbol{z}_2\|^2 \\ \left\|\frac{\partial V_{\boldsymbol{z}_2}}{\partial \boldsymbol{z}_2}\right\| &\leq c_4\|\boldsymbol{z}_2\|\,, \end{aligned} \tag{5.15}$$

implying that the $\dot{\boldsymbol{z}}_2 = \boldsymbol{f}_2(\boldsymbol{\xi}, \boldsymbol{z}_1, \boldsymbol{z}_2)$ dynamics, with $\boldsymbol{\xi}$, $\boldsymbol{z}_1$ as inputs, are input-to-state stable. The following upper bound can be immediately derived

$$\begin{aligned} \dot{V}_{\boldsymbol{z}_2} &= \frac{\partial V_{\boldsymbol{z}_2}}{\partial \boldsymbol{z}_2}\boldsymbol{f}_2(\boldsymbol{\xi}, \boldsymbol{z}_1, \boldsymbol{z}_2) = \frac{\partial V_{\boldsymbol{z}_2}}{\partial \boldsymbol{z}_2}\boldsymbol{f}_2(0,0,\boldsymbol{z}_2) + \frac{\partial V_{\boldsymbol{z}_2}}{\partial \boldsymbol{z}_2}\boldsymbol{f}_2(\boldsymbol{\xi}, \boldsymbol{z}_1, \boldsymbol{z}_2) - \frac{\partial V_{\boldsymbol{z}_2}}{\partial \boldsymbol{z}_2}\boldsymbol{f}_2(0,0,\boldsymbol{z}_2) \\ &\leq -c_3\|\boldsymbol{z}_2\|^2 + c_4c_5\|\boldsymbol{z}_2\|\|\bar{\boldsymbol{\xi}}\| \leq -\frac{3c_3}{4}\|\boldsymbol{z}_2\|^2 + \frac{(c_4c_5)^2}{c_3}\|\bar{\boldsymbol{\xi}}\|^2\,, \end{aligned} \tag{5.16}$$

where c_5 is the Lipschitz constant of $\boldsymbol{f}_2(\boldsymbol{\xi}, \boldsymbol{z}_1, \boldsymbol{z}_2)$ in $\bar{\boldsymbol{\xi}} \triangleq \begin{bmatrix} \boldsymbol{\xi}^T & \boldsymbol{z}_1^T \end{bmatrix}^T$.

Assumption 5.3. *Let β_i's and c_5 be such that Q in (5.11) can be chosen to satisfy*

$$Q_m > 3 + 2\delta_1\|PB_2\| + \frac{(c_4c_5)^2}{c_3} + \frac{(2\|PB_2\|\beta_2)^2}{c_3}\,, \tag{5.17}$$

where Q_m is the minimum eigenvalue of Q, $\delta_1 \triangleq \max\{\beta_0, \beta_1\}$, and the matrix B_2 has the following structure $B_2^T = \begin{bmatrix} 0 & I & 0 \end{bmatrix}$, $I \in \mathbb{R}^{(n_m-r)\times(n_m-r)}$.

Remark 5.2. Assumptions 5.2 and 5.3 basically state the relationship between the nonlinear system in (5.3) and the linear model in (5.6), used for the design of the linear controller. In case $n_m = n$ there are no $\boldsymbol{z}_2$ dynamics, and the relationship in (5.12) implies that the zero-dynamics in (5.6) represent the internal dynamics of (5.3) up to the accuracy of $\boldsymbol{\Delta}_2$. Also notice, that the upper bound in (5.14) along with the lower bound in (5.17), which in the absence of $\boldsymbol{z}_2$ will involve only the first two terms, specify the dependence between the linear design gains involved in $\bar{A}$, choice of the matrix Q, and the unmatched uncertainty $\boldsymbol{\Delta}_2$. More insight on this will be presented after the stability proof. Finally, if $n_m < n$, Assumption 5.2 permits existence of globally exponentially stable dynamics in (5.3) not captured in (5.6), like that of $\boldsymbol{z}_2$, while Assumption 5.3 restricts the choice of the matrix Q and the linear design gains in $\bar{A}$.

The last equation in (5.3) can be put in the following form

$$h_i(\boldsymbol{\xi}, \boldsymbol{z}, \boldsymbol{u}) = \boldsymbol{h}_i^T \boldsymbol{z}_1 + \boldsymbol{a}_i^T \boldsymbol{\xi} + \boldsymbol{b}_i^T (\boldsymbol{u} + \boldsymbol{\Delta}_1) \tag{5.18}$$

where $\boldsymbol{b}_i^T \boldsymbol{\Delta}_1(\boldsymbol{\xi}, \boldsymbol{z}, \boldsymbol{u}) = h_i(\boldsymbol{\xi}, \boldsymbol{z}, \boldsymbol{u}) - \boldsymbol{h}_i^T \boldsymbol{z}_1 - \boldsymbol{a}_i^T \boldsymbol{\xi} - \boldsymbol{b}_i^T \boldsymbol{u}$ can be viewed as the portion of the modeling error that lies in the range space of the control. Augment the linear controller in (5.7) with an adaptive signal:

$$\boldsymbol{u} = \boldsymbol{u}_{lc} - \boldsymbol{u}_{ad}, \tag{5.19}$$

where $\boldsymbol{u}_{ad}$ is designed to approximately and *adaptively* cancel $\boldsymbol{\Delta}_1$. Notice from (5.19) and (5.18) that $\boldsymbol{\Delta}_1$ depends on $\boldsymbol{u}_{ad}$ through $\boldsymbol{u}$, and that the role of $\boldsymbol{u}_{ad}$ is to cancel $\boldsymbol{\Delta}_1$. The following assumption introduces a sufficient condition for the existence and uniqueness of a solution for $\boldsymbol{u}_{ad}$.

Assumption 5.4. *The mapping $\boldsymbol{u}_{ad} \mapsto \boldsymbol{\Delta}_1$ is a contraction.*

Contraction mapping is defined by the following condition:

$$\left\| \frac{\partial \boldsymbol{\Delta}_1}{\partial \boldsymbol{u}_{ad}} \right\| < 1 \,.$$

In the case of a completely decoupled MIMO system is equivalent to the conditions in [62]

$$\operatorname{sgn}\left(\partial h_i / \partial u_i\right) = \operatorname{sgn}(b_i), \quad i = 1, \cdots, m \tag{5.20}$$

$$|b_i| > |\partial h_i / \partial u_i| / 2 > 0, \quad i = 1, \cdots, m. \tag{5.21}$$

The first condition states that unmodeled control reversal is not permissible, and the second condition places a lower bound on the estimate of the control effectiveness, b_i.

For the design of the adaptive controller, we will refer to the universal approximation property of NN as in (3.2) in a MIMO setting.

Theorem 5.1. *Given arbitrary $\epsilon > 0$, there exists a set of bounded weights M, N and a positive time delay $d > 0$, such that the modeling error $\boldsymbol{\Delta}_1(\boldsymbol{\xi}, \boldsymbol{z}, \boldsymbol{u})$ in (5.18) can be approximated over a compact set $\mathcal{D}_x \times \mathcal{D}_u$ by a SHL NN*

$$\boldsymbol{\Delta}_1(\boldsymbol{\xi}, \boldsymbol{z}, \boldsymbol{u}) \;\; = \;\; M^T \boldsymbol{\sigma}(N^T \boldsymbol{\eta}) + \boldsymbol{\varepsilon}(\boldsymbol{\eta}), \quad \|\boldsymbol{\varepsilon}\| < \epsilon \tag{5.22}$$

using the input vector:

$$\boldsymbol{\eta}(t) = \left[\begin{array}{ccc} 1 & \bar{\boldsymbol{y}}_d^T(t) & \bar{\boldsymbol{u}}_d^T(t) \end{array}\right]^T, \quad \|\boldsymbol{\eta}\| \leq \eta^*, \tag{5.23}$$

where $\bar{\boldsymbol{y}}_d(t), \bar{\boldsymbol{u}}_d(t)$ are the vectors of delayed values of the measurement and control variables respectively, and η^* is a known uniform bound on $\mathcal{D}_x \times \mathcal{D}_u$.

5.4 Adaptive Controller, Error Dynamics and Adaptation Laws

The adaptive signal u_{nn} is designed as in (4.14)

$$\boldsymbol{u}_{ad} = \widehat{M}^T \boldsymbol{\sigma}(\widehat{N}^T \boldsymbol{\eta}), \tag{5.24}$$

where $\widehat{M}$ and $\widehat{N}$ are estimates of M and N to be adapted online. Using (5.18), (5.13), and (5.12), the nonlinear system in (5.3) under the regulation of (5.19) along with (5.7) can be written as

$$\begin{aligned} \dot{\boldsymbol{x}} &= \bar{A}\boldsymbol{x} + \bar{B}\boldsymbol{y}_c - B_1 \boldsymbol{u}_{ad} + \boldsymbol{\Delta} \\ \dot{\boldsymbol{z}}_2 &= \boldsymbol{f}_2(\boldsymbol{\xi}, \boldsymbol{z}_1, \boldsymbol{z}_2) \\ \boldsymbol{y} &= \bar{C}\boldsymbol{x}\,, \end{aligned} \tag{5.25}$$

in which

$$\boldsymbol{x} = \left[\begin{array}{c} \boldsymbol{\xi} \\ \boldsymbol{z}_1 \\ \boldsymbol{x}_c \end{array}\right], \quad B_1 = \left[\begin{array}{c} B \\ 0 \\ 0 \end{array}\right]_{(n_m+n_c)\times m},$$

$$\boldsymbol{\Delta} = \left[\begin{array}{c} \bar{\boldsymbol{\Delta}}_1 \\ \boldsymbol{\Delta}_2 \\ 0 \end{array}\right], \quad \bar{\boldsymbol{\Delta}}_1 = \left[\begin{array}{c} \boldsymbol{\Delta}_1^1 \\ \vdots \\ \boldsymbol{\Delta}_1^m \end{array}\right], \quad \boldsymbol{\Delta}_1^i = \left[\begin{array}{c} 0 \\ \vdots \\ \boldsymbol{b}_i^T \boldsymbol{\Delta}_1 \end{array}\right]_{r_i \times 1}.$$

With the following definition of the error vector

$$\boldsymbol{E} \triangleq \left[\begin{array}{ccc} (\boldsymbol{\xi}_l - \boldsymbol{\xi})^T & (\boldsymbol{z}_l - \boldsymbol{z}_1)^T & (\boldsymbol{x}_{cl} - \boldsymbol{x}_c)^T \end{array}\right]^T \tag{5.26}$$

following (5.10) and (5.25), the error dynamics can be expressed as

$$\begin{aligned}\dot{\boldsymbol{E}} =& \bar{A}\boldsymbol{E} + B_1(\boldsymbol{u}_{ad} - \bar{\boldsymbol{\Delta}}_1) - B_2\boldsymbol{\Delta}_2 \\ \dot{\boldsymbol{z}}_2 =& \boldsymbol{f}_2(\boldsymbol{\xi}, \boldsymbol{z}_1, \boldsymbol{z}_2) \\ \boldsymbol{Z} =& \bar{C}\boldsymbol{E}\,,\end{aligned} \tag{5.27}$$

where $\boldsymbol{Z}$ represents the signals available for feedback

$$\boldsymbol{Z} = \begin{bmatrix} \boldsymbol{y}_l - \boldsymbol{y} \\ \boldsymbol{x}_{cl} - \boldsymbol{x}_c \end{bmatrix} = \bar{C}\boldsymbol{E}\,. \tag{5.28}$$

Notice that (5.27) has the same form as (4.10) with the only difference being the input/output dimension. Thus, the remaining control design procedure is the same as that in Section 4.3. We introduce the following linear error observer for the dynamics in (5.27)

$$\begin{aligned}\dot{\widehat{\boldsymbol{E}}} &= \bar{A}\widehat{\boldsymbol{E}} + K(\boldsymbol{z} - \hat{\boldsymbol{z}}) \\ \hat{\boldsymbol{z}} &= \bar{C}\widehat{\boldsymbol{E}},\end{aligned} \tag{5.29}$$

where K is chosen to make $\tilde{A} \triangleq \bar{A} - K\bar{C}$ Hurwitz, and the following adaptive laws

$$\begin{aligned}\dot{\widehat{M}} =& -\Gamma_M[(\hat{\boldsymbol{\sigma}} - \hat{\sigma}'\widehat{N}^T\boldsymbol{\eta})\widehat{\boldsymbol{E}}^T P B_1 + k\widehat{M}] \\ \dot{\widehat{N}} =& -\Gamma_N[\boldsymbol{\eta}\widehat{\boldsymbol{E}}PB_1\widehat{M}^T\hat{\sigma}' + k\widehat{N}]\,,\end{aligned} \tag{5.30}$$

in which the NN parameters have the same meaning as in (3.49). This choice of adaptive laws is based on Lyapunov's direct method and partially cancels out the uncertainties in the error dynamics as it will be demonstrated in Section 5.5.

The stability of the closed-loop system should be addressed along with the observer error dynamics. Define the signal $\widetilde{\boldsymbol{E}} = \widehat{\boldsymbol{E}} - \boldsymbol{E}$. Then

$$\dot{\widetilde{\boldsymbol{E}}} = \widetilde{A}\widetilde{\boldsymbol{E}} - B_1(\boldsymbol{u}_{ad} - \bar{\boldsymbol{\Delta}}_1) + B_2\boldsymbol{\Delta}_2. \tag{5.31}$$

We immediately note that given Hurwitz $\widetilde{A}$, there exists a unique positive definite matrix $\widetilde{P} = \widetilde{P}^T$, solving the Lyapunov equation for arbitrary $\widetilde{Q} > 0$

$$\widetilde{A}^T\widetilde{P} + \widetilde{P}\widetilde{A} + \widetilde{Q} = 0. \tag{5.32}$$

5.5 Stability Analysis

In this section we will show through Lyapunov's direct method that both the tracking and observation errors $\boldsymbol{E}, \widetilde{\boldsymbol{E}}$ along with the NN weight errors $\widetilde{M} \triangleq \widehat{M} - M, \quad \widetilde{N} \triangleq \widehat{N} - N$ are ultimately bounded. Consider the following composite error vector

$$\boldsymbol{\zeta} = \left[\begin{array}{cccc} \boldsymbol{E}^T & \widetilde{\boldsymbol{E}}^T & \boldsymbol{z}_2 & \mathbf{vec}\widetilde{Z} \end{array} \right]^T , \tag{5.33}$$

where $\widetilde{Z} \triangleq \left[\begin{array}{cc} \widetilde{M} & 0 \\ 0 & \widetilde{N} \end{array} \right]$, and the operator **vec** is stacking a matrix into a vector. Notice that the following upper bounds can be immediately derived:

$$\|\widehat{M}\|_F < \|\widetilde{M}\|_F + M^*, \quad \|\widehat{N}\|_F < \|\widetilde{N}\|_F + N^* , \tag{5.34}$$

where M^*, N^* are known upper bounds on the Frobenius norms of the weights in (5.22):

$$\|M\|_F < M^*, \quad \|N\|_F < N^*. \tag{5.35}$$

With (5.34), the forcing term in (5.27) and (5.31) can be upper bounded in terms of some constants α_1 and α_2

$$\|\widehat{M}^T\boldsymbol{\sigma}(\widehat{N}^T\boldsymbol{\eta}) - M^T\boldsymbol{\sigma}(N^T\boldsymbol{\eta}) - \boldsymbol{\varepsilon}\| \leq \alpha_1\|\widetilde{Z}\|_F + \alpha_2, \quad \alpha_1 > 0, \quad \alpha_2 > 0 . \tag{5.36}$$

For the stability proof we need the following representations

$$\widehat{M}^T\boldsymbol{\sigma}(\widehat{N}^T\boldsymbol{\eta}) - M^T\boldsymbol{\sigma}(N^T\boldsymbol{\eta}) - \boldsymbol{\varepsilon} \;\; = \;\; \widetilde{M}^T\left(\hat{\boldsymbol{\sigma}} - \hat{\sigma}'\widehat{N}^T\boldsymbol{\eta}\right) + \widehat{M}^T\hat{\sigma}'\widetilde{N}^T\boldsymbol{\eta} + \boldsymbol{w} - \boldsymbol{\varepsilon}, \tag{5.37}$$

where

$$\boldsymbol{w} = \widetilde{M}^T\hat{\sigma}'N^T\boldsymbol{\eta} - M^T\mathcal{O}(\widetilde{N}^T\boldsymbol{\eta})^2 . \tag{5.38}$$

This is achieved via Taylor series expansion of $\boldsymbol{\sigma}(N^T\boldsymbol{\eta})$ around the estimate $\widehat{N}^T\boldsymbol{\eta}$ [120]. Over the compact set $\mathcal{D}_x \times \mathcal{D}_u$ the following upper bounds can be derived [120]

$$\|\boldsymbol{w} - \boldsymbol{\varepsilon}\| \leq \gamma_1\|\widetilde{Z}\|_F + \gamma_2 , \qquad \gamma_1 > 0, \quad \gamma_2 > 0 , \tag{5.39}$$

where γ_1, γ_2 are constants, such that γ_1 depends upon η^*, while γ_2 depends upon ϵ.

Notice that the upper bound introduced in (5.14) can be further upper bounded

$$\|\boldsymbol{\Delta}_2\| \leq \delta_1 \Big\{ \|\boldsymbol{E}\| + \|\boldsymbol{x}_l\| \Big\} + \beta_2 \|\boldsymbol{z}_2\| + \beta_3 \tag{5.40}$$

Given Hurwitz $\bar{A}$ in (5.10) and the bound in (5.8), with $\left\| e^{\bar{A}t} \right\| \leq k_0 e^{A_M t}$, we immediately conclude that

$$\|\boldsymbol{x}_l\| \leq k_0 e^{A_M t} \|\boldsymbol{x}_l(0)\| + \frac{k_0}{A_M} \|\bar{B}\| \beta_c \triangleq \beta_4 \,, \tag{5.41}$$

where A_M is introduced for the maximum eigenvalue of A. Thus, the bound in (5.40) can be rewritten

$$\begin{aligned} \|\boldsymbol{\Delta}_2\| &\leq \delta_1 \Big\{ \|\boldsymbol{E}\| + \beta_4 \Big\} + \beta_2 \|\boldsymbol{z}_2\| + \beta_3 \\ &= \delta_1 \|\boldsymbol{E}\| + \delta_1 \beta_4 + \beta_2 \|\boldsymbol{z}_2\| + \beta_3 \end{aligned} \tag{5.42}$$

and ultimately put in the form:

$$\|\boldsymbol{\Delta}_2\| \leq \delta_1 \|\boldsymbol{E}\| + \beta_2 \|\boldsymbol{z}_2\| + \delta_2 \,, \tag{5.43}$$

where $\delta_2 = \delta_1 \beta_4 + \beta_3$. With the same rationale, the relation in (5.16) can be upper bounded

$$\dot{V}_{\boldsymbol{z}_2} \leq -\frac{c_3}{2} \|\boldsymbol{z}_2\|^2 + \frac{(c_4 c_5)^2}{c_3} \|\bar{\boldsymbol{\xi}}\|^2 \leq -\frac{3c_3}{4} \|\boldsymbol{z}_2\|^2 + \frac{(c_4 c_5)^2}{c_3} \|\bar{\boldsymbol{E}}\|^2 + \frac{(c_4 c_5)^2}{c_3} \beta_4^2 \,. \tag{5.44}$$

With the upper bounds derived in (5.34), (5.36), (5.39) and (5.43), using Lyapunov's direct method, we will prove that the error signals are ultimately bounded. For that we need to introduce a positive invariant set in the error space to which the initial errors can belong. Later, we will show that given an initial condition in that set, the error signals will be ultimately bounded. Notice that the error vector in (5.33) has been defined using the state variables $\boldsymbol{\xi}, \boldsymbol{\xi}_l, \boldsymbol{z}_1, \boldsymbol{z}_l, \boldsymbol{x}_c, \boldsymbol{x}_{cl}, \boldsymbol{z}_2, \widehat{\boldsymbol{E}}, \widehat{Z}$ and the constant matrix Z:

$$\boldsymbol{\zeta} = \boldsymbol{F}(\boldsymbol{\xi}, \boldsymbol{\xi}_l, \boldsymbol{z}_1, \boldsymbol{z}_l, \boldsymbol{x}_c, \boldsymbol{x}_{cl}, \boldsymbol{z}_2, \widehat{\boldsymbol{E}}, \widehat{Z}, Z) \,, \tag{5.45}$$

where $\widehat{Z} = \begin{bmatrix} \widehat{M} & 0 \\ 0 & \widehat{N} \end{bmatrix}$, $Z = \begin{bmatrix} M & 0 \\ 0 & N \end{bmatrix}$, and $\boldsymbol{F}$ represents an *implicit* mapping from the original domains of the arguments to the space of error variables. Recall that (5.22) introduces the set $\mathcal{D}_x \times \mathcal{D}_u$ in the state space over which the NN approximation is valid.

Based on the definition of error variables and continuity of solutions of differential equations, this set maps onto a bounded set $\Omega_{\boldsymbol{\zeta}}$ in the error space. Introduce the largest hypersphere which is included in $\Omega_{\boldsymbol{\zeta}}$ in the error space:

$$B_R \triangleq \{\boldsymbol{\zeta} \mid \|\boldsymbol{\zeta}\| \leq R\}\,, \quad R > 0\,. \tag{5.46}$$

For every $\boldsymbol{\zeta} \in B_R$, we have $(\boldsymbol{x}, \boldsymbol{u}) \in \mathcal{D}_x \times \mathcal{D}_u$, ensuring that the NN approximation in (5.22) remains valid. Consider the following gain matrices:

$$T_1 \triangleq \frac{1}{2}\begin{bmatrix} 2P & 0 & 0 & 0 & 0 \\ 0 & 2\tilde{P} & 0 & 0 & 0 \\ 0 & 0 & \Gamma_M^{-1} & 0 & 0 \\ 0 & 0 & 0 & \Gamma_N^{-1} & 0 \\ 0 & 0 & 0 & 0 & c_1 I \end{bmatrix}, \quad T_2 \triangleq \frac{1}{2}\begin{bmatrix} 2P & 0 & 0 & 0 & 0 \\ 0 & 2\tilde{P} & 0 & 0 & 0 \\ 0 & 0 & \Gamma_M^{-1} & 0 & 0 \\ 0 & 0 & 0 & \Gamma_N^{-1} & 0 \\ 0 & 0 & 0 & 0 & c_2 I \end{bmatrix}, \tag{5.47}$$

where I is the identity matrix of dimension $(n - n_m) \times (n - n_m)$ and the following positive definite function, which will further be used for the stability analysis:

$$V(\boldsymbol{\zeta}) = \boldsymbol{E}^T P \boldsymbol{E} + \tilde{\boldsymbol{E}}^T \tilde{P} \tilde{\boldsymbol{E}} + \frac{1}{2}\mathrm{tr}(\widetilde{M}^T \Gamma_M^{-1} \widetilde{M}) + \frac{1}{2}\mathrm{tr}(\widetilde{N}^T \Gamma_N^{-1} \widetilde{N}) + V_{\boldsymbol{z}_2}(\boldsymbol{z}_2)\,. \tag{5.48}$$

Notice that the bounds in (5.15) immediately imply:

$$\boldsymbol{\zeta}^T T_1 \boldsymbol{\zeta}^T \leq V(\boldsymbol{\zeta}) \leq \boldsymbol{\zeta}^T T_2 \boldsymbol{\zeta}^T\,. \tag{5.49}$$

Let

$$\alpha \triangleq \min_{\|\boldsymbol{\zeta}\|=R} \boldsymbol{\zeta}^T T_1 \boldsymbol{\zeta}^T = R^2 T_{1_m}\,,$$

where T_{1_m} is the minimum eigenvalue of T_1. Introduce the following set:

$$\Omega_\alpha = \{\boldsymbol{\zeta} \in B_R \mid V(\boldsymbol{\zeta}) \leq \alpha\}\,. \tag{5.50}$$

Assumption 5.5. *Assume*

$$R > \gamma \sqrt{\frac{T_{2_M}}{T_{1_m}}} \geq \gamma\,, \tag{5.51}$$

where T_{2_M} is the maximum eigenvalue of the matrix T_2, defined in (5.47), γ is defined as:

$$\begin{aligned}
\gamma &= \max(C_1, C_2, C_3, C_4) \\
C_1 &= \sqrt{\frac{\|PB_1\|^2\gamma_2^2 + \kappa_2^2 + \bar{Z} + \delta_2^2(\|PB_2\|^2 + \|\tilde{P}B_2\|^2) + \frac{(c_4c_5)^2}{c_3}\beta_4^2}{Q_m - 3 - 2\delta_1\|PB_2\| - \frac{(c_4c_5)^2}{c_3} - \frac{(2\|PB_2\|\beta_2)^2}{c_3}}} \\
C_2 &= \sqrt{\frac{\|PB_1\|^2\gamma_2^2 + \kappa_2^2 + \bar{Z} + \delta_2^2(\|PB_2\|^2 + \|\tilde{P}B_2\|^2) + \frac{(c_4c_5)^2}{c_3}\beta_4^2}{\tilde{Q}_m - 3 - 2\delta_1\|\tilde{P}B_2\| - \frac{(2\|\tilde{P}B_2\|\beta_2)^2}{c_3}}} \\
C_3 &= \sqrt{\frac{\|PB_1\|^2\gamma_2^2 + \kappa_2^2 + \bar{Z} + \delta_2^2(\|PB_2\|^2 + \|\tilde{P}B_2\|^2) + \frac{(c_4c_5)^2}{c_3}\beta_4^2}{\frac{k}{2} - \kappa_1^2 - [\gamma_1\|PB_1\|]^2}} \\
C_4 &= 2\sqrt{\frac{\|PB_1\|^2\gamma_2^2 + \kappa_2^2 + \bar{Z} + \delta_2^2(\|PB_2\|^2 + \|\tilde{P}B_2\|^2) + \frac{(c_4c_5)^2}{c_3}\beta_4^2}{c_3}}
\end{aligned}$$

where $\bar{Z} = \frac{k}{2}\left[\|M\|_F^2 + \|N\|_F^2\right]$, $\kappa_1 = \Theta\alpha_1 + \|PB_1\|\gamma_1$, $\kappa_2 = \Theta\alpha_2 + \|PB_1\|\gamma_2$, $\Theta \triangleq \|PB_1\| + \|\tilde{P}B_1\|$. Further assume that δ_1 is such that the matrix $\widetilde{Q}$ in the Lyapunov equation in (5.32) can be chosen to satisfy the following condition

$$\widetilde{Q}_m > 3 + 2\delta_1\|\tilde{P}B_2\| + \frac{(2\|\tilde{P}B_2\|\beta_2)^2}{c_3}. \tag{5.52}$$

And finally let the σ-modification gain satisfy the following lower bound $k > 2\left[\kappa_1^2 + \gamma_1^2\|PB_1\|^2\right]$.

The significance of this Assumption is discussed in Remarks 5.3 and 5.4. We are now ready to state the main result.

Theorem 5.2. *Let Assumptions 5.1-5.5 hold. Then, if the initial error $\boldsymbol{\zeta}(0)$ belongs to the compact set Ω_α, defined in (5.50), the feedback control law given by (5.19), (5.24), along with (5.30), guarantees that the signals $\boldsymbol{E}, \tilde{\boldsymbol{E}}, \boldsymbol{z}_2, \widetilde{M}, \widetilde{N}$ in the closed loop system are ultimately bounded.*

Proof. See Appendix.

Remark 5.3. The bounded analysis explicitly shows the "price" of the error in modelling of non-minimum phase zeros on the tracking performance. If $\boldsymbol{\Delta}_2 = 0$, implying $\beta_i = 0,\ i = 0, 1, 2, 3,\ \delta_1 = \delta_2 = 0$, Lyapunov analysis results in the ultimate bounds in (C.8), as one can find in [63] where a similar approach has been developed for minimum phase systems. The terms, involving c_i's and β_4 in the ultimate bounds, indicate the price of the

unmodeled dynamics on the tracking performance. The ultimate bounds also imply that the non-minimum phase zeros of the nonlinear system and the unmodeled dynamics are compensated by the linear design gains, and *not* by adaptation. This defines the approach to be *robust adaptive* in a sense that adaptation is compensating only for the matched uncertainties in the error dynamics.

Remark 5.4. Assumption 5.5 may be interpreted as implying both an upper and lower bound for the adaptation gains. Define $\bar{\gamma} \triangleq \max(\lambda_{\max}(F), \lambda_{\max}(G))$, $\underline{\gamma} \triangleq \min(\lambda_{\min}(F), \lambda_{\min}(G))$ and $\bar{\lambda} \triangleq \max(\lambda_{\max}(P), \lambda_{\max}(\tilde{P}))$ and $\underline{\lambda} \triangleq \min(\lambda_{\min}(P), \lambda_{\min}(\tilde{P}))$, where $\lambda(\cdot)$ denotes the eigenvalue. Then an upper bound for the adaptation gains results when $2\bar{\lambda}\underline{\gamma} > 1$ and $2\underline{\lambda}\bar{\gamma} > 1$, for which the relation in (5.51) reduces to $\bar{\gamma} < R^2/(2\gamma^2\bar{\lambda})$. A lower bound for the adaptation gains results when $2\bar{\lambda}\underline{\gamma} < 1$ and $2\underline{\lambda}\bar{\gamma} < 1$, for which (5.51) reduces to $\underline{\gamma} > \gamma^2/(2R^2\underline{\lambda})$.

Remark 5.5. The assumption on global exponential stability and global Lipschitz of the $\boldsymbol{z}_2$ dynamics in (5.13) can be relaxed to input-to-state practical stabilizability assumption [121], if instead of conic sector bound on $\boldsymbol{\Delta}_2$ one considers constant norm bound. The proof can be completed without the use of $V_{\boldsymbol{z}_2}$ in the Lyapunov function.

Remark 5.6. In many applications it is very often the case that the available linear model and the linear control design for it are predetermined and cannot be altered. If this linear controller does not ensure that the conditions in (5.17), (5.51), (5.52) can be satisfied, then an additional linear controller u_{dc} can be introduced to "speed up" the error dynamics following the procedure described after Theorem 4.1. In this case, the conceptual layout for the overall design process is summarized in Figure 4.1.

5.6 Simulation Results

Consider the system depicted in Figure 5.1. An inverted pendulum of mass m is connect by a massless rod to a cart of mass M_1, which is in turn connected to additional carts of mass M_2, M_3 serially through springs and dampers. The equations of motion for the system can

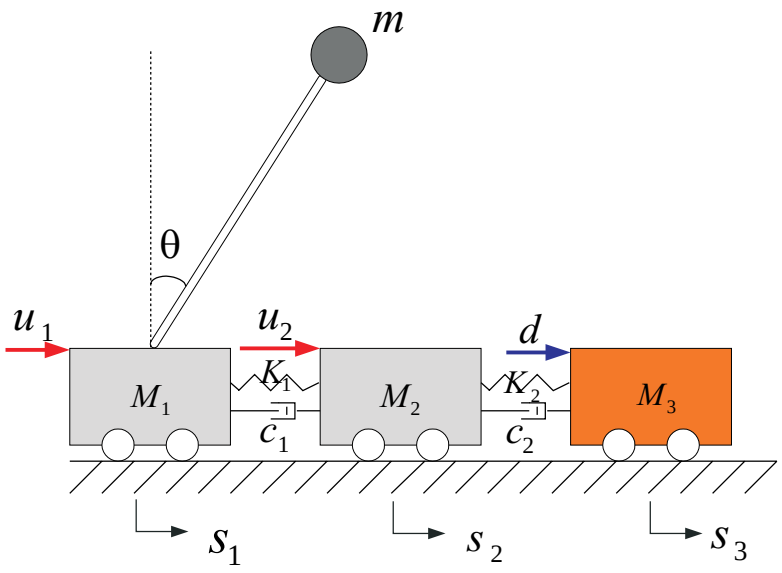

Fig. 5.1: An Inverted Pendulum with Coupled Masses.

be described as follows:

$$\begin{aligned}
&(M_1+m)\ddot{s}_1 + c_1(\dot{s}_1-\dot{s}_2) + K_1(s_1-s_2) + mL(\ddot{\theta}\cos\theta - \dot{\theta}^2\sin\theta) = u_1\\
&mL(\ddot{s}_1 + L\ddot{\theta} - g\sin\theta) = 0\\
&M_2\ddot{s}_2 - c_1(\dot{s}_1-\dot{s}_2) - K_1(s_1-s_2) + c_2(\dot{s}_2-\dot{s}_3) + K_2(s_2-s_3) = u_2\\
&M_3\ddot{s}_3 - c_2(\dot{s}_2-\dot{s}_3) - K_2(s_2-s_3) = d
\end{aligned} \tag{5.53}$$

where u_1, u_2 are input forces, d is an external disturbance, L is is the length of the rod, g is the gravitational acceleration, K_1, K_2 are the spring constants, and c_1, c_2 are the damping coefficients. The parameter values are: $M_1 = M_2 = 1.378, m = M_3 = 0.051, g = 9.8, L = 0.325, K_1 = 15, K_2 = 20, c_1 = 2.7, c_2 = 2.2$. The measured variables consist of the displacements of the carts s_1, s_2, and the angle of the pendulum θ. The control objective is to have s_1, s_2 track reference commands s_{1_c}, s_{2_c} while balancing the pendulum.

With the definition: $\xi_1^1 = s_1, \xi_1^2 = \dot{s}_1, \xi_2^1 = s_2, \xi_2^2 = \dot{s}_2, z_1^1 = \theta, z_1^2 = \frac{\dot{s}_1}{L}\cos\theta + \dot{\theta}, z_2^1 =$

$s_3, z_2^2 = \dot{s}_3$, the system in (5.53) is put into its normal form:

$$
\begin{aligned}
\dot{\xi}_1^1 &= \xi_1^2 \\
\dot{\xi}_1^2 &= \frac{1}{M_1 + m\sin^2 z_1^1}[-K_1(\xi_1^1 - \xi_2^1) - c_1(\xi_1^2 - \xi_2^2) - mg\sin z_1^1 \cos z_1^1 + mL\dot{\theta}^2 \sin z_1^1] \\
&\quad + \frac{1}{M_1 + m\sin^2 z_1^1} u_1 \\
\dot{\xi}_2^1 &= \xi_2^2 \\
\dot{\xi}_2^2 &= \frac{1}{M_2}[K_1(\xi_1^1 - \xi_2^1) + c_1(\xi_1^2 - \xi_2^2) - K_2(\xi_2^1 - z_2^1) - c_2(\xi_2^2 - z_2^2)] \\
&\quad + \frac{1}{M_2} u_2 \\
\dot{z}_1^1 &= z_1^2 - \frac{\xi_1^2}{L}\cos z_1^1 \\
\dot{z}_1^2 &= \frac{g}{L}\sin z_1^1 - \frac{\xi_1^2}{L}\dot{\theta}\sin z_1^1 \\
\dot{z}_2^1 &= z_2^2 \\
\dot{z}_2^2 &= \frac{1}{M_3}[K_2(\xi_2^1 - z_2^1) + c_2(\xi_2^2 - z_2^2)] + \frac{d}{M_3}
\end{aligned}
\tag{5.54}
$$

Its zero dynamics are given by:

$$
\begin{aligned}
\dot{z}_1^1 &= z_1^2 \\
\dot{z}_1^2 &= \frac{g}{L}\sin z_1^1 \\
\dot{z}_2^1 &= z_2^2 \\
\dot{z}_2^2 &= \frac{1}{M_3}[-K_2 z_2^1 - c_2 z_2^2] + \frac{d}{M_3}.
\end{aligned}
\tag{5.55}
$$

Linearization of z_1^1, z_1^2 dynamics in (5.55) about vertical-up position (0,0) reveals an unstable mode at $\sqrt{\frac{g}{L}}$. Therefore the system is non-minimum phase.

The linear design model in (5.6) is constructed by linearizing Eq.(5.53) with respect to its zero position. Further, the dynamics associated with M_3 are ignored. With $d = 0$, the function $\boldsymbol{f}_2$ in (5.13) is written as:

$$
\boldsymbol{f}_2(\boldsymbol{\xi}, \boldsymbol{z}_1, \boldsymbol{z}_2) = \begin{bmatrix} z_2^2 \\ \frac{1}{M_3}[K_2(\xi_2^1 - z_2^1) + c_2(\xi_2^2 - z_2^2)] \end{bmatrix}. \tag{5.56}
$$

The zero solution for $\dot{\boldsymbol{z}}_2 = \boldsymbol{f}_2(0, 0, \boldsymbol{z}_2)$ is globally exponentially stable, and $\boldsymbol{f}_2$ is globally Lipschitz in its arguments. With the variables: $\xi_{l_1}^1 = s_1, \xi_{l_1}^2 = \dot{s}_1, \xi_{l_2}^1 = s_2, \xi_{l_2}^2 = \dot{s}_2, z_{l_1}^1 =$

$\theta, z_{l_1}^2 = \frac{\dot{s}_1}{L} + \dot{\theta}$, the normal form for the linear model leads to the following system matrices:

$$
\begin{aligned}
A_{11} &= \begin{bmatrix} 0 & 1 \\ -\frac{\hat{K}_1}{\hat{M}_1} & -\frac{\hat{c}_1}{\hat{M}_1} \end{bmatrix}, \quad A_{12} = \begin{bmatrix} 0 & 0 \\ \frac{\hat{K}_1}{\hat{M}_1} & \frac{\hat{c}_1}{\hat{M}_1} \end{bmatrix}, \quad B_z^1 = \begin{bmatrix} 0 & 0 \\ -\frac{\hat{m}}{\hat{M}_1} g & 0 \end{bmatrix}, B_1 = \begin{bmatrix} 0 & 0 \\ \frac{1}{\hat{M}_1} & 0 \end{bmatrix} \\
A_{21} &= \begin{bmatrix} 0 & 0 \\ \frac{\hat{K}_1}{\hat{M}_2} & \frac{\hat{c}_1}{\hat{M}_2} \end{bmatrix}, \quad A_{22} = \begin{bmatrix} 0 & 1 \\ -\frac{\hat{K}_1}{\hat{M}_2} & -\frac{\hat{c}_1}{\hat{M}_2} \end{bmatrix}, \quad B_z^2 = \begin{bmatrix} 0 & 0 \\ 0 & 0 \end{bmatrix}, \quad B_2 = \begin{bmatrix} 0 & 0 \\ 0 & \frac{1}{\hat{M}_2} \end{bmatrix} \\
G_o &= \begin{bmatrix} 0 & -\frac{1}{L} & 0 & 0 \\ 0 & 0 & 0 & 0 \end{bmatrix}, \quad F_o = \begin{bmatrix} 0 & 1 \\ \frac{g}{L} & 0 \end{bmatrix}
\end{aligned}
\tag{5.57}
$$

where $\hat{M}_1, \hat{M}_2, \hat{m}, \hat{K}_1, \hat{c}_1$ are estimates for parameters M_1, M_2, m, K_1, c_1. These are chosen as: $\hat{M}_1 = \hat{M}_2 = 1.8, \hat{m} = 0.14, \hat{K}_1 = 10, \hat{c}_1 = 1.0$. Each parameter has at least 25% parametric error in its value. Comparing (5.54) to the plant model described by the system matrices in (5.57) leads to the following expressions for the modelling errors:

$$
\begin{aligned}
\Delta_1^1 &= \frac{\hat{M}_1}{M_1 + m\sin^2 z_1^1}[-K_1(\xi_1^1 - \xi_2^1) - c_1(\xi_1^2 - \xi_2^2) - mg\sin z_1^1 \cos z_1^1 + mL\dot{\theta}^2 \sin z_1^1] \\
&\quad + \frac{\hat{M}_1}{M_1 + m\sin^2 z_1^1} u_1 + [\hat{K}_1(\xi_1^1 - \xi_2^1) + \hat{c}_1(\xi_1^2 - \xi_2^2) + \hat{m}g z_1^1] - u_1 \\
\Delta_1^2 &= \frac{\hat{M}_2}{M_2}[K_1(\xi_1^1 - \xi_2^1) + c_1(\xi_1^2 - \xi_2^2) - K_2(\xi_2^1 - z_2^1) - c_2(\xi_2^2 - z_2^2)] + \frac{\hat{M}_2}{M_2} u_2 \\
&\quad - [\hat{K}_1(\xi_1^1 - \xi_2^1) + \hat{c}_1(\xi_1^2 - \xi_2^2)] - u_2 \\
\Delta_2^1 &= -\frac{\xi_1^2}{L}\cos z_1^1 + \frac{\xi_1^2}{L} \\
\Delta_2^2 &= \frac{g}{L}\sin z_1^1 - \frac{\xi_1^2}{L}\dot{\theta}\sin z_1^1 - \frac{g}{L} z_1^1.
\end{aligned}
\tag{5.58}
$$

The dynamic compensator in (5.7) is designed as a Linear Quadratic Gaussian (LQG) controller based on the linear model in (5.57), in which three measured outputs $\xi_{l_1}^1 (= s_1), \xi_{l_2}^1 (= s_2), z_l^1 (= \theta)$ are available for control design. Its design follows a non-zero regulation procedure used in [118] to track the given reference command $\boldsymbol{y}_c^T = [s_{1_c},\ s_{2_c}]^T$. Since $\boldsymbol{x}_{cl} - \boldsymbol{x}_c$ is available, we employ a reduced order observer to obtain estimates for unavailable errors $[(\boldsymbol{\xi}_l - \boldsymbol{\xi})^T, (\boldsymbol{z}_l - \boldsymbol{z}_1)^T]^T$.

The SHL NN consists of 6 neurons, 12 inputs and 2 outputs. Its learning rate F, G are tuned as a diagonal matrices. The $\sigma-$modification factor $k = 10.5$. The simulations are

run with the following initial conditions:

$$s_1(0) = -0.1, \dot{s}_1(0) = 0, s_2(0) = 0.01, \dot{s}_2(0) = 0, s_3(0) = \dot{s}_3(0) = 0, \theta(0) = 25^\circ, \dot{\theta}(0) = 10^\circ/s,$$

and the reference commands s_{1_c}, s_{2_c} are square waves having a magnitude of 0.1 m and a frequency of 1/30 Hz. These reference commands correspond to synchronous motion for the first two carts. Figure 5.2 compares s_1, s_2 with and without augmentation, for $d = 0$. The system regulated by the linear controller goes unstable. The augmented system not only stabilizes the system but also suppresses the oscillatory responses. Furthermore, the

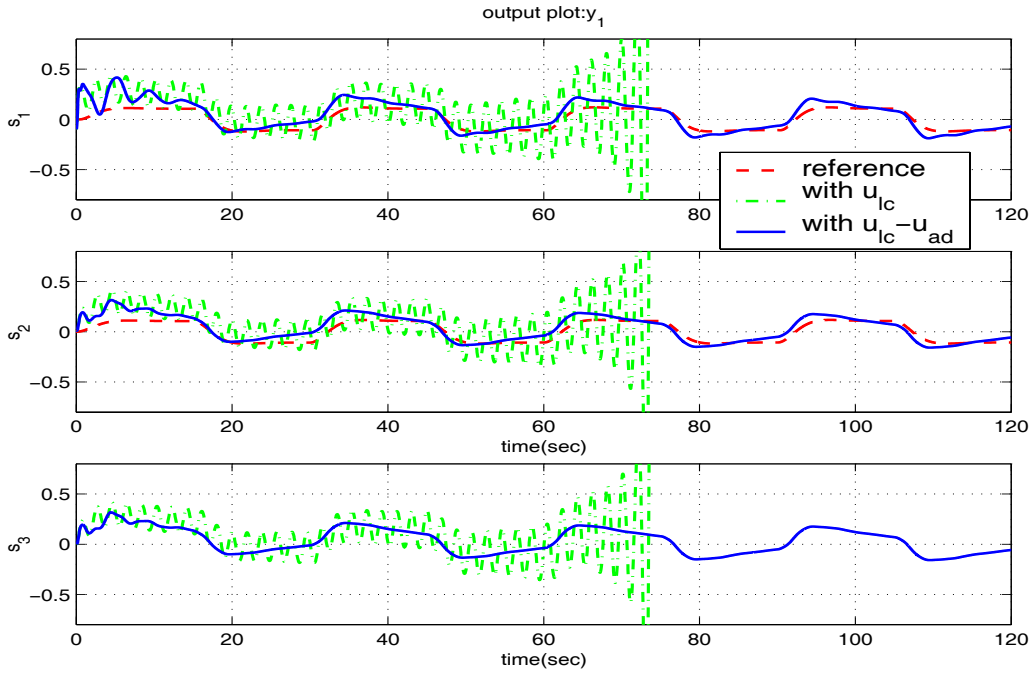

Fig. 5.2: Comparison of Regulated Outputs with/without Augmentation

motion of the unmodelled cart (s_3) is also synchronized. Figure 5.3 compares the adaptive signals and the modelling error that they are intended to approximately cancel. Large oscillations up to 10 sec. are mainly caused by initial conditions. The decay in the modelling errors, after 10 sec., can be explained by the fact that the effects of springs and dampers become negligible as synchronized motion is achieved, and the nonlinear terms related to the pendulum dynamics become small as it is balanced.

Figures 5.4 and 5.5 depict stabilization and tracking with disturbance $d(t) = 0.1(\sin 1t + \sin 3t + \sin 5t + \sin 10t + \sin 20t)$. Note that excellent disturbance rejection is achieved.

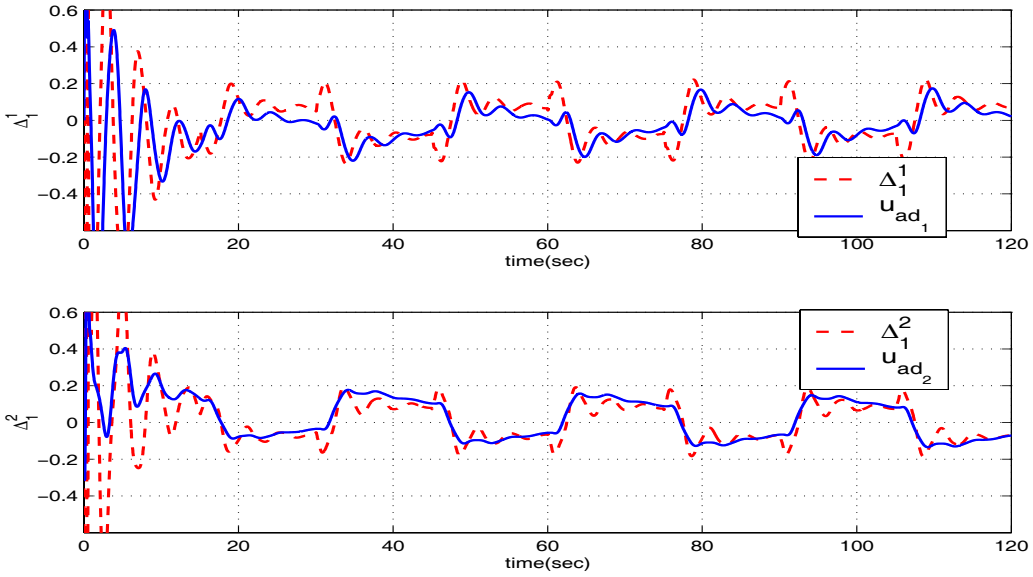

Fig. 5.3: Matched Uncertainty $\boldsymbol{\Delta}_1$ and Adaptive Signal $\boldsymbol{u}_{ad}$.

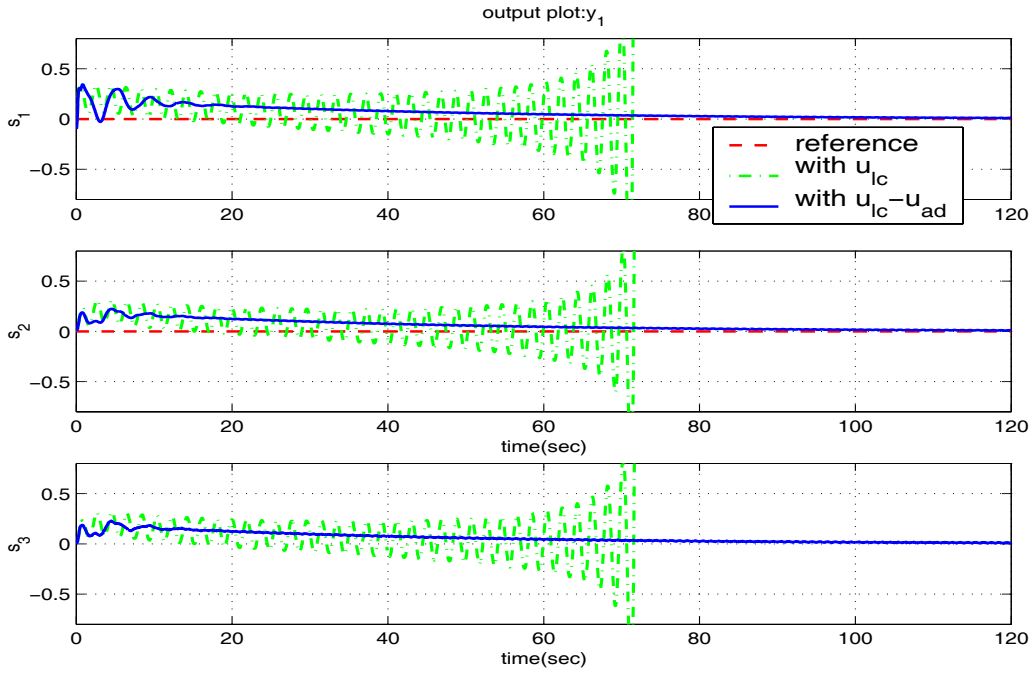

Fig. 5.4: Stabilization of the Carts with/without Augmentation when subjected to an External Disturbance

That is, the disturbance is not attenuated, but rather nearly cancelled by adaptation.

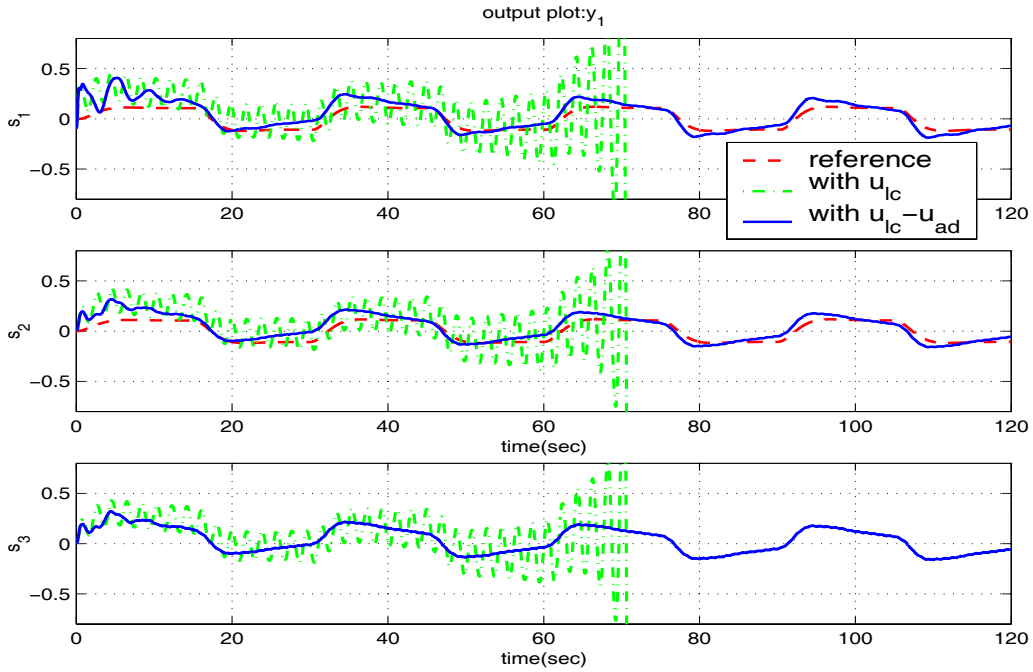

Fig. 5.5: Displacements of the Carts with/without Augmentation when subjected to an External Disturbance

5.7 Conclusion

This chapter describes an approach for augmenting a linear controller with an output feedback adaptive element in a MIMO setting. The approach is applicable to non-minimum phase nonlinear systems. The key properties of the design are that *only* output variables are used, and the design is adaptive to both parametric errors and unmodelled dynamics. The main assumptions are that the vector relative degree of the regulated output is known, and the unmatched uncertainty in the error dynamics satisfies a conic sector bound.

CHAPTER 6

COORDINATED DECENTRALIZED CONTROL OF INTERCONNECTED SYSTEMS

In this chapter, we describe a decentralized adaptive output feedback control design for large-scale interconnected systems. It is assumed that all the controllers share prior information about the system reference models. Based on that information, a linearly parameterized NN is introduced for each subsystem to partially cancel the effect of the interconnections on tracking performance. Boundedness of error signals is shown through Lyapunov's direct method.

6.1 Introduction

With the advent of complex engineering systems, interest in design of decentralized controllers has especially increased. The problem can be briefly formulated as a control design for a system composed of several *dynamically interconnected* subsystems, such that the output of each subsystem has to track a prescpecified reference trajectory, while no communication is allowed between the controllers. The problem was first introduced in [122] for *weakly* interconnected subsystems that have regulated outputs with relative degree 1 or 2. In [123, 124] a framework for model reference adaptive control has been developed under restrictive assumptions: i) positive definiteness of an M-matrix involving unknown constants, ii) relative degrees of outputs being one or two, iii) and matched uncertainties. The first condition was relaxed in [124] using an alternative adaptive high-gain approach, assuming a standard strict matching condition on the disturbances. Relaxation of the condition on subsystem relative degrees was first tried in [125]. Only partially decentralized adaptive controllers were designed. The design relies on bounds for the effects of interactions from the subsystems. In [126] this restriction is relaxed by employing parameter projection together with static normalization. Ref. [127] attempted to remove this condition using

Morse's dynamic certainty equivalence principle. Ref. [128] made a similar attempt using integrator backstepping. Stability results using an indirect pole assignment scheme, without restriction on the relative degrees, were reported in [129–131]. Efforts in relaxing the relative degree constraint in the case of direct adaptive control have been made in [132–134] by using advanced adaptive strategies. Ref. [135] relaxed the assumption on the type of uncertain interconnections, considering a class of large-scale systems with general polynomial-type interconnections with matching conditions. Ref. [136] relaxed the strict matching assumption by combining a high-gain approach with adaptive backstepping. In [137,138], sufficient conditions are derived for asymptotic stabilization of large-scale systems via decentralized controllers. However, these design procedures are not appropriate for systems in which the interconnections are uncertain. In [139–141] large-scale systems have been considered without the matching condition, using polynomial growth conditions on the interconnections, and restricted output nonlinearities. Furthermore, the system nonlinearities are allowed to depend upon unmeasured zero dynamics.

Here we formulate and solve the problem of decentralized adaptive output feedback control for a class of nonlinear subsystems with known relative degrees, subject to unknown interconnections with known upper bound. We depart from attempting to obtain global results, and restrict the synthesis approach to a domain over which the interconnections and nonlinearities can be approximated by a linearly parameterized NN. Similar attempts of incorporating neural networks into decentralized adaptive control have have been reported in [41, 142–145] for design of *state feedback* controllers. Following [84, 85, 146], we assume that the desired trajectories are known to all the controllers, i.e. the controllers share prior information about their goals, and we develop an *adaptive output feedback* synthesis approach that achieves ultimate boundedness of tracking errors. As in [84, 85], we will say that the controllers are engaged in *implicit cooperation*. While most of the existing results in decentralized control literature rely on the definition of a robust controller for dominating the interconnections, we show through Lyapunov's direct method that a linearly parameterized NN, operating over reference model states, can *partially* cancel the interconnection effects. The adaptive laws are based on the adaptive output feedback theory developed

in Chapter 4 for centralized design. Ultimate boundedness of error signals is shown using Lyapunov's direct method. This decentralized method should be viewed as the extension of adaptive output feedback control approach developed in Chapter 4 for centralized control to a decentralized setup, using the viewpoint of [84, 85, 146] for definition of *implicit cooperation*.

This chapter is organized as follows. In Section 6.2 we state the problem formulation and assumptions about the subsystem dynamics. In Section 6.3 we develop the approach and define the error dynamics. In Section 6.4 we introduce a linear observer for the tracking error dynamics that provides a training signal for the adaptation laws. In Section 6.5, we define the adaptive controller for each subsystem and derive associated bounds. Section 6.6 provide a stability analysis. In Section 6.7, we illustrate the theoretical results on a non-minimum phase system consisting of three inverted pendulums connected by springs and dampers. Conclusions are given in Section 6.8.

6.2 System Description and Problem Formulation

Let the large-scale system be composed of m *stabilizable* nonlinear single-input single-output (SISO) subsystems, represented in the following normal form:

$$\begin{aligned} \dot{\boldsymbol{x}}_i &= A_i \boldsymbol{x}_i + B_i \boldsymbol{z}_i + \boldsymbol{b}_i \left[u_i + f_i(\boldsymbol{x}_1, \boldsymbol{z}_1, \ldots, \boldsymbol{x}_m, \boldsymbol{z}_m) \right] \quad i = 1, \cdots, m, \\ \dot{\boldsymbol{z}}_i &= C_i \boldsymbol{x}_i + D_i \boldsymbol{z}_i + \boldsymbol{g}_i(\boldsymbol{x}_1, \boldsymbol{z}_1, \ldots, \boldsymbol{x}_m, \boldsymbol{z}_m) \\ y_i &= \boldsymbol{c}_i^T \boldsymbol{x}_i \,, \end{aligned} \tag{6.1}$$

where $\left[\begin{array}{cc} \boldsymbol{x}_i^T & \boldsymbol{z}_i^T \end{array} \right]^T \in \mathbb{R}^{r_i + (n_i - r_i)}$ is the state vector of the realization of the i^{th} subsystem in normal form, r_i representing the relative degree, $u_i \in \mathbb{R}$ and $y_i \in \mathbb{R}$ are the control and measurement of the i^{th} subsystem, $f_i : \mathbb{R}^{n_1 + \cdots + n_m} \rightarrow \mathbb{R}$, $\boldsymbol{g}_i : \mathbb{R}^{n_1 + \cdots + n_m} \rightarrow \mathbb{R}^{n_i - r_i}$ are sufficiently smooth unknown functions, representing the modelling errors and interconnection

effects, while $A_i, B_i, \boldsymbol{b}_i, \boldsymbol{c}_i$ are matrices and vectors corresponding to the normal realization:

$$A_i = \begin{bmatrix} 0 & 1 & \cdots & 0 \\ 0 & 0 & \ddots & 0 \\ \vdots & \vdots & \ddots & 1 \\ a_{i_1} & a_{i_2} & \cdots & a_{i_{r_i}} \end{bmatrix}, \quad B_i = \begin{bmatrix} 0 & 0 & \cdots & 0 \\ 0 & 0 & \ddots & 0 \\ \vdots & \vdots & \ddots & 0 \\ c_{i_1} & c_{i_2} & \cdots & c_{i_{n_i - r_i}} \end{bmatrix}, \quad \boldsymbol{b}_i = \begin{bmatrix} 0 \\ 0 \\ \vdots \\ b_i \end{bmatrix}, \quad \boldsymbol{c}_i = \begin{bmatrix} 1 \\ 0 \\ \vdots \\ 0 \end{bmatrix} \tag{6.2}$$

Assumption 6.1. *The functions $\boldsymbol{g}_i(\boldsymbol{x}_1, \boldsymbol{z}_1, \ldots, \boldsymbol{x}_m, \boldsymbol{z}_m)$ are bounded as follows:*

$$\|\boldsymbol{g}_i(\boldsymbol{x}_1, \boldsymbol{z}_1, \ldots, \boldsymbol{x}_m, \boldsymbol{z}_m)\| \leq \sum_{j=1}^{m} \alpha_i \left\| \left[\boldsymbol{x}_j^T \;\; \boldsymbol{z}_j^T \right]^T \right\|, \quad \alpha_i > 0\,, \quad i = 1, \cdots, m \tag{6.3}$$

Problem formulation. The objective is to synthesize *decentralized adaptive output feedback* control laws u_i, such that $y_i(t)$ tracks a smooth *bounded* reference trajectory $y_{l_i}(t)$ with bounded errors for all $i = 1, \cdots, m$, under the assumption that the i^{th} controller knows the *desired* states of all the subsystems $j = 1, \cdots, m$, while having access only to its own measurement $y_i(t)$.

Following [84, 85, 146], we introduce the following assumption.

Assumption 6.2. *The signals $y_{l_i}(t)$ are assumed to be generated by the following **stable** linear closed-loop reference models*

$$\dot{\boldsymbol{\xi}}_{l_i} = \bar{A}_i \boldsymbol{\xi}_{l_i} + \boldsymbol{b}_{r_i} y_{c_i} \tag{6.4}$$

$$y_{l_i} = \bar{\boldsymbol{c}}_i^T \boldsymbol{\xi}_{l_i}\,, \tag{6.5}$$

consisting of an open loop system

$$\begin{aligned} \dot{\boldsymbol{x}}_{l_i} &= A_i \boldsymbol{x}_{l_i} + B_i \boldsymbol{z}_{l_i} + \boldsymbol{b}_i u_{l_i} \\ \dot{\boldsymbol{z}}_{l_i} &= C_i \boldsymbol{x}_{l_i} + D_i \boldsymbol{z}_{l_i} \\ y_{l_i} &= \boldsymbol{c}_i^T \boldsymbol{x}_{l_i}\,, \quad i = 1, \cdots, m \end{aligned} \tag{6.6}$$

and a stabilizing dynamic compensator:

$$\begin{aligned} \dot{\boldsymbol{x}}_{c_i} &= A_{c_i} \boldsymbol{x}_{c_i} + \boldsymbol{b}_{c_i}(y_{c_i} - y_{l_i}) \\ u_{l_i} &= \boldsymbol{c}_{c_i}^T \boldsymbol{x}_{c_i} + d_{c_i}(y_{c_i} - y_{l_i})\,, \quad i = 1, \cdots, m\,, \end{aligned} \tag{6.7}$$

where

$$\bar{A}_i = \begin{bmatrix} A_i - \boldsymbol{b}_i d_{c_i} \boldsymbol{c}_i^T & B_i & \boldsymbol{b}_i \boldsymbol{c}_{c_i}^T \\ C_i & D_i & 0 \\ -\boldsymbol{b}_{c_i} \boldsymbol{c}_i^T & 0 & A_{c_i} \end{bmatrix}, \quad \boldsymbol{\xi}_{l_i} = \begin{bmatrix} \boldsymbol{x}_{l_i} \\ \boldsymbol{z}_{l_i} \\ \boldsymbol{x}_{c_i} \end{bmatrix}, \quad \boldsymbol{b}_{r_i} = \begin{bmatrix} \boldsymbol{b}_i d_{c_i} \\ 0 \\ \boldsymbol{b}_{c_i} \end{bmatrix}, \quad \bar{\boldsymbol{c}}_i = \begin{bmatrix} \boldsymbol{c}_i \\ 0 \\ 0 \end{bmatrix} \tag{6.8}$$

and y_{c_i} *is a bounded input of interest to track, while* $\boldsymbol{x}_{c_i} \in \mathcal{D}_{\boldsymbol{x}_{c_i}} \subset \mathbb{R}^{n_{c_i}}$. *The matrices* $A_i, B_i, \boldsymbol{b}_i, \boldsymbol{c}_i$ *correspond to the normal realization, as defined in (6.2), so that* $\dim \boldsymbol{x}_{l_i} = \dim \boldsymbol{x}_i$, *and* $\dim \boldsymbol{z}_{l_i} = \dim \boldsymbol{z}_i$. *Notice that this choice of the open loop system in (6.6) implies that the relative degree of the* i^{th} *open-loop reference model equals that of the* i^{th} *open-loop subsystem. The following bounds are known:*

$$\left\| \begin{bmatrix} \boldsymbol{x}_{l_i}^T & \boldsymbol{z}_{l_i}^T \end{bmatrix}^T \right\| \leq \beta_i \,, \quad i = 1, \cdots, m. \tag{6.9}$$

Remark 6.1. In [84], this problem formulation has been addressed for linear subsystems, and, by a proper choice of robustifying signal, it has been shown that global asymptotic tracking can be achieved if the robustifying gain satisfies a lower bound, depending upon the number of subsystems and the apriori known bound on the interconnection effects. In [85], these results have been extended to nonlinear interconnections, modelled by *known* nonlinear functions. Moreover, output feedback has been formulated and solved for the case of subsystems having regulated outputs with relative degree 1. Our approach is different in two perspectives: i) we formulate the problem in output feedback *for arbitrary relative degree* by extending the results of Chapter 4 for centralized control, ii) we use an *adaptive* signal for overcoming the effect of interconnections on the tracking performance. On the other hand it should be understood that, due to results in [147], one cannot expect global results while using dynamic output feedback compensators with the class of nonlinear systems presented here.

6.3 Controller Design and Tracking Error Dynamics

The control design for each of the subsystems will be based on the logic of combining a linear controller, that stabilizes the nominal linear model in the absence of interconnections, with a NN that approximately cancels the interconnection effects in the controllable range.

Towards this end, introduce the following control signal

$$u_i = u_{c_i} - u_{ad_i}\,, \tag{6.10}$$

where u_{c_i} is the output of the following dynamic compensator

$$\begin{aligned} \dot{\boldsymbol{\eta}}_{c_i} &= A_{c_i}\boldsymbol{\eta}_{c_i} + \boldsymbol{b}_{c_i}(y_{c_i} - y_i) \\ u_{c_i} &= \boldsymbol{c}_{c_i}^T\boldsymbol{\eta}_{c_i} + d_{c_i}(y_{c_i} - y_i)\,, \quad i = 1, \cdots, m\,, \end{aligned} \tag{6.11}$$

where $\boldsymbol{\eta}_{c_i} \in \mathcal{D}_{\boldsymbol{\eta}_{c_i}} \subset \mathbb{R}^{n_{c_i}}$, $A_{c_i}, \boldsymbol{b}_{c_i}, \boldsymbol{c}_{c_i}, d_{c_i}$ are introduced in (6.7), and the adaptive signal u_{ad_i} will be defined later. This results in the following closed-loop subsystem dynamics:

$$\dot{\boldsymbol{\xi}}_i = \bar{A}_i\boldsymbol{\xi}_i + \boldsymbol{b}_{r_i}y_{c_i} - \bar{\boldsymbol{b}}_i(u_{ad_i} - f_i) + \bar{\boldsymbol{g}}_i \tag{6.12}$$

$$y_i = \bar{\boldsymbol{c}}_i^T\boldsymbol{\xi}_i\,, \qquad i = 1, \cdots, m\,, \tag{6.13}$$

where

$$\boldsymbol{\xi}_i = \begin{bmatrix} \boldsymbol{x}_i \\ \boldsymbol{z}_i \\ \boldsymbol{\eta}_{c_i} \end{bmatrix}, \quad \bar{\boldsymbol{b}}_i = \begin{bmatrix} \boldsymbol{b}_i \\ 0 \\ 0 \end{bmatrix}, \quad \bar{\boldsymbol{g}}_i = \begin{bmatrix} 0 \\ \boldsymbol{g}_i \\ 0 \end{bmatrix}. \tag{6.14}$$

Following [85], define the error vector $\boldsymbol{E}_i = \boldsymbol{\xi}_{l_i} - \boldsymbol{\xi}_i$, and write the tracking error dynamics:

$$\begin{aligned} \dot{\boldsymbol{E}}_i &= \bar{A}_i\boldsymbol{E}_i + \bar{\boldsymbol{b}}_i(u_{ad_i} - f_i) - \bar{\boldsymbol{g}}_i \\ \bar{\boldsymbol{y}}_i &= \bar{C}_i\boldsymbol{E}_i, \qquad i = 1, \cdots, m\,, \end{aligned} \tag{6.15}$$

where $\bar{C}_i = \begin{bmatrix} \bar{\boldsymbol{c}}_i^T & I \end{bmatrix}^T$ separates the signals available for feedback.

6.4 Error Observer Dynamics

Following the previous work on centralized adaptive output feedback [63,83,148], we propose a linear observer for the tracking error dynamics (6.15). This observer gives estimates of the tracking error states that will later be used in the adaptive laws (6.26). Towards this end, consider the following linear observers for the tracking error dynamics in (6.15):

$$\begin{aligned} \dot{\widehat{\boldsymbol{E}}}_i &= \bar{A}_i\widehat{\boldsymbol{E}}_i + K_i\,(\bar{\boldsymbol{y}}_i - \hat{\boldsymbol{y}}_i) \\ \hat{\boldsymbol{y}}_i &= \bar{C}_i\widehat{\boldsymbol{E}}_i, \quad i = 1, \cdots, m, \end{aligned} \tag{6.16}$$

where K_i is a gain matrix, and should be chosen such that $\bar{A}_i - K_i\bar{C}_i$ is asymptotically stable. Let

$$\widetilde{A}_i \triangleq \bar{A}_i - K_i\bar{C}_i, \quad \widetilde{\boldsymbol{E}}_i = \boldsymbol{E}_i - \widehat{\boldsymbol{E}}_i, \quad i = 1, \cdots, m. \tag{6.17}$$

The observer error dynamics can be written:

$$\dot{\widetilde{\boldsymbol{E}}}_i = \widetilde{A}_i\widetilde{\boldsymbol{E}}_i + \bar{\boldsymbol{b}}_i(u_{ad_i} - f_i) - \bar{\boldsymbol{g}}_i, \quad i = 1, \cdots, m. \tag{6.18}$$

We immediately note that for arbitrary positive definite $\widetilde{Q}_i > 0$ matrix there exists a unique solution $\widetilde{P}_i = \widetilde{P}_i^T > 0$ such that

$$\widetilde{A}_i^T\widetilde{P}_i + \widetilde{P}_i\widetilde{A}_i = -\widetilde{Q}_i\,. \tag{6.19}$$

6.5 Neural Network Approximation of Nonlinearities

6.5.1 Neural Network Approximation of Interconnections

Following [93], given arbitrary $\epsilon^* > 0$ and a continuous function $\boldsymbol{f}(\boldsymbol{x}) : \mathbb{R}^n \to \mathbb{R}^m$, defined on a compact set $\boldsymbol{x} \in \mathcal{D} \subset \mathbb{R}^n$, there exists a set of bounded constant weights W, and a set of basis functions $\boldsymbol{\phi}(\boldsymbol{x})$, such that the following representation holds $\forall \boldsymbol{x} \in \mathcal{D}$:

$$\boldsymbol{f}(\boldsymbol{x}) = W^T\boldsymbol{\phi}(\boldsymbol{x}) + \boldsymbol{\epsilon}(\boldsymbol{x})\,, \quad \|\boldsymbol{\epsilon}(\boldsymbol{x})\| < \epsilon^*\,. \tag{6.20}$$

Thus, one can model the interconnections

$$f_i(\boldsymbol{x}_1, \boldsymbol{z}_1, \cdots, \boldsymbol{x}_m, \boldsymbol{z}_m) = \boldsymbol{W}_i^T\boldsymbol{\phi}_i(\boldsymbol{Y}) + \epsilon_i(\boldsymbol{Y}), \quad |\epsilon_i| < \epsilon_i^*\,, \quad \|\boldsymbol{W}_i\| \le W_i^*\,, \tag{6.21}$$

using the following input vector

$$\boldsymbol{Y} = \begin{bmatrix} \boldsymbol{x}_1^T & \boldsymbol{z}_1^T & \cdots & \boldsymbol{x}_m^T & \boldsymbol{z}_m^T \end{bmatrix}^T \in \mathcal{D} \subset \mathbb{R}^{n_1+\cdots+n_m} \tag{6.22}$$

and a vector of the radial basis functions

$$\boldsymbol{\phi}_i(\boldsymbol{Y}) = \begin{bmatrix} \phi_{i_1}(\boldsymbol{Y}) & \cdots & \phi_{i_{N_i}}(\boldsymbol{Y}) \end{bmatrix}^T, \quad \phi_{i_k}(\boldsymbol{Y}) = e^{-\|\boldsymbol{Y}-\boldsymbol{Y}_{i_{c_k}}\|^2/2\sigma_{i_k}}\,, \tag{6.23}$$

where N_i is the number of basis functions to be used by the i^{th} subsystem, $\boldsymbol{Y}_{i_{c_k}}$ is the vector of centers of the basis functions used by the i^{th} subsystem, having the same dimension as $\boldsymbol{Y}$ in (6.22), while σ_{i_k} specifies the width of the k^{th} basis function in the i^{th} subsystem.

6.5.2 Adaptive control

Since our interest is in decentralized design, the states of other subsystems are not available to individual controllers, therefore the input vector defined in (6.22) cannot be used in designing adaptive elements. Based on the assumption that the controllers share prior information about their reference models, the adaptive control signal for the i^{th} subsystem can be designed following the same logic as in [85]:

$$u_{ad_i} = \widehat{\boldsymbol{W}}_i^T \boldsymbol{\phi}_i(\boldsymbol{Y}_l), \tag{6.24}$$

where the vector $\boldsymbol{Y}_l$ is defined as:

$$\boldsymbol{Y}_l = \begin{bmatrix} \boldsymbol{x}_{l_1}^T & \boldsymbol{z}_{l_1}^T & \cdots & \boldsymbol{x}_{l_m}^T & \boldsymbol{z}_{l_m}^T \end{bmatrix}^T \tag{6.25}$$

having the states of all the subsystems in (6.22) replaced by their corresponding reference states. Notice that following (6.9) there exists a set $\mathcal{D}_l$ in the extended space such that $\boldsymbol{Y}_l \in \mathcal{D}_l$. The adaptive laws for $\widehat{\boldsymbol{W}}_i$ are similar to those in [63]:

$$\dot{\widehat{\boldsymbol{W}}}_i = -F_i \left[2\boldsymbol{\phi}_i(\boldsymbol{Y}_l) \widehat{\boldsymbol{E}}_i^T P_i \bar{\boldsymbol{b}}_i + k_i \widehat{\boldsymbol{W}}_i \right], \tag{6.26}$$

in which P_i is the solution of the Lyapunov equation

$$\bar{A}_i^T P_i + P_i \bar{A}_i = -Q_i \,, \tag{6.27}$$

for some $Q_i > 0$, and $F_i, k_i > 0$ are adaptation gains. The error dynamics in (6.15) can be expressed as:

$$\begin{aligned} \dot{\boldsymbol{E}}_i &= \bar{A}_i \boldsymbol{E}_i + \bar{\boldsymbol{b}}_i \left[\widehat{\boldsymbol{W}}_i^T \boldsymbol{\phi}_i(\boldsymbol{Y}_l) - \boldsymbol{W}_i^T \boldsymbol{\phi}_i(\boldsymbol{Y}) - \epsilon_i \right] - \bar{\boldsymbol{g}}_i \\ \bar{\boldsymbol{y}}_i &= \bar{C}_i \boldsymbol{E}_i. \end{aligned} \tag{6.28}$$

Through several algebraic manipulations and, using the mean value theorem, one can obtain

$$\begin{aligned} u_{ad_i} - f_i &= \widehat{\boldsymbol{W}}_i^T \boldsymbol{\phi}_i(\boldsymbol{Y}_l) - \boldsymbol{W}_i^T \boldsymbol{\phi}_i(\boldsymbol{Y}) - \epsilon_i = \widehat{\boldsymbol{W}}_i^T \boldsymbol{\phi}_i(\boldsymbol{Y}_l) + \boldsymbol{W}_i^T \boldsymbol{\phi}_i(\boldsymbol{Y}_l) - \boldsymbol{W}_i^T \boldsymbol{\phi}_i(\boldsymbol{Y}_l) \\ &\quad - \boldsymbol{W}_i^T \boldsymbol{\phi}_i(\boldsymbol{Y}) - \epsilon_i = \widehat{\boldsymbol{W}}_i^T \boldsymbol{\phi}_i(\boldsymbol{Y}_l) - \boldsymbol{W}_i^T \boldsymbol{\phi}_i(\boldsymbol{Y}_l) + \boldsymbol{W}_i^T (\boldsymbol{\phi}_i(\boldsymbol{Y}_l) - \boldsymbol{\phi}_i(\boldsymbol{Y})) - \epsilon_i \\ &= \widetilde{\boldsymbol{W}}_i^T \boldsymbol{\phi}_i(\boldsymbol{Y}_l) + \boldsymbol{W}_i^T \boldsymbol{\phi}_i'(\boldsymbol{Y}^*) \tilde{\boldsymbol{Y}} - \epsilon_i \,, \end{aligned}$$

where

$$\tilde{\boldsymbol{Y}} = \left[\begin{array}{cccccc} \tilde{\boldsymbol{x}}_1^T & \tilde{\boldsymbol{z}}_1^T & \cdots & \tilde{\boldsymbol{x}}_m^T & \tilde{\boldsymbol{z}}_m^T \end{array} \right]^T \quad (\tilde{\boldsymbol{x}}_i = \boldsymbol{x}_{l_i} - \boldsymbol{x}_i, \quad \tilde{\boldsymbol{z}}_i = \boldsymbol{z}_{l_i} - \boldsymbol{z}_i) \tag{6.29}$$

is comprised of the tracking errors of all the subsystems, and $\boldsymbol{\phi}_i'(\boldsymbol{Y}^*)$ is the bounded derivative of the basis function in an intermediate point $\boldsymbol{Y}^* = \boldsymbol{Y}_l + (1-\lambda)\boldsymbol{Y}$, $0 < \lambda < 1$, and $\widetilde{\boldsymbol{W}}_i \triangleq \widehat{\boldsymbol{W}}_i - \boldsymbol{W}_i$ is the parameter error vector. The following upper bound follows from the definition of $\boldsymbol{E}_j$ and $\tilde{\boldsymbol{Y}}$:

$$\|\tilde{\boldsymbol{Y}}\| \leq \sum_{j=1}^{j=m} \|\boldsymbol{E}_j\| \,. \tag{6.30}$$

6.6 Stability Analysis

In this section we show through Lyapunov's direct method that the error signals $\boldsymbol{E}_i, \widetilde{\boldsymbol{E}}_i, \widetilde{\boldsymbol{W}}_i$, $i = 1, \cdots, m$, are ultimately bounded. To this end, introduce the composite error vector

$$\boldsymbol{\zeta} \triangleq \left[\boldsymbol{E}_1^T \ \cdots \ \boldsymbol{E}_m^T \ \widetilde{\boldsymbol{E}}_1^T \ \cdots \ \widetilde{\boldsymbol{E}}_m^T \ \widetilde{\boldsymbol{W}}_1^T \ \cdots \ \widetilde{\boldsymbol{W}}_m^T \right]^T \in \mathbb{R}^{2(n_1+\cdots+n_m)} \times \mathbb{R}^{N_1+\cdots+N_m} \tag{6.31}$$

and consider the following positive definite function

$$V(\boldsymbol{\zeta}) \triangleq \boldsymbol{\zeta}^T T \boldsymbol{\zeta} \tag{6.32}$$

where $T = blockdiag \left[\begin{array}{cccccccc} P_1 & \cdots & P_m & \widetilde{P}_1 & \cdots & \widetilde{P}_m & \frac{1}{2}F_1^{-1} & \cdots & \frac{1}{2}F_m^{-1} \end{array} \right]$. Further, notice that the compact set $\mathcal{D}$ over which (6.22) defines the RBF network approximation can be arbitrarily large. Based on the definition of the compact set $\mathcal{D}_l$, and the boundedness of $\boldsymbol{x}_{c_i}$ and $\boldsymbol{\eta}_{c_i}$, in the subspace of the error variables consider the following compact set $\Omega_{\boldsymbol{E}}$ of possible initial errors

$$\Omega_{\boldsymbol{E}} = \left\{ \left[\begin{array}{ccc} \boldsymbol{E}_1^T & \cdots & \boldsymbol{E}_m^T \end{array} \right]^T \in \mathbb{R}^{n_1+\cdots+n_m} \ : \ \boldsymbol{Y} \in \mathcal{D}, \ \boldsymbol{Y}_l \in \mathcal{D}_l, \ \boldsymbol{x}_c \in \mathcal{D}_{\boldsymbol{x}_c}, \ \boldsymbol{\eta}_c \in \mathcal{D}_{\boldsymbol{\eta}_c} \right\}$$

where $\boldsymbol{x}_c \triangleq [\boldsymbol{x}_{c_1}^T \ \cdots \boldsymbol{x}_{c_m}^T]^T$, $\mathcal{D}_{\boldsymbol{x}_c} = \mathcal{D}_{\boldsymbol{x}_{c_1}} \times \cdots \times \mathcal{D}_{\boldsymbol{x}_{c_m}}$, $\boldsymbol{\eta}_c \triangleq [\boldsymbol{\eta}_{c_1}^T \ \cdots \boldsymbol{\eta}_{c_m}^T]^T$, $\mathcal{D}_{\boldsymbol{\eta}_c} = \mathcal{D}_{\boldsymbol{\eta}_{c_1}} \times \cdots \times \mathcal{D}_{\boldsymbol{\eta}_{c_m}}$. In the expanded space of the composite error variable $\boldsymbol{\zeta} \in \mathbb{R}^{2(n_1+\cdots+n_m)} \times \mathbb{R}^{N_1+\cdots+N_m}$, consider the largest level set of $V(\boldsymbol{\zeta}) = \boldsymbol{\zeta}^T T \boldsymbol{\zeta}$ such that its projection on the subspace of the error variable $[\boldsymbol{E}_1^T \ \cdots \ \boldsymbol{E}_m^T]^T$ completely lies in $\Omega_{\boldsymbol{E}}$. Introduce the largest ball that lies

inside that level set $\mathcal{B}_R = \{\boldsymbol{\zeta} \mid \|\boldsymbol{\zeta}\| \leq R\}$. Let α be the minimum value of $V(\boldsymbol{\zeta}) = \boldsymbol{\zeta}^T T \boldsymbol{\zeta}$ on the boundary of $\mathcal{B}_R$:

$$\alpha \triangleq \min_{\|\boldsymbol{\zeta}\|=R} V(\boldsymbol{\zeta}) = R^2 \lambda_{\min}(T)\,, \tag{6.33}$$

where $\lambda_{\min}(T)$ is introduced for the minimum eigenvalue of T. Introduce the following set:

$$\Omega_\alpha \triangleq \{\boldsymbol{\zeta} \in \mathcal{B}_R \mid V(\boldsymbol{\zeta}) \leq \alpha\} \tag{6.34}$$

Assumption 6.3. *Let*

$$R > \gamma \sqrt{\lambda_{\max}(T)/\lambda_{\min}(T)} \tag{6.35}$$

where $\lambda_{\max}(T)$ is introduced for the maximum eigenvalue of T, while

$$\gamma = \max\left(\sqrt{\frac{\omega}{\lambda_{\min}(D)}}, \sqrt{\frac{\omega}{\lambda_{\min}(\tilde{D})}}, \sqrt{\frac{\omega}{\lambda_{\min}(\Lambda)}}\right)\,, \tag{6.36}$$

in which

$$\begin{aligned}
D &\triangleq \operatorname{diag}\begin{bmatrix} \theta_1 & \cdots & \theta_m \end{bmatrix}, \\
&\quad \theta_i = \lambda_{\min}(Q_i) - 2m\alpha_i \lambda_{\max}(P_i) - (m\phi_i^* + 1)\|P_i \bar{\boldsymbol{b}}_i\| \\
&\quad - \sum_{j=1}^{j=m} (2\|P_j \bar{\boldsymbol{b}}_j\| + \Theta_j)\phi_j^* - \alpha_i \left(\lambda_{\max}(P_i) + \lambda_{\max}(\widetilde{P}_i)\right) > 0 \\
\tilde{D} &\triangleq \operatorname{diag}\begin{bmatrix} \tilde{\theta}_1 & \cdots & \tilde{\theta}_m \end{bmatrix}, \\
&\quad \tilde{\theta}_i = \lambda_{\min}(\widetilde{Q}_i) - 2m\alpha_i \lambda_{\max}(\widetilde{P}_i) - (m\phi_i^* + 1)\left(\|P_i \bar{\boldsymbol{b}}_i\| + \mu_i\right) - \mu_i \|\boldsymbol{\phi}_i(\boldsymbol{Y}_l)\| > 0 \\
\Lambda &\triangleq \operatorname{diag}\begin{bmatrix} \lambda_1 & \cdots & \lambda_m \end{bmatrix}, \quad \lambda_i = \frac{k_i}{2} - \mu_i \|\boldsymbol{\phi}_i(\boldsymbol{Y}_l)\| > 0 \\
\omega &\triangleq \sum_{i=1}^{m} \left(\frac{k_i}{2}(W_i^*)^2 + \left(2\|P_i \bar{\boldsymbol{b}}_i\| + \mu_i\right)(\epsilon_i^*)^2 + \alpha_i \left(\lambda_{\max}(P_i) + \lambda_{\max}(\widetilde{P}_i)\right) \sum_{j=1}^{j=m} \beta_j^2 \right) \\
\phi_i^* &\triangleq W_i^* \|\boldsymbol{\phi}_i'(\boldsymbol{Y}^*)\|, \quad \mu_i \triangleq \|\widetilde{P}_i \bar{\boldsymbol{b}}_i + P_i \bar{\boldsymbol{b}}_i\|\,.
\end{aligned} \tag{6.37, 6.38}$$

This assumption implies upper and lower bounds for the adaptation gains, as discussed by the end of the proof.

Theorem 6.1. *Let Assumptions 6.1, 6.2 and 6.3 hold. Then, if the initial errors lie in Ω_α, defined in (6.34), the feedback control law given by (6.10), along with (6.11), (6.24), (6.26), guarantees that the signals $\boldsymbol{E}_i, \widetilde{\boldsymbol{E}}_i, \widetilde{\boldsymbol{W}}_i, i = 1, \cdots, m$, in the closed loop system are ultimately bounded.*

Remark 6.2. The results obtained above can be extended to the case where the modeling errors also depend upon the control signal, i.e. in (6.1) one can have $f_i(u_i, \boldsymbol{x}_1, \boldsymbol{z}_1, \ldots, \boldsymbol{x}_m, \boldsymbol{z}_m)$, subject to $\partial f_i/\partial u_i \neq 0$. Notice then that due to (6.10) the adaptive signal in (6.24) will be introduced to cancel a function $f_i(u_i(u_{ad_i}(\cdot), \cdot)$ of itself. To avoid this algebraic loop, one way of implementing this is to use a one step delayed value of the control signal $u_i(t-d)$, where $d > 0$ is sufficiently small.

Remark 6.3. The synthesis approach presented here is "robust adaptive" in a sense that it ensures that the modeling error associated with the zero dynamics, represented by $\boldsymbol{g}_i$, is dominated by the linear design, while adaptation ensures approximate cancellation of the modeling error presented by f_i, that lies in the controllable subspace.

Remark 6.4. Assumption 6.3 may be interpreted as placing both upper and lower bounds on the adaptation gains. Let $\bar{\gamma} \triangleq \max(\lambda_{\max}(F_i))$, $\underline{\gamma} \triangleq \min(\lambda_{\min}(F_i))$, $\bar{\lambda} \triangleq \max(\lambda_{\max}(P_i), \lambda_{\max}(\widetilde{P}_i))$, $\underline{\lambda} \triangleq \min(\lambda_{\min}(P_i), \lambda_{\min}(\widetilde{P}_i))$, $i = 1, \cdots, m$. Then an upper bound for the adaptation gains results when $2\bar{\lambda}\underline{\gamma} > 1$ and $2\underline{\lambda}\bar{\gamma} > 1$, for which the relation in (6.35) reduces to $\bar{\gamma} < R^2/(2\gamma^2\bar{\lambda})$. A lower bound for the adaptation gains results when $2\bar{\lambda}\underline{\gamma} < 1$ and $2\underline{\lambda}\bar{\gamma} < 1$, for which the relation in (6.35) reduces to $\underline{\gamma} > \gamma^2/(2R^2\underline{\lambda})$. Notice that the upper bound for the adaptation gain has R in the numerator, while the lower bound has R in the denominator. Therefore, R can be selected sufficiently large to ensure that $\underline{\gamma} < \bar{\gamma}$.

Remark 6.5. The adaptive laws in (6.10) are based on backpropagation along with $\sigma-$modification term for preventing the parameter drift. One can alternatively use the projection based adaptive algorithm to ensure boundedness of the RBF weights by definition [149].

6.7 Simulations

We consider three inverted pendulums mounted on carts, as depicted in Figure 6.1. The carts are connected by springs and dampers. In each subsystem, we assume that the position of the cart (x_i) and the angle of the pendulum (θ_i) are measured and the cart is regulated

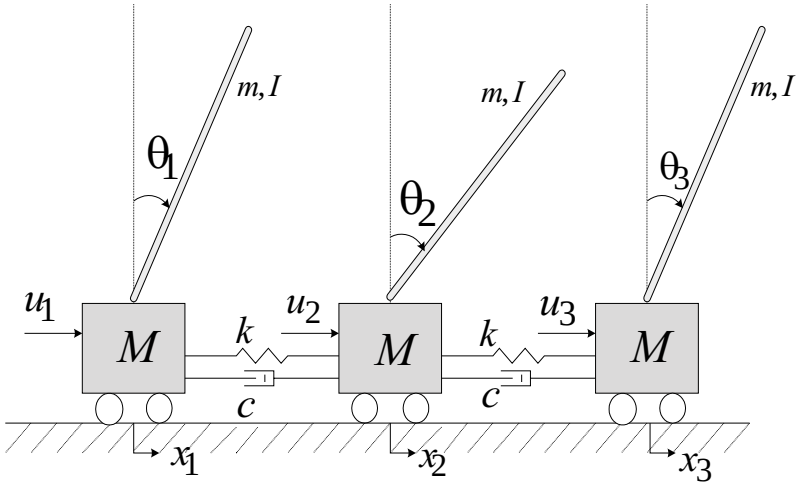

Fig. 6.1: System Configuration: Three inverted pendulums on Three Carts Connected by Springs and Dampers

by input forces (u_i). The equations of motion for the system are described as follows:

$$(M+m)\ddot{x}_1 + ml_p\ddot{\theta}_1\cos\theta_1 - ml_p\dot{\theta}_1^2\sin\theta_1 = u_1 + s_1 \tag{6.39}$$

$$ml_p\cos\theta_1\ddot{x}_1 + (I+ml_p^2)\ddot{\theta}_1 - mgl_p\sin\theta_1 = 0 \tag{6.40}$$

$$(M+m)\ddot{x}_2 + ml_p\ddot{\theta}_2\cos\theta_2 - ml_p\dot{\theta}_2^2\sin\theta_2 = u_2 - s_1 + s_2 \tag{6.41}$$

$$ml_p\cos\theta_2\ddot{x}_2 + (I+ml_p^2)\ddot{\theta}_2 - mgl_p\sin\theta_2 = 0 \tag{6.42}$$

$$(M+m)\ddot{x}_3 + ml_p\ddot{\theta}_3\cos\theta_3 - ml_p\dot{\theta}_3^2\sin\theta_3 = u_3 - s_2 \tag{6.43}$$

$$ml_p\cos\theta_3\ddot{x}_3 + (I+ml_p^2)\ddot{\theta}_3 - mgl_p\sin\theta_3 = 0 \tag{6.44}$$

where u_1, u_2, u_3 are input forces to the carts(N), M is the mass of the cart (kg), m is the mass of the rod (kg), l_p is the distance from the pivot on the cart to the center of gravity of the rod(half of full length)(m), $I(=\frac{1}{3}ml_p^2)$ is the moment of inertia of the rod with respect to its center of mass (kg·m^2), g is the gravitational acceleration (kg·m/sec^2), k is the spring constant (N/m), c is the damping constant (N·sec/m), $s_1 = k(x_2 - x_1) + c(\dot{x}_2 - \dot{x}_1), s_2 = k(x_3 - x_2) + c(\dot{x}_3 - \dot{x}_2)$ are interconnection forces due to springs and dampers. The parameter values are: $M = 0.9, m = 0.18, l_p = 0.305, g = 9.8, k = 1, c = 2\times10^{-5}$. Our control objective is to regulate the displacements of the carts $\boldsymbol{x}_i$ while balancing the inverted rods on the carts without velocity measurements.

The open loop subsystem in (6.6) is derived after the dynamics in (6.39)–(6.44) are first

linearized with respect to equilibrium position $x_i = \theta_i = 0$, and then put into a normal form by the transformation: $x_{l_{i_1}} = x_i, x_{l_{i_2}} = \dot{x}_i, z_{l_{i_1}} = \theta_i, z_{l_{i_2}} = \frac{\dot{x}_i}{l_p} + \dot{\theta}_i$. The linear subsystem, for $i = 1, 2, 3$, is described by the following system matrices:

$$
\begin{aligned}
A_i &= \begin{bmatrix} 0 & 1 \\ 0 & 0 \end{bmatrix}, \; B_i = \begin{bmatrix} 0 & 0 \\ -\frac{\hat{m}}{\hat{M}} & 0 \end{bmatrix}, \; \boldsymbol{b}_i = \begin{bmatrix} 0 \\ \frac{1}{\hat{M}} \end{bmatrix} \\
C_i &= \begin{bmatrix} 0 & -\frac{1}{l_p} \\ 0 & 0 \end{bmatrix}, \; D_i = \begin{bmatrix} 0 & 1 \\ \frac{g}{l_p} & 0 \end{bmatrix}, \; \boldsymbol{c}_i = \begin{bmatrix} 1 \\ 0 \end{bmatrix}
\end{aligned}
\tag{6.45}
$$

The constants $\hat{M} = 0.815, \hat{m} = 0.21$ represent parameter estimates for M, m respectively. Further, in this linear model, the inverted rod is treated as a lumped mass located on its center of mass, i.e., $I = 0$. Putting each subsystem in (6.39)–(6.44) into normal form leads to the following modelling errors and interconnection effects defined in (6.1):

$$
\begin{aligned}
f_i &= \left[\frac{\hat{M}}{M + m(1 - 3/4 \cos\theta_i^2)} \left(u_i + m l_p \dot{\theta}_i^2 \sin\theta_i - \frac{3}{4} mg \sin\theta_i \cos\theta_i + \tau_i \right) + \hat{m} g \theta_i - u_i \right] \\
\boldsymbol{g}_i &= \begin{bmatrix} -\frac{\cos\theta_i}{l_p} x_{i_2} - \frac{1}{3}\dot{\theta}_i + \frac{1}{l_p} x_{i_2} \\ \frac{g}{l_p} \sin\theta_i - \frac{1}{l_p} x_{i_2} \dot{\theta}_i \sin\theta_i - \frac{g}{l_p} \theta_i \end{bmatrix}
\end{aligned}
\tag{6.46}
$$

where $\tau_1 = s_1, \; \tau_2 = -s_1 + s_2, \; \tau_3 = -s_2$. The term τ_i in Eq.(6.46) implies that the spring and the damper are not considered in the open loop model. The term u_i means that the modelling error also depends on the control signal as in Remark 6.2. Note that the interconnection between two carts and modelling errors contain velocity terms which are not measured. This implies that the existing adaptive output feedback approaches in the decentralized control literature, such as the ones developed in [136, 140] and many others cannot be applied. Moreover, regulation of x_i using u_i to the carts renders the control problem *non-minimum* phase. (Linearization of each subsystem about vertical-up position leads to unstable zero $\sqrt{\frac{g}{L}}$.) These issues make the control problem even more challenging.

The dynamic compensator in (6.11) for each subsystem is designed as a LQG controller based on the open loop model in (6.45), in which two measured outputs x_i, θ_i are available for control design. The error observer in (6.16) is designed such that the smallest eigenvalue

of $\widetilde{A}_i$ in (6.18) equals approximately five times the smallest eigenvalue of $\bar{A}_i$. The basis functions have the following structures for three subsystems:

$$\phi_{i_k}(\boldsymbol{Y}_l) = e^{-\|\boldsymbol{Y}_l - \boldsymbol{Y}_{i_{c_k}}\|^2/2\sigma_{i_k}}, \sigma_{i_k} = 1, i = 1,2,3,\ k = 1,\ldots,N_i \tag{6.47}$$

where $N_1 = N_3 = 7, N_2 = 9$. The centers $\boldsymbol{Y}_{i_{c_k}}$ are randomly selected over a grid of possible values for the vector $\boldsymbol{Y}_l$. All of the NN inputs are normalized using an estimate for their maximum values. Since the dynamics of the first and third carts are coupled only through the dynamics of the middle cart, and the modelling error contains a control signal, we choose the NN input vectors as:

$$\begin{aligned}
\boldsymbol{Y}_{l_1}^T &= \begin{bmatrix} u_1 & x_{l_{1_1}} & x_{l_{1_2}} & z_{l_{1_1}} & z_{l_{1_2}} & x_{l_{2_1}} & x_{l_{2_2}} & 0 & 0 & 0 & 0 & 0 & 0 \end{bmatrix} \\
\boldsymbol{Y}_{l_2}^T &= \begin{bmatrix} u_2 & x_{l_{1_1}} & x_{l_{1_2}} & 0 & 0 & x_{l_{2_1}} & x_{l_{2_2}} & z_{l_{2_1}} & z_{l_{2_2}} & x_{l_{3_1}} & x_{l_{3_2}} & 0 & 0 \end{bmatrix} \\
\boldsymbol{Y}_{l_3}^T &= \begin{bmatrix} u_3 & 0 & 0 & 0 & 0 & x_{l_{2_1}} & x_{l_{2_2}} & 0 & 0 & x_{l_{3_1}} & x_{l_{3_2}} & z_{l_{3_1}} & z_{l_{3_2}} \end{bmatrix}
\end{aligned}$$

where $\boldsymbol{Y}_{l_i}$ represents the NN input vector for the ith subsystem. Adaptation gains are chosen as: $F_i = 0.5I, k_i = 0.05$.

Figure 6.2 compares output tracking performances when the reference command $y_{c_i}, i = 1,2,3$ is a square wave signal of magnitude 0.15m at 0.05 Hz. The pendulum angles are shown in Figure 6.3. The initial conditions are:

$$\begin{aligned}
&x_1(0) = \dot{x}_1(0) = 0,\ \theta_1(0) = -30^o,\ \dot{\theta}_1(0) = -10^o/sec \\
&x_2(0) = \dot{x}_2(0) = 0,\ \theta_2(0) = 30^o,\ \dot{\theta}_2(0) = 10^o/sec \\
&x_3(0) = \dot{x}_3(0) = 0,\ \theta_3(0) = 20^o,\ \dot{\theta}_3(0) = -10^o/sec
\end{aligned} \tag{6.48}$$

Without adaptive control compensation, the system goes unstable. When each control is augmented with an adaptive term, the three carts are in synchronous motion with each inverted pendulum balanced, implying implicit cooperation for output tracking. The decentralized coordination of three carts can be further illustrated by the control signals in Figure 6.4. In contrast to the disharmony between three control signals in Figure 6.4(a), the control signals in Figure 6.4(b) become almost identical after an initial transient period.

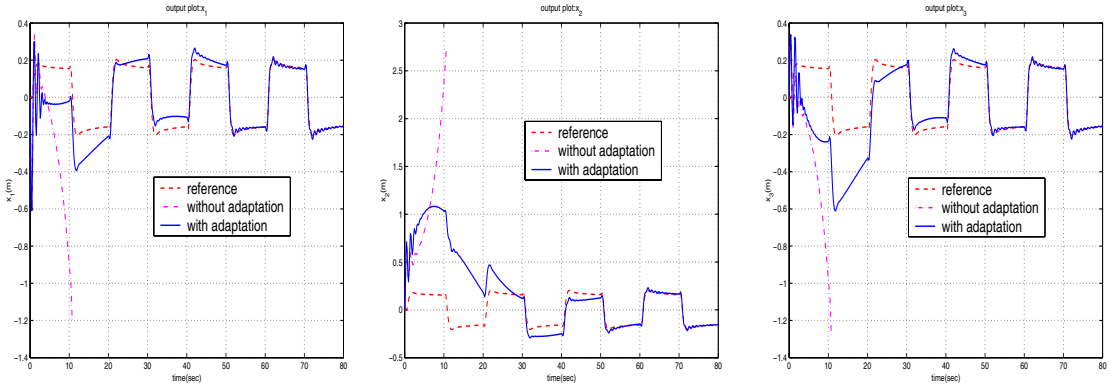

(a) x_1 (b) x_2 (c) x_3

Fig. 6.2: Comparison of the Cart Displacements with/without Adaptive Signal u_{ad_i}.

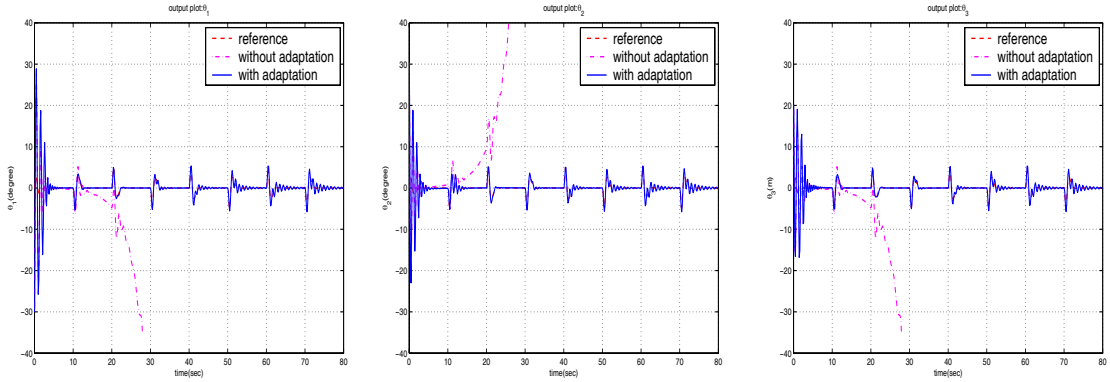

(a) θ_1 (b) θ_2 (c) θ_3

Fig. 6.3: Comparison of the Rod Angles with/without Adaptive Signal u_{ad_i}.

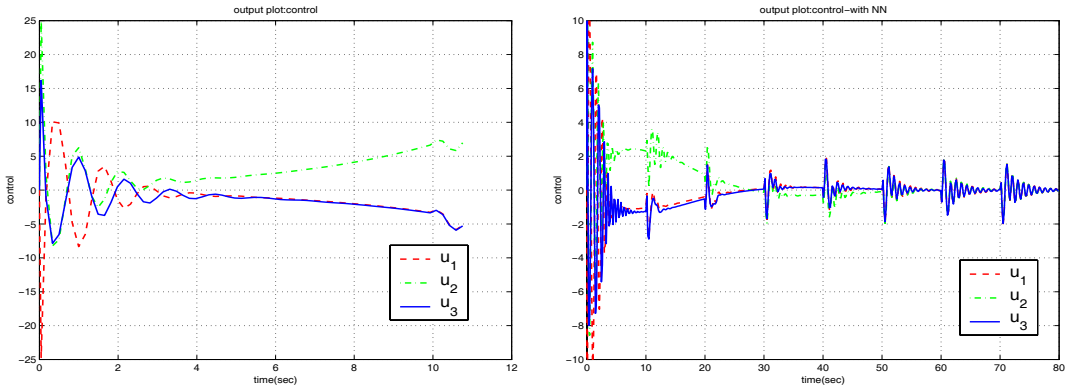

(a) without adaptive signal (b) with adaptive signal

Fig. 6.4: Comparison of Control Signals with/without Adaptive Signal u_{ad_i}.

6.8 Conclusions

In this chapter we have presented a methodology for adaptive output feedback decentralized control design under the assumption that the reference trajectories are known to all subsystems. A linearly parameterized neural network is used to model the interconnection effects on-line. Boundedness of error signals is shown using Lyapunov's direct method. The methodology is applicable to non-minimum phase subsystems.

CHAPTER 7

ADAPTIVE OBSERVER-BASED OUTPUT FEEDBACK CONTROL

A method of adaptive output feedback control design for an uncertain nonlinear system is presented. The control design augments a state observer based linear control law by an adaptive observer in a manner that adaptive estimation and control augmentation is achieved through a single neural network. In this process, we show how unmatched uncertainty can be managed by an adaptive signal. The proposed synthesis can be applied to non-affine systems having parametric and dynamic uncertainties. The approach is also applicable to non-minimum phase systems if the non-minimum phase zero dynamics are treated in the linear control design. We illustrate the effectiveness of the approach using an inverted pendulum example.

7.1 Introduction

In this chapter we consider the problem of augmenting an observer-based linear control law with adaptive signals. It is assumed that the linear controller is designed using a linear model for the system dynamics. A linear observer for the linear model of the system dynamics is augmented by an adaptive NN as in [86]. The main contribution of this chapter is to show how the linear controller, based on these state estimates, can be augmented by the *same* NN employed for the adaptive observer, to achieve adaptation both in the observer and in the controller design process. This is in contrast to the control architecture in [42, 43] where two NNs are used for the observer and controller design. The approach is applicable to non-minimum phase systems if the unstable zero dynamics are modelled in the linear design.

This chapter is organized as follows: We formulate the control problem in Section 7.2. The process of augmenting a linear observer using a NN is presented in Section 7.3. The

adaptive control design, which utilizes estimates for the uncertainty generated by the NN, is explained in Section 7.4. Next, a stability analysis is presented in Section 7.5. Simulation results with an inverted pendulum follow to illustrate the approach for a non-minimum phase system in Section 7.6. Finally, conclusions are given in Section 7.7.

7.2 Problem Formulation

Consider an *observable and stabilizable* nonlinear system in its *normal* form:

$$\begin{aligned}
\dot{\boldsymbol{z}}_1 =& F_0 \boldsymbol{z}_1 + \boldsymbol{g}_0 x_1 + \boldsymbol{\phi}_2(\boldsymbol{z}_1, \boldsymbol{z}_2, \boldsymbol{\xi}) \\
\dot{x}_1 =& x_2 \\
& \vdots \\
\dot{x}_r =& h(\boldsymbol{z}_1, \boldsymbol{z}_2, \boldsymbol{\xi}, u) \\
=& \boldsymbol{h}_0^T \boldsymbol{z}_1 + a_1 x_1 + \cdots + a_r x_r + d_r[u + \phi_1(\boldsymbol{z}_1, \boldsymbol{z}_2, \boldsymbol{\xi}, u)] \\
\dot{\boldsymbol{z}}_2 =& \boldsymbol{f}_2(\boldsymbol{z}_1, \boldsymbol{z}_2, \boldsymbol{\xi}) \\
y =& x_1,
\end{aligned} \tag{7.1}$$

where $\boldsymbol{\xi} = [x_1, \ldots, x_r]^T \in \mathbb{R}^r$. The linear plant model, which is used to design a linear control law, is written in a compact form:

$$\begin{aligned}
\dot{\boldsymbol{x}} =& A\boldsymbol{x} + \boldsymbol{b}u \\
y =& \boldsymbol{c}^T \boldsymbol{x},
\end{aligned} \tag{7.2}$$

where $\boldsymbol{x} = \begin{bmatrix} \boldsymbol{\xi}^T & \boldsymbol{z}_1^T \end{bmatrix}^T \in \mathbb{R}^m$. The system matrices are defined as:

$$A = \begin{bmatrix} A_m & B_z \\ \boldsymbol{g}_0 \boldsymbol{c}_m^T & F_0 \end{bmatrix}, \ \boldsymbol{b} = \begin{bmatrix} \boldsymbol{b}_m \\ \boldsymbol{0} \end{bmatrix}, \ \boldsymbol{c} = \begin{bmatrix} \boldsymbol{c}_m \\ \boldsymbol{0} \end{bmatrix}, \tag{7.3}$$

where

$$\begin{aligned}
A_m =& \begin{bmatrix} 0 & 1 & 0 & \cdots & 0 \\ 0 & 0 & 1 & \cdots & 0 \\ \vdots & \vdots & \vdots & \vdots & \vdots \\ a_1 & a_2 & \cdots & a_{r-1} & a_r \end{bmatrix}_{r \times r}, \ B_z = \begin{bmatrix} 0 \\ 0 \\ \vdots \\ \boldsymbol{h}_0^T \end{bmatrix}_{r \times (m-r)} \\
\boldsymbol{b}_m^T =& \begin{bmatrix} 0 & 0 & \ldots & d_r \end{bmatrix}_r, \ \boldsymbol{c}_m^T = [\ 1 \quad 0 \quad \cdots \quad 0\ ]_r.
\end{aligned} \tag{7.4}$$

In (7.1), the variable $\boldsymbol{z}_1 \in \Omega_{z_1} \subset \mathbb{R}^{m-r}$ represents the part of the states of the internal dynamics that are modelled, $\boldsymbol{z}_2 \in \Omega_{z_2} \subset \mathbb{R}^{n-m}$ represents any unmodelled dynamics, $u \in \mathcal{D}_u \subset \mathbb{R}^1$ and $y \in \mathbb{R}^1$ are control and measurement variables, and r is the known relative degree of the system [90]. The terms ϕ_1 and $\boldsymbol{\phi}_2$ represent matched and unmatched uncertainties respectively as in (4.2). They are unknown continuous functions, and $\phi_1(0,0,0,0) = 0, \phi_2(0,0,0) = 0$.

Assumption 7.1. *The zero solution of $\dot{\boldsymbol{z}}_2 = \boldsymbol{f}_2(0, \boldsymbol{z}_2, 0)$ is globally exponentially stable, and the function $\boldsymbol{f}_2(\boldsymbol{z}_1, \boldsymbol{z}_2, \boldsymbol{\xi})$ is globally Lipschitz in its arguments.*

Consider the following *state feedback* controller for the dynamics in (7.2), which is designed to track a given *bounded* reference command y_c:

$$u_{lc} = -\boldsymbol{k}^T \boldsymbol{x} + k_c y_c, \tag{7.5}$$

where $k_c y_c$ represents a feedforward term. The plant model in (7.2), when regulated by (7.5), constitutes the *reference model*, which is the nominal closed loop system. The reference model is described as follows:

$$\begin{aligned} \dot{\boldsymbol{x}}_l &= \bar{A}\boldsymbol{x}_l + \boldsymbol{b}k_c y_c, \quad \boldsymbol{x}_l \in \Omega_{\boldsymbol{x}_l} \subset \mathbb{R}^m \\ y_m &= \boldsymbol{c}^T \boldsymbol{x}_l, \end{aligned} \tag{7.6}$$

where $\bar{A} = A - \boldsymbol{b}\boldsymbol{k}^T$.

When compared to (7.2), the system in (7.1) can be written in a compact form:

$$\begin{aligned} \dot{\boldsymbol{x}} &= A\boldsymbol{x} + \boldsymbol{b}u + \boldsymbol{b}_d \boldsymbol{\phi}(\boldsymbol{x}, \boldsymbol{z}_2, u), \\ y &= \boldsymbol{c}^T \boldsymbol{x} \\ \dot{\boldsymbol{z}}_2 &= \boldsymbol{f}_2(\boldsymbol{x}, \boldsymbol{z}_2), \end{aligned} \tag{7.7}$$

where $\boldsymbol{x} \in \Omega_{\boldsymbol{x}} \triangleq \Omega_{\boldsymbol{\xi}} \times \Omega_{\boldsymbol{z}_1} \subset \mathbb{R}^m$, and

$$\boldsymbol{b}_d = \begin{bmatrix} \boldsymbol{b}_m & \boldsymbol{0} \\ \boldsymbol{0} & I \end{bmatrix}, \quad \boldsymbol{\phi}(\boldsymbol{x}, \boldsymbol{z}_2, u) = \begin{bmatrix} \phi_1(\boldsymbol{x}, \boldsymbol{z}_2, u) \\ \boldsymbol{\phi}_2(\boldsymbol{x}, \boldsymbol{z}_2) \end{bmatrix}. \tag{7.8}$$

The control objective is to design a control law $u(\cdot)$ for the dynamics in (7.7) so that its output y tracks the reference model output y_m. We achieve this goal through the following steps:

1. We use the adaptive observer from [86] to generate the state estimates $\hat{\boldsymbol{x}}$ to implement the control law in (7.5) as follows:

$$u_{lc} = -\boldsymbol{k}^T \hat{\boldsymbol{x}} + k_c y_c. \tag{7.9}$$

2. The linear control law u_{lc} is augmented by an adaptive control u_{ad}, as follows:

$$u = u_{lc} + u_{ad}, \tag{7.10}$$

where u_{ad} is designed using the estimates for the uncertainties generated by the NN in the process of state estimation.

7.3 Adaptive Observer Design

The adaptive observer design in [86] makes use of the linear model in (7.2) and augments the following linear observer:

$$\begin{aligned} \dot{\hat{\boldsymbol{x}}} &= A\hat{\boldsymbol{x}} + \boldsymbol{b}u + \boldsymbol{L}(y - \hat{y}) \\ \hat{y} &= \boldsymbol{c}^T \hat{\boldsymbol{x}}, \end{aligned} \tag{7.11}$$

by a SHL NN which approximates the modelling error $\boldsymbol{\phi}$. As in Theorem 3.2. for arbitrary $\epsilon^* > 0$, there exist bounded constant weights M, N such that:

$$\boldsymbol{\phi}(\boldsymbol{x}, \boldsymbol{z}_2, u) = M^T \boldsymbol{\sigma}(N^T \boldsymbol{\eta}) + \boldsymbol{\varepsilon}(\boldsymbol{\eta}),\ \|\boldsymbol{\varepsilon}(\boldsymbol{\eta})\| \leq \epsilon^*,\ \forall (\boldsymbol{x}, \boldsymbol{z}_2, u) \in \Omega_{\boldsymbol{x}} \times \Omega_{\boldsymbol{z}_2} \times \mathcal{D}_u, \tag{7.12}$$

where the NN input $\boldsymbol{\eta}$ is the same as in Theorem 3.2.

The adaptive observer is defined as:

$$\begin{aligned} \dot{\hat{\boldsymbol{x}}} &= A\hat{\boldsymbol{x}} + \boldsymbol{b}u + \boldsymbol{b}_d \hat{\boldsymbol{\phi}} + \boldsymbol{L}(y - \hat{y}), \quad \hat{\boldsymbol{x}} \in \Omega_{\hat{\boldsymbol{x}}} \subset \mathbb{R}^m \\ \hat{y} &= \boldsymbol{c}^T \hat{\boldsymbol{x}}, \end{aligned} \tag{7.13}$$

where $\boldsymbol{L}$ is an observer gain matrix designed to make $F \triangleq A - \boldsymbol{L}\boldsymbol{c}^T$ stable, and $\hat{\boldsymbol{\phi}}$ is the estimate for the modelling error:

$$\hat{\boldsymbol{\phi}} = \widehat{M}^T \boldsymbol{\sigma}(\widehat{N}^T \boldsymbol{\eta}), \tag{7.14}$$

where $\widehat{M}$ and $\widehat{N}$ are estimates of M and N to be adapted on-line. Denote the observation error vectors $\boldsymbol{E} = \hat{\boldsymbol{x}} - \boldsymbol{x},\ z = \hat{y} - y$. Then the observation error dynamics can be written as:

$$\begin{aligned} \dot{\boldsymbol{E}} &= F\boldsymbol{E} + \boldsymbol{b}_d[\hat{\boldsymbol{\phi}} - \boldsymbol{\phi}],\ \boldsymbol{E} \in \Omega_{\boldsymbol{E}} \subset \mathbb{R}^m \\ z &= \boldsymbol{c}^T\boldsymbol{E}. \end{aligned} \tag{7.15}$$

Since F is Hurwitz, for any $Q > 0$, there exists a $P > 0$ such that:

$$F^T P + PF + Q = 0. \tag{7.16}$$

The NN weights are updated using the teaching signal generated by the linear observer for the dynamics in (7.15):

$$\begin{aligned} \dot{\widehat{\boldsymbol{E}}} &= F\widehat{\boldsymbol{E}} + \boldsymbol{H}(z - \hat{z}) \\ \hat{z} &= \boldsymbol{c}^T\widehat{\boldsymbol{E}}, \end{aligned} \tag{7.17}$$

where $\boldsymbol{H}$ is a gain matrix chosen such that $\widetilde{F} \triangleq F - \boldsymbol{H}\boldsymbol{c}^T$ is stable. This observer is used only to generate an error signal needed in adapting the NN weights [86]. Let $\widetilde{\boldsymbol{E}} = \widehat{\boldsymbol{E}} - \boldsymbol{E}$. Then, the estimation error dynamics for $\boldsymbol{E}$ is written as:

$$\dot{\widetilde{\boldsymbol{E}}} = \widetilde{F}\widetilde{\boldsymbol{E}} - \boldsymbol{b}_d[\hat{\boldsymbol{\phi}} - \boldsymbol{\phi}], \quad \widetilde{\boldsymbol{E}} \in \Omega_{\widetilde{\boldsymbol{E}}} \subset \mathbb{R}^m. \tag{7.18}$$

Since $\widetilde{F}$ is Hurwitz, for any $\widetilde{Q} > 0$, there exists a $\widetilde{P} > 0$ such that:

$$\widetilde{F}^T\widetilde{P} + \widetilde{P}\widetilde{F} + \widetilde{Q} = 0. \tag{7.19}$$

The NN weights $\widehat{M},\ \widehat{N}$ are updated according to the following adaptation laws [86]:

$$\begin{aligned} \dot{\widehat{M}} &= -\Gamma_M[(\hat{\boldsymbol{\sigma}} - \hat{\sigma}'\widehat{N}^T\boldsymbol{\eta})\widehat{\boldsymbol{E}}^T P\boldsymbol{b}_d + k\widehat{M}] \\ \dot{\widehat{N}} &= -\Gamma_N[\boldsymbol{\eta}\widehat{\boldsymbol{E}}P\boldsymbol{b}_d\widehat{M}^T\hat{\sigma}' + k\widehat{N}] \end{aligned} \tag{7.20}$$

in which the NN parameters are the same as those in (3.49).

Following the analysis in Section 5.5, the forcing term $\hat{\boldsymbol{\phi}} - \boldsymbol{\phi}$ in (7.15) and (7.18) allows for the following upper bound [86]:

$$\|\hat{\boldsymbol{\phi}} - \boldsymbol{\phi}\| \leq \alpha_1\|\widetilde{Z}\|_F + \alpha_2, \quad \alpha_1, \alpha_2 > 0. \tag{7.21}$$

Following the lines in Section 5.5 , the NN approximation error $\hat{\boldsymbol{\phi}} - \boldsymbol{\phi}$ can be described as

$$\hat{\boldsymbol{\phi}} - \boldsymbol{\phi} = \widetilde{M}(\hat{\sigma} - \hat{\sigma}'\widehat{N}^T\boldsymbol{\eta}) + \widehat{M}^T\hat{\sigma}'\widetilde{N}^T\boldsymbol{\eta} + \boldsymbol{w} - \boldsymbol{\varepsilon} \tag{7.22}$$

where $\boldsymbol{\omega} - \boldsymbol{\varepsilon}$ can be bounded as follows:

$$\|\boldsymbol{w} - \boldsymbol{\varepsilon}\| \leq \gamma_1\|\tilde{Z}\|_F + \gamma_2, \quad \gamma_1, \gamma_2 > 0. \tag{7.23}$$

It has been shown in [86] that, with $u \equiv 0$, $\boldsymbol{E}$ in (7.15) and $\widetilde{\boldsymbol{E}}$ in (7.18) and $\widetilde{M}$, $\widetilde{N}$ are bounded under a set of assumptions about $Q, \widetilde{Q}, k$. The following Lyapunov function was used that in that analysis

$$\begin{aligned} V_o(\boldsymbol{E}, \widetilde{\boldsymbol{E}}, \widetilde{M}, \widetilde{N}) =& \boldsymbol{E}^T P \boldsymbol{E} + \widetilde{\boldsymbol{E}}^T \widetilde{P} \widetilde{\boldsymbol{E}} + \text{tr}\left(\widetilde{M}^T \Gamma_M^{-1} \widetilde{M}\right) \\ &+ \text{tr}\left(\widetilde{N}^T \Gamma_N^{-1} \widetilde{N}\right), \end{aligned} \tag{7.24}$$

where $P, \widetilde{P}$ are defined in (7.16), (7.19) respectively.

7.4 Adaptive Control design

When the control law in (7.10) is applied, with u_{lc} in (7.9) being implemented using $\hat{\boldsymbol{x}}$ in (7.13), the closed loop system in (7.7) is written as:

$$\dot{\boldsymbol{x}} = A\boldsymbol{x} + \boldsymbol{b}k_c y_c - \boldsymbol{b}\boldsymbol{k}^T\hat{\boldsymbol{x}} + \boldsymbol{b}u_{ad} + \boldsymbol{b}_d\boldsymbol{\phi}. \tag{7.25}$$

Let $u_{ad} = u_{ad_1} + u_{ad_2}$. Adding and subtracting $\boldsymbol{b}\boldsymbol{k}^T\boldsymbol{x}, \boldsymbol{b}_d\hat{\boldsymbol{\phi}}$, the dynamics in (7.25) can be further arranged as follows:

$$\begin{aligned} \dot{\boldsymbol{x}} = \bar{A}\boldsymbol{x} + \boldsymbol{b}k_c y_c - \boldsymbol{b}\boldsymbol{k}^T\boldsymbol{E} + \boldsymbol{b}(u_{ad_1} + \hat{\phi}_1) + \boldsymbol{b}u_{ad_2} + \begin{bmatrix} 0 \\ \hat{\boldsymbol{\phi}}_2 \end{bmatrix} \\ + \boldsymbol{b}_d[\boldsymbol{\phi} - \hat{\boldsymbol{\phi}}]. \end{aligned} \tag{7.26}$$

Define tracking error vector as follows:

$$\boldsymbol{e}_l = \boldsymbol{x}_l - \boldsymbol{x}, \quad \boldsymbol{e}_l \in \Omega_{\boldsymbol{e}_l} \quad \text{when } \boldsymbol{x}_l \in \Omega_{\boldsymbol{x}_l},\ \boldsymbol{x} \in \Omega_{\boldsymbol{x}}. \tag{7.27}$$

Note that $\boldsymbol{e}_l$ represents the trajectory deviations of the closed loop system in (7.26) from those of the reference model in (7.6). Its dynamics are given by

$$\dot{\boldsymbol{e}}_l = \bar{A}\boldsymbol{e}_l + \boldsymbol{b}\boldsymbol{k}^T\boldsymbol{E} - \boldsymbol{b}(u_{ad_1} + \hat{\phi}_1) - \boldsymbol{b}u_{ad_2} - \begin{bmatrix} 0 \\ \hat{\boldsymbol{\phi}}_2 \end{bmatrix} - \boldsymbol{b}_d[\boldsymbol{\phi} - \hat{\boldsymbol{\phi}}]. \tag{7.28}$$

The control signal u_{ad_1} is designed in the same manner as in [150], to approximately cancel ϕ_1:

$$u_{ad_1} = -\hat{\phi}_1. \tag{7.29}$$

Notice from (7.29) and the form of ϕ_1 that $\phi_1(\cdot, u)$ depends on u_{ad_1} through u, and that the role of u_{ad_1} is to cancel ϕ_1.

Assumption 7.2. *There exist a fixed point solution to the equation* $u_{ad_1} = -\phi_1(\cdot,\ u_{ad_1})$ *uniformly in* $(\boldsymbol{x}, \boldsymbol{z}_2) \in \Omega_{\boldsymbol{x}} \times \Omega_{z_2}$ *on* $\mathcal{D}_u$.

With u_{ad_1} in (7.29), the tracking error dynamics become:

$$\dot{\boldsymbol{e}}_l = \bar{A}\boldsymbol{e}_l + \boldsymbol{b}\boldsymbol{k}^T\boldsymbol{E} - \boldsymbol{b}u_{ad_2} - \begin{bmatrix} 0 \\ \hat{\boldsymbol{\phi}}_2 \end{bmatrix} - \boldsymbol{b}_d[\boldsymbol{\phi} - \hat{\boldsymbol{\phi}}]. \tag{7.30}$$

Note that with $u_{ad_2} = 0$, the unmatched uncertainty $\boldsymbol{\phi}_2$ directly enters the tracking error dynamics. To remedy this situation, we consider the following Lyapunov function for the tracking error dynamics in (7.30):

$$V_{\boldsymbol{e}_l} = \boldsymbol{e}_l^T P_l \boldsymbol{e}_l, \tag{7.31}$$

where P_l is the positive definite solution to the following Lyapunov equation:

$$\bar{A}^T P_l + P_l \bar{A} + Q_l = 0, \tag{7.32}$$

for some $Q_l > 0$. The main idea for u_{ad_2} is to determine the control law so that it reduces the effect of the unmatched uncertainty on the time derivative of $V_{\boldsymbol{e}_l}$ in (7.31).

With (7.30) and (7.32), the time derivative of $V_{\boldsymbol{e}_l}$ is described by:

$$\dot{V}_{\boldsymbol{e}_l} = -\boldsymbol{e}_l^T Q_l \boldsymbol{e}_l - 2\boldsymbol{e}_l^T P_l \boldsymbol{b} u_{ad_2} - 2\boldsymbol{e}_l^T P_l \begin{bmatrix} 0 \\ \hat{\boldsymbol{\phi}}_2 \end{bmatrix} - 2\boldsymbol{e}_l^T P_l \boldsymbol{b}_d[\boldsymbol{\phi} - \hat{\boldsymbol{\phi}}] + 2\boldsymbol{e}_l^T P_l \boldsymbol{b}\boldsymbol{k}^T\boldsymbol{E}. \tag{7.33}$$

One can see from this expression that it is desirable to design the signal u_{ad_2} in a way that

$$\boldsymbol{e}_l^T P_l \boldsymbol{b} u_{ad_2} + \boldsymbol{e}_l^T P_l \begin{bmatrix} 0 \\ \hat{\boldsymbol{\phi}}_2 \end{bmatrix} = 0. \tag{7.34}$$

However, since $\boldsymbol{e}_l$ is not available, we use $\hat{\boldsymbol{e}}_l \triangleq \boldsymbol{x}_l - \hat{\boldsymbol{x}} \in \Omega_{\hat{\boldsymbol{e}}_l} \in \mathbb{R}^m$. Towards this end, the expression in (7.33) is rewritten as:

$$\begin{aligned}\dot{V}_{\boldsymbol{e}_l} = -\boldsymbol{e}_l^T Q_l \boldsymbol{e}_l - 2\hat{\boldsymbol{e}}_l^T P_l \boldsymbol{b} u_{ad_2} - 2\hat{\boldsymbol{e}}_l^T P_l \begin{bmatrix} 0 \\ \hat{\boldsymbol{\phi}}_2 \end{bmatrix} - 2\boldsymbol{E}^T P_l \boldsymbol{b} u_{ad_2} \\ - 2\boldsymbol{E}^T P_l \begin{bmatrix} 0 \\ \hat{\boldsymbol{\phi}}_2 \end{bmatrix} - 2\boldsymbol{e}_l^T P_l [\boldsymbol{\phi} - \hat{\boldsymbol{\phi}}] + 2\boldsymbol{e}_l^T P_l \boldsymbol{b} \boldsymbol{k}^T \boldsymbol{E}.\end{aligned} \tag{7.35}$$

With the following definition:

$$\hat{s} = \hat{\boldsymbol{e}}_l^T P_l \boldsymbol{b}, \quad \hat{\psi} = \hat{\boldsymbol{e}}_l^T P_l \begin{bmatrix} 0 \\ \hat{\boldsymbol{\phi}}_2 \end{bmatrix}, \tag{7.36}$$

the adaptive signal u_{ad_2} is designed as:

$$u_{ad_2} = \mathcal{N}(\hat{s}) = \begin{cases} -\frac{1}{\hat{s}}\hat{\psi} & \text{if} \quad |\hat{s}| > \mu \\ -\frac{1}{2}\frac{\hat{\psi}}{\hat{s}}\left[\sin\frac{4\pi}{3}\left(\frac{\hat{s}^2}{\mu^2} - \frac{5}{8}\right) + 1\right] & \text{if} \quad \frac{\mu}{2} < |\hat{s}| \leq \mu \\ 0 & \text{if} \quad |\hat{s}| \leq \frac{\mu}{2} \end{cases} \tag{7.37}$$

where $\mu > 0$ is a design factor introduced to reduce the control action u_{ad_2} when $\hat{s}$ is small, and to prevent u_{ad_2} from becoming unbounded when $\hat{s} = 0$. This case may occur if $\hat{\boldsymbol{e}}_l \perp P_l \boldsymbol{b}, \hat{\boldsymbol{e}}_l (\neq 0)$. The control signal u_{ad_2} is smooth and motivated by a switching $\sigma-$modification [151]. The overall control signal is summarized as follows:

$$u = u_{lc} + u_{ad_1} + u_{ad_2} = -\boldsymbol{k}^T \hat{\boldsymbol{x}} + k_c y_c - \hat{\phi}_1 + \mathcal{N}(\hat{s}). \tag{7.38}$$

7.5 Stability Analysis

Before we develop the proof of boundednessf, we need to derive bounds for $\hat{\boldsymbol{\phi}}$ and $\hat{\psi}$ in terms of $\widetilde{Z}$ defined after (5.33). With the following bound for each element of the estimate for the unmatched uncertainty $\hat{\boldsymbol{\phi}}_2$:

$$|\hat{\boldsymbol{\phi}}_{2_i}| \leq p_i \|\widetilde{Z}\|_F + q_i, \quad i = r+1, \ldots, m, \quad p_i, q_i > 0, \tag{7.39}$$

the overall bound for $\hat{\boldsymbol{\phi}}_2$ can be expressed as:

$$\left\|\hat{\boldsymbol{\phi}}_2\right\| \leq c_1 \|\widetilde{Z}\|_F + c_2, \tag{7.40}$$

where $c_1 = \sum_{i=r+1}^{m} p_i$, $c_2 = \sum_{i=r+1}^{m} q_i$. The bound in (7.39) can be derived using $\|\hat{\boldsymbol{\phi}}_{2_i}\| \leq \|\widehat{M}_i\| \leq c\|\widehat{M}\|_F \leq c\|\widetilde{M}\|_F + cM^*$ with $c > 0$, where $\widehat{M}_i$ represents the row vector of $\widehat{M}$ which corresponds to $\hat{\boldsymbol{\phi}}_{2_i}$.

In order to derive a bound for $\hat{\psi}$ in (7.36), we define constants $\pi_i,\ i = r+1, \ldots, m$, according to the following inequalities:

$$|\hat{\boldsymbol{e}}_l^T P_{l_i}| \leq \varphi_i(\hat{\boldsymbol{e}}_l)|\hat{s}| \leq \pi_i|\hat{s}|, \quad \text{when} \quad \hat{\boldsymbol{e}}_l \in \Omega_{\hat{\boldsymbol{e}}_l} \setminus B_\mu \left(\triangleq \{\hat{\boldsymbol{e}}_l \in \Omega_{\hat{\boldsymbol{e}}_l} \ : \ |\hat{s}| < \frac{\mu}{2}\} \right), \tag{7.41}$$

where $\varphi_i(\hat{\boldsymbol{e}}_l) = \left| \frac{\hat{\boldsymbol{e}}_l^T P_{l_i}}{\hat{\boldsymbol{e}}_l^T P_l \boldsymbol{b}} \right| \leq \frac{2|\hat{\boldsymbol{e}}_l^T P_{l_i}|}{\mu}$, $\pi_i = \sup_{\hat{\boldsymbol{e}}_l \in \Omega_{\hat{\boldsymbol{e}}_l} \setminus B_\mu} \varphi_i(\hat{\boldsymbol{e}}_l)$, and P_{l_i} represents the ith column of P_l. Using (7.39) and (7.41),

$$\begin{aligned} |\hat{\psi}| = \Big| \sum_{i=r+1}^{m} \hat{\boldsymbol{e}}_l^T P_{l_i} \hat{\boldsymbol{\phi}}_{2_i} \Big| &\leq \sum_{i=r+1}^{m} \pi_i |\hat{s}| |\hat{\boldsymbol{\phi}}_{2_i}| \leq |\hat{s}| \sum_{i=r+1}^{m} \pi_i \left[p_i \|\widetilde{Z}\|_F + q_i \right] \\ &\leq |\hat{s}| \left[\pi_1 \|\widetilde{Z}\|_F + \pi_2 \right] \quad \text{when} \quad \hat{\boldsymbol{e}}_l \in \Omega_{\hat{\boldsymbol{e}}_l} \setminus B_\mu, \end{aligned} \tag{7.42}$$

where $\pi_1 = \sum_{i=r+1}^{m} \pi_i p_i,\ \pi_2 = \sum_{i=r+1}^{m} \pi_i q_i$.

We will show that the signals $\boldsymbol{e}_l$ in (7.30), $\boldsymbol{E}$ in (7.15), $\widetilde{\boldsymbol{E}}$ in (7.18), and NN weight errors $\widetilde{Z}$ are bounded,, using the following Lyapunov candidate function:

$$V(\boldsymbol{e}_l, \boldsymbol{E}, \widetilde{\boldsymbol{E}}, \widetilde{M}, \widetilde{N}) = V_{\boldsymbol{e}_l} + V_o(\boldsymbol{e}_l, \boldsymbol{E}, \widetilde{\boldsymbol{E}}, \widetilde{M}, \widetilde{N}), \tag{7.43}$$

where $V_{\boldsymbol{e}_l},\ V_o$ are defined in (7.31), (7.24) respectively. With this objective in mind, we define the error vector $\zeta^T \triangleq \left[\begin{array}{cccc} \boldsymbol{e}_l^T & \boldsymbol{E}^T & \widetilde{\boldsymbol{E}}^T & \mathbf{vec}(\widetilde{Z})^T \end{array} \right]$ and the ball $\mathcal{B}_R \triangleq \{\zeta | \|\zeta\| \leq R,\ R > 0\} \subseteq \Omega_{\boldsymbol{e}_l} \times \Omega_{\boldsymbol{E}} \times \Omega_{\widetilde{\boldsymbol{E}}} \times \Omega_{\widetilde{\boldsymbol{Z}}}$ such that for every $\zeta \in \mathcal{B}_R$, the control signal u in (7.38) belongs to $\mathcal{D}_u$, and $\|\boldsymbol{\eta}\| \leq \eta^*$, thus NN approximation implied in (7.12) is valid. With the definition of ζ, the Lyapunov function in (7.43) can be compactly written as:

$$V(\zeta) = \zeta^T T \zeta, \tag{7.44}$$

where T is defined to be:

$$T = \frac{1}{2} \begin{bmatrix} 2P_l & 0 & 0 & 0 & 0 \\ 0 & 2P & 0 & 0 & 0 \\ 0 & 0 & 2\widetilde{P} & 0 & 0 \\ 0 & 0 & 0 & 2\Gamma_M^{-1} & 0 \\ 0 & 0 & 0 & 0 & 2\Gamma_N^{-1} \end{bmatrix}. \tag{7.45}$$

Let T_m, T_M be minimal and maximal eigenvalues of T. Then, $T_m\|\zeta\|^2 \leq V(\zeta) \leq T_M\|\zeta\|^2$. Introduce the following set:

$$\alpha = \sqrt{\frac{T_m}{T_M}}R, \quad \mathcal{B}_\alpha = \{\zeta \in \mathcal{B}_R \mid \|\zeta\| \leq \alpha\}. \tag{7.46}$$

Theorem 7.1. *Suppose $\zeta(0) \in \mathcal{B}_\alpha$ and $R > C$, C being defined in (E.14). Subject to Assumptions 7.1-7.2, the control design described in (7.38) guarantees that the signal ζ is uniformly ultimately bounded, provided the following conditions hold:*

$$\begin{aligned} &\lambda_{\min}(Q_l) > \ 3, \quad \lambda_{\min}(Q) > \ 2 + \|P_l \boldsymbol{b}\boldsymbol{k}^T\|^2, \quad \lambda_{\min}(\widetilde{Q}) > \ 2 \\ &k > \ \max\Big\{\frac{\mu\pi_1}{2} + \alpha_1^2\lambda_{\max}(P_l)^2 + \delta_1^2 + \Theta^2, \\ &\qquad (\alpha_1 + c_1)^2)\lambda_{\max}(P_l)^2 + \delta_1'^2 + \Theta^2\Big\}, \end{aligned} \tag{7.47}$$

where $\delta_1 = c_1\lambda_{\max}(P_l) + (\pi_1 + \gamma_1)\|P\boldsymbol{b}_d\|$, $\delta_1' = \gamma_1\|P\boldsymbol{b}_d\|$, $\Theta = \gamma_1\|P\boldsymbol{b}_d\| + \alpha_1\|(P + \widetilde{P})\boldsymbol{b}_d\|$.

Proof. See Appendix E. □

Theorem 7.1 implies that $\boldsymbol{x}$ is bounded since $\boldsymbol{x}_l$ in (7.6) and $\boldsymbol{e}_l$ in (7.30) are bounded. Then Assumption 7.1 ensures that $\boldsymbol{z}_2$ is bounded since it is input-to-state stable [91]. The assumption that $u \in \mathcal{D}_u$ and $\|\boldsymbol{\eta}\| \leq \eta^*$ is also guaranteed, since $\mathcal{B}_\alpha \subseteq \mathcal{B}_R$ is positively invariant set. Hence all the signals in the closed loop system are bounded.

7.6 Simulation Results with an Inverted Pendulum

We illustrate the proposed approach using the inverted pendulum mechanism depicted in Figure 4.6. The mechanism is described in Section 4.5. In the simulation, the system parameters are $M = 1.2$, $m = 0.15$, $l_p = 0.305$, $g = 9.8$, $a_1 = 1.72$, $a_2 = 7.68$. Also $\Psi(x, \dot{x}) = 0$ in (4.26). Its normal form and the definitions for the matched uncertainty and unmatched uncertainty are obtained by setting $\Psi(x, \dot{x}) = 0$ in (4.28) and (4.31). The plant model is given in (4.30). The control objective is to regulate the displacement of the cart x, using measured outputs x, θ to track given command y_c. A linear quadratic regulator(LQR) compensator is designed so that y_m tracks y_c. Its parameters are

$$\boldsymbol{k}^T = [-7.1, 8.1, -43.3, -8.1], \quad k_c = -7.1. \tag{7.48}$$

The linear observer in (7.11) is designed such that its closed poles are located at $-2.2 \pm 0.6i$, $-11.6 \pm 2.0i$. The observer poles for the teaching signal of the NN are at $-75.4 \pm 13.2i, -14.1 \pm 4.0i$. Since two outputs are available, network inputs are constructed as follows:

$$\boldsymbol{\eta}^T = [x_1,\ x_1(t-d),\ z_1,\ z_1(t-d), u],\ d = 0.04\ sec. \tag{7.49}$$

The modelling error $\boldsymbol{\phi}$ is approximated by 3 NNs rather than 1 NN because it allows easy tuning for its parameters and learning rates to approximate each uncertainty. This is equivalent to the use of 1 NN [36]. The design parameters μ in (7.37) are chosen as 0.02.

Figure 7.1 compares the output ($\boldsymbol{x}$) responses of the closed loop system regulated by the linear controller, the LQR controller in (7.48) combined with the linear observer, and the one regulated by the proposed controller when the reference command is a square wave of .15(m) at .05 Hz. The initial conditions are:

$$x(0) = \dot{x}(0) = \dot{\theta}(0) = 0,\ \theta(0) = 5^o. \tag{7.50}$$

The proposed control achieves significant reduction in output oscillations. To compare the

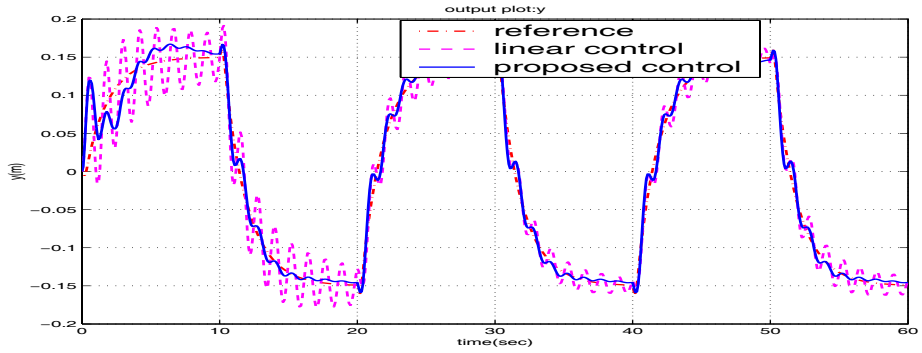

Fig. 7.1: Comparison of Output Responses of the Linear Control and the Proposed Control

performances of the linear observer and the adaptive observer, the estimation errors for $\dot{x}$ and $\dot{\theta}$, i.e. the 2nd and 4th elements of $\boldsymbol{E}$ are shown in Figure 7.2. The importance of u_{ad} is verified when we set the initial conditions as:

$$x(0) = \dot{x}(0) = 0,\ \theta(0) = 50^o,\ \dot{\theta}(0) = 5^o/sec. \tag{7.51}$$

In this case, the linear control law combined with the adaptive observer fails to regulate the

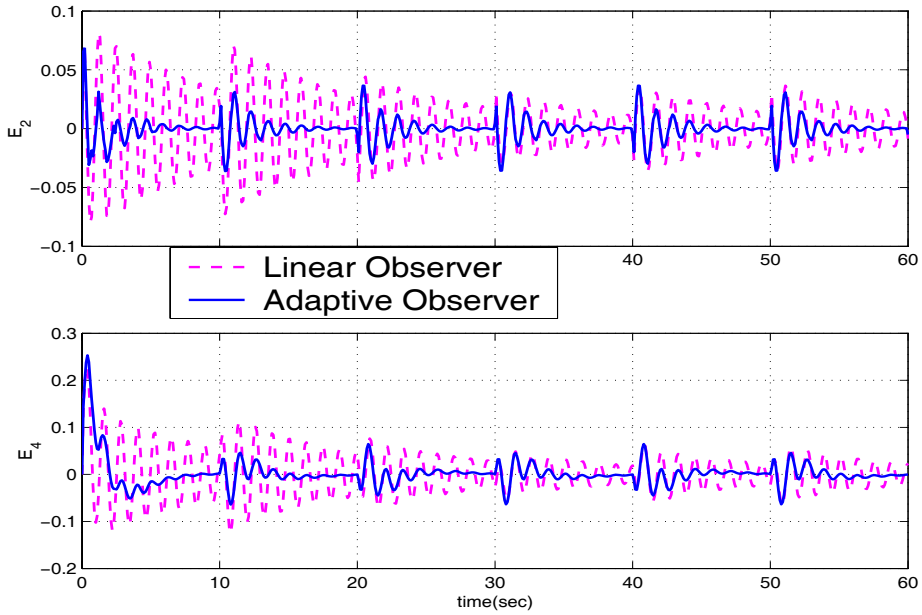

Fig. 7.2: Comparison of Estimation Errors by the Linear Observer and the Adaptive Observer : a) $\dot{x}$ Estimation Error b) $\dot{\theta}$ Estimation Error

system. With the adaptive law u_{ad}, on the other hand, Figure 7.3 shows that following a large transient, the control system recovers output tracking.

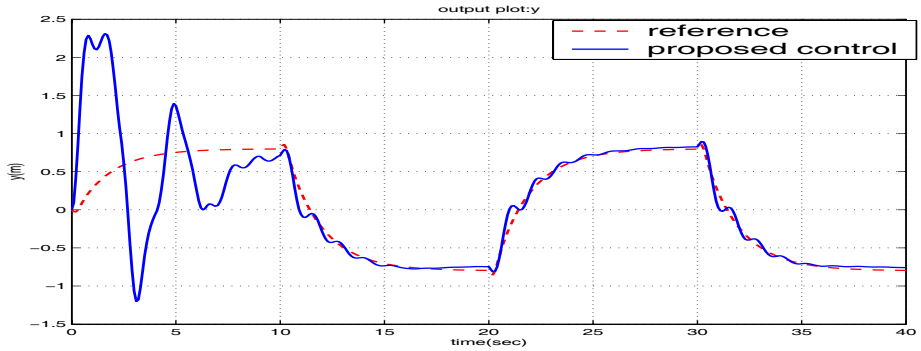

Fig. 7.3: Output Response of the Proposed Controller with the Initial Condition for which a Linear Control Law is not Valid

7.7 Conclusions

This chapter presents an approach for adaptive output feedback control of uncertain nonlinear systems. The control is based on augmentation of a linear control law, which uses states generated by an adaptive observer. To compensate for the uncertainties, the linear

controller is augmented by an adaptive element. This approach is applicable to both minimum phase and non-minimum phase nonlinear systems. The key properties of the design are that only output variables are used and the unmatched uncertainty is compensated by adaptive control. The main assumption is that the relative degree of the regulated output is known. Simulation results with an inverted pendulum demonstrate the validity of the approach for control of a nonlinear non-minimum phase system.

CHAPTER 8

APPLICATION TO A FLEXIBLE ROBOT CONTROL

This chapter addresses adaptive augmentation of an existing inertial damping mechanism, for controlling a micromanipulator that is serially attached to a macromanipulator. The objective of the control design is to compensate for the flexibility of the macromanipulator, and suppress vibrations. An experimental testbed is used to demonstrate the theoretical approach. In the testbed, the micromanipulator is mounted at the tip of a cantilevered beam which resembles a macromanipulator with its joint locked. The inertial damping control combines acceleration feedback with a separately designed position control for the micromanipulator. There were several design challenges that had to be faced from an adaptive control perspective. One challenge was the presence of a non-minimum phase zero in an output feedback adaptive control design setting in which the regulated output variable has zero relative degree. Other challenges included flexibility in the actuation devices, lack of control degrees of freedom, and high dimensionality of the system dynamics. In this paper we describe how we overcame these difficulties. Experimental results are provided to illustrate the effectiveness of the augmenting approach to adaptive output feedback control design.

8.1 Introduction

A rigid micromanipulator attached serially to a macromanipulator is used in industrial robotics where a lightweight and long-reach capability is needed, such as might be the case in a space robotics application. To achieve tip positioning with high accuracy within acceptable time, the flexibility in the macromanipulator necessitates the design of a control system that includes provision for vibration damping. Inertial damping control has experimentally proven effective using the test bed in the Intelligent Machine Dynamics Laboratory (IMDL) at Georgia Tech., in which a micromanipulator, SAMII (Small Articulated Manipulator

II), is mounted at the tip of a cantilevered beam fixed to the ceiling, the base motion of which is similar to that at the tip of a flexible manipulator with locked joints [152–154]. In inertial damping control, the micromanipulator is commanded so as to produce inertial forces that damp the unwanted vibration in the base. Therefore, the method generally requires a relatively accurate model for the interactions between the micromanipulator and the base, which is essential to avoid particular locations where coupling effects between the micromanipulator and the base are not suitable for vibration damping. In the design, it is important to limit the control gain to ensure that model uncertainties do not lead to instabilities. Also, it is important to maintain a proper link configuration so that inertial effects dominate the interaction forces [155].

When the robot executes its task in a real-time environment, however, the control method which requires a sound model for its dynamic process may be deficient due to inherent uncertainties in the system modelling and operating conditions. In [156], it is shown that modal uncertainty associated with the macromanipulator dynamics can lead to controller induced instabilities. Thus, uncertainty in the system dynamics and operating conditions makes the design of an augmenting adaptive controller highly desirable for this application.

In this chapter we implement adaptive control in Chapter 4 to augment the existing inertial damping control system given in [156] for suppressing flexible base vibration. After all, the approach allows the system to be non-minimum phase and thus can be applied to control of flexible-link robot arms that can be non-minimum phase when actuators and sensors are not collocated [157, pp.20-26]. Beyond the non-minimum phase aspect of the problem, several challenges need to be addressed. For one, the output regulated variable has zero relative degree. In addition, the actuation device exhibits significant flexibility [158]. Furthermore, the control degrees of freedom is smaller than the coupled number of outputs to be regulated. That is, the existing system combines both position control and vibration control in a single input design setting. Finally, the dimension of the system dynamics increase as the second mode of base vibration is considered in design of the existing controller.

The chapter is organized as follows: In Section 8.2, we describe the essential features of IMDL testbed. In Section 8.3, the existing control system is presented. Next, the details of the augmenting adaptive controller design are given in Section 8.4, with emphasis on how the approach in Chapter 4 was adapted to address the challenges in this application. In Section 8.5, experimental results are described that support the validity of the overall approach. Conclusion are given in Section 8.6.

8.2 System Description

Figure 8.1 depicts SAMII mounted serially to the 5-m long cantilevered beam suspended from an I-beam of the building. The actuators of the system are hydraulic servo motors at

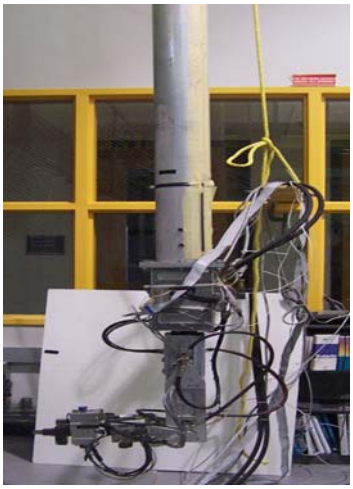

Fig. 8.1: Testbed at the Intelligent Machine Dynamics Laboratory (IMDL) at Georgia Tech.

the joints of SAMII. These are rotary vane actuators with electro-hydraulic servo valves. Optical encoders located on the shaft of each joint perform measurement of the rotational position of the joints. For vibration control, accelerations are measured by accelerometers located at the beam tip. Figure 8.2 defines the coordinates related to the control design. With the definitions given in Figure 8.2, the configuration in Figure 8.1 is described by $\theta_1 = -90°$, $\theta_2 = 90°$, and $\theta_3 = 90°$, and $x = 0$, which represents the initial position where the control system starts. The existing control system considers only vibration control of a single direction (x) by implementing an inertial damping controller to a single link (link 2) while the other links and the wrist are under decoupled position control, using proportional

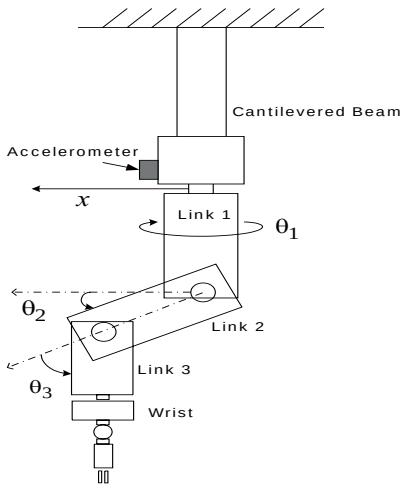

Fig. 8.2: Definitions of Coordinates in the Existing Control System

feedback control. Therefore, only the variable θ_2 among joint angles is used in design of the control system, and the notation θ is used in place of θ_2 throughout the chapter.

The hydraulic actuator model in [156], a linear model derived by curve fitting experimental data obtained with the configuration as shown in Figure 8.1, is as follows:

$$\frac{\theta}{u} = P_\theta(s) = \frac{K_1[(s/\omega_2)^2 + 2\zeta_2(s/\omega_2) + 1]}{s(s/\tau + 1)[(s/\omega_p)^2 + 2\zeta_p(s/\omega_p) + 1]}, \tag{8.1}$$

where θ° is in degrees, and u is the input voltage to the hydraulic actuator. The parameters in this model are: $K_1 = 20,\ \omega_d = 8.2Hz, \zeta_d = 0.11,\ \omega_2 = 10Hz, \zeta_2 = 0.06,\ \tau = 30Hz$. Figure 8.3 compares the frequency response of the model in Eq.(8.1) to that of experimental data. Note that the model in (8.1) includes flexibility in the actuator model, in contrast to that in [152, 155].

In the same manner, the acceleration of the base is modelled as a transfer function. This linear model implies that the Coriolis term and centrifugal forces are negligible in the interaction forces. The transfer function for the base acceleration with the joint angle θ as input is given in [156] as

$$\begin{aligned} \frac{\ddot{x}}{\theta} = P_f(s) = & \frac{s^4 B_1 \phi_1(L)}{(s/\omega_1)^2 + 2\zeta_1(s/\omega_1) + 1} \\ & + \frac{s^4 B_2 \phi_2(L)}{(s/\omega_2)^2 + 2\zeta_2(s/\omega_2) + 1}, \end{aligned} \tag{8.2}$$

where x represents the displacement of the point on which the accelerometer is mounted (see Figure 8.2), and $B_1 = -1/475000, \omega_1 = 1.75Hz, \zeta_1 = 0.05,\ B_2 = 1/(3 \times 10^6)$. The

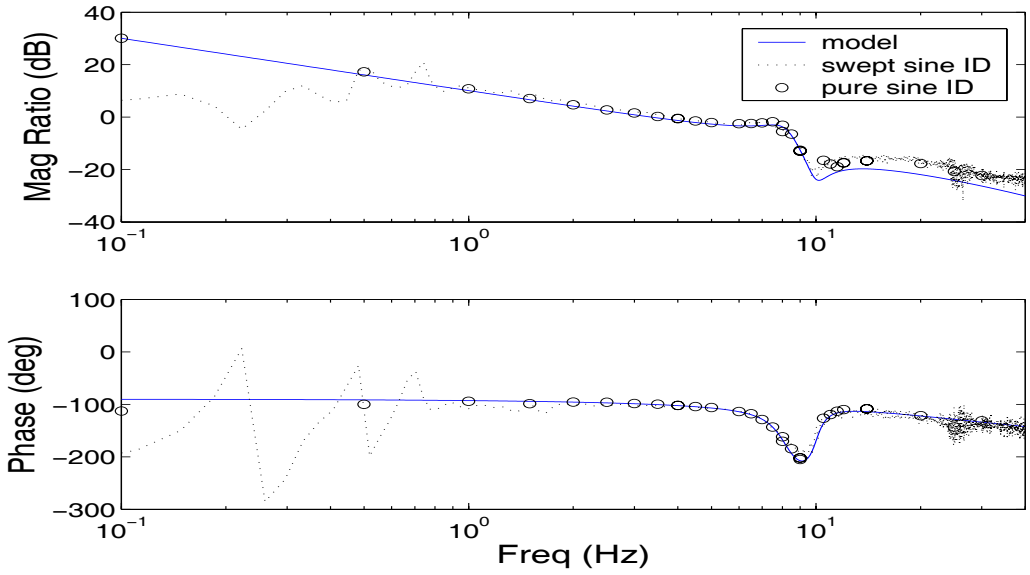

Fig. 8.3: Comparison of Frequency Response of the Actuator Model in (8.1) to Experimental Data

terms ϕ_1 and ϕ_2 represent the normalized mode shapes so that $\phi_1(L) = \phi_2(L) = 1$. The frequency response of the model in (8.2) is compared to the experimental data in Figure 8.4. Note that the model in (8.2) is only valid up to a frequency of 20 Hz. This means that the dynamics at high frequency are essentially unknown. Furthermore, with 4 zeros at the origin (s^4) , the opposite sign of B_1 and B_2 in (8.2) results in right-half plane zeros and renders the acceleration output with the input u non-minimum phase. This is physically due to the sensor location which is not collocated with the hydraulic actuator as explained in [156] (See also Figure 8.2). The uncertainty in high frequency dynamics together with its non-minimum phase property severely restricts the control gains, and thus renders the design of a high-performance vibration controller a challenging task.

8.3 Existing Control System

The existing control system consists of a position controller combined with an inertial damping controller which is *separately* designed to suppress vibration. In spirit, the control scheme is based on separation of bandwidths, or two time-scales, in which the fact that the base vibration is relatively "fast" compared to the robot motion is exploited [154]. The rationale can be understood from block diagram depicted in Figure 8.5. The position

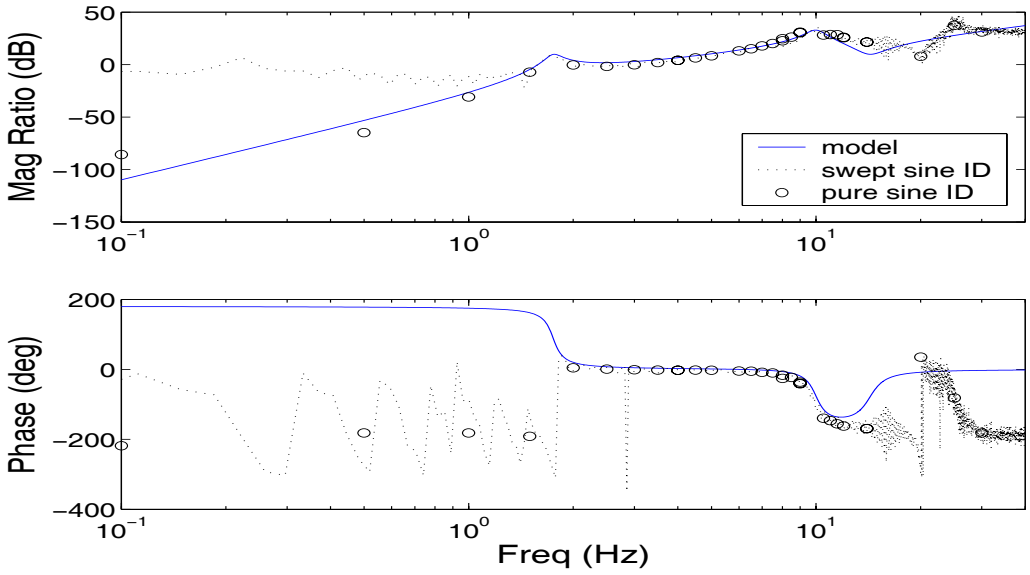

Fig. 8.4: Comparison of the Base Acceleration Model in (8.2) to Experimental Data

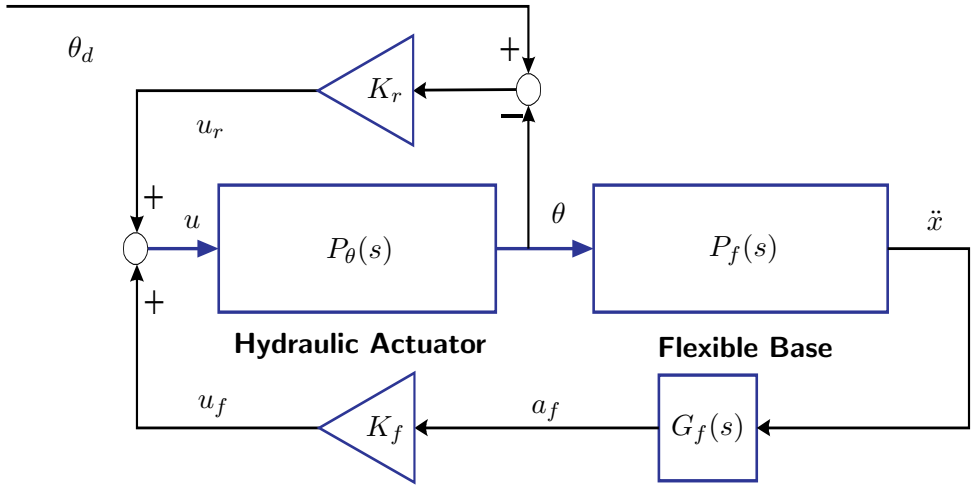

Fig. 8.5: Existing Control System Architecture

controller for the rigid link is a proportional feedback

$$u_r = K_r(\theta_d - \theta), \tag{8.3}$$

where θ_d is the position command for the link, and $K_r = 1$. Proportional acceleration feedback, with $K_f = -1.435$, is used to suppress vibrations, based on the assumption that the hydraulic actuator results in a velocity proportional to voltage. As can be seen from

Figure 8.3, this is approximately true up to a bandwidth of 8 Hz. However, according to the analysis in [156], with B_1 and B_2 in (8.2) having opposite signs, this proportional feedback results in a design that adds damping to the first mode, at the expense of reducing the damping in the second mode. Therefore, a butterworth low-pass filter, $G_f(s)$, is introduced before $\ddot{x}$ is used for feedback purpose. That is,

$$a_f = G_f(s)\ddot{x} = \frac{1}{(s/\omega_c)^2 + 2\zeta_c(s/\omega_c) + 1}\ddot{x} \tag{8.4}$$

where $\omega_c = 2Hz = 12.6rad/s$, $\zeta_c = 0.707$. Subsequently, the acceleration controller is realized as

$$u_f = K_f a_f. \tag{8.5}$$

A more description of the existing control system can be found in [156].

8.4 Adaptive Control Augmentation

8.4.1 Addressing Main Challenges

When attempting to apply the adaptive approach in Chapter 4 to this system, one immediate difficulty is the lack of control degrees of freedom, i.e., a single control input needs to achieve combined position and vibration control with measurements of joint angle and base vibration. Thus, a new regulated output variable is defined by blending these two outputs

$$y_o = W_1\theta + W_2'\frac{\ddot{x}}{L\omega_1^2} = W_1\theta + W_2\ddot{x}. \tag{8.6}$$

The weights $W_1 = 0.5$ and $W_2 = -0.5$ were intentionally selected due to the fact that the control has an opposite effect on the base acceleration and the link 2 (Moving the link in positive θ direction leads to negative $\ddot{x}$). The blended output y_o has relative degree zero, as can be seen by combining transfer functions in (8.1) and (8.2). On the other hand, if we use a_f in (8.4) in blending process,

$$y_b = W_1\theta + W_2G_f(s)\ddot{x} \tag{8.7}$$

the blended output has relative degree 2. Since the approach in Chapter 4 assumes that the relative degree of the regulated output is greater than zero, the variable y_b in (8.7) is selected

as regulated output variable. This is also in accordance with the philosophy of the existing inertial damping control system. That is, high frequency in the measurement is suppressed by the low-pass filter. In addition, since the electro-hydraulic servo valve dynamics lie outside bandwidth of our design ($\tau = 30$ Hz), y_b is treated as having a practical relative degree of 1.

The adaptive design concerns the two-time scale approach used to design the existing control system. This renders difficult to define a reference model for the adaptive portion of the design, for the reference model should be defined so that it represents the closed loop dynamics of the plant model being regulated by the existing controller. According to the results in [156], the overall performance of the of the system could be significantly improved if a coupled single controller were designed for the combined dynamics in (8.1) and (8.2). Hence, the reference model for the adaptive design was defined in a way so as to achieve a higher level of performance.

8.4.2 Reference Model Design

We start to design the reference model by selecting the plant model. The hydraulic actuator *design model* is chosen as

$$\frac{\theta_m}{u} = \frac{K_1}{s[(s/\omega_p)^2 + 2\zeta_p(s/\omega_p) + 1]}. \tag{8.8}$$

This model ignores the elector-hydraulic servo valve dynamics and its high frequency zero. The model of the base acceleration is selected by considering only the first mode,

$$\frac{\ddot{x}_m}{\theta_m} = \frac{s^4 B_1 \phi_1(L)}{(s/\omega_1)^2 + 2\zeta_1(s/\omega_1) + 1}. \tag{8.9}$$

Finally, regulated output is defined without the low-pass filter

$$y_{m_b} = W_1\theta_m + W_2\ddot{x}_m, \tag{8.10}$$

since the second mode of the base is not considered in the design model. The resulting blended output has relative degree 1 and matches that in (8.7) within the bandwidths of interest, as shown in Figure 8.6. In this figure , the frequency response of the blended output in (8.10) is compared to that in (8.7) assuming the effect of electro-hydraulic servo

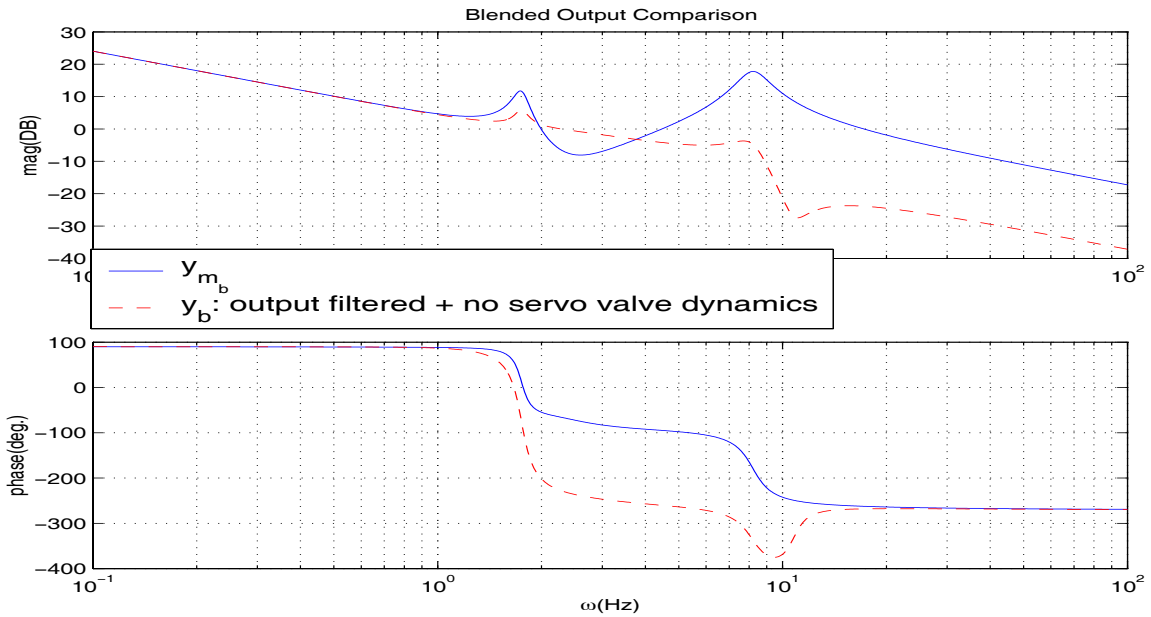

Fig. 8.6: Comparison of the Blended Output of the Design Model to that in (8.7) without Servo Valve Dynamics

valve dynamics are not present. The combined dynamics of the transfer functions in (8.8) and (8.9), together with the blended output in (8.10), are described in the following state space form

$$\begin{aligned} \dot{\boldsymbol{\chi}} &= A_m \boldsymbol{\chi} + \boldsymbol{b}_m u, \\ y_{m_b} &= \boldsymbol{c}_m^T \boldsymbol{\chi}. \end{aligned} \tag{8.11}$$

As a next step, we design a linear quadratic regulator (LQR) controller for the design model in (8.11), which minimizes the cost integral

$$J = \int_0^\infty (\boldsymbol{\chi}^T Q \boldsymbol{\chi} + R u^2) dx, \tag{8.12}$$

where $Q = \text{diag}[.5\ .5\ .5\ 1.5\ 2.5]$ and $R = 0.01$. The resulting controller is as follows:

$$u_{lqr} = -K_{lqr}(\boldsymbol{\chi} - \boldsymbol{\chi}_d), \tag{8.13}$$

where $\boldsymbol{\chi}_d = [\theta_d\ 0\ 0\ 0\ 0\ ]^T$ represents the steady state vector which generates the desired position angle θ_d for the link and $K_{lqr} = [\ 7.46\ 8.94\ 7.07\ 4.41\ 19.46\ ]$.

Now the reference model is put into its normal form. Since y_{m_b} is of relative degree 1,

the normal form is written as

$$\begin{aligned}\dot{\xi}_m &= a_1\xi_m + +\boldsymbol{h}_m^T\boldsymbol{z}_m + bu\\ \dot{\boldsymbol{z}}_m &= F_m\boldsymbol{z}_m + \boldsymbol{g}_m\xi_m\\ y_{m_b} &= \xi_m,\end{aligned} \tag{8.14}$$

where $\xi_m \in R,\ \boldsymbol{z}_m \in R^4$, $b = -85.58$, and

$$\begin{aligned}a_1 = -11.4,\ \boldsymbol{h}_m^T &= \begin{bmatrix} -309.57 & -1.12 & -68.23 & 13.05 \end{bmatrix}\\ F_m = \begin{bmatrix} 0 & -9.70 & -0.67 & -9.16\\ 32 & 0 & 0 & 0\\ 0 & 16 & 0 & 0\\ 0 & 0 & 8 & 0 \end{bmatrix},\ \boldsymbol{g}_m &= \begin{bmatrix} 8\\ 0\\ 0\\ 0 \end{bmatrix}.\end{aligned} \tag{8.15}$$

Using the same transformation, the LQR controller in (8.13) can be expressed as

$$u_{lqr} = -k_1\xi_m - \boldsymbol{k}_2^T\boldsymbol{z}_m + k_1\theta_d, \tag{8.16}$$

where $k_1 = -3.23,\ \boldsymbol{k}_2^T = [-22.96,\ -5.48,\ -5.38,\ 1.20]$. The design model in (8.14) regulated by the controller in (8.16) leads to the reference model in the normal form

$$\begin{aligned}\dot{\boldsymbol{x}}_l &= \bar{A}\boldsymbol{x}_l + \bar{\boldsymbol{b}}k_1\theta_d, \quad \boldsymbol{x}_l \in R^5\\ y_{m_b} &= \bar{\boldsymbol{c}}^T\boldsymbol{x}_l\end{aligned} \tag{8.17}$$

where $\boldsymbol{x}_l^T = \begin{bmatrix} \xi_m & \boldsymbol{z}_m^T \end{bmatrix}$, and

$$\begin{aligned}\bar{A} &= \begin{bmatrix} a_1 - bk_1 & \boldsymbol{h}_m^T - b\boldsymbol{k}_2^T\\ \boldsymbol{g}_m & F_m \end{bmatrix},\\ \bar{\boldsymbol{b}} = \begin{bmatrix} b\\ 0_{4\times 1} \end{bmatrix},\ \bar{\boldsymbol{c}} &= \begin{bmatrix} 1\\ 0_{4\times 1} \end{bmatrix}.\end{aligned} \tag{8.18}$$

The performance of the reference model is compared to that of the combined model of (8.1) and (8.2) regulated by the existing controller of (8.3) and (8.4) in Figures 8.7 and 8.8 for a reference command corresponding to the step response of the following command filter

$$R(s) = \frac{1}{(s/\omega_d)^2 + 2\zeta_d(s/\omega_d) + 1}, \tag{8.19}$$

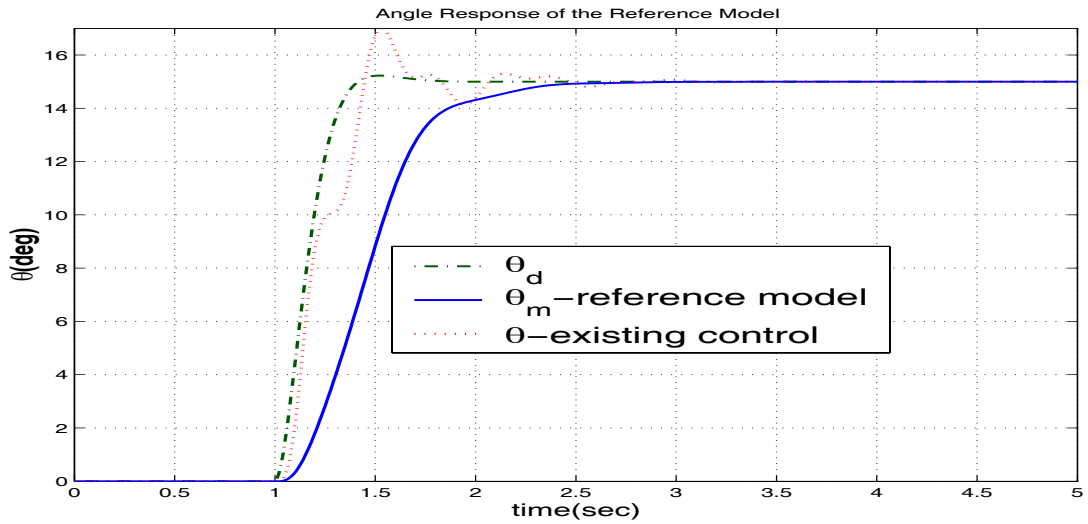

Fig. 8.7: Comparison of the Joint Angle Response between the Reference Model and the Combined Model of (8.1) and (8.2) regulated by the Existing Controller

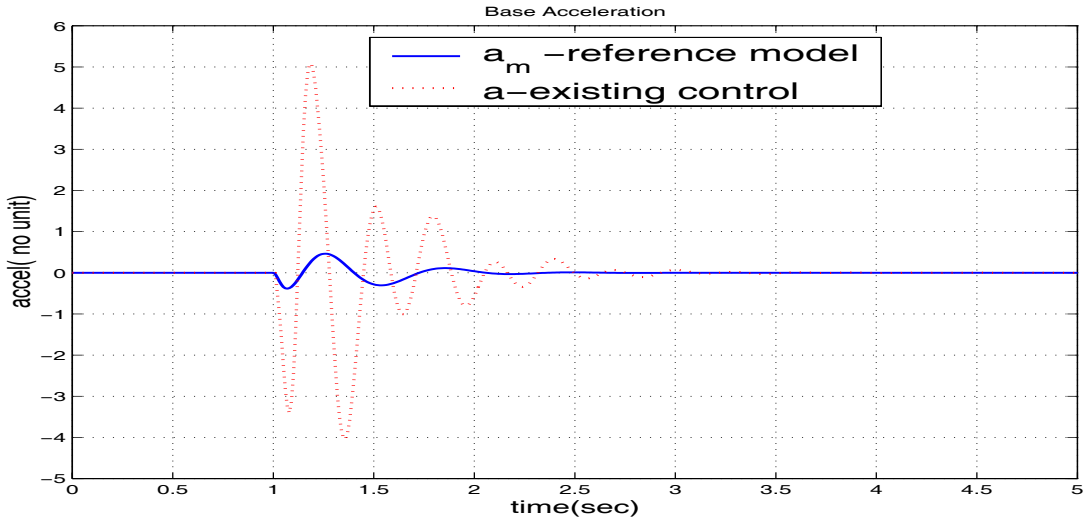

Fig. 8.8: Comparison of the Base Acceleration Response between the Reference Model and the Combined Model of (8.1) and (8.2) regulated by the Existing Controller

where $w_d = 10rad/s,\ \zeta_d = 0.8$.

The reference model achieves less oscillatory tracking response in the position control of the link with much less vibration in the base compared to the closed loop of the combined model of (8.1) and (8.2) under the regulation of the existing controller. Thus use of this reference model in the adaptive design implies that we expect the adaptive controller to achieve a higher level of performance in the presence of modelling error, than that of the existing controller operating in the absence of modelling error.

8.4.3 Augmenting Adaptive Elements

To employ the adaptive approach in Chapter 4, the system dynamics are, with the regulated output y_b in (8.7), expressed in normal form

$$\begin{aligned}
\dot{\xi} &= a_1\xi + \boldsymbol{h}_m^T\boldsymbol{z}_1 + bu + \phi_1(\boldsymbol{z}_1, \boldsymbol{z}_2, u) \\
\dot{\boldsymbol{z}}_1 &= F_m\boldsymbol{z}_1 + \boldsymbol{g}_m\xi + \boldsymbol{\phi}_2(\xi, \boldsymbol{z}_1, \boldsymbol{z}_2) \\
\dot{\boldsymbol{z}}_2 &= \boldsymbol{f}_2(\xi, \boldsymbol{z}_1, \boldsymbol{z}_2) \\
y_b &= \xi,
\end{aligned} \tag{8.20}$$

where $\boldsymbol{z}_1$ are the states of the internal dynamics modelled through $\boldsymbol{z}_m$ in (8.14), $\boldsymbol{z}_2$ are the states of unmodelled dynamics which are assumed to be input-to-state stable with $\xi, \boldsymbol{z}_2$ viewed as input, $\phi_1(\boldsymbol{z}_1, \boldsymbol{z}_2, u)$ represents the matched uncertainty, and $\boldsymbol{\phi}_2(\xi, \boldsymbol{z}_1, \boldsymbol{z}_2)$ represents the unmatched uncertainty.

Define,

$$u = u_{lc} + u_{ad} \tag{8.21}$$

where u_{lc} represents the output of the existing controller, and u_{ad} is the output of the adaptive controller. The first equation in (8.20) is rearranged as

$$\begin{aligned}
\dot{\xi} =& (a_1 - bk_1)\xi + (\boldsymbol{h}_m^T - b\boldsymbol{k}_2^T)\boldsymbol{z}_1 + bk_1\theta_d \\
&+ b(u_{ad} + \Delta_1),
\end{aligned} \tag{8.22}$$

where the uncertainty Δ_1 is defined by

$$\Delta_1 = \frac{1}{b}\phi_1(\boldsymbol{z}_1, \boldsymbol{z}_2, u) + k_1\xi + \boldsymbol{k}_2^T\boldsymbol{z}_1 + k_1\theta_d + u_{lc}, \tag{8.23}$$

which will be approximated and cancelled by u_{ad}. Define the error vector

$$\boldsymbol{E} = \begin{bmatrix} e_1 \\ \tilde{\boldsymbol{z}}_1 \end{bmatrix} = \begin{bmatrix} \xi_m - \xi \\ \boldsymbol{z}_m - \boldsymbol{z}_1 \end{bmatrix}, \quad \boldsymbol{E} \in \mathbb{R}^5. \tag{8.24}$$

Comparing (8.20), with its first equation as in (8.22), to (8.17) leads to the following expression for the *error dynamics*

$$\begin{aligned}
\dot{\boldsymbol{E}} =& \bar{A}\boldsymbol{E} + \bar{\boldsymbol{b}}(-u_{ad} - \Delta_1) - \bar{\boldsymbol{b}}_u\boldsymbol{\Delta}_2, \\
\dot{\boldsymbol{z}}_2 =& \boldsymbol{f}_2(\xi, \boldsymbol{z}_1, \boldsymbol{z}_2), \\
e_1 =& \bar{\boldsymbol{c}}^T\boldsymbol{E}
\end{aligned} \tag{8.25}$$

where

$$\bar{\boldsymbol{b}}_u = \begin{bmatrix} 0 \\ I_{4\times 4} \end{bmatrix}, \ \boldsymbol{\Delta}_2 = \begin{bmatrix} 0 \\ \boldsymbol{\phi}_2(\xi, \boldsymbol{z}_1, \boldsymbol{z}_2) \end{bmatrix}. \tag{8.26}$$

The error dynamics (8.25) have the same form as that in (4.10). Define,

$$u_{ad} = -u_{nn} - u_{dc}, \tag{8.27}$$

where u_{nn} is the adaptive NN output variable, and u_{dc} is output of a linear controller introduced to further robustify the design. In this case, we designed it as a lead compensator,

$$u_{dc} = 0.2\frac{s/3+1}{s/20+1}e_1, \tag{8.28}$$

which is described by the state space form as

$$\begin{aligned} \dot{x}_a &= a_c x_a + b_c e_1 \\ u_{dc} &= c_c x_a + d_c e_1. \end{aligned} \tag{8.29}$$

Applying the controller in (8.28) to the dynamics in (8.25) leads to the following redefined error dynamics:

$$\dot{\boldsymbol{E}}_a = L_a \boldsymbol{E}_a + \begin{bmatrix} \bar{\boldsymbol{b}} \\ 0 \end{bmatrix} (u_{nn} - \Delta_1) - \begin{bmatrix} \bar{\boldsymbol{b}}_u \\ 0 \end{bmatrix} \boldsymbol{\Delta}_2 \,. \tag{8.30}$$

where

$$\boldsymbol{E}_a = \begin{bmatrix} \boldsymbol{E} \\ x_a \end{bmatrix} \in \mathbb{R}^6, \ L_a = \begin{bmatrix} \bar{A} + \bar{\boldsymbol{b}} d_c \bar{\boldsymbol{c}}^T & \bar{\boldsymbol{b}} c_c \\ b_c \bar{\boldsymbol{c}}^T & a_c \end{bmatrix}. \tag{8.31}$$

Since L_a is Hurwitz by design, there exist a $P = P^T > 0$ such that, for some $Q_e > 0$,

$$\bar{A}^T P + P\bar{A} + Q_e = 0. \tag{8.32}$$

For this design we used $Q_e = 1.1 I_{6\times 6}$.

Notice from (8.21) and (8.27) that Δ_1 in (8.23) depends on u_{nn} through u, and that the role of u_{nn} is to cancel Δ_1. This constitutes a fixed point problem. Within the range of bandwidths of interest, if we assume that the frequency response model in Figure 8.6 is a close approximate for the physical system, it can be easily seen that the conditions in (2.17)

are satisfied. Thus Assumption 4.2 is assured. To circumvent a fixed point iteration in the real-time environment, the control signal is delayed by the single sampling time before it is used as a network input. In a preliminary simulation, this was compared to obtaining a fixed point solution, and the results were not distinguishable.

A SHLNN is used to approximate Δ_1 in (8.23). Since the system dimension is not exactly known, 9 delayed values of y_b in (8.7) and 8 delayed values of the input u, with delay $d = 0.06$ sec., are combined to realize the NN input signal in (4.13). The squashing functions are chosen as sigmoidal functions

$$[\boldsymbol{\sigma}(N^T\boldsymbol{\eta})]_i = \frac{1}{1+e^{-a(N^T\boldsymbol{\eta})_i}},\ i = 1, \cdots, 6, \tag{8.33}$$

where $a = 1$ represents the activation potential.

The adaptive signal u_{nn} is expressed in the form

$$u_{nn} = \hat{M}^T\boldsymbol{\sigma}(\hat{N}^T\boldsymbol{\eta}) \tag{8.34}$$

where $\hat{M}$ and $\hat{N}$ are weights that are adapted on-line. The weight adaptation law in (3.49) used in Chapter 4 requires construction of an estimator for *all of the states* $\boldsymbol{E}_a$ in (8.30), or $\boldsymbol{E}$ in (8.25) in case the state of the additional controller x_c are excluded from the estimated states. However, the method in [63] does not require an error observer in case the output has relative degree 1. Thus, we utilized the following update law

$$\begin{aligned}\dot{\hat{M}} &= -\Gamma_M[(\hat{\boldsymbol{\sigma}} - \hat{\sigma}'\hat{N}^T\boldsymbol{\eta})e_1P_{11}b + k\hat{M}] \\ \dot{\hat{N}} &= -\Gamma_N[e_1P_{11}b\boldsymbol{\eta}\hat{M}^T\hat{\sigma}' + k\hat{N}]\,,\end{aligned} \tag{8.35}$$

in which P_{11} is obtained from the decomposition of P in (8.32) as follows:

$$P = \begin{bmatrix} P_{11} & P_{12} \\ P_{12}^T & P_{22} \end{bmatrix},\ P_{11} \in \mathbb{R},\ P_{22} \in \mathbb{R}^{5\times 5}. \tag{8.36}$$

The following parameters are used for the adaptive law in (8.35)

$$\Gamma_M = 0.017I_{7\times 7},\ \Gamma_N = 0.068I_{20\times 20},\ k = 0.24. \tag{8.37}$$

The overall NN-based adaptive control architecture is depicted in Figure 8.9, where the elements used to augment the existing control system are shaded.

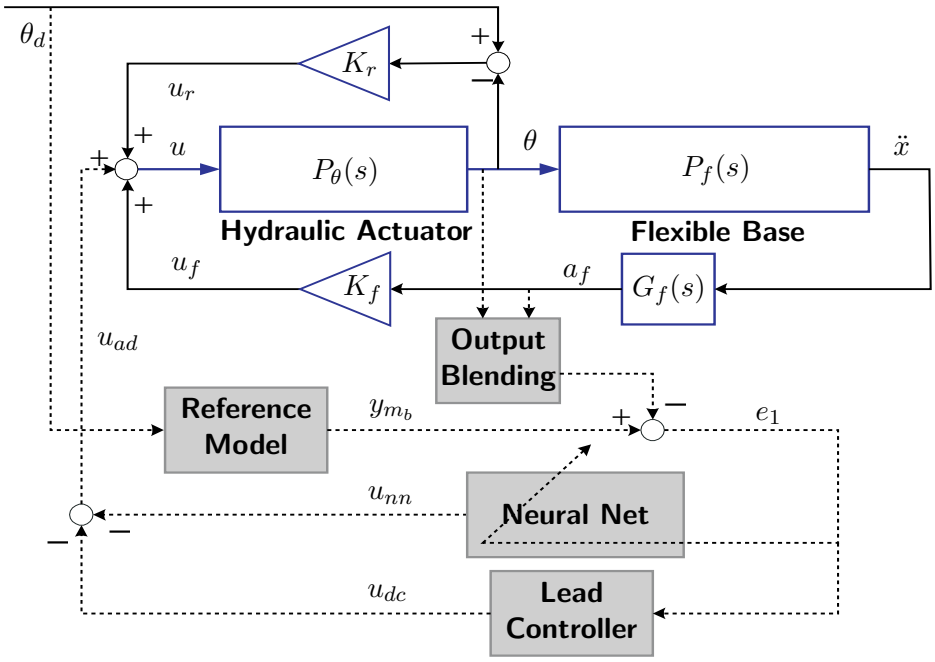

Fig. 8.9: Adaptive Control Augmenting Architecture with Flexible Robot

8.5 Experimental Results

To analyze the effectiveness of the existing control scheme and the NN-based augmenting scheme during two-dimensional robot motion, a square wave of magnitude 15° and frequency of 0.025 Hz is applied through the command filter in (8.19) with all other degrees of freedom locked. The control objective is to achieve inertial tip positioning of the end effector attached to the micromanipulator. Relative rotation of the joint angle with respect to the base is measured by an encoder, and the base acceleration is measured by an accelerometer (See Figure 8.2).

The joint angle θ and the base acceleration $\ddot{x}$ responses are shown in Figures 8.10 and 8.11. Dashed lines represent the responses without the inertial damping controller, dotted lines represent the responses with the inertial damping controller, and the solid lines represent the responses with adaptive augmentation. Due to the scale used in these figures, the differences in responses are hard to distinguish, but selected regions are zoomed into in successive figures below.

Figures 8.12 and 8.13 show the differences in transient response for each of the different

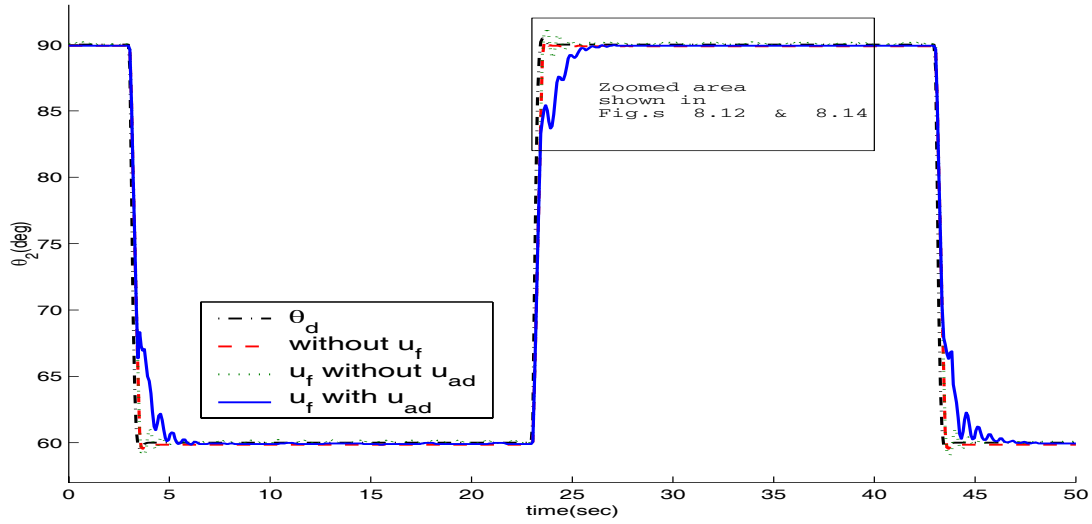

Fig. 8.10: Comparison of the Joint Angle Responses with a Square Wave Reference Command

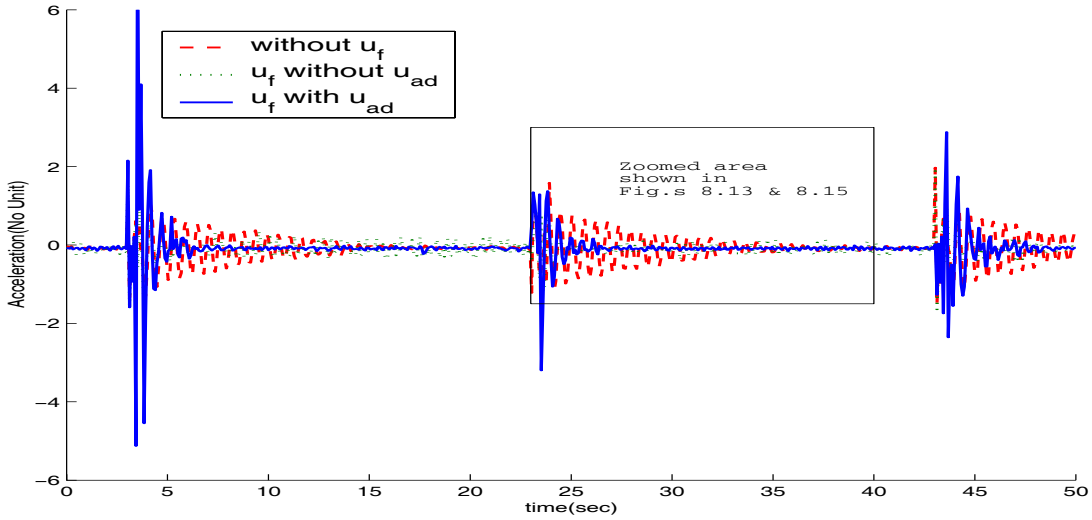

Fig. 8.11: Comparison of the Base Acceleration with a Square Wave Reference Command

control strategies. Without damping control, the joint angle tracks the reference command very closely, but the base acceleration is completely uncontrolled. This results in a long settling time because of the long vibration decay time. In contrast, with the inertial damping control added ("u_f without u_{ad}"), the responses in Figures 8.12 and 8.13 show that the micromanipulator is moved in a manner to damp the base vibration. At the expense of a slight overshoot with oscillations in the joint angle, the acceleration in the flexible base is greatly diminished. The frequency content observed in the joint angle shows that

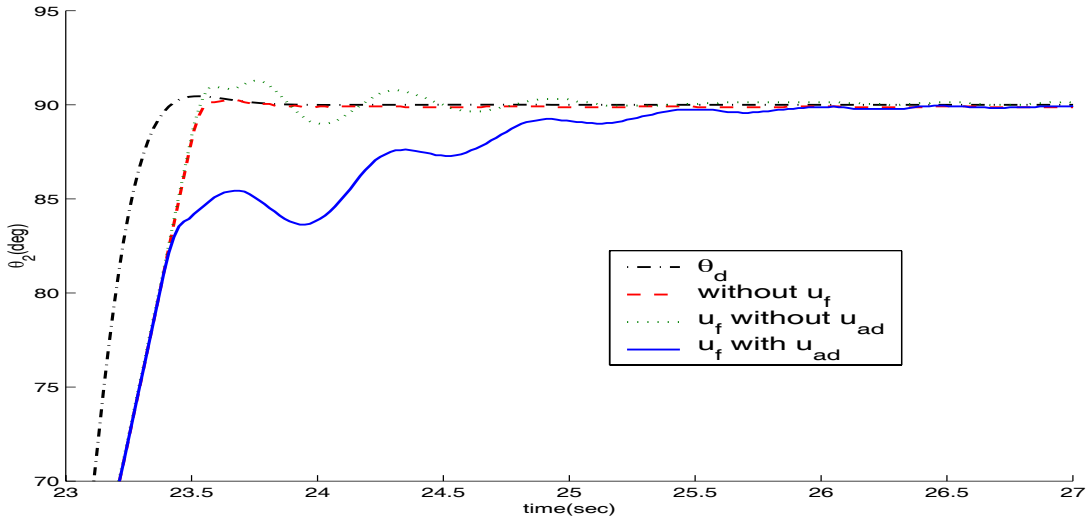

Fig. 8.12: Comparison of Transient Responses for the Joint Angle

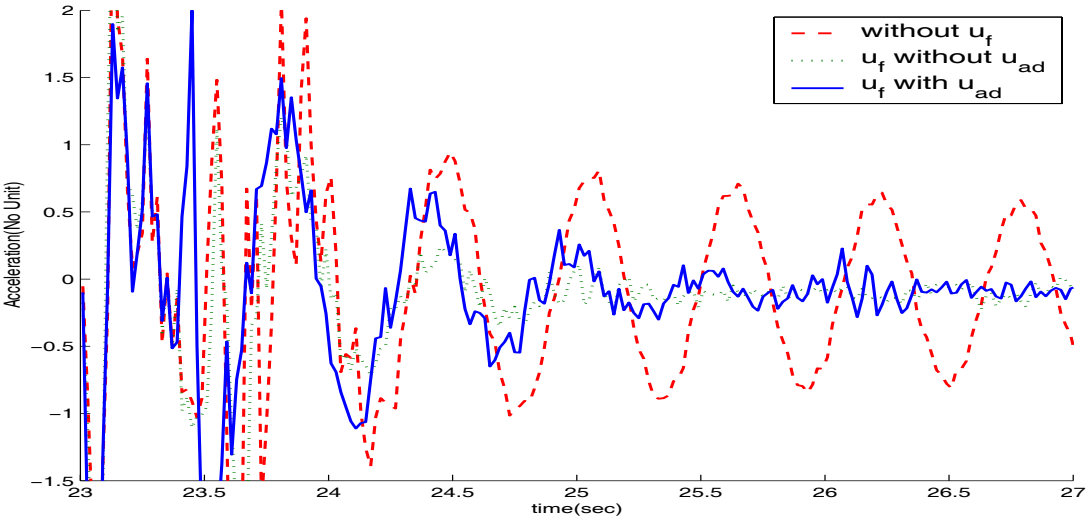

Fig. 8.13: Comparison of Transient Responses for the Base Acceleration

the first mode vibration is damped. Similar oscillations are also observed when adaptive augmentation is applied ("u_f with u_{ad}").

Inspection of the steady state responses from Figures 8.10 and 8.11 as shown in Figures 8.14 and 8.15 reveals interesting features of the different controllers. With the existing control system, the base vibrates continuously, and this vibration is also reflected in the oscillating joint angle. This kind of behavior is problematic if the manipulator is to be employed for tasks requiring high precision. In contrast, the augmented control regulates the joint angle close to the accuracy of the encoder resolution (0.044°), and it suppresses

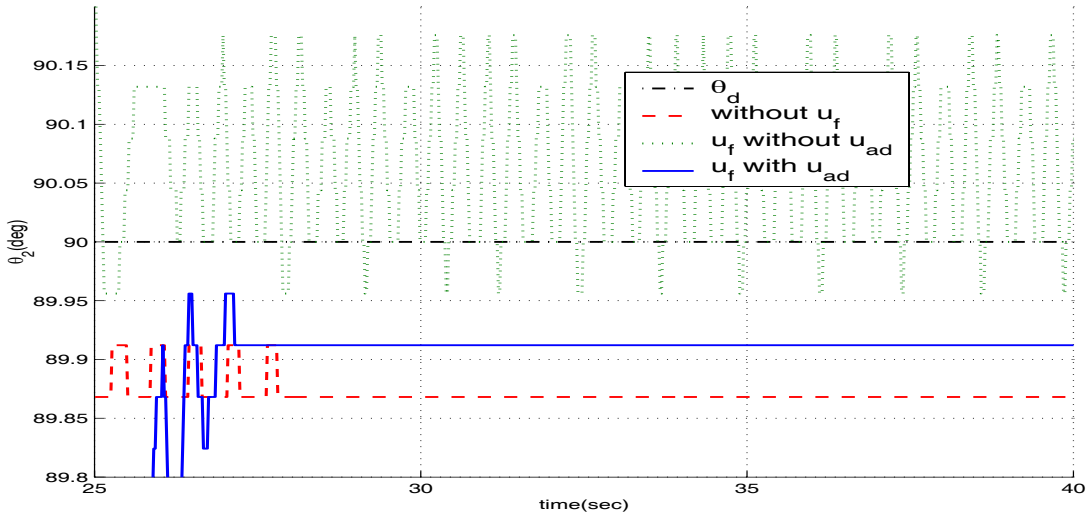

Fig. 8.14: Comparison of Steady State Responses for the Joint Angle

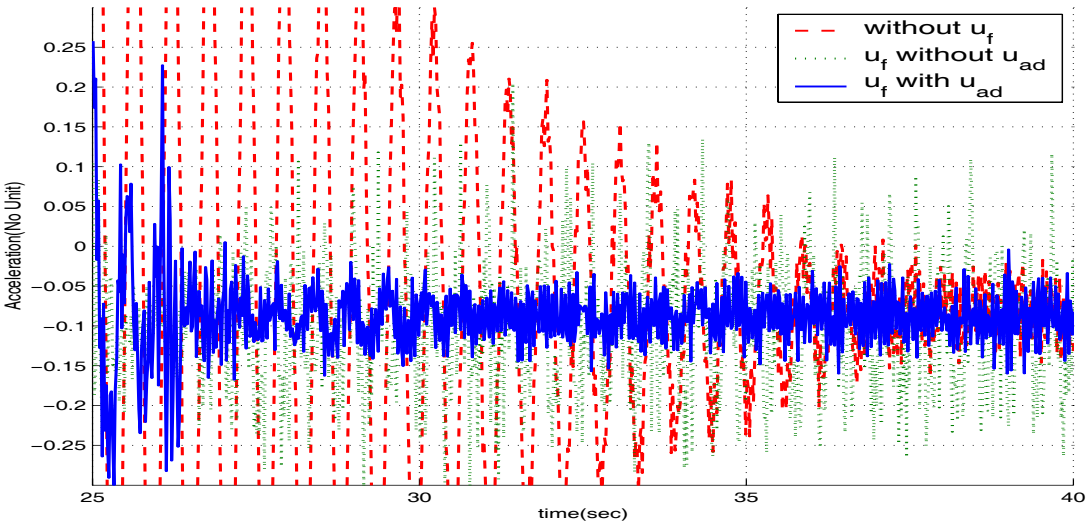

Fig. 8.15: Comparison of Steady State Responses for the Base Acceleration

the vibration to the level of that without damping control (Without damping control, the vibration decays completely to zero in its steady state response, thus oscillations in the acceleration measurement are due to sensor noise).

Investigation of the joint angle steady state reveals another interesting phenomenon in the existing control system: the joint angle oscillates around a value that is offset from the desired angle due to actuator nonlinearities such as dead zone and stiction. These nonlinearities in the actuation are configuration dependent and time-varying, depending on operating conditions. In tests it was observed that this phenomenon became prominent and

the existing control system exhibited a large steady state error (about 2°). Figures 8.16 and 8.17 illustrate the joint angle and the base acceleration responses for such a case. The steady state error in the joint angle is clearly visible when the system is under the regulation of the existing control system. This indicates that the fixed gain control deviates when it encounters an uncertain operating condition. When the adaptive elements are turned on, however, the steady state error quickly decays to zero while the remaining vibration of the base is damped out. The action of the adaptive elements in augmenting the existing control

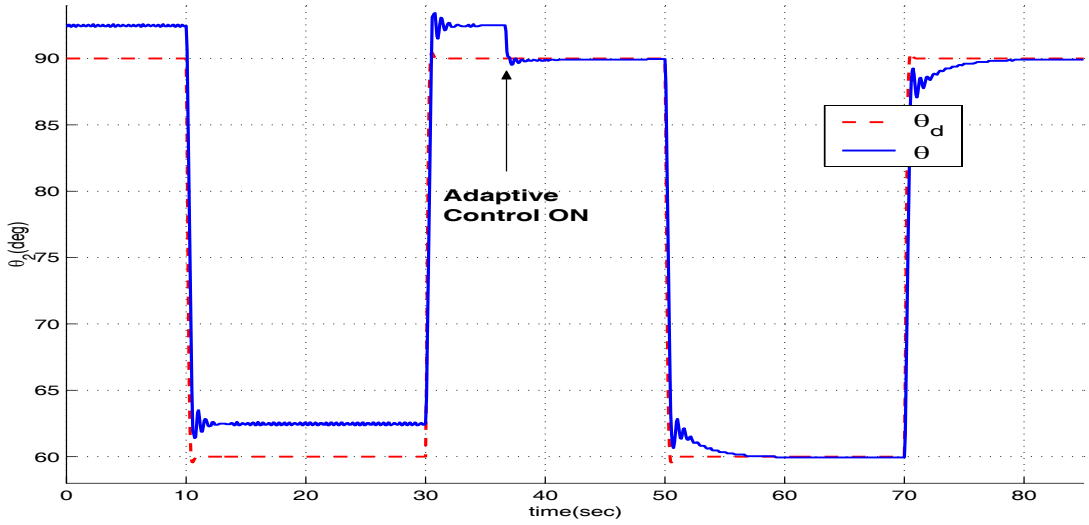

Fig. 8.16: Joint Angle Responses in the case of a Large Steady State Error in the Joint Angle

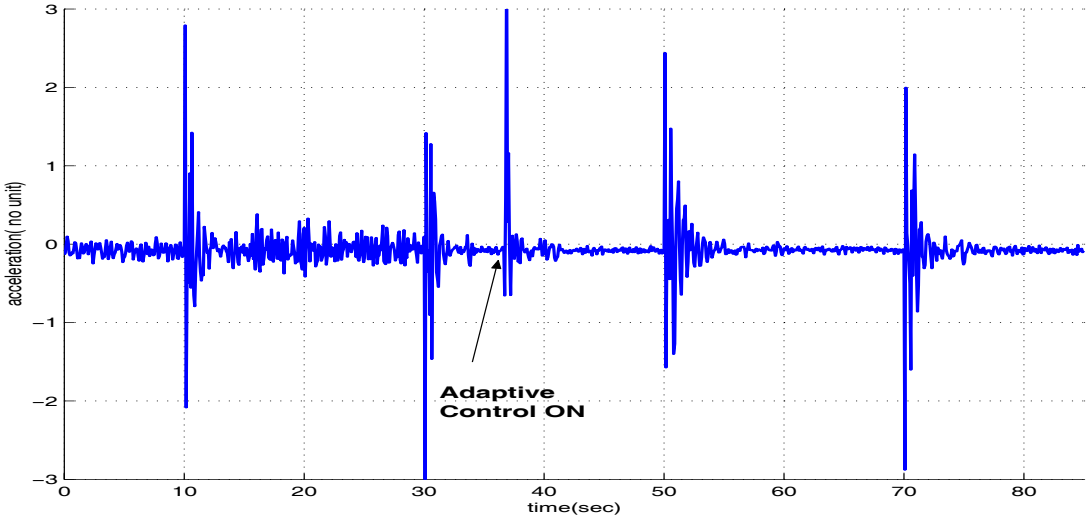

Fig. 8.17: Base Acceleration in the case of a Large Steady State Error in the Joint Angle

can be explained by investigating the tracking error e_1 in (8.24). This error is the deviation of the regulated output from that of the reference model, and Figure 8.18 shows this error. As soon as the adaptive control is turned on, the error is regulated to zero. This is only possible when the regulation of the joint angle and the suppression of the base vibration are achieved simultaneously, because the regulated output combines the joint angle and the base vibration.

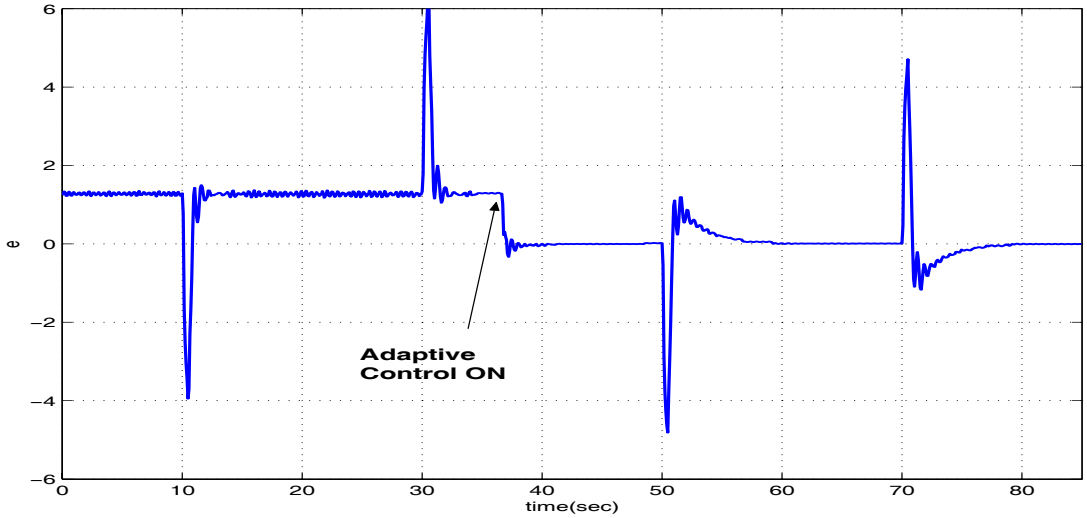

Fig. 8.18: Tracking Error e_1 in (8.24) in the case of a Large Steady State Error in the Joint Angle

Finally, to more fully illustrate the potential benefits of the augmenting adaptive controller, the acceleration gain for the inertial damping control is increased from $K_f = -1.435$ to $K_f = -3.28$. In this case, the closed loop system under regulation by the existing controller becomes highly unstable and requires increasing the gain in the lead compensator in (8.28) from 0.2 to 0.6. Figures 8.19, 8.20, and 8.21 show the responses of the joint angle, the base acceleration, and the tracking error e_1, respectively. Without the augmenting elements, the existing system immediately goes unstable while the augmented control system maintains good performance.

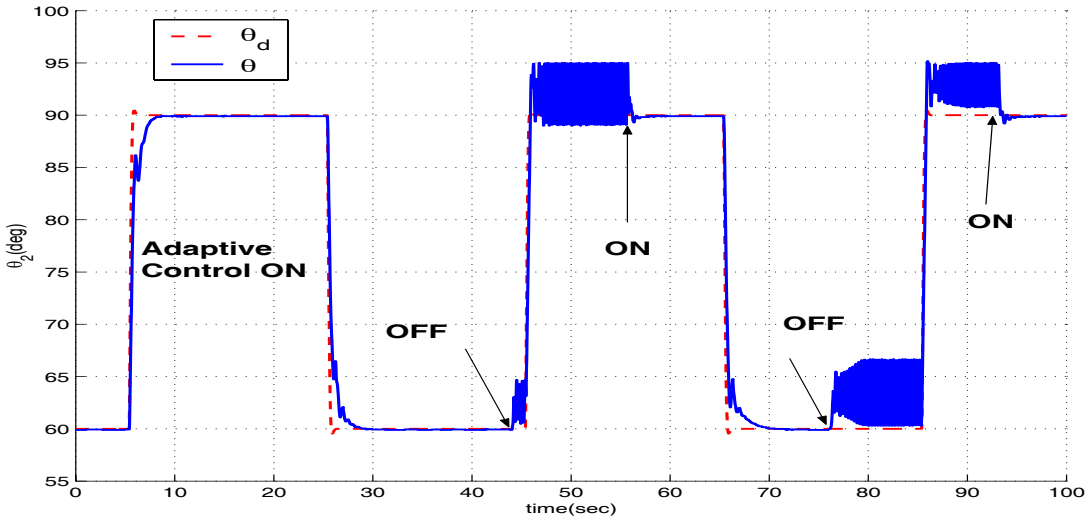

Fig. 8.19: Joint Angle Responses with Increased Acceleration Control Gain

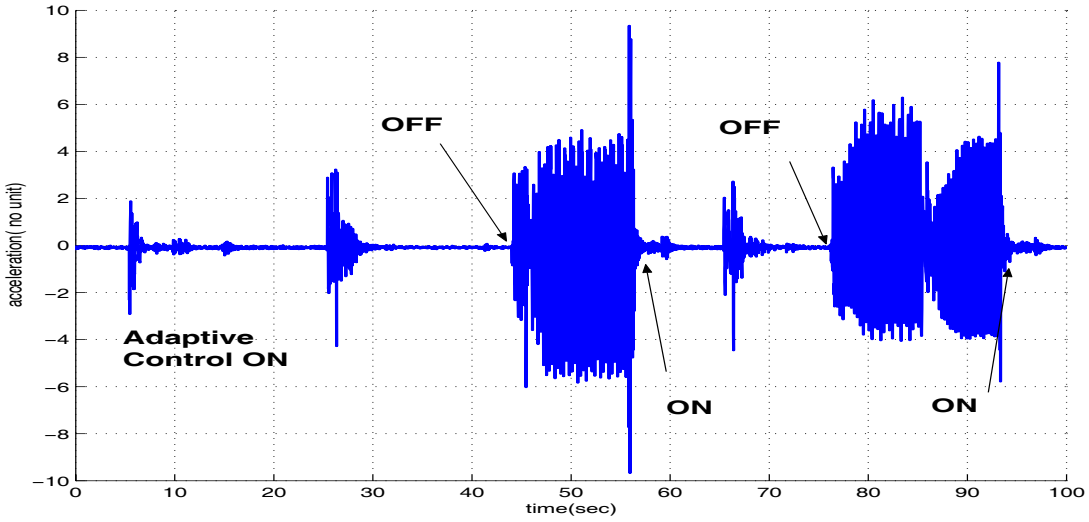

Fig. 8.20: Base Acceleration with Increased Acceleration Control Gain

8.6 Conclusions

This chapter addresses NN-based adaptive output feedback augmentation of an existing combined position and vibration control system. The method involves applying the approach in Chapter 4 to an existing linear two time-scale controller. Both the nonadaptive and the adaptive controllers with damping control are effective in reducing the transient time of the vibration. However, in steady state, with adaptation the micromanipulator achieves a level of accuracy on the order of the encoder resolution. Furthermore, adaptation overcomes the effects of actuation nonlinearities due to dead zone and stiction, providing highly

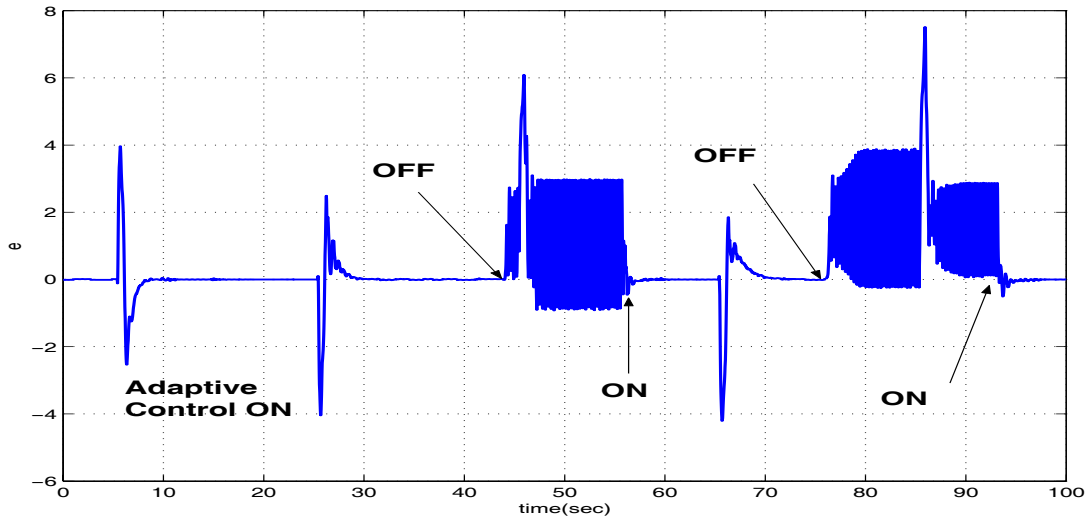

Fig. 8.21: The Tracking Error e_1 in (8.24) with the Increased Acceleration Control Gain

accurate tip positioning.

CHAPTER 9

CONCLUDING REMARKS

9.1 Conclusions

This thesis describes NN-based adaptive output feedback control methods with flexible systems as the main application. The adaptive control is assumed to augment an existing linear controller. The main assumption is that the relative degree of the regulated output is known. When the regulated output is minimum phase, internal model-following control is shown to be effective in compensating for modelling errors, external disturbances, and actuator nonlinearities. The implementation results with a three-disk torsional system illustrates its effectiveness in a real-time environment. External model-following control does not rely on inversion, thus it can be applied to non-minimum phase systems. Its effectiveness in both minimum phase systems and non-minimum phase systems is illustrated through experiments with the three-disk torsional system, an inverted pendulum, and a flexible-base manipulator. This approach is further extended so that it can be applied to control of MIMO non-minimum phase systems and, in a decentralized setting, to a large-scale interconnected systems. The flexibility of the external model-following control is further shown by employing the control architecture in order to adaptively augment a linear observer-based controller. In this approach, a single neural network is used for adaptation in the observer and controller simultaneously, resulting in an adaptive control method that compensates for the unmatched uncertainty as well.

9.2 Recommended Future Research

There are three areas in which further theoretical research is recommended. The first is to mathematically clarify some issues regarding the use of a set of input/output delayed values to approximate an uncertainty. The issue concerns the fixed-point problem in the NN-based adaptive output feedback methods. This problem arises due to the fact that the

uncertainty $\Delta(\cdot, u)$ is, through u, a function of the adaptive signal u_{ad} while the goal of u_{ad} is to approximately cancel $\Delta(\cdot, u)$. The *existence* of a fixed-point solution is not restrictive, and this point has been addressed in Section 2.3. In a real-time environment, however, the algebraic loop is broken by implementing a delayed values for the control input to the NN. This process has been justified in [89], in which the mean value theorem is utilized to eliminate the fixed-point assumption. However, with a fixed-point assumption, this is mainly justified by simulation studies in which the use of delayed control signal produces the same result as the fixed-point iteration. Mathematical justification for this process is a current research topic.

Another issue related to the use of input/output pairs concerns the stability proofs presented in this thesis. According to the analysis in [65], the NN approximation theorem based on a finite history of input/output pairs is only valid for a class of *bounded* nonlinear processes. However, when combined with control synthesis, boundedness of all the closed-loop signals are in turn guaranteed by properly designing a control law. To break this seemingly circular argument, one must show that all the signals remain bounded *a posteriori* when the system is regulated by the NN-based adaptive controller. In a state feedback setting, this has been shown for a given controller by identifying a positively invariant set to which the initial conditions are required to belong [41]. In the stability proofs in this thesis (for example, see Section 5.5), the compact set for initial conditions is determined by an *implicit* mapping rather than an explicit mapping. Defining the compact set by an explicit mapping is a topic currently under investigation.

Together with a proof of ultimate boundedness, equally important is the issue of the "size" of the ultimate bound. The stability proofs in this thesis do not provide a means for achieving an arbitrarily small ultimate bound. In state feedback settings, an arbitrarily small ultimate bound has been implied by employing a high-gain controller [36, 37, 40]. Recent progress includes guaranteeing an arbitrary bound, as a function of design parameters, on tracking error [**?**]. In output feedback settings, most approaches [40, 41] have attacked this problem by employing a high-gain observer [13]. Addressing this problem, especially in relation to the error observer in [63], is a remaining research topic. It is expected that

with employing a high-gain observer for the *error* dynamics, an arbitrarily small bound for tracking error can be assured.

The third issue is related to the uncertainty for which a NN is employed. In Section 3.3, we address compensation for actuator nonlinearities such as dead zone, backlash, and hysteresis based on the results in [77] in which a class of nonlinearities that can be decomposed as a linear portion and a Lipschitz-type nonlinearity are considered. When a NN is employed to compensate for this class of nonlinearities as in Section 3.3, the question about the capability of a NN for this class of nonlinearities naturally arises. In particular, a hysteresis with nonlocal memory [159, pp. 14-17 in Introduction] involves a dependency from the *history* of its input. This implies, unlike dead zone, backlash, and a single relay hysteresis, that hysteresis with nonlocal memory may be better described by input-output dynamic operators. For example, in [160], the input-output passivity of the classical Preisach model [159] pointed out in [161] is used to analyze and design controllers for linear systems with hysteretic actuators. The NN-based hysteresis identification schemes have used a NN either as an substitute for hysteresis [162,163] or as an approximator for unknown weights with its input preprocessed by elementary hysteretic operators [164–166]. The approaches in [167–169] utilize a different set of inputs for NNs instead of introducing internal states. The analysis of a proper NN structure, with its theoretical clarification and simulation studies in relation to the well-developed Preisach hysteresis model, remains a topic for future research.

From the perspective of applications, we need to further explore issues related to nonlinear actuation, sensor noise, and unmodelled dynamics. Control hedging, or its analogous mechanism, pseudo-control hedging in augmenting an inverting controller, has been relatively well tested through many flight control systems and other laboratory settings [66, 67, 99]. The disturbance observer-based compensation for actuator nonlinearities has not been tested yet. Evaluation of this method using, for example, an inverted pendulum apparatus should be done. Such an apparatus, if based on a rack-and-pinion gear and torque motor actuation system, will likely exhibit a highly nonlinear behavior at low command levels due to high stiction in the gears and to slight asymmetry in the behavior. As a result, regulating the displacement of the cart with high precision will further test the use

of a disturbance observer-based compensation for actuator nonlinearities. The modelling of this apparatus necessarily involves zeros in the plant model whether it is obtained from linearization with respect to the vertical-up position (unstable, non-minimum phase) or the vertical-down position (stable, minimum phase). However, the result in Section 3.3 requires that the plant model is fully linearizable. This calls for extension of the approach to address an augmenting design problem in which the plant model contains zero dynamics. In parallel with this development, the development of a control algorithm to compensate for actuator nonlinearities in the external model-following control will be a challenging but fruitful research topic. It is expected that the structure of RIC will play a key role in implementing a disturbance observer-based design within the external model-following control framework because it does not require any property of the system regarding zero dynamics or stability [82].

The problem of sensor noise is especially problematic for those output feedback approaches that employ a high-gain observer in the estimation process. The high-gain observer may also cause implementation problems due to limited sampling frequency in most available laboratory systems. Ref. [15] illustrates how carefully it should be designed in relation to sampling frequency. In [170], it has been pointed out that the full order observer in Chapter 4 is more sensitive to sensor noise compared to a reduced observer. This idea is exploited in control of the flexible-base manipulator where the measurements of base accelerations are highly noisy. To circumvent the estimation problem, experiments with the relative degree of the regulated output equal to 1 were carried out, utilizing a new update law that requires only the tracking error. The stability proof of this approach, in which the NN weights are updated using only estimates of the reduced error observer, remains a future research topic. In addition, research on how to solve for an optimal solution when multiple objectives among performance requirements and robustness need to be synthesized will be vital for successful implementation of the NN-based adaptive algorithm in highly complex, multi-degree-of-freedom systems. In general, for complex systems the performance specifications tend to be diverse and complex. One viable solution, when multiple objectives are

need to be met, is to utilize multi-objective LMI [171, 172] to provide systematic performance tuning while the adaptation is used to compensate for uncertainties in the control system.

From implementation of the adaptive control in the flexible base manipulator, we obtained promising results in control of a single degree of freedom system. Subsequent research must verify that adaptation is useful for compensating for changes in inertia and system configuration that result when the robot executes tasks such as picking up an object and carry it through the workspace. The implementation of the adaptive approach in a full 6 degree-of-freedom system will be a challenging and very insightful excursion into real-world applications.

The decentralized approach in this thesis is formulated with the assumption that unmodelled dynamics are not present. This is not the case in most large-scale interconnected systems, in which a certain degree of unmodelled dynamics are unavoidable in practice. When we attempt to extend the approach to allow for unmodelled dynamics, we encounter the issues of how to achieve an implicit cooperation for the whole system consisting of completely independent subsystems, and how to specify an observability condition for the whole composite system at the level of each subsystem, without communication among the subsystems. In the approach of this thesis, the issue of implicit cooperation was treated by sharing the states of the reference models among every subsystem. This somewhat violates the concept of " completely decentralized control" because the approach allows a central information flow to every subsystem. It is proposed that research on properly restricting reference commands should relax the above need. That is, by restricting reference commands to those realizable by the whole composite system and not by each decoupled subsystems, the implicit coordination should be achieved without any communication between subsystems. The other problem of observability can be tackled by investigating the observability of a local group consisting a subsystem and its neighbors. By concentrating on local groups instead of the whole system, the problem of observability can be addressed in a rather "small scale." By this, we can limit the dimension of the NN input required to reconstruct an unknown process, and this prevents it from growing proportionally to the

dimension of the whole system.

Finally, a critical assumption in this thesis is the knowledge of the relative degree of the system. Considering that frequency response is the most common form of system identification, it is desirable that we develop the approach that requires the knowledge of the relative degree within the bandwidth of interests. The problem of practical relative degree versus the absolute relative degree has typically been addressed by a singular perturbation approach [173,174] in which the stability of the original system is analyzed by investigating a reduced model consisting of the degenerate system when a very small parameter is replaced by zero. Addressing this problem in the setting of ultimate boundedness has not been reported in the literature, and research on this topic is expected to further justify a practical use of adaptive control in industry.

APPENDIX A

CHAPTER 2 PROOFS

Proof of Theorem 2.3 : By the Popov-Belevitch-Hautus(PBH) test [175], the linear system defined with matrices in (2.35) is observable *iff*

$$\text{rank} \begin{bmatrix} C_p & \begin{bmatrix} D_p \\ -B_p \end{bmatrix} C_d \\ sI_{n_p} - A_p & \\ 0 & sI_{n_d} - A_d \end{bmatrix} = n_p + n_d, \quad \forall s \in \mathbb{C}. \tag{A.1}$$

Due to the zero block in (A.1), when A_p and A_d have no common eigenvalues, observability of (2.35) is assured if (A_p, C_p) is observable and $(A_d, \bar{C})$ is observable, where $\bar{C} = \begin{bmatrix} D_p \\ -B_p \end{bmatrix} C_d$. It remains to be shown that observability of $(A_d, \bar{C})$ is equivalent to observability of (A_d, C_d). From the PBH eigenvector test [175], $(A_d, \bar{C})$ is not observable *iff* there exists a vector $\boldsymbol{q} \neq \mathbf{0}$ such that $A_d\boldsymbol{q} = \lambda\boldsymbol{q}$ and $\bar{C}\boldsymbol{q} = \mathbf{0}$. By assumption 3 in Theorem 2.3, $\bar{C}\boldsymbol{q} = \mathbf{0}$ *iff* $C_d\boldsymbol{q} = \mathbf{0}$. □

Proof of Corollary 2.1 : If A_p and A_d do not share a common eigenvalue, then from Theorem 2.3 it follows that (A, C) in (2.35) is observable. Suppose A_p and A_d do share a common eigenvalue at $s = \lambda$. Then by PBH eigenvector test (A, C) is not observable *iff* there exist $\bar{\boldsymbol{q}} \neq \mathbf{0}$ such that

$$\begin{bmatrix} C_p & \begin{bmatrix} D_p \\ -B_p \end{bmatrix} C_d \\ \lambda I_{n_p} - A_p & \\ 0 & \lambda I_{n_d} - A_d \end{bmatrix} \bar{\boldsymbol{q}} = \mathbf{0}.$$

Let $\boldsymbol{q}_2$ be an eigenvector of A_d corresponding to λ, then there exists a $\boldsymbol{q}_1$ such that $\begin{bmatrix} C_p \\ \lambda I_{n_p} - A_p \end{bmatrix} \boldsymbol{q}_1 + \bar{C}\boldsymbol{q}_2 = \mathbf{0}$, *iff* $\bar{C}\boldsymbol{q}_2$ lies in the column space of $\begin{bmatrix} C_p^T & \lambda I_{n_p} - A_p^T \end{bmatrix}$. □

APPENDIX B

CHAPTER 3 PROOF

Proof of Theorem 3.1 : Consider the Lyapunov function candidate V in (3.19). With NN update rule in (2.34) and using $\boldsymbol{z}^T P\boldsymbol{b}_{cl} = \boldsymbol{z}^T\boldsymbol{c}_{cl} = \tilde{y}_{ad}$ from (2.31), together with the dynamics described in (3.7), (2.29), and (2.32), the time derivative $\dot{V}$ is described by

$$\begin{aligned}\dot{V} =& -\frac{1}{2}\boldsymbol{e}_m{}^T Q_n \boldsymbol{e}_m + \boldsymbol{e}_m^T P_n[-\bar{\boldsymbol{b}}_c e_1 + \bar{\boldsymbol{b}}u_h] \\ &-\frac{1}{2}\boldsymbol{z}^T Q\boldsymbol{z} + \boldsymbol{z}^T P\boldsymbol{b}_{cl}(\theta - \varepsilon_f) \\ &-\frac{1}{2}\boldsymbol{z}_f^T Q_f \boldsymbol{z}_f + \boldsymbol{z}_f^T P_f \boldsymbol{b}_f \boldsymbol{\phi} - \sigma \mathrm{tr}\{\widetilde{\boldsymbol{W}}^T(\widetilde{\boldsymbol{W}} + \boldsymbol{W})\},\end{aligned} \tag{B.1}$$

where Q_n, Q, Q_f are defined in (3.8), (2.31), and (2.33) respectively. Assuming that the filter $T^{-1}(s)$ is scaled so that its maximum gain is unity, the filtered error ε_f can be bounded as

$$|\varepsilon_f| \leq \epsilon^*. \tag{B.2}$$

With this bound, the time derivative $\dot{V}$ is upper bounded by

$$\begin{aligned}\dot{V} \leq& -\frac{1}{2} q_n \|\boldsymbol{e}_m\| + \|\boldsymbol{e}_m\| \|\boldsymbol{z}\| \left\|P_n \bar{\boldsymbol{b}}_c \boldsymbol{c}_{e_1}^T\right\| + \|\boldsymbol{e}_m\| \left\|P_n \bar{\boldsymbol{b}}\right\| |u_h| \\ &-\frac{1}{2} q \|\boldsymbol{z}\| + \|\boldsymbol{z}\| \|P\boldsymbol{b}_{cl}\| [|\theta| + \epsilon^*] \\ &-\frac{1}{2} q_f \|\boldsymbol{z}_f\| + \|\boldsymbol{z}_f\| \|P_f \boldsymbol{b}_f \boldsymbol{\phi}\| - \sigma \mathrm{tr}\{\widetilde{\boldsymbol{W}}^T(\widetilde{\boldsymbol{W}} + \boldsymbol{W})\},\end{aligned} \tag{B.3}$$

where $q_n = \lambda_{\min}(Q_n),\ q = \lambda_{\min}(Q),\ q_f = \lambda_{\min}(Q_f)$. Using the inequality in (3.17), $\dot{V}$ is arranged as

$$\begin{aligned}\dot{V} \leq& -\gamma_1 \|\boldsymbol{e}_m\|^2 + \gamma_2 \|\boldsymbol{e}_m\| \|\boldsymbol{z}\| + \gamma_3 \|\boldsymbol{e}_m\| \left\|\widetilde{\boldsymbol{W}}\right\| + \gamma_4 \|\boldsymbol{e}_m\| \\ &-\frac{1}{2} q \|\boldsymbol{z}\|^2 + \beta_1 \|\boldsymbol{z}\| \left\|\widetilde{\boldsymbol{W}}\right\| + \beta_2 \|\boldsymbol{z}\| \\ &-\frac{1}{2} q_f \|\boldsymbol{z}_f\|^2 + \beta_3 \|\boldsymbol{z}_f\| - \sigma \left\|\widetilde{\boldsymbol{W}}\right\|_F^2 + \sigma \left\|\widetilde{\boldsymbol{W}}\right\| W^*,\end{aligned} \tag{B.4}$$

where

$$\gamma_1 = \frac{1}{2} q_n - \mu_1 \left\|P_n \bar{\boldsymbol{b}}\right\|,\ \gamma_2 = \left\|P_n \bar{\boldsymbol{b}}_c \boldsymbol{c}_{e_1}^T\right\| + \mu_2 \left\|P_n \bar{\boldsymbol{b}}\right\|,\ \gamma_3 = \mu_3 \left\|P_n \bar{\boldsymbol{b}}\right\|,\ \gamma_4 = \mu_4 \left\|P_n \bar{\boldsymbol{b}}\right\|$$

$$\beta_1 = \alpha \|P\boldsymbol{b}_{cl}\|,\ \beta_2 = \epsilon^* \|P\boldsymbol{b}_{cl}\|,\ \beta_3 = \|P_f \boldsymbol{b}_f \boldsymbol{\phi}\|,\ \|\boldsymbol{W}\| \leq W^*.$$

Upon completion of square, $\dot{V}$ can be regrouped as

$$\begin{aligned}\dot{V} \leq & -\frac{\gamma_1}{2}\|\boldsymbol{e}_m\|^2 - \frac{\gamma_1}{4}\left[\|\boldsymbol{e}_m\| - \frac{2\gamma_2}{\gamma_1}\|\boldsymbol{z}\|\right]^2 + \frac{\gamma_2^2}{\gamma_1}\|\boldsymbol{z}\|^2 \\ & - \frac{\gamma_1}{4}\left[\|\boldsymbol{e}_m\| - \frac{2\gamma_3}{\gamma_1}\left\|\widetilde{\boldsymbol{W}}\right\|_F\right]^2 + \frac{\gamma_3^2}{\gamma_1}\left\|\widetilde{\boldsymbol{W}}\right\|_F + \gamma_4\|\boldsymbol{e}_m\| \\ & - \frac{1}{4}q\|\boldsymbol{z}\|^2 - \frac{q}{4}\left[\|\boldsymbol{z}\| - \frac{2\beta_1}{q}\left\|\widetilde{\boldsymbol{W}}\right\|_F\right]^2 + \frac{\beta_1^2}{q}\left\|\widetilde{\boldsymbol{W}}\right\|_F^2 + \beta_2\|\boldsymbol{z}\| \\ & - \frac{1}{2}q_f\|\boldsymbol{z}_f\|^2 + \beta_3\|\boldsymbol{z}_f\| - \sigma\left\|\widetilde{\boldsymbol{W}}\right\|_F^2 + \sigma\left\|\widetilde{\boldsymbol{W}}\right\|_F W^*.\end{aligned} \tag{B.5}$$

The terms that involve products of variables and are linear in the variables are upper bounded as follows:

$$\begin{aligned}&\gamma_4\|\boldsymbol{e}_m\| \leq \frac{\gamma_4}{2}[\|\boldsymbol{e}_m\|^2 + 1], \\ &\beta_2\|\boldsymbol{z}\| \leq \frac{\beta_2}{2}[\|\boldsymbol{z}\|^2 + 1],\ \beta_3\|\boldsymbol{z}_f\| \leq \frac{\beta_3}{2}[\|\boldsymbol{z}_f\|^2 + 1], \\ &\sigma\left\|\tilde{\boldsymbol{W}}\right\|_F W^* \leq \left\|\widetilde{\boldsymbol{W}}\right\|_F^2 + \left(\frac{\sigma W^*}{2}\right)^2.\end{aligned} \tag{B.6}$$

Using the bounds in (B.6), the time derivative $\dot{V}$ in (B.5) is finally bounded as

$$\dot{V} \leq -\kappa_{\boldsymbol{e}_m}\|\boldsymbol{e}_m\|^2 - \kappa_{\boldsymbol{z}}\|\boldsymbol{z}\|^2 - \kappa_{\boldsymbol{z}_f}\|\boldsymbol{z}_f\|^2 - \kappa_W\left\|\widetilde{\boldsymbol{W}}\right\|_F^2 + \Upsilon^2, \tag{B.7}$$

where $\kappa_{\boldsymbol{e}_m} = \frac{1}{2}(\gamma_1 - \gamma_4)$, $\kappa_{\boldsymbol{z}} = \frac{1}{4}q - \frac{\beta_2}{2} - \frac{\gamma_2^2}{\gamma_1}$, $\kappa_{\boldsymbol{z}_f} = \frac{1}{2}(q_f - \beta_3)$, $\kappa_W = \sigma - 1 - \frac{\gamma_3^2}{\gamma_1} - \frac{\beta_1^2}{q}$, $\Upsilon^2 = \frac{1}{2}[\gamma_4 + \beta_2 + \beta_3 + \frac{\sigma^2 W^{*2}}{2}]$.

Define a compact set $\mathcal{B}_C = \{\zeta \in \mathcal{B}_R \ : \ \|\zeta\| \leq C\}$, where

$$C = \max\left\{\sqrt{\frac{\Upsilon^2}{\kappa_{\boldsymbol{e}_m}}},\ \sqrt{\frac{\Upsilon^2}{\kappa_{\boldsymbol{z}}}},\ \sqrt{\frac{\Upsilon^2}{\kappa_{\boldsymbol{z}_f}}},\ \sqrt{\frac{\Upsilon^2}{\kappa_W}}\right\}. \tag{B.8}$$

Then $\dot{V} < 0$ when $\|\zeta\| > C$. Define $\rho = \sqrt{\frac{T_M}{T_m}}C$, $\mathcal{B}_\rho = \{\zeta \in \mathcal{B}_R \ : \ \|\zeta\| \leq \rho\}$, then ζ is uniformly ultimately bounded in $\mathcal{B}_\rho$ [91, Corollary 5.1]. □

APPENDIX C

CHAPTER 5 PROOF

Proof of Theorem 5.2 : Consider the following positive definite radially unbounded function as a candidate Lyapunov function for the dynamics in (5.27), (5.30), (5.31)

$$V(\boldsymbol{E},\widetilde{\boldsymbol{E}},\boldsymbol{z}_2,\widetilde{Z}) = \boldsymbol{E}^T P\boldsymbol{E} + \widetilde{\boldsymbol{E}}^T P\widetilde{\boldsymbol{E}} + \frac{1}{2}\mathrm{tr}(\widetilde{M}^T\Gamma_M^{-1}\widetilde{M}) + \frac{1}{2}\mathrm{tr}(\widetilde{N}^T\Gamma_N^{-1}\widetilde{N}) + V_{\boldsymbol{z}_2}(\boldsymbol{z}_2). \quad \text{(C.1)}$$

Its derivative along (5.27), (5.31) will be

$$\begin{aligned}\dot{V} &= -\boldsymbol{E}^T Q\boldsymbol{E} - \widetilde{\boldsymbol{E}}^T\widetilde{Q}\widetilde{\boldsymbol{E}} + 2\boldsymbol{E}^T PB_1\Big[\boldsymbol{u}_{ad} - \bar{\boldsymbol{\Delta}}_1\Big] - 2\boldsymbol{E}^T PB_2\boldsymbol{\Delta}_2 \\ &\quad -2\widetilde{\boldsymbol{E}}^T\widetilde{P}B_1\Big[\boldsymbol{u}_{ad} - \bar{\boldsymbol{\Delta}}_1\Big] + 2\widetilde{\boldsymbol{E}}^T\widetilde{P}B_2\boldsymbol{\Delta}_2 + \mathrm{tr}(\widetilde{M}^T\Gamma_M^{-1}\dot{\widetilde{M}}) + \mathrm{tr}(\widetilde{N}^T\Gamma_N^{-1}\dot{\widetilde{N}}) + \dot{V}_{\boldsymbol{z}_2}(\boldsymbol{z}_2).\end{aligned}$$

With the definition of $\widetilde{\boldsymbol{E}} = \widehat{\boldsymbol{E}} - \boldsymbol{E}$ and (5.37), this can be written

$$\begin{aligned}\dot{V} &= -\boldsymbol{E}^T Q\boldsymbol{E} - \widetilde{\boldsymbol{E}}^T\widetilde{Q}\widetilde{\boldsymbol{E}} + 2\widehat{\boldsymbol{E}}^T PB_1\Big[\widehat{M}^T\Big(\hat{\sigma} - \hat{\sigma}'\widehat{N}^T\boldsymbol{\eta}\Big) + \widehat{M}^T\hat{\sigma}'\widetilde{N}^T\boldsymbol{\eta} + \boldsymbol{w} - \boldsymbol{\varepsilon}] - 2\boldsymbol{E}^T PB_2\boldsymbol{\Delta}_2 \\ &\quad -2\widetilde{\boldsymbol{E}}^T(\widetilde{P}B_1 + PB_1)\Big[\boldsymbol{u}_{ad} - \bar{\boldsymbol{\Delta}}_1\Big] + 2\widetilde{\boldsymbol{E}}^T\widetilde{P}B_2\boldsymbol{\Delta}_2 + \mathrm{tr}(\widetilde{M}^T\Gamma_M^{-1}\dot{\widetilde{M}}) + \mathrm{tr}(\widetilde{N}^T\Gamma_N^{-1}\dot{\widetilde{N}}) + \dot{V}_{\boldsymbol{z}_2}(\boldsymbol{z}_2).\end{aligned}$$

Substituting the adaptive laws implies

$$\begin{aligned}\dot{V} &= -\boldsymbol{E}^T Q\boldsymbol{E} - \widetilde{\boldsymbol{E}}^T\widetilde{Q}\widetilde{\boldsymbol{E}} + 2\widehat{\boldsymbol{E}}^T PB_1\Big[\boldsymbol{w} - \boldsymbol{\varepsilon}\Big] - 2\boldsymbol{E}^T PB_2\boldsymbol{\Delta}_2 \\ &\quad -2\widetilde{\boldsymbol{E}}^T(\widetilde{P}B_1 + PB_1)\Big[\boldsymbol{u}_{ad} - \bar{\boldsymbol{\Delta}}_1\Big] + 2\widetilde{\boldsymbol{E}}^T\widetilde{P}B_2\boldsymbol{\Delta}_2 \\ &\quad -k\mathrm{tr}\Big[\widetilde{M}^T\widehat{M}\Big] - k\mathrm{tr}\Big[\widetilde{N}^T\widehat{N}\Big] + \dot{V}_{\boldsymbol{z}_2}(\boldsymbol{z}_2).\end{aligned}$$

Using upper bounds from (5.36), (5.39), (5.43), (5.44), the derivative of the Lyapunov

function candidate can be upper bounded as

$$\begin{aligned}
\dot{V} \;\leq\; & -Q_m\|\boldsymbol{E}\|^2 - \widetilde{Q}_m\|\widetilde{\boldsymbol{E}}\|^2 + 2\|\boldsymbol{E}\|\|PB_2\|\left[\delta_1\|\boldsymbol{E}\| + \beta_2\|\boldsymbol{z}_2\| + \delta_2\right] \\
& +2\|PB_1\|\|\widehat{\boldsymbol{E}}\|\left[\gamma_1\|\widetilde{Z}\|_F + \gamma_2\right] + 2\Theta\|\widetilde{\boldsymbol{E}}\|\left[\alpha_1\|\widetilde{Z}\|_F + \alpha_2\right] \\
& +2\|\widetilde{\boldsymbol{E}}\|\|\widetilde{P}B_2\|\left[\delta_1\|\boldsymbol{E}\| + \beta_2\|\boldsymbol{z}_2\| + \delta_2\right] \\
& -\frac{k}{2}\|\widetilde{M}\|_F^2 - \frac{k}{2}\|\widehat{M}\|_F^2 + \frac{k}{2}\|M\|_F^2 - \\
& -\frac{k}{2}\|\widetilde{N}\|_F^2 - \frac{k}{2}\|\widehat{N}\|_F^2 + \frac{k}{2}\|N\|_F^2 \\
& -\frac{3c_3}{4}\|\boldsymbol{z}_2\|^2 + \frac{(c_4c_5)^2}{c_3}\|\boldsymbol{E}\|^2 + \frac{(c_4c_5)^2}{c_3}\beta_4^2, \qquad \text{(C.2)}
\end{aligned}$$

where the following property for matrices has been used

$$\operatorname{tr}\left[\widetilde{W}^T(\widehat{W})\right] \;=\; \frac{1}{2}\|\widetilde{W}\|^2 + \frac{1}{2}\|\widehat{W}\|^2 - \frac{1}{2}\|W\|^2.$$

Completion of squares implies

$$\begin{aligned}
\dot{V} \;\leq\; & -\left(Q_m - 1 - 2\delta_1\|PB_2\| - \frac{(c_4c_5)^2}{c_3} - \frac{(2\|PB_2\|\beta_2)^2}{c_3}\right)\|\boldsymbol{E}\|^2 + (\delta_2\|PB_2\|)^2 \\
& -\left(\widetilde{Q}_m - 1 - 2\delta_1\|\widetilde{P}B_2\| - \frac{(2\|\widetilde{P}B_2\|\beta_2)^2}{c_3}\right)\|\widetilde{\boldsymbol{E}}\|^2 + (\delta_2\|\widetilde{P}B_2\|)^2 \\
& +2\|PB_1\|(\|\boldsymbol{E}\| + ||\widetilde{\boldsymbol{E}}||)\left[\gamma_1\|\widetilde{Z}\|_F + \gamma_2\right] + 2\Theta\|\widetilde{\boldsymbol{E}}\|\left[\alpha_1\|\widetilde{Z}\|_F + \alpha_2\right] \\
& -\frac{k}{2}\|\widetilde{Z}\|_F^2 + \bar{Z} - \frac{c_3}{4}\|\boldsymbol{z}_2\|^2 + \frac{(c_4c_5)^2}{c_3}\beta_4^2\,. \qquad \text{(C.3)}
\end{aligned}$$

Grouping terms, (C.3) can be written

$$\begin{aligned}
\dot{V} \;\leq\; & -\left(Q_m - 1 - 2\delta_1\|PB_2\| - \frac{(c_4c_5)^2}{c_3} - \frac{(2\|PB_2\|\beta_2)^2}{c_3}\right)\|\boldsymbol{E}\|^2 + (\delta_2\|PB_2\|)^2 \\
& -\left(\widetilde{Q}_m - 1 - 2\delta_1\|\widetilde{P}B_2\| - \frac{(2\|\widetilde{P}B_2\|\beta_2)^2}{c_3}\right)\|\widetilde{\boldsymbol{E}}\|^2 + (\delta_2\|\widetilde{P}B_2\|)^2 \\
& +2\|PB_1\|\|\boldsymbol{E}\|\left[\gamma_1\|\widetilde{Z}\|_F + \gamma_2\right] + 2\|\widetilde{\boldsymbol{E}}\|\left[\Theta\left(\alpha_1\|\widetilde{Z}\|_F + \alpha_2\right) + \|PB_1\|\left(\gamma_1\|\widetilde{Z}\|_F + \gamma_2\right)\right] \\
& -\frac{k}{2}\|\widetilde{Z}\|_F^2 + \bar{Z} - \frac{c_3}{4}\|\boldsymbol{z}_2\|^2 + \frac{(c_4c_5)^2}{c_3}\beta_4^2, \qquad \text{(C.4)}
\end{aligned}$$

and further put in the form

$$\begin{aligned}\dot{V} \leq & -\left(Q_m - 1 - 2\delta_1\|PB_2\| - \frac{(c_4c_5)^2}{c_3} - \frac{(2\|PB_2\|\beta_2)^2}{c_3}\right)\|\boldsymbol{E}\|^2 + (\delta_2\|PB_2\|)^2 \\ & - \left(\widetilde{Q}_m - 1 - 2\delta_1\|\widetilde{P}B_2\| - \frac{(2\|\widetilde{P}B_2\|\beta_2)^2}{c_3}\right)\|\widetilde{\boldsymbol{E}}\|^2 + (\delta_2\|\widetilde{P}B_2\|)^2 \\ & + 2\|PB_1\|\|\boldsymbol{E}\|\left[\gamma_1\|\widetilde{Z}\|_F + \gamma_2\right] + 2\|\widetilde{\boldsymbol{E}}\|\left[\kappa_1\|\widetilde{Z}\|_F + \kappa_2\right] \\ & - \frac{k}{2}\|\widetilde{Z}\|_F^2 + \bar{Z} - \frac{c_3}{4}\|\boldsymbol{z}_2\|^2 + \frac{(c_4c_5)^2}{c_3}\beta_4^2\,.\end{aligned} \tag{C.5}$$

Upon completion of squares, we get

$$\begin{aligned}\dot{V} \leq & -\left(Q_m - 2 - 2\delta_1\|PB_2\| - \frac{(c_4c_5)^2}{c_3} - \frac{(2\|PB_2\|\beta_2)^2}{c_3}\right)\|\boldsymbol{E}\|^2 + 2\gamma_2\|PB_1\|\|\boldsymbol{E}\| + (\delta_2\|PB_2\|)^2 \\ & - \left(\widetilde{Q}_m - 2 - 2\delta_1\|\widetilde{P}B_2\| - \frac{(2\|\widetilde{P}B_2\|\beta_2)^2}{c_3}\right)\|\widetilde{\boldsymbol{E}}\|^2 + 2\kappa_2\|\widetilde{\boldsymbol{E}}\| + (\delta_2\|\widetilde{P}B_2\|)^2 \\ & + \kappa_1^2\|\widetilde{Z}\|_F^2 + [\gamma_1\|PB_1\|]^2\|\widetilde{Z}\|_F^2 - \frac{k}{2}\|\widetilde{Z}\|_F^2 + \bar{Z} - \frac{c_3}{4}\|\boldsymbol{z}_2\|^2 + \frac{(c_4c_5)^2}{c_3}\beta_4^2\,.\end{aligned} \tag{C.6}$$

One more completion of squares allows for the following upper bound:

$$\begin{aligned}\dot{V} \leq & -\left(Q_m - 3 - 2\delta_1\|PB_2\| - \frac{(c_4c_5)^2}{c_3} - \frac{(2\|PB_2\|\beta_2)^2}{c_3}\right)\|\boldsymbol{E}\|^2 + \gamma_2^2\|PB_1\|^2 + (\delta_2\|PB_2\|)^2 \\ & - \left(\widetilde{Q}_m - 3 - 2\delta_1\|\widetilde{P}B_2\| - \frac{(2\|\widetilde{P}B_2\|\beta_2)^2}{c_3}\right)\|\widetilde{\boldsymbol{E}}\|^2 + \kappa_2^2 + (\delta_2\|\widetilde{P}B_2\|)^2 \\ & - \left(\frac{k}{2} - \kappa_1^2 - [\gamma_1\|PB_1\|]^2\right)\|\widetilde{Z}\|_F^2 - \frac{c_3}{4}\|\boldsymbol{z}_2\|^2 + \bar{Z} + \frac{(c_4c_5)^2}{c_3}\beta_4^2.\end{aligned} \tag{C.7}$$

Either of the following conditions

$$\begin{aligned}\|\boldsymbol{E}\| &> \sqrt{\frac{\|PB_1\|^2\gamma_2^2 + \kappa_2^2 + \bar{Z} + \delta_2^2(\|PB_2\|^2 + \|\widetilde{P}B_2\|^2) + \frac{(c_4c_5)^2}{c_3}\beta_4^2}{Q_m - 3 - 2\delta_1\|PB_2\| - \frac{(c_4c_5)^2}{c_3} - \frac{(2\|PB_2\|\beta_2)^2}{c_3}}} \\ \|\widetilde{\boldsymbol{E}}\| &> \sqrt{\frac{\|PB_1\|^2\gamma_2^2 + \kappa_2^2 + \bar{Z} + \delta_2^2(\|PB_2\|^2 + \|\widetilde{P}B_2\|^2) + \frac{(c_4c_5)^2}{c_3}\beta_4^2}{\widetilde{Q}_m - 3 - 2\delta_1\|\widetilde{P}B_2\| - \frac{(2\|\widetilde{P}B_2\|\beta_2)^2}{c_3}}} \\ \|\widetilde{Z}\|_F &> \sqrt{\frac{\|PB_1\|^2\gamma_2^2 + \kappa_2^2 + \bar{Z} + \delta_2^2(\|PB_2\|^2 + \|\widetilde{P}B_2\|^2) + \frac{(c_4c_5)^2}{c_3}\beta_4^2}{\frac{k}{2} - \kappa_1^2 - [\gamma_1\|PB_1\|]^2}} \\ \|\boldsymbol{z}_2\| &> 2\sqrt{\frac{\|PB_1\|^2\gamma_2^2 + \kappa_2^2 + \bar{Z} + \delta_2^2(\|PB_2\|^2 + \|\widetilde{P}B_2\|^2) + \frac{(c_4c_5)^2}{c_3}\beta_4^2}{c_3}}\end{aligned} \tag{C.8}$$

will render $\dot{V} < 0$ outside a compact set. To complete the proof, consider the hypershere

$$B_\gamma = \{\boldsymbol{\zeta} \in B_R \mid \|\boldsymbol{\zeta}\| < \gamma\}$$

in the space of the error vector $\boldsymbol{\zeta}$ outside of which $\dot{V}(\boldsymbol{\zeta}) < 0$. Notice from (5.51), that $B_\gamma \subset B_R$. Let

$$\Gamma \triangleq \max_{\|\boldsymbol{\zeta}\|=\gamma} \boldsymbol{\zeta}^T T_2 \boldsymbol{\zeta}^T = \gamma^2 T_{2_M} .$$

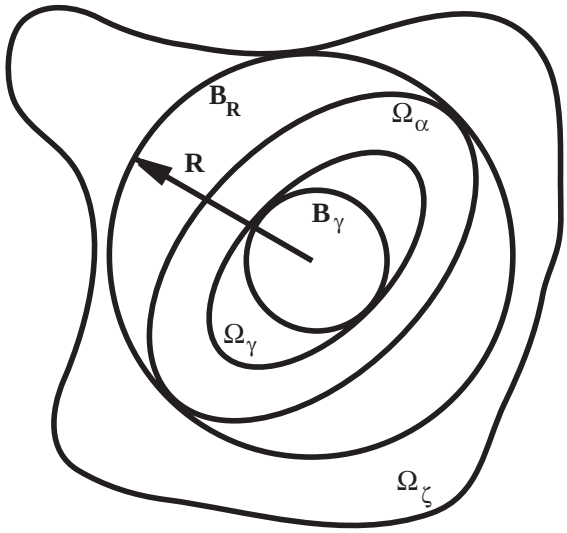

Fig. C.1: Geometric Representation of the Sets in Error Space.

Introduce the set, Figure C.1:

$$\Omega_\gamma = \left\{\boldsymbol{\zeta} \mid \boldsymbol{\zeta}^T T_2 \boldsymbol{\zeta} \leq \Gamma\right\} .$$

The condition in (5.51) ensures that $\Omega_\gamma \subset \Omega_\alpha$. Thus, if the initial error $\boldsymbol{\zeta}_0 = \boldsymbol{\zeta}(0)$ belongs to Ω_α, then there exists a time instant $t_{\boldsymbol{\zeta}}(\boldsymbol{\zeta}_0)$, such that $\boldsymbol{\zeta}(t)$ will enter the set Ω_γ at $t_{\boldsymbol{\zeta}}$ and remain inside it for all $t > t_{\boldsymbol{\zeta}}$. This implies ultimate boundedness of $\boldsymbol{\zeta}$ and completes the proof. □

APPENDIX D

CHAPTER 6 PROOF

Proof of Theorem 6.1 : Consider the following Lyapunov function candidate for each of the subsystems:

$$V_i(\boldsymbol{E}_i, \widetilde{\boldsymbol{E}}_i, \widetilde{\boldsymbol{W}}_i) = \boldsymbol{E}_i^T P_i \boldsymbol{E}_i + \widetilde{\boldsymbol{E}}_i^T \widetilde{P}_i \widetilde{\boldsymbol{E}}_i + \frac{1}{2} \widetilde{\boldsymbol{W}}_i^T F_i^{-1} \widetilde{\boldsymbol{W}}_i \,. \tag{D.1}$$

The derivative of V_i along (6.28), (6.18) will be

$$\begin{aligned} \dot{V}_i &= -\boldsymbol{E}_i^T Q_i \boldsymbol{E}_i - \widetilde{\boldsymbol{E}}_i^T \widetilde{Q}_i \widetilde{\boldsymbol{E}}_i + 2\boldsymbol{E}_i^T P_i \bar{\boldsymbol{b}}_i \Big[u_{ad_i} - f_i \Big] + 2\boldsymbol{E}_i^T P_i \bar{\boldsymbol{g}}_i \\ &\quad + 2\widetilde{\boldsymbol{E}}_i^T \widetilde{P}_i \bar{\boldsymbol{b}}_i \Big[u_{ad_i} - f_i \Big] + 2\widetilde{\boldsymbol{E}}_i^T \widetilde{P}_i \bar{\boldsymbol{g}}_i + \widetilde{\boldsymbol{W}}_i^T F_i^{-1} \dot{\widetilde{\boldsymbol{W}}}_i . \end{aligned}$$

With the definition of $\widetilde{\boldsymbol{E}}_i = \boldsymbol{E}_i - \widehat{\boldsymbol{E}}_i$, this can be written as

$$\begin{aligned} \dot{V}_i &= -\boldsymbol{E}_i^T Q_i \boldsymbol{E}_i - \widetilde{\boldsymbol{E}}_i^T \widetilde{Q}_i \widetilde{\boldsymbol{E}}_i + 2\widehat{\boldsymbol{E}}_i^T P_i \bar{\boldsymbol{b}}_i \Big[\widehat{\boldsymbol{W}}_i^T \boldsymbol{\phi}_i(\boldsymbol{Y}_l) - \boldsymbol{W}_i^T \boldsymbol{\phi}_i(\boldsymbol{Y}) - \epsilon_i \Big] + 2\boldsymbol{E}_i^T P_i \bar{\boldsymbol{g}}_i \\ &\quad + 2\widetilde{\boldsymbol{E}}_i^T (\widetilde{P}_i \bar{\boldsymbol{b}}_i + P_i \bar{\boldsymbol{b}}_i) \Big[\widehat{\boldsymbol{W}}_i^T \boldsymbol{\phi}_i(\boldsymbol{Y}_l) - \boldsymbol{W}_i^T \boldsymbol{\phi}_i(\boldsymbol{Y}) - \epsilon_i \Big] + 2\widetilde{\boldsymbol{E}}_i^T \widetilde{P}_i \bar{\boldsymbol{g}}_i + \widetilde{\boldsymbol{W}}_i^T F_i^{-1} \dot{\widetilde{\boldsymbol{W}}}_i . \end{aligned}$$

With the representation in (6.29), we have

$$\begin{aligned} \dot{V}_i &= -\boldsymbol{E}_i^T Q_i \boldsymbol{E}_i - \widetilde{\boldsymbol{E}}_i^T \widetilde{Q}_i \widetilde{\boldsymbol{E}}_i + 2\widehat{\boldsymbol{E}}_i^T P_i \bar{\boldsymbol{b}}_i \Big[\widetilde{\boldsymbol{W}}_i^T \boldsymbol{\phi}_i(\boldsymbol{Y}_l) + \boldsymbol{W}_i^T \boldsymbol{\phi}_i'(\boldsymbol{Y}^*) \tilde{\boldsymbol{Y}} - \epsilon_i \Big] + 2\boldsymbol{E}_i^T P_i \bar{\boldsymbol{g}}_i \\ &\quad + 2\widetilde{\boldsymbol{E}}_i^T (\widetilde{P}_i \bar{\boldsymbol{b}}_i + P_i \bar{\boldsymbol{b}}_i) \Big[\widetilde{\boldsymbol{W}}_i^T \boldsymbol{\phi}_i(\boldsymbol{Y}_l) + \boldsymbol{W}_i^T \boldsymbol{\phi}_i'(\boldsymbol{Y}^*) \tilde{\boldsymbol{Y}} - \epsilon_i \Big] + 2\widetilde{\boldsymbol{E}}_i^T \widetilde{P}_i \bar{\boldsymbol{g}}_i + \widetilde{\boldsymbol{W}}_i^T F_i^{-1} \dot{\widetilde{\boldsymbol{W}}}_i . \end{aligned}$$

Substituting the adaptive laws from (6.26) implies

$$\begin{aligned} \dot{V}_i &= -\boldsymbol{E}_i^T Q_i \boldsymbol{E}_i - \widetilde{\boldsymbol{E}}_i^T \widetilde{Q}_i \widetilde{\boldsymbol{E}}_i + 2\widehat{\boldsymbol{E}}_i^T P_i \bar{\boldsymbol{b}}_i \Big[\boldsymbol{W}_i^T \boldsymbol{\phi}_i'(\boldsymbol{Y}^*) \tilde{\boldsymbol{Y}} - \epsilon_i \Big] + 2\boldsymbol{E}_i^T P_i \bar{\boldsymbol{g}}_i \\ &\quad + 2\widetilde{\boldsymbol{E}}_i^T (\widetilde{P}_i \bar{\boldsymbol{b}}_i + P_i \bar{\boldsymbol{b}}_i) \Big[\widetilde{\boldsymbol{W}}_i^T \boldsymbol{\phi}_i(\boldsymbol{Y}_l) + \boldsymbol{W}_i^T \boldsymbol{\phi}_i'(\boldsymbol{Y}^*) \tilde{\boldsymbol{Y}} - \epsilon_i \Big] + 2\widetilde{\boldsymbol{E}}_i^T \widetilde{P}_i \bar{\boldsymbol{g}}_i - k_i \left[\widetilde{\boldsymbol{W}}_i \widehat{\boldsymbol{W}}_i \right] . \end{aligned}$$

Notice that using the bound in (6.9), the upperbound in (6.3) can be represented as

$$\|\boldsymbol{g}_i\| \leq \sum_{j=1}^{j=m} \alpha_i [\|\boldsymbol{E}_j\| + \beta_j] \tag{D.2}$$

Then using (6.30), the following upper bound can be derived

$$\begin{aligned}
\dot{V}_i &\leq -\lambda_{\min}(Q_i)\|\boldsymbol{E}_i\|^2 - \lambda_{\min}(\widetilde{Q}_i)\|\widetilde{\boldsymbol{E}}_i\|^2 \\
&\quad +2\left(\|\widetilde{\boldsymbol{E}}_i\| + \|\boldsymbol{E}_i\|\right)\|P_i\bar{\boldsymbol{b}}_i\|\left[\phi_i^* \sum_{j=1}^{j=m}\|\boldsymbol{E}_j\| + \epsilon_i^*\right] \\
&\quad +2\alpha_i\lambda_{\max}(P_i)\|\boldsymbol{E}_i\|\sum_{j=1}^{j=m}[\|\boldsymbol{E}_j\| + \beta_j] \\
&\quad +2\|\widetilde{\boldsymbol{E}}_i\|\mu_i\left[\|\widetilde{\boldsymbol{W}}_i\|\|\boldsymbol{\phi}_i(\boldsymbol{Y}_l)\| + \phi_i^*\sum_{j=1}^{j=m}\|\boldsymbol{E}_j\| + \epsilon_i^*\right] \\
&\quad +2\alpha_i\lambda_{\max}(\widetilde{P}_i)\|\widetilde{\boldsymbol{E}}_i\|\sum_{j=1}^{j=m}[\|\boldsymbol{E}_j\| + \beta_j] - k_i\left[\widetilde{\boldsymbol{W}}_i\widehat{\boldsymbol{W}}_i\right].
\end{aligned}$$

Completing the squares, this can be reduced to

$$\begin{aligned}
\dot{V}_i &\leq -\lambda_{\min}(Q_i)\|\boldsymbol{E}_i\|^2 - \lambda_{\min}(\widetilde{Q}_i)\|\widetilde{\boldsymbol{E}}_i\|^2 \\
&\quad +\|P_i\bar{\boldsymbol{b}}_i\|\left[\phi_i^*\sum_{j=1}^{j=m}\left[2\|\boldsymbol{E}_j\|^2 + \|\widetilde{\boldsymbol{E}}_i\|^2 + \|\boldsymbol{E}_i\|^2\right] + 2\left(\epsilon_i^*\right)^2 + \|\widetilde{\boldsymbol{E}}_i\|^2 + \|\boldsymbol{E}_i\|^2\right] \\
&\quad +2\alpha_i\lambda_{\max}(P_i)\|\boldsymbol{E}_i\|\sum_{j=1}^{j=m}[\|\boldsymbol{E}_j\| + \beta_j] \\
&\quad +\mu_i\left[\phi_i^*\sum_{j=1}^{j=m}\left[\|\boldsymbol{E}_j\|^2 + \|\widetilde{\boldsymbol{E}}_i\|^2\right] + \left(\|\widetilde{\boldsymbol{E}}_i\|^2 + \|\widetilde{\boldsymbol{W}}_i\|^2\right)\|\boldsymbol{\phi}_i(\boldsymbol{Y}_l)\| + (\epsilon_i^*)^2 + \|\widetilde{\boldsymbol{E}}_i\|^2\right] \\
&\quad +2\alpha_i\lambda_{\max}(\widetilde{P}_i)\|\widetilde{\boldsymbol{E}}_i\|\sum_{j=1}^{j=m}[\|\boldsymbol{E}_j\| + \beta_j] - \frac{k_i}{2}\|\widetilde{\boldsymbol{W}}_i\|^2 - \frac{k_i}{2}\|\widehat{\boldsymbol{W}}_i\|^2 + \frac{k_i}{2}\|\boldsymbol{W}_i\|^2
\end{aligned}$$

where the following property for vectors has been used

$$\widetilde{\boldsymbol{W}}^T\widehat{\boldsymbol{W}} = \frac{1}{2}\|\widetilde{\boldsymbol{W}}\|^2 + \frac{1}{2}\|\widehat{\boldsymbol{W}}\|^2 - \frac{1}{2}\|\boldsymbol{W}\|^2.$$

Another completion of squares will reduce to the following upper bound

$$\begin{aligned}
\dot{V}_i \;\leq\; & -\lambda_{\min}(Q_i)\|\boldsymbol{E}_i\|^2 - \lambda_{\min}(\widetilde{Q}_i)\|\widetilde{\boldsymbol{E}}_i\|^2 \\
& + \|P_i\bar{\boldsymbol{b}}_i\| \left[\phi_i^* \sum_{j=1}^{j=m} \left[2\|\boldsymbol{E}_j\|^2 + \|\widetilde{\boldsymbol{E}}_i\|^2 + \|\boldsymbol{E}_i\|^2 \right] + 2\left(\epsilon_i^*\right)^2 + \|\widetilde{\boldsymbol{E}}_i\|^2 + \|\boldsymbol{E}_i\|^2 \right] \\
& + \alpha_i \lambda_{\max}(P_i) \sum_{j=1}^{j=m} \left[2\|\boldsymbol{E}_i\|^2 + \|\boldsymbol{E}_j\|^2 + \beta_j^2 \right] \\
& + \mu_i \left[\phi_i^* \sum_{j=1}^{j=m} \left[\|\boldsymbol{E}_j\|^2 + \|\widetilde{\boldsymbol{E}}_i\|^2 \right] + \left(\|\widetilde{\boldsymbol{E}}_i\|^2 + \|\widetilde{\boldsymbol{W}}_i\|^2 \right) \|\boldsymbol{\phi}_i(\boldsymbol{Y}_l)\| + (\epsilon_i^*)^2 + \|\widetilde{\boldsymbol{E}}_i\|^2 \right] \\
& + \alpha_i \lambda_{\max}(\widetilde{P}_i) \sum_{j=1}^{j=m} \left[2\|\widetilde{\boldsymbol{E}}_i\|^2 + \|\boldsymbol{E}_j\|^2 + \beta_j^2 \right] - \frac{k_i}{2}\|\widetilde{\boldsymbol{W}}_i\|^2 - \frac{k_i}{2}\|\widehat{\boldsymbol{W}}_i\|^2 + \frac{k_i}{2}(W_i^*)^2
\end{aligned}$$

Further regrouping

$$\begin{aligned}
\dot{V}_i \;\leq\; & -\left(\lambda_{\min}(Q_i) - 2m\alpha_i\lambda_{\max}(P_i) - (m\phi_i^* + 1)\|P_i\bar{\boldsymbol{b}}_i\|\right)\|\boldsymbol{E}_i\|^2 \\
& - \Big(\lambda_{\min}(\widetilde{Q}_i) - 2m\alpha_i\lambda_{\max}(\widetilde{P}_i) - (m\phi_i^* + 1)\left(\|P_i\bar{\boldsymbol{b}}_i\| + \mu_i\right) - \mu_i\|\boldsymbol{\phi}_i(\boldsymbol{Y}_l)\|\Big)\|\widetilde{\boldsymbol{E}}_i\|^2 \\
& - \left(\frac{k_i}{2} - \mu_i\|\boldsymbol{\phi}_i(\boldsymbol{Y}_l)\|\right)\|\widetilde{\boldsymbol{W}}_i\|^2 \\
& + \sum_{j=1}^{j=m} \left[(2\|P_i\bar{\boldsymbol{b}}_i\| + \mu_i)\phi_i^* + \alpha_i\left(\lambda_{\max}(P_i) + \lambda_{\max}(\widetilde{P}_i)\right)\right]\|\boldsymbol{E}_j\|^2 \\
& + \frac{k_i}{2}(W_i^*)^2 + \left(2\|P_i\bar{\boldsymbol{b}}_i\| + \mu_i\right)\left(\epsilon_i^*\right)^2 + \alpha_i\left(\lambda_{\max}(P_i) + \lambda_{\max}(\widetilde{P}_i)\right)\sum_{j=1}^{j=m}\beta_j^2
\end{aligned}$$

Now introduce the following Lyapunov function for the whole system

$$V = \sum_{i=1}^{m} V_i\,. \tag{D.3}$$

Then, using the notations in (6.37), the upper bound reduces to:

$$\begin{aligned}
\dot{V} \;=\; & \sum_{i=1}^{m} \dot{V}_i \leq \\
& \sum_{i=1}^{m} \Big[-\left(\lambda_{\min}(Q_i) - 2m\alpha_i\lambda_{\max}(P_i) - (m\phi_i^* + 1)\|P_i\bar{\boldsymbol{b}}_i\|\right)\|\boldsymbol{E}_i\|^2 - \tilde{\theta}_i\|\widetilde{\boldsymbol{E}}_i\|^2 - \lambda_i\|\widetilde{\boldsymbol{W}}_i\|^2 \\
& + \sum_{j=1}^{j=m} \left[(2\|P_i\bar{\boldsymbol{b}}_i\| + \mu_i)\phi_i^* + \alpha_i\left(\lambda_{\max}(P_i) + \lambda_{\max}(\widetilde{P}_i)\right)\right]\|\boldsymbol{E}_j\|^2 \Big] + \omega.
\end{aligned} \tag{D.4}$$

Regrouping, this can be written as

$$\begin{aligned}\dot{V} &= \sum_{i=1}^{m} \dot{V}_i \leq \\ &\sum_{i=1}^{m} \Big[-\theta_i \|\boldsymbol{E}_i\|^2 - \tilde{\theta}_i \|\widetilde{\boldsymbol{E}}_i\|^2 - \lambda_i \|\widetilde{\boldsymbol{W}}_i\|^2 \Big] + \omega. \end{aligned} \tag{D.5}$$

Following an argument similar to that in [142], define the vectors $\boldsymbol{E} \triangleq \left[\begin{array}{ccc} \|\boldsymbol{E}_1\| & \cdots & \|\boldsymbol{E}_m\| \end{array} \right]^T$, $\widetilde{\boldsymbol{E}} \triangleq \left[\begin{array}{ccc} \|\widetilde{\boldsymbol{E}}_1\| & \cdots & \|\widetilde{\boldsymbol{E}}_m\| \end{array} \right]^T$, $\widetilde{\boldsymbol{W}} \triangleq \left[\begin{array}{ccc} \|\widetilde{\boldsymbol{W}}_1\| & \cdots & \|\widetilde{\boldsymbol{W}}_m\| \end{array} \right]^T$. Then the expression in (D.5) can be put into the following form:

$$\dot{V} \leq -\boldsymbol{E}^T D \boldsymbol{E} - \widetilde{\boldsymbol{E}}^T \tilde{D} \widetilde{\boldsymbol{E}} - \widetilde{\boldsymbol{W}}^T \Lambda \widetilde{\boldsymbol{W}} + \omega \,.$$

The following upper bound

$$\dot{V} \leq -\lambda_{\min}(D)\|\boldsymbol{E}\|^2 - \lambda_{\min}(\tilde{D})\|\widetilde{\boldsymbol{E}}\|^2 - \lambda_{\min}(\Lambda)\|\widetilde{\boldsymbol{W}}\|^2 + \omega$$

implies that either of the following conditions:

$$\begin{aligned} \|\boldsymbol{E}\| &> \sqrt{\frac{\omega}{\lambda_{\min}(D)}}, \\ \left\|\widetilde{\boldsymbol{E}}\right\| &> \sqrt{\frac{\omega}{\lambda_{\min}(\tilde{D})}}, \\ \|\widetilde{\boldsymbol{W}}\| &> \sqrt{\frac{\omega}{\lambda_{\min}(\Lambda)}} \end{aligned} \tag{D.6}$$

will render $\dot{V} < 0$ outside the compact set $\mathcal{B}_\gamma = \{\boldsymbol{\zeta} \mid \|\boldsymbol{\zeta}\| \leq \gamma\}$. Notice from (6.35) that $\mathcal{B}_\gamma \in \mathcal{B}_R$. Let Γ be the maximum value of the function $V(\boldsymbol{\zeta})$ on the edge of $\mathcal{B}_\gamma$

$$\Gamma \triangleq \max_{\|\boldsymbol{\zeta}\|=\gamma} V = \gamma^2 \lambda_{\max}(T) \,.$$

Introduce the level set of $V(\boldsymbol{\zeta})$, that touches the ball $\mathcal{B}_\gamma$ from outside:

$$\Omega_\gamma = \{\boldsymbol{\zeta} \mid V = \Gamma\} \,.$$

The condition in (6.35) ensures that $\Omega_\gamma \subset \Omega_\alpha$. Thus, if the initial error $\boldsymbol{\zeta}_0 = \boldsymbol{\zeta}(0)$ belongs to Ω_α, then there exists a time instant $t_{\boldsymbol{\zeta}}(\boldsymbol{\zeta}_0)$, such that $\boldsymbol{\zeta}(t)$ will enter the set Ω_γ at $t_{\boldsymbol{\zeta}}$ and remain inside it for all $t > t_{\boldsymbol{\zeta}}$. This implies ultimate boundedness of $\boldsymbol{\zeta}$ and completes the proof.

□

APPENDIX E

CHAPTER 7 PROOF

Proof of Theorem 7.1 : Consider the Lyapunov function in (7.44). Following similar lines in the stability proof given in [63], with the dynamics in (7.33), (7.15), (7.18) and the NN weights update rules in (7.20), it is straightforward to show that:

$$\begin{aligned}\dot{V} = &-\boldsymbol{e}_l^T Q_l \boldsymbol{e}_l - 2\boldsymbol{e}_l^T P_l \boldsymbol{b} u_{ad_2} - 2\boldsymbol{e}_l^T P_l \begin{bmatrix} 0 \\ \hat{\boldsymbol{\phi}}_2 \end{bmatrix} - 2\boldsymbol{e}_l^T P_l [\boldsymbol{\phi} - \hat{\boldsymbol{\phi}}] \\ &+ 2\boldsymbol{e}_l^T P_l \boldsymbol{b}\boldsymbol{k}^T \boldsymbol{E} - \boldsymbol{E}^T Q \boldsymbol{E} + 2\widehat{\boldsymbol{E}}^T P \boldsymbol{b}_d(\omega - \varepsilon) - \widetilde{\boldsymbol{E}}^T \widetilde{Q} \widetilde{\boldsymbol{E}} \\ &- 2\widetilde{\boldsymbol{E}}^T [P\boldsymbol{b}_d + \widetilde{P}\boldsymbol{b}_d](\hat{\boldsymbol{\phi}} - \boldsymbol{\phi}) - 2k\mathrm{tr}\left(\widetilde{M}^T \widehat{M}\right) - 2k\mathrm{tr}\left(\widetilde{N}^T \hat{N}\right).\end{aligned} \tag{E.1}$$

The stability proof is carried out depending upon $|\hat{s}|$ due to u_{ad_2} in (7.37).

(i) when $|\hat{s}| > \mu$, i.e., $u_{ad_2} = -\frac{1}{\hat{s}}\hat{\psi}$

The time derivative $\dot{V}$ in (E.1) can be arranged as:

$$\begin{aligned}\dot{V} = &-\boldsymbol{e}_l^T Q_l \boldsymbol{e}_l - 2\underbrace{\left\{\hat{\boldsymbol{e}}_l^T P_l \boldsymbol{b} u_{ad_2} + \hat{\boldsymbol{e}}_l^T P_l \begin{bmatrix} 0 \\ \hat{\boldsymbol{\phi}}_2 \end{bmatrix}\right\}}_{(*)} - 2\boldsymbol{E}^T P_l \boldsymbol{b} u_{ad_2} \\ &- 2\boldsymbol{E}^T P_l \begin{bmatrix} 0 \\ \hat{\boldsymbol{\phi}}_2 \end{bmatrix} - 2\boldsymbol{e}_l^T P_l [\boldsymbol{\phi} - \hat{\boldsymbol{\phi}}] + 2\boldsymbol{e}_l^T P_l \boldsymbol{b}\boldsymbol{k}^T \boldsymbol{E} \\ &- \boldsymbol{E}^T Q \boldsymbol{E} + 2\widehat{\boldsymbol{E}}^T P \boldsymbol{b}_d(\omega - \varepsilon) - \widetilde{\boldsymbol{E}}^T \widetilde{Q} \widetilde{\boldsymbol{E}} \\ &- 2\widetilde{\boldsymbol{E}}^T [P\boldsymbol{b}_d + \widetilde{P}\boldsymbol{b}_d](\hat{\boldsymbol{\phi}} - \boldsymbol{\phi}) - 2k\mathrm{tr}\left(\widetilde{M}^T \widehat{M}\right) - 2k\mathrm{tr}\left(\widetilde{N}^T \hat{N}\right).\end{aligned} \tag{E.2}$$

The term $(*)$ in (E.2) is zero as a consequence of the choice of u_{ad_2}. Using (7.42), the following bound is immediate:

$$\left| -\boldsymbol{E}^T P_l \boldsymbol{b} \frac{\hat{\psi}}{\hat{s}} \right| \leq \|\boldsymbol{E}\| \|P_l \boldsymbol{b}\| \left[\pi_1 \|\widetilde{Z}\|_F + \pi_2\right]. \tag{E.3}$$

Using the upper bounds from (7.40) and (E.3), $\dot{V}$ can be bounded by (see [63] for details):

$$\begin{aligned}\dot{V} \leq & -q_l\|\boldsymbol{e}_l\|^2 + 2\beta_1\|\boldsymbol{e}_l\|\|\boldsymbol{E}\| + 2\beta_2\|\boldsymbol{e}_l\|\|\widetilde{Z}\|_F + 2\beta_3\|\boldsymbol{e}_l\| \\ & - q\|\boldsymbol{E}\|^2 + 2\delta_1\|\boldsymbol{E}\|\|\widetilde{Z}\|_F + 2\delta_2\|\boldsymbol{E}\| \\ & - \tilde{q}\|\widetilde{\boldsymbol{E}}\|^2 + 2\Theta\|\widetilde{\boldsymbol{E}}\|\|\widetilde{Z}\|_F + 2\nu\|\widetilde{\boldsymbol{E}}\| \\ & - k\|\widetilde{Z}\|_F^2 + \bar{Z},\end{aligned} \tag{E.4}$$

where $q_l = \lambda_{\min}(Q_l), q = \lambda_{\min}(Q), \tilde{q} = \lambda_{\min}(\widetilde{Q})$, and

$$\begin{aligned}&\beta_1 = \|P_l\boldsymbol{b}\boldsymbol{k}^T\|,\ \beta_2 = \alpha_1\lambda_{\max}(P_l),\ \beta_3 = \alpha_2\lambda_{\max}(P_l) \\ &\delta_2 = 2c_2\lambda_{\max}(P_l) + (\pi_2 + \gamma_2)\|P\boldsymbol{b}_d\| \\ &\nu = \gamma_2\|P\boldsymbol{b}_d\| + \alpha_2\|(P + \widetilde{P})\boldsymbol{b}_d\|,\ \bar{Z} = k\left[\|M\|_F^2 + \|\boldsymbol{N}\|_F^2\right].\end{aligned} \tag{E.5}$$

Upon completion of squares, $\dot{V}$ can be bounded by:

$$\begin{aligned}\dot{V} \leq & -(q_l - 3)\|\boldsymbol{e}_l\|^2 - (q - 2 - \beta_1^2)\|\boldsymbol{E}\|^2 - (\tilde{q} - 2)\|\widetilde{\boldsymbol{E}}\|^2 \\ & - (k - \beta_2^2 - \delta_1^2 - \Theta^2)\|\widetilde{Z}\|_F^2 + \Upsilon_1, \\ & \text{where } \Upsilon_1 = \beta_3^2 + \delta_2^2 + \nu^2 + \bar{Z}.\end{aligned} \tag{E.6}$$

(ii) When $\mu/2 < |\hat{s}| \leq \mu$, i.e., $u_{ad_2} = -\frac{1}{2}\frac{\hat{\psi}}{\hat{s}}\left[\sin\frac{4\pi}{3}\left(\frac{\hat{s}^2}{\mu^2} - \frac{5}{8}\right) + 1\right]$.

The term $(*)$ in (E.2), using (7.42), can be bounded as follows:

$$\left|-\frac{1}{2}\hat{\psi}\left[\sin\frac{4\pi}{3}\left(\frac{\hat{s}^2}{\mu^2} - \frac{5}{8}\right) + 1\right] + \hat{\psi}\right| \leq \mu\left[\pi_1\|\widetilde{Z}\|_F + \pi_2\right]. \tag{E.7}$$

And the same bound for $|\boldsymbol{E}^T P_l\boldsymbol{b}\frac{\hat{\psi}}{\mu}|$ as in (E.3) leads to the following:

$$\dot{V} \leq \dot{V}_{(E.4)} + \mu\left[\pi_1\|\widetilde{Z}\|_F + \pi_2\right]. \tag{E.8}$$

With the following bound:

$$\mu\pi_1\|\widetilde{Z}\|_F \leq \frac{\mu\pi_1}{2}\left[\|\widetilde{Z}\|_F^2 + 1\right], \tag{E.9}$$

the time derivative of the Lyapunov function $\dot{V}$ is written as:

$$\begin{aligned}\dot{V} \leq & -(q_l - 3)\|\boldsymbol{e}_l\|^2 - (q - 2 - \beta_1^2)\|\boldsymbol{E}\|^2 - (\tilde{q} - 2)\|\widetilde{\boldsymbol{E}}\|^2 \\ & - (k - \frac{\mu\pi_1}{2} - \beta_2^2 - \delta_1^2 - \Theta^2)\|\widetilde{Z}\|_F^2 + \Upsilon_2, \\ & \text{where} \quad \Upsilon_2 = \Upsilon_1 + \mu(\frac{\pi_1}{2} + \pi_2).\end{aligned} \tag{E.10}$$

(iii) When $|\hat{s}| \leq \mu/2$, i.e., $u_{ad_2} = 0$

In this case, using (7.40), $\dot{V}$ in (E.1) can be bounded as:

$$\begin{aligned}\dot{V} \leq & -q_l\|\boldsymbol{e}_l\|^2 + 2\beta_1\|\boldsymbol{e}_l\|\|\boldsymbol{E}\| + 2\beta_2'\|\boldsymbol{e}_l\|\|\widetilde{Z}\|_F + 2\beta_3'\|\boldsymbol{e}_l\| \\ & - q\|\boldsymbol{E}\|^2 + 2\delta_1'\|\boldsymbol{E}\|\|\widetilde{Z}\|_F + 2\delta_2'\|\boldsymbol{E}\| \\ & - \tilde{q}\|\widetilde{\boldsymbol{E}}\|^2 + 2\Theta\|\widetilde{\boldsymbol{E}}\|\|\widetilde{Z}\|_F + 2\nu\|\widetilde{\boldsymbol{E}}\| \\ & - k\|\widetilde{Z}\|_F^2 + \bar{Z},\end{aligned} \tag{E.11}$$

where $\beta_2' = (\alpha_1 + c_1)\lambda_{\max}(P_l)(\ > \beta_2)$, $\beta_3' = (\alpha_2 + c_2)\lambda_{\max}(P_l)(\ > \beta_3)$, $\delta_1' = \gamma_1\|P\boldsymbol{b}_d\|(\ < \delta_1)$, $\delta_2' = \gamma_2\|P\boldsymbol{b}_d\|(\ < \delta_2)$. Upon completion of squares, $\dot{V}$ can be bounded as:

$$\begin{aligned}\dot{V} \leq & -(q_l - 3)\|\boldsymbol{e}_l\|^2 - (q - 2 - \beta_1^2)\|\boldsymbol{E}\|^2 - (\tilde{q} - 2)\|\widetilde{\boldsymbol{E}}\|^2 \\ & - (k - \beta_2'^2 - \delta_1'^2 - \Theta^2)\|\widetilde{Z}\|_F^2 + \Upsilon_3, \\ & \text{where} \quad \Upsilon_3 = \beta_3'^2 + \delta_2'^2 + \nu^2 + \bar{Z}.\end{aligned} \tag{E.12}$$

From **(i)**, **(ii)**, **(iii)**, either of the following conditions:

$$\|\boldsymbol{e}_l\| > C_1, \quad \|\boldsymbol{E}\| > C_2, \quad \|\widetilde{\boldsymbol{E}}\| > C_4, \quad \|\widetilde{Z}\|_F > C_4 \tag{E.13}$$

will render $\dot{V} < 0$, where $C_1 = \max\left\{\sqrt{\frac{\Upsilon_2}{q_l - 3}}, \sqrt{\frac{\Upsilon_3}{q_l - 3}}\right\}$, $C_2 = \max\left\{\sqrt{\frac{\Upsilon_2}{q - 2 - \beta_1^2}}, \sqrt{\frac{\Upsilon_3}{q - 2 - \beta_1^2}}\right\}$, $C_3 = \max\left\{\sqrt{\frac{\Upsilon_2}{\tilde{q} - 2}}, \sqrt{\frac{\Upsilon_3}{\tilde{q} - 2}}\right\}$, $C_4 = \max\left\{\sqrt{\frac{\Upsilon_2}{k - \frac{\mu\pi_1}{2} - \beta_2^2 - \delta_1^2 - \Theta^2}}, \sqrt{\frac{\Upsilon_3}{k - \beta_2'^2 - \delta_1'^2 - \Theta^2}}\right\}$. Further, with the definition:

$$C = \max\{C_1, C_2, C_3, C_3\}, \quad \mathcal{B}_C \triangleq \{\zeta \in \mathcal{B}_R | \|\zeta\| \leq C\}, \tag{E.14}$$

$\dot{V} < 0$ outside the compact set $\mathcal{B}_C$. Define

$$\rho = \sqrt{\frac{T_M}{T_m}}C, \ \mathcal{B}_\rho = \{\zeta \in \mathcal{B}_R | \|\zeta\| \leq \rho\} \subset \mathcal{B}_\alpha, \tag{E.15}$$

then ζ is ultimately bounded in $\mathcal{B}_\rho$ [91, Corollary 5.1]. □

REFERENCES

[1] Ioannou, P. and Kokotović, P., *Adaptive Systems with Reduced Models*, Springer-Verlag, Berlin;New York, 1983.

[2] Sastry, S. and Bodson, M., *Adaptive Control: Stability, Convergence, and Robustness*, Prentice-Hall, Englewood Cliffs, NJ, 1989.

[3] Åström, K. J. and Wittenmark, B., *Adaptive Control*, Addison-Wesley, Berlin;New York, 1995.

[4] Ioannou, P. and Sun, J., *Robust Adaptive Control*, Prentice-Hall, Englewood Cliffs, NJ, 1996.

[5] Sastry, S. and Isidori, A., "Adaptive Control of Linearizable Systems," *IEEE Transactions on Automatic Control*, Vol. 34, No. 11, 1989, pp. 1123–1131.

[6] Roup, A. V. and Bernstein, D. S., "Adaptive Stabilization of a Class of Nonlinear Systems With Nonparametric Uncertainty," *IEEE Transactions on Automatic Control*, Vol. 46, No. 11, November 2003, pp. 1821–1825.

[7] Chellaboina, V., Haddad, W. M., and Hayakawa, T., "Direct Adaptive Control for Nonlinear Matrix Second-Order Dynamical Systems with State-Dependent Uncertainty," *Systems & Control Letters*, Vol. 48, 2003, pp. 53–67.

[8] Esfandiari, F. and Khalil, H., "Output feedback stabilization of fully linearizable systems," *International Journal of Control*, Vol. 56, 1992, pp. 1007–1037.

[9] Tornambe, A., "Output Feedback Stabilization of a class of Non-Minimum Phase Nonliner Systems," *Systems & Control Letters*, Vol. 19, 1992, pp. 193–204.

[10] Teel, A. and Praly, L., "Global stabilizability and observability imply semi-global stabilizability by output feedback," *Systems and Control Letters*, Vol. 22, 1994, pp. 313–325.

[11] Aloliwi, B. and Khalil, H., "Adaptive output feedback regulation of a class of nonlinear systems: convergence and robustness," *IEEE Transactions on Automatic Control*, Vol. 42, 1997, pp. 1714–1716.

[12] Atassi, A. and Khalil, H., "A Separation Principle for the Stabilization of a Class of Nonlinear Systems," *IEEE Transactions on Automatic Control*, Vol. 44, No. 9, Sep. 1999, pp. 1672–1687.

[13] Khalil, H., "High-Gain Observers in Nonlinear Feedback Control," *New Directions in Nonlinear and Observer Design*, edited by H. Nijmeijer and T. Fossen, Springer, New York, 1999.

[14] Isidori, A., "A Tool for Semiglobal Stabilization of Uncertain Non-Minimum-Phase Nonlinear Systems via Output Feedback," *IEEE Transactions on Automatic Control*, Vol. 45, No. 10, 2000, pp. 1817–1827.

[15] Dabroom, A. M. and Khalil, H., "Output Feedback Sampled-Data Control of Nonlinear Systems Using High-Gain Observers," *IEEE Transactions on Automatic Control*, Vol. 46, No. 11, 2001, pp. 1712–1725.

[16] Sussmann, H. and Kokotović, P., "The peaking phenomenon and the global stabilization of nonlinear systems," *IEEE Transactions on Automatic Control*, Vol. 36, 1991, pp. 424–439.

[17] Sepulchre, R., Jankovic, M., and Kokotović, P., *Constructive Nonlinear Control*, Springer-Verlag, 1997.

[18] Kanellakopoulos, I., "Adaptive Control of Nonlinear Systems: A Tutorial," *Adaptive Control, Filtering, and Signal Processing*, edited by K. Åström, G. Goodwin, and P. Kumar, Springer-Verlag, 1995.

[19] Krstić, M., Kanellakopoulos, I., and Kokotović, P. V., *Nonlinear and Adaptive Control Design*, John Wiley & Sons, New York, 1995.

[20] Marino, R. and Tomei, P., *Nonlinear Control Design: Geometric, Adaptive, & Robust*, Prentice Hall, New Jersey, 1995.

[21] Narendra, K. and Annaswamy, A., *Stable Adaptive Control*, Prentice-Hall, 1989.

[22] Funahashi, K., "On the Approximate Realization of Continuous Mappings by Neural Networks," *Neural Networks*, Vol. 2, 1989, pp. 183–192.

[23] Hornik, N., Stinchcombe, M., and White, H., "Multilayer feedforward networks are universal approximators," *Neural Networks*, Vol. 2, 1989, pp. 359–366.

[24] Chowdhury, F., Wahi, R., and Kaminedi, S., "A Survey of Neural Networks Applications in Automatic Control," *Proceedings of the* 33^{rd} *Southeastern Symposium on System Theory*, 2001, pp. 349–353.

[25] Narendra, K. and Parthasarathy, K., "Identification and control of dynamical systems using neural networks," *IEEE Transactions on Neural Networks*, Vol. 1, Mar. 1990, pp. 4–27.

[26] Narendra, K., "Adaptive control using neural networks," *Neural Networks for Control*, edited by W. Miller, R. Sutton, and P. Werbos, MIT Press, Cambridge, MA, 1990.

[27] Narendra, K., "Adaptive Control of Dynamical Systems Using Neural Networks," *Handbook of Intelligent Control*, edited by D. A. White and D. A. Sofge, Van Nostrand Reinhold, New York, 1992.

[28] Narendra, K., "Neural Networks for Control: Theory and Practice," *Proceedings of the IEEE*, Vol. 84, No. 10, Oct. 1996, pp. 1385–1996.

[29] Rao, V., Damle, R., Tebbe, C., , and Kern, F., "The adaptive control of smart structures using neural networks," *Smart Materials and Structures*, Vol. 3, 1994, pp. 354–366.

[30] Hyland, D. C., "Neural Network Architecture for On-Line System Identification and Adaptively Optimized Control," *Proceedings of the Conference on Decision and Control*, Brighton, England, Dec. 1991, pp. 2552–2557.

[31] Hyland, D. C., "Adaptive Neural Control for Flexible Aerospace Systems: Progress and Prospects," *10th IEEE International Symposium on Intelligent Control*, 1995, pp. 3–8.

[32] Davis, L., Hyland, D., Yen, G., and Das, A., "Adaptive neural control for space structure vibration suppression," *Smart Materials and Structures*, Vol. 8, 1999, pp. 753–766.

[33] KrishnaKumar, K. and Montgomery, L., "Adaptive neuro-control for large flexible structures," *Smart Materials and Structures*, Vol. 1, 1992, pp. 312–323.

[34] Chen, F.-C. and Liu, C.-C., "Adatively Controlling Nonlinear Continous-time Systems using Multilayer Neural Networks," *IEEE Transactions on Automatic Control*, Vol. 39, No. 6, 1994, pp. 1306–1310.

[35] Polycarpou, M., "Stable Adaptive Neural Control Scheme for Nonlinear Systems," *IEEE Transactions on Automatic Control*, Vol. 41, No. 3, 1996, pp. 447–451.

[36] Lewis, F., Jagannathan, S., and Yeşildirek, A., *Neural Network Control of Robot Manipulators and Nonlinear Systems*, Taylor & Francis, 1999.

[37] Rovithakis, G. A. and Christodoulou, M. A., *Adaptive Control with Recurrent High-order Neural Networks*, Springer-Verlag, London, 2000.

[38] Gutiérrez, L., Lewis, F., and Lowe, A., "Implementation of a Neural Network Tracking Controller for a Single Flexible Link: Comparison with PD and PID controllers," *IEEE Transactions on Industrial Electronics*, Vol. 45, No. 2, April 1998.

[39] Seshagiri, S. and Khalil, H., "Output Feedback Control of Nonlinear Systems Using RBF Neural Networks," *IEEE Transactions on Neural Network*, Vol. 11, No. 1, Jan 2000, pp. 69–79.

[40] Ge, S., Hang, C., Lee, T., and Zhang, T., *Stable Adaptive Neural Network Control*, Kluwer Academic Publishers, Boston, 2002.

[41] Spooner, J. T., Maggiore, M., Ordóñez, R., and Passino, K. M., *Stable Adaptive Control and Estimation for Nonlinear Systems- Neural and Fuzzy Approximator Techniques*, John Wiley & Sons, New York, NY, 2002.

[42] Kim, Y. and Lewis, F., *High-Level Feedback Control with Neural Networks*, World Scientific, Singapore; River Edge,NJ, 1998.

[43] Hovakimyan, N., Nardi, F., Calise, A., and Lee, H., "Adaptive Output Feedback Control of a Class of Nonlinear Systems Using Neural Networks," *International Journal of Control*, Vol. 74, No. 12, 2001, pp. 1161–1169.

[44] Ananthakrishnan, S., "Adaptive Tachometer Feedback Augmentation of the Shuttle Remote Manipulator Control System," *IEEE International Conference on Robotics and Automation*, 1995.

[45] Wen, C. and Gibbard, M., "Conventional Power Systems Stabilizer with Auxiliary Self-Tuning/Fixed-Parameter Controller," *Electrical Power & Engergy Systems*, Vol. 17, No. 1, 1995, pp. 39–49.

[46] Dash, P., Elangovan, S., and Liew, A., "Design of Nonlinear Expert Supervisory Controllers for Power System Stabilization," *Eleictric Power Systems Research*, Vol. 33, 1995, pp. 25–32.

[47] Anderson, C., Hittle, D., Katz, A., and Kretchmar, R., "Synthesisof reinforcement learning, neural networks and PI control applied to a simulated heating coil," *Artificial Intelligence in Engineering*, Vol. 11, 1997, pp. 421–429.

[48] Bodson, M. and Groszkiewicz, J., "Multivariable Adaptive Algorithms for Reconfigurable Fligh Control," *IEEE Transactions on Control Systems Technology*, Vol. 5, No. 2, 1997, pp. 217–229.

[49] Wohletz, J., Paduano, J., and Annaswamy, A., "Retrofit Systems for Reconfiguration in Civil Aviation," *Proceedings of the AIAA Guidance, Navigation, and Control Conference*, AIAA-99-3964, Portland, OR, 1999.

[50] Rovithakis, G., "Robustifying Nonlinear Systems Using High-Order Neural Network Controller," *IEEE Transactions on Automatic Control*, Vol. 44, 1999, pp. 102–108.

[51] Li, Y., Sundararajan, N., and Saratchandran, P., "Neuro-Controller design for nonlinear fighter aircraft maneuver using fully tuned RBF networks," *Automatica*, Vol. 37, No. 8, 2001, pp. 1293–1301.

[52] Kim, B. S. and Calise, A. J., "Nonlinear Flight Control Using Neural Networks," *AIAA Journal of Guidance, Control & Dynamics*, Vol. 20-1, 1997, pp. 26–33.

[53] Rysdyk, R. and Calise, A., "Adaptive Model Inversion Flight Control for Tilt-Rotor Aircraft," *AIAA Journal of Guidance,Control, and Dynamics*, Vol. 22, No. 3, 1999, pp. 402–407.

[54] Calise, A. J., Sharma, M., and Lee, S., "Adaptive Autopilot Design for Guided Munitions," *AIAA Journal of Guidance, Control & Dynamics*, Vol. 23, No. 5, 2000.

[55] Mcfarland, M. and Calise, A., "Adaptive Nonlinear Control of Agile Antiair Missiles using Neural Networks," *IEEE Transactions on Control Systems Technology*, Vol. 8, No. 5, Sep 2000, pp. 749–756.

[56] Calise, A. J., Lee, S., and Sharma, M., "Development of a Reconfigurable Flight Control Law for Tailless Aircraft," *AIAA Journal of Guidance, Control & Dynamics*, Vol. 24, No. 5, 2001, pp. 896–902.

[57] Johnson, E. N. and Calise, A. J., "Limited Authority Adaptive Flight Control for Reusable Launch Vehicles," *AIAA Journal of Guidance, Control & Dynamics*, Vol. 26, No. 6, 2003, pp. 906–913.

[58] McFarland, M., "Augmentation of Gain-Scheduled Missile Autopilots using Adaptive Neural Networks," *Proceedings of AIAA guidance,navigation and control conference*, AIAA-98-4491, Reston,VA, 1998.

[59] McFarland, M. and Stansbery, D., "Adaptive Nonlinear Autopilot for Air-To-Air Missiles," Tech. Rep. AD-A356503, 1998, presented at AIAA Missiles Sciences Conference, Monterey, CA, 1998.

[60] Campa, G., Sharma, M., Calise, A., and Innocenti, M., "Neural Network Augmentation of Linear Controllers With Application to Underwater Vehicles," *Proceedings of the American Control Conference*, Chicago,IL, June 2000, pp. 75–79.

[61] Sharma, M. and Calise, A., "Neural Network Augmentation of Existing Linear Controllers," *Proceedings of the AIAA Guidance, Navigation, and Control Conference*, AIAA-2001-4163, Montreal, Canada, August 2001.

[62] Calise, A., Hovakimyan, N., and Idan, M., "Adaptive Output Feedback Control of Nonlinear Systems using Neural Networks," *Automatica*, Vol. 37, No. 8, 2001, pp. 1201–1211.

[63] Hovakimyan, N., Nardi, F., Kim, N., and Calise, A., "Adaptive Output Feedback Control of Uncertain Systems using Single Hidden Layer Neural Networks," *IEEE Transactions on Neural Networks*, Vol. 13, No. 6, 2002.

[64] Hovakimyan, N., Lee, H., and Calise, A., "On Approximate NN Realization of an Unknown Dynamic System from its Input-Output History," *Proceedings of the American Control Conference*, Chicago, IL, 2000, pp. 919–923.

[65] Lavretsky, E., Hovakimyan, N., and Calise, A., "Upper Bounds for Approximation of Continuous-Time Dynamics Using Delayed Outputs and Feedforward Neural Networks," *IEEE Transactions on Automatic Control*, Vol. 48, No. 9, 2003, pp. 1606–1610.

[66] Kutay, A. T., Calise, A. J., Idan, M., and Hovakimyan, N., "Experimental Results on Adaptive Output Feedback Control Using a Laboratory Model Helicopter," *Proceedings of AIAA guidance,navigation and control conference*, No. AIAA-2002-4921, Monterey, CA, August 2002.

[67] Kim, N., Calise, A. J., Hovakimyan, N., Prasad, J., and Corban, J. E., "Adaptive Output Feedback for High-Bandwidth Flight Control," *AIAA Journal of Guidance, Control & Dynamics*, Vol. 25, No. 6, 2002, pp. 993–1002.

[68] Isidori, A., *Nonlinear Control Systems*, Springer-Verlag, Berlin;New York, 3rd ed., 1995.

[69] Johnson, C., "Theory of Disturbance-Accomodating Controllers," *Control and Dynamic Systems:Advances in Theory and Applications*, edited by C. Leondes, Vol. 12, Academic Press, New York, NY, 1976, pp. 387–487.

[70] Johnson, E. N., *Limited Authority Adaptive Flight Control*, Ph.D. thesis, Georgia Institute of Technology, School of Aerospace Engineering, Dec. 2000.

[71] Karason, S. and Annaswamy, A., "Adaptive Control in the Presence of Input Constraints," *IEEE Transactions on Automatic Control*, Vol. 39, No. 11, 1994, pp. 1–6.

[72] Bernstein, D. and Michel, A., "A Chronological Bibliography on Saturating Actuators," *International Journal Robust and Nonlinear Control*, Vol. 5, 1995, pp. 375–380.

[73] Saberi, A., Stoorvogel, A. A., and Sannuti, P., *Control Of Linear Systems with Regulation and Input Constraints*, Springer-Verlag, London, 2000.

[74] Leonessa, A., Haddad, W. M., and Hayakawa, T., "Adaptive Tracking for Nonlinear Systems with Control Constraints," *Proceedings of the American Control Conference*, Arlington, Virginia, jun 2001.

[75] Polycarpou, M., Farrell, J., and Sharma, M., "On-Line Approximation Control of Uncertain Nonlinear Systems: Issues with Control Input Saturation," *Proceedings of the American Control Conference*, Denver, CO, June 2003, pp. 543–548.

[76] Tao, G. and Kokotović, P. V., *Adaptive Control of Systems with Actuator and Sensor Nonlinearities*, John Wiley & Sons, Inc., New York, NY, 1996.

[77] Shahruz, S., "Performance Enhancement of a Class of Nonlinear Systems by Disturbance Observers," *IEEE/ASME Transactions on Mechatronics*, Vol. 5, No. 3, Sept. 2000, pp. 319–323.

[78] Šelmić, R. R. and Lewis, F. L., "Deadzone Compensation in Motion control Systems Using Neural Networks," *IEEE Transactions on Automatic Control*, Vol. 45, No. 4, April 2000, pp. 602–613.

[79] Selmic, R. R. and Lewis, F. L., "Neural-Network Approximation of Piecewise Continuous Functions: Application to Friction Compensation," *IEEE Transactions on Neural Networks*, Vol. 13, No. 3, 2002.

[80] Taware, A. and Tao, G., *Control of Sandwich Nonlinear Systems*, Springer-Verlag, New York, NY, 2003.

[81] Schrijver, E., Dijk, J. v., and Nijmeijer, H., "Equivalence of Disturbance Observer Structures for Linear Systems," *Proceedings of Conference on Decision and Control*, Sydney,Australia, 2000, pp. 4518–4519.

[82] Kim, B. K. and Chung, W. K., "Performance Tuning of Robust Motion Controllers for High-Accuracy Positioning Systems," *IEEE/ASME Tansactions on Mechatronics*, Vol. 7, No. 4, Dec. 2002, pp. 500–514.

[83] Hovakimyan, N. and Calise, A., "Adaptive Output Feedback Control of Uncertain Multi-Input Multi-Output Systems using Single Hidden Layer Neural Networks," *Proceedings of the American Control Conference*, Anchorage,AL, May 2002.

[84] Narendra, K. and Oleng, N., "Exact Output Tracking in Decentralized Adaptive Control Systems," *IEEE Transactions on Automatic Control*, Vol. 47, No. 2, 2002, pp. 390–395.

[85] Narendra, K. and Oleng, N., "Decentralized Adaptive Control," *Proceedings of American Control Conference*, 2002.

[86] Hovakimyan, N., Calise, A., and Venkatesh, M., "An Adaptive Observer Design Methodology for Bounded Nonlinear Processes," *Proceedings of Conference on Decision and Control*, Las Vegas, NV, 2002, pp. 4700–4705.

[87] Wohletz, J., Paduano, J., and Maine, T., "Retrofit Reconfiguration System for a Commercial Transport," *Proceedings of the AIAA Guidance, Navigation, and Control Conference*, AIAA-2000-4041, Denver, CO, 2000.

[88] King, B. and Hovakimyan, N., "An Adaptive Approach to Control of Distributed Parameter Systems," *Proceedings of the Conference on Decision and Control*, Maui, HI, Dec. 2003, pp. 5715–5720.

[89] Kim, N., *Improved Methods in Neural Network Based Adaptive Output Feedback Control with Application to Flight Control*, Ph.D. thesis, Georgia Institute of Technology, School of Aerospace Engineering, 2003.

[90] Sastry, S., *Nonlinear Systems*, Springer-Verlag, 1999.

[91] Khalil, H., *Nonlinear Systems*, Prentice-Hall, Upper Saddle River, NJ, 1996.

[92] Bartle, R. G., *The Elements of Real Analysis*, John Wiley & Sons, New York, 2nd ed., 1976.

[93] Sanner, R. and Slotine, J., "Gaussian Networks for Direct Adaptive Control," *IEEE Transactions on Neural Networks*, Vol. 3, No. 6, 1992, pp. 837–864.

[94] Sontag, E., *Mathematical Control Theory*, Springer-Verlag, New York, 1998.

[95] "Torsion Pendulum Appratus, ECP Systems, Inc." `http://www.ecpsystems.com/controls_torplant.htm`.

[96] De Doná, J. A. and Goodwin, G. C., "A general scheme that combines piecewise-linear control, low-high-gain control and over-saturation to achieve high performance in the presence of input saturation," *Proceedings of American Control Conference*, Chicago, IL, June 2000.

[97] Johnson, E. N. and Calise, A. J., "Neural Network Adaptive Control of Systems with Input Saturation," *Proceedings of the American Control Conference*, Arlington, Virginia, jun 2001.

[98] Hovakimyan, N., Kim, N., Calise, A., Prasad, J., and Corban, E., "Adaptive Output Feedback for High-Bandwidth Control of an Unmanned Helicopter," *Proceedings of the AIAA Guidance, Navigation, and Control Conference*, Montreal, Canada, August 2001.

[99] Johnson, E. N. and Kannan, S. K., "Adaptive Flight Control for an Autonomous Unmanned Helicopter," *Proceedings of AIAA guidance,navigation and control conference*, No. AIAA-2002-4439, Monterey, CA, August 2002.

[100] Calise, A., Yang, B.-J., and Craig, J., "An Augmenting Adaptive Approach to Control of Flexible Systems," *Proceedings of AIAA guidance,navigation and control conference*, AIAA-2002-4942, 2002.

[101] Yang, B.-J., Calise, A., and Craig, J., "Adaptive Output Feedback Control with Input Saturation," *Proceedings of the American Control Conference*, Denver, CO, 2003, pp. 1572–1577.

[102] Umeno, T. and Hori, Y., "Robust Speed Control of DC Servomotors Using Modern Two Degrees-of-Freedom Controller Design," *IEEE Transactions on Industrial Electronics*, Vol. 38, No. 5, 1991, pp. 363–368.

[103] Choi, Y., Chung, W. K., and Youm, Y., "Disturbance Observer in $\mathcal{H}_\infty$ Frameworks," *Proceedings of the 1996 IEEE IECON 22nd International Conference on Industrial Electronics,Control, and Instrumentation*, Vol. 3, 1996, pp. 1394–1400.

[104] Yi, L. and Tomizuka, M., "Two-degree-of-freedom control with robust feedback control for hard disk servo systems," *IEEE/ASME Tansactions on Mechatronics*, Vol. 4, No. 1, 1999, pp. 17–24.

[105] Oh, Y. and Chung, W. K., "Disturbance-Observer-Based Motion Control of Redundant Manipulators Using Inertially Decoupled Dynamics," *IEEE Tansactions on Mechatronics*, Vol. 4, No. 2, Jun. 1999, pp. 133–146.

[106] Tesfaye, A., Lee, H. S., and Tomizuka, M., "A Sensitivity Optimization Approach to Design of a Disturbance Observer in Digital Motion Control Systems," *IEEE Tansactions on Mechatronics*, Vol. 5, No. 1, Mar. 2000, pp. 32–38.

[107] Umeno, T., Kaneko, T., and Hori, Y., "Robust Servosystem Design with Two Degrees of Freedom and its Application to Novel Motion Control of Robot Manipulators," *IEEE Transactions on Industrial Electronics*, Vol. 40, No. 5, 1993, pp. 473–485.

[108] Canudas de Wit, C., Olsson, H., Åström, K., and Lischinsky, P., "A New Model for Control of Systems with Friction," *IEEE Transactions on Automatic Control*, Vol. 40, No. 3, 1995, pp. 419–425.

[109] Maulana, A. P., Ohmori, H., and Sano, A., "Friction Compensation via Smooth Adaptive Dynamic Surface Control," *Proceedings of the American Control Conference*, San Diego,CA, 1999, pp. 540–541.

[110] Xu, L. and Yao, B., "Adaptive Robust Control of Mechanical Systems with Nonlinear Dynamic Friction Compensation," *Proceedings of the American Control Conference*, Chicago, IL, 2000, pp. 2595–2599.

[111] Isidori, A. and Byrnes, C., "Output Regulation of Nonlinear Systems," *IEEE Transactions on Automatic Control*, Vol. 35, No. 2, 1990, pp. 131–140.

[112] Devasia, S., Chen, D., and Paden, B., "Nonlinear Inversion-Based Output Tracking," *IEEE Transactions on Automatic Control*, Vol. 41, No. 7, 1996, pp. 930–942.

[113] Tomlin, C. and Sastry, S., "Bounded Tracking for Non-Minimum Phase Systems with Fast Zero Dynamics," *International Journal of Control*, Vol. 68, No. 7, 1998, pp. 819–847.

[114] Seron, M. M., Braslavsky, J. H., and Goodwin, G. C., *Fundamental Limitations in Filtering and Control*, Springer-Verlag, London, 1998.

[115] Chen, Y., "Design of Robust Controllers for Uncertain Dynamical Systems," *IEEE Transactionson Automatic Control*, Vol. 33, No. 5, 1988, pp. 487–491.

[116] Huang, J., "Asymptotic Tracking of a Nonminimum Phase Nonlinear System with Nonhyperbolic Zero Dynamics," *IEEE Transactions on Automatic Control*, Vol. 45, No. 3, 2000, pp. 542–546.

[117] "Inverted Pendulum, Quanser Inc." `http://www.quanser.com/english/html/challenges/fs_chall_linear_flash.htm`.

[118] Stengel, R. F., *Optimal Control and Estimation*, Dover, 1994.

[119] Zhou, K., Doyle, J. C., and Glover, K., *Robust and Optimal Control*, Prentice-Hall, Upper Saddle River, NJ, 1995.

[120] Lewis, F. L., Yeşildirek, A., and Liu, K., "Multilayer Neural-Net Robot Controller with Guaranteed Tracking Performance," *IEEE Transactions on Neural Networks*, Vol. 7, No. 2, 1996, pp. 1–12.

[121] Sontag, E. and Wang, Y., "New characterizations of the input to state stability property," *IEEE Transactions on Automatic Control*, Vol. 41, 1996, pp. 1283–1294.

[122] Ioannou, P., "Decentralized Adaptive Control of Interconnected Systems," *IEEE Transactions on Automatic Control*, Vol. 31, No. 4, 1986, pp. 291–298.

[123] Ioannou, P. and Kokotovic, P., "Decentralized Adaptive Control of Interconnected Systems with Reduced Order Models," *Automatica*, Vol. 21, No. 4, 1985, pp. 401–412.

[124] Gavel, D. and Siljak, D., "Decentralized adaptive control: structural conditions for stability," *IEEE Transactions on Automatic Control*, Vol. 34, No. 4, 1989, pp. 413–426.

[125] Datta, A. and Ioannou, P., "Decentralized adaptive control," *Adavances in Control and Dynamic Systems, Academic Press*, 1992.

[126] Wen, C. and Soh, Y., "Decentralized Model Reference Adaptive Control Without Restriction on Subsystem Relative Degree," *IEEE Transactions on Automatic Control*, Vol. 44, No. 7, 1999, pp. 1464–1469.

[127] Ortega, R. and Herrera, A., "Solution to the decentralized stabilization problem," *Systems & Control Letters*, Vol. 20, No. 4, 1993, pp. 299–306.

[128] Wen, C., "Decentralized Adaptive Regulation," *IEEE Transactions on Automatic Control*, Vol. 39, No. 10, 1994, pp. 2163–2166.

[129] Wen, C. and Hill, D., "Global Boundedness Of Discrete-Time Adaptive Control Just Using Estimator Projection," *Automatica*, Vol. 28, No. 6, 1992, pp. 1143–1157.

[130] Wen, C. and Hill, D., "Decentralized Adaptive Control Of Linear Time Varying Systems," *Proc. 11th World Congr. Automatic Control*, Vol. 4, 1990.

[131] Wen, C., "Indirect Robust Totally Decentralized Adaptive Control Of Continuous-Time Interconnected Systems," *IEEE Transactions on Automatic Control*, Vol. 40, 1995, pp. 1122–1126.

[132] Ortega, R., "An energy amplification condition for decentralized adaptive stabilization," *IEEE Transactions on Automatic Control*, Vol. 41, 1996, pp. 285–288.

[133] Krstić, M., Kanellakopoulos, I., and Kokotović, P. V., "Nonlinear Design of Adaptive Controllers for Linear Systems," *IEEE Transactions on Automatic Control*, Vol. 39, No. 4, 1994, pp. 738–752.

[134] Wen, C. and Soh, Y., "Decentralized Adaptive Control using Integrator Backstepping," *Automatica*, Vol. 33, No. 9, 1997, pp. 1719–1724.

[135] Shi, L. and Singh, S., "Decentralized adaptive controller design for large scale systems with higher order interconnections," *IEEE Transactions on Automatic Control*, Vol. 37, No. 8, 1992, pp. 1106–1118.

[136] Jain, S. and Khorrami, F., "Decentralized Adaptive Output Feedback Design for Large Scale Nonlinear Systems," *IEEE Transactions on Automatic Control*, Vol. 42, No. 4, 1997, pp. 729–735.

[137] Geromel, J., Bernussou, J., and Oliveira, M., "Norm Optimization with Constrained Dynamic Output Feedback Controllers: Decentralized and Reliable Control," *IEEE Transactions on Automatic Control*, Vol. 44, No. 7, 1999, pp. 1449–1454.

[138] Yang, G., Wang, J., Soh, C., and Lam, J., "Decentralized Controller Design for Nonlinear systems," *IEEE Transactions on Automatic Control*, Vol. 44, No. 3, 1999, pp. 578–583.

[139] Jiang, Z., "New results in decentralized adaptive nonlinear control with output feedback," 1999, pp. 4772–4777.

[140] Jiang, Z., "Decentralized and adaptive nonlinear tracking of large-scale systems via output feedback," *IEEE Transactions on Automatic Control*, Vol. 45, No. 11, 2000, pp. 2122 –2128.

[141] Jiang, Z., "Decentralized disturbance attenuating output feedback trackers for large-scale nonlinear systems," *Automatica*, Vol. 38, No. 8, 2002, pp. 1407–1415.

[142] Spooner, J. and Passino, K., "Decentralized adaptive control of nonlinear systems using radial basis neural networks," *IEEE Transactions on Automatic Control*, Vol. 44, No. 11, 1999, pp. 2050–2057.

[143] Feipeng, D., "Decentralized sliding mode adaptive controller design based on fuzzy neural networks for interconnected uncertain nonlinear systems," *IEEE Transactions on Neural Networks*, Vol. 11, No. 6, 2000, pp. 1471–1480.

[144] Karakasoglu, A., Sudharsanan, I., and Sudareshan, M., "Identification and Decentralized adaptive control using dynamical neural networks with application to robtoic manipulators," *IEEE Transactions on Neural Networks*, Vol. 4, No. 6, 1993, pp. 919–930.

[145] Yen, G., "Decentralized neural controller design for space structural platforms," *IEEE International Conference on Systems, Man and Cybernetics*, 1994, pp. 2126–2131.

[146] Mirkin, B., " Comments on "Exact Output Tracking in Decentralized Adaptive Control Systems"," *IEEE Transactions on Automatic Control*, Vol. 48, No. 2, 2003, pp. 348–350.

[147] Mazenc, F., Praly, L., and W., D., "Global Stabilization by Output Feedback: examples and counterexamples," *Systems & Control Letters*, Vol. 23, 1994, pp. 119–125.

[148] Hovakimyan, N., Nardi, F., and Calise, A., "A Novel error Observer based Adaptive Output Feedback Approach for Control of Uncertain Systems," *IEEE Transactions on Automatic Control*, Vol. 47, No. 8, 2002, pp. 1310–1314.

[149] Pomet, J. and Praly, L., " Adaptive Nonlinear Regulation: Estimation from the Lyapunov Equation," *IEEE Transactions on Automatic Control*, Vol. 37, No. 6, 1992, pp. 729–740.

[150] Hovakimyan, N., Yang, B.-J., and Calise, A., "An Adaptive Output Feedback Control Methodology for Non-Minimum Phase Systems," *Proceedings of Conference on Decision and Control*, Las Vegas, NV, 2002, pp. 949–954.

[151] Ikhouane, F. and Krstić, M., "Robustness of the Tuning Functions Adaptive Backstepping Design for Linear Systems," *Proceedings of Conference on Decision and Control*, New Orleans, LA, 1995, pp. 159–164.

[152] Loper, J. C., *Vibration Cancellation and Disturbance Rejection in Serially Linked Micro/Macro Manipulators*, Master's thesis, Georgia Institute of Technology, School of Mechanical Engineering, March 1998.

[153] Book, W. and Loper, J., "Inverse Dynamics for Commanding Micromanipulator Inertial Force to Damp Macromanipulator Vibration," *Proceedings of the IEEE/RSJ International Conference on Intelligent Robotics and Systems*, 1999.

[154] George, L. and Book, W. J., "Inertial Vibration Damping Control of a Flexible Base Manipulator," *IEEE/ASME Tansactions on Mechatronics*, Vol. 8, No. 2, 2003, pp. 268–271.

[155] George, L. E., *Active Vibration Control of a Flexible Base Manipulator*, Ph.D. thesis, Georgia Institute of Technology, School of Mechanical Engineering, 2002.

[156] Krauss, R. and Book, W. J., "Stability and Observability in Active Mass Damping Control of a Flexible Robot," *Proceedings of IEEE Aerospace Conference*, Big Sky, Montana, 2003.

[157] Moallem, M., Patel, R., and Khorasani, K., *Flexible-link Robot Manipulators: Control Techniques and Structural Design*, Lecture Notes in Control and Information Sciences 257, Springer-Verlag, London, 2000.

[158] Heintze, J., Schothorst, G., and Weiden, A.J.J. v.d., T. P., "Modeling and Control of an industrial hydraulic rotary vane actuator," *Proceedings of Conference on Decision and Control*, San Antonio, TX, 1993, pp. 1913–1918.

[159] Mayergoyz, I., *Mathematical Models of Hysteresis*, Springer-Verlag, New York, NY, 1991.

[160] Haddad, W. M., Chellaboina, V., and Oh, J., "Linear Controller Analysis and Design for Systems with Input Hystereses Nonlinearities," *Journal of Franklin Institute*, Vol. 340, 2003, pp. 371–390.

[161] Gorbet, R. B., Morris, K. A., and Wang, D. W., "Passivity-Based Stability and Control of Hysteresis in Smart Actuators," *IEEE Transactions on Control Systems Technology*, Vol. 9, No. 1, January 2001, pp. 5–16.

[162] Nafalski, A., Hoskins, B. G., Kundu, A., and Doan, T., "The use of neural networks in describing magnetisation phenomena," *Journal of Magnetism and Magnetic Materials*, Vol. 160, 1996, pp. 84–86.

[163] Saliah, H. and Lowther, D., "The use of neural networks in magnetic hysteresis identification," *Physica B*, Vol. 233, 1997, pp. 318–323.

[164] Serpico, C. and Visone, C., "Magnetic Hysteresis Modeling via Feed-Forward Neural Networks," *IEEE Transactions on Magnetics*, Vol. 34, No. 3, May 1998, pp. 623–628.

[165] Adly, A. and Abd-El-Hafiz, S., "Using Neural Networks in the Identification of Preisach-Type Hysteresis Models," *IEEE Transactions on Magnetics*, Vol. 34, No. 3, May 1998, pp. 629–635.

[166] Kuczmann, M. and Iványi, A., "A New Neural-Network-Based Scalar Hysteresis Model," *IEEE Transactions on Magnetics*, Vol. 385, No. 2, March 2002, pp. 857–860.

[167] Beuschel, M., Hangl, F., and Schröder, D., "A General Approach for Hysteresis Modeling and Identification using Neural Networks," *Neural Networks Proceedings,1998. IEEE World Congress on Computational Intelligence. The 1998 IEEE International Joint Conference on*, Vol. 3, May 1998, pp. 2425–2428.

[168] Makaveev, D., Dupré, L., De Wulf, M., and Melkebeek, J., "Modelling of quasistatic magnetic hysteresis with feed-forward neural networks," *Journal of Applied Physics*, Vol. 89, No. 11, June 2001, pp. 6737–6739.

[169] Li, C. and Tan, Y., "A Neural Networks Model for Hysteresis Nonlinearity," *Sensors and Actuators A*, 2004, Article in Press.

[170] Kutay, A., Calise, A., and Hovakimyan, N., "Adaptive Output Feedback Control with Reduced Sensitivity to Sensor Noise," *Proceedings of the American Control Conference*, 2003.

[171] Scherer, C., Gahinet, P., and Chilali, M., "Multiobjective Output-Feedback Control via LMI Optimization," *IEEE Transactions on Automatic Control*, Vol. 42, No. 7, 1997, pp. 896–911.

[172] Chilali, M., Gahinet, P., and Apkarian, P., "Robust Pole Placement in LMI Regions," *IEEE Transactions on Automatic Control*, Vol. 44, No. 12, 1999, pp. 2257–2270.

[173] Kokotović, P., Khalil, H., and O'Reilly, J., *Singular Perturbation Methods in Control: Analysis and Design*, Academic Press, 1986.

[174] Sastry, S., Hauser, J., and Kokotovicć, P., "Zero dynamics of regularly perturbed systems may be singularly perturbed," *Systems & Control Letters*, Vol. 13, 1989, pp. 299–314.

[175] Kailath, T., *Linear Systems*, Prentice-Hall, Englewood Cliffs, NJ, 1980.

VITA

Bong-Jun Yang was born on November 2, 1969, in Cheju-Do, South Korea. He is the son of Ho-Nam Yang and Myung-Ja Choi. He attended the Seoul National University, obtaining a Bachelor of Science in Aeronautical and Astronautical engineering in 1994. Then, he attended Stanford University and completed a Master of Science degree in Astro/Aeronautics in 1998. In 1999, he entered the School of Aerospace Engineering at Georgia Institute of Technology to pursue a Doctor of Philosophy degree. He is the member of the Control System Society (CSS) at the Institute of Electrical and Electronics Engineers (IEEE) and the American Institute of Aeronautics and Astronautics (AIAA).